

Winter 2003

The central New England sea breeze study

Samuel T K Miller

University of New Hampshire, Durham

Follow this and additional works at: <https://scholars.unh.edu/dissertation>

Recommended Citation

Miller, Samuel T K, "The central New England sea breeze study" (2003). *Doctoral Dissertations*. 196.
<https://scholars.unh.edu/dissertation/196>

This Dissertation is brought to you for free and open access by the Student Scholarship at University of New Hampshire Scholars' Repository. It has been accepted for inclusion in Doctoral Dissertations by an authorized administrator of University of New Hampshire Scholars' Repository. For more information, please contact nicole.hentz@unh.edu.

THE CENTRAL NEW ENGLAND SEA BREEZE STUDY

BY

SAMUEL T. K. MILLER

B.S., University of New Hampshire, 1996

M.S., University of New Hampshire, 1999

DISSERTATION

Submitted to the University of New Hampshire
in Partial Fulfillment of
the Requirements for the Degree of

Doctor of Philosophy
in
Earth Sciences

December, 2003

UMI Number: 3111509

Copyright 2004 by
Miller, Samuel T. K.

All rights reserved.

INFORMATION TO USERS

The quality of this reproduction is dependent upon the quality of the copy submitted. Broken or indistinct print, colored or poor quality illustrations and photographs, print bleed-through, substandard margins, and improper alignment can adversely affect reproduction.

In the unlikely event that the author did not send a complete manuscript and there are missing pages, these will be noted. Also, if unauthorized copyright material had to be removed, a note will indicate the deletion.

UMI[®]

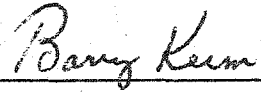
UMI Microform 3111509

Copyright 2004 by ProQuest Information and Learning Company.

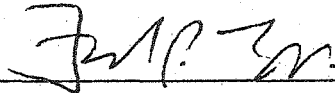
All rights reserved. This microform edition is protected against unauthorized copying under Title 17, United States Code.

ProQuest Information and Learning Company
300 North Zeeb Road
P.O. Box 1346
Ann Arbor, MI 48106-1346

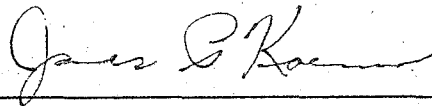
This dissertation has been examined and approved.



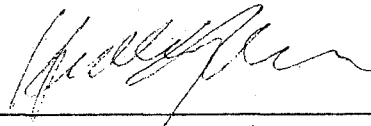
Dissertation Director
Dr. Barry Keim, Former UNH Associate Professor
of Geography and Earth, Oceans, and Space



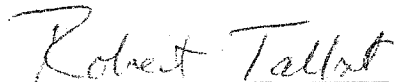
Dr. Frank Colby, Professor of Meteorology
University of Massachusetts - Lowell
Department of Earth, Environmental, and
Atmospheric Sciences



Dr. James Koerner, Professor of Meteorology
Plymouth State University
Department of Natural Sciences



Dr. Huiting Mao, Research Assistant Professor
Climate Change Research Center



Dr. Robert Talbot, Research Professor of Earth Sciences
and Earth, Oceans, and Space

10-29-03

Date

DEDICATION

This work is dedicated to Catherine, Virginia, and Sabina.

ACKNOWLEDGMENTS

I would like to thank Dr. Barry Keim and the other members of my dissertation committee, as well as Ms. Kristi Donahue, Dr. Mike Prentice, Ms. LeeAnn Stevens, Mr. Yuanli Wang, and Mr. Dan Woods for their generous assistance with this work.

This work was supported by the Atmospheric Investigation, Regional Modeling, Analysis, and Prediction (AIRMAP) Project, under NOAA grants NA07RP0475 and NA17RP1488.

TABLE OF CONTENTS

DEDICATION.....	iii
ACKNOWLEDGMENTS.....	iv
LIST OF TABLES.....	ix
LIST OF FIGURES.....	xi
ABSTRACT.....	xiv

CHAPTER	PAGE
1. INTRODUCTION.....	1
2. THE SEA BREEZE: STRUCTURE, FORECASTING, AND IMPACTS.....	11
Introduction.....	11
Ancient history.....	16
Modern understanding.....	19
Forcing.....	20
The role of sound waves.....	21
Sea-breeze circulation and the Bjerknes circulation theorem.....	24
More complete models and topography.....	28
Structure.....	33
Prefrontal phenomena.....	34
SBC response to the synoptic-scale wind.....	35
Sea-breeze gravity current and Kelvin- Helmholtz Billows.....	50
Sea-breeze front (SBF).....	55
Interactions with external meteorological phenomena.....	73
Daily life-cycle.....	76
Forecasting.....	79
Occurrences.....	79
Surface wind.....	83

Extent of inland penetration.....	92
Air quality impact mechanisms.....	100
Summary.....	112
3. SYNOPTIC-SCALE CONTROLS ON THE SEA BREEZE OF THE CENTRAL NEW ENGLAND COAST.....	116
Introduction.....	118
Pertinent literature.....	119
Methods.....	121
Event identification.....	126
Definition of synoptic classes.....	130
Synoptic classes associated with sea breeze events, marginal events, and non-sea-breeze events.....	138
Meso-alpha temperature gradients and geostrophic wind components.....	141
Summary and conclusions.....	160
4. SYNOPTIC-SCALE CONTROLS ON THE SEA BREEZE OF THE CENTRAL NEW ENGLAND COAST, PART II: TIME-EVOLUTION OF MESO-ALPHA FORCING.....	165
Introduction.....	167
Background.....	168
Methods.....	174
Results.....	178
Synoptic class 1.....	178
Synoptic class 2.....	179
Synoptic class 3.....	183
Synoptic class 4.....	186
Synoptic class 5.....	190
Synoptic class 6.....	193
Discussion.....	196
Summary.....	205

5.	THE SEA-BREEZE -- MESO-ALPHA FORCING AND MESO-BETA RESPONSE, PART I: CIRCULATION AND GRAVITY CURRENT.....	209
	Introduction.....	210
	Scope and methods.....	218
	Results.....	225
	Isentropic patterns.....	227
	Kinematic patterns.....	237
	Discussion.....	248
	Development of sea-breeze gravity current....	248
	Decay of sea-breeze gravity current.....	249
	Annual variation in most developed state of sea-breeze gravity current.....	250
	Isentropic patterns with winter sea breeze events.....	251
	Kinematic patterns associated with pure, corkscrew, and backdoor sea-breeze circulation.....	251
	Along-shore variation associated with weak sea breeze events.....	253
	Differing scales of sea-breeze forcing and response.....	255
	Forecasting the most developed state of the sea-breeze gravity current.....	262
	Forecasting time-of-onset and maximum inland penetration of the sea-breeze circulation.....	264
	Summary and conclusions.....	268
6.	THE SEA-BREEZE -- MESO-ALPHA FORCING AND MESO-BETA RESPONSE, PART II: FRONTAL BEHAVIOR.....	272
	Introduction.....	274
	Scope and methods.....	281
	Results.....	287
	Discussion.....	294

Morning development of cross-shore gradients.....	294
Kinematic and thermodynamic fronts develop in different locations.....	295
Evening persistence of circulation.....	295
Dual peaks in magnitude of thermodynamic front.....	296
Dual peaks in magnitude of kinematic front.....	297
Bifurcation of the thermodynamic front.....	297
Persistent zone of convergence.....	299
Bifurcation of the kinematic front.....	299
Distribution and forecasting of peak isentropic and kinematic gradients.....	300
Forecasting peak meso- β frontogenesis.....	305
Summary.....	309
7. SUMMARY AND CONCLUSIONS.....	313
Summary of research results.....	314
Directions for future research.....	325
Concluding remarks	333
REFERENCES.....	335
APPENDIX 1: TERMINOLOGY.....	354
APPENDIX 2: SUMMARY OF SYMBOLS.....	363
APPENDIX 3: SCALING AND LIMITATIONS OF THE KINEMATIC FRONTOGENESIS FUNCTION.....	365
APPENDIX 4: COMPLETE LIST OF SEA-BREEZE, MARGINAL, AND NON-SEA BREEZE EVENTS AND THEIR ASSOCIATED SYNOPTIC CLASSES.....	369
APPENDIX 5: MISCELLANEOUS TABLES.....	373

LIST OF TABLES

No.	TITLE	PAGE
2.1	Summary of subjects discussed in sea breeze literature.....	21
2.2	Varying extent of the sea breeze's inland penetration in different parts of the world....	93
2.3	Summary of controls on the inland penetration of the sea breeze.....	98
3.1	Occurrences of synoptic classes and associated percentages of all occurrences.....	138
3.2	Comparison of sea-breeze, marginal, and non-sea-breeze events to synoptic classes.....	139
4.1	Description of synoptic classes defined in Chapter 3.....	172
4.2	Summary of case studies.....	197
4.3	Observed meso- α forcing and sea-breeze response by synoptic class.....	199
5.1	Case study dates, synoptic classes, and event types.....	220
5.2	General category of sea-breeze and marginal events observed in case-studies.....	253
5.3	Evolution of May 9, 2001 isentropic and kinematic patterns.....	257
5.4	Evolution of May 10, 2001 isentropic and kinematic patterns.....	262
6.1	Case study dates, synoptic classes, and event types.....	283
6.2	Peak sea-breeze related isentropic gradients and wind divergence values.....	301
A2.1	Summary of symbols.....	363
A3.1	Base variables for scaling the KFF.....	365
A3.2	Summary of KFF model limitations when using in the horizontal plain.....	368
A4.1	List of Year-2001 Events and Associated Synoptic Classes.....	369
A5.1	Description of Isentropic Patterns.....	373

A5.2	Description of Kinematic Patterns.....	376
A5.3	Sequence of Isentropic and Kinematic Patterns with Sea-Breeze and Marginal Events.....	379
A5.4	Summary of $ \nabla\theta $ and $\nabla \cdot V$ field evolution during Sea-Breeze and Marginal events.....	382

LIST OF FIGURES

No.	TITLE	PAGE
1.1	Sea-breeze system.....	4
1.2	Study area and location map.....	6
2.1	Sea-breeze system.....	15
2.2	Sea breeze and the Bjerknes circulation theorem.....	26
2.3	Development of pure, corkscrew, and backdoor sea breezes.....	38
2.4	New England Air Quality Study, 2002, sea breeze study area.....	43
2.5	Pure sea breeze event, 3 August 2002.....	45
2.6	Corkscrew sea breeze event, 21 July 2002.....	47
2.7	Backdoor sea breeze event, 24 July 2002.....	49
2.8	Simpson's [1997] shadowgraph of a laboratory gravity current.....	55
2.9	Simplified two-dimensional flow associated with a gravity current in presence of surface friction.....	56
2.10	Australian Morning Glory, as seen from the wing of a glider about one kilometer AGL.....	71
2.11	Atmospheric SO ₂ concentration levels at two stations in Boston, Massachusetts.....	103
2.12	Convective Internal Boundary Layer (CIBL) formed by advection of cool marine air over a warm land surface.....	104
2.13	Ground-level O ₃ concentration levels at three stations north of New York City.....	111
3.1	Study area and location map.....	123
3.2	Synoptic class 1.....	132
3.3	Synoptic class 2.....	133
3.4	Synoptic class 3.....	134
3.5	Synoptic class 4.....	135
3.6	Synoptic class 5.....	136
3.7	Synoptic class 6.....	137
3.8	Nowcast diagram.....	145

3.9	Nowcast diagram for synoptic classes 1, 2, and 3.....	148
3.10	Nowcast diagram for synoptic classes 1, 2, and 3.....	150
3.11	Nowcast diagram for synoptic classes 4 and 5	152
3.12	Dates associated with class 4 and 5 non-sea-breeze events.....	155
3.13	Nowcast diagram for synoptic class 6.....	156
3.14	Onset hour [UTC] of sea-breeze and marginal events, all synoptic classes.....	158
4.1	Study area and location map.....	170
4.2	Synoptic classes.....	173
4.3	Summary of 32 case-studies selected from 2001.....	175
4.4	Time evolution of meso- α forcing during SB, MAR, and NSB events associated with synoptic class 1.....	179
4.5	Time evolution of meso- α forcing during SB, MAR, and NSB events associated with synoptic class 2.....	180
4.6	Time evolution of meso- α forcing during NSB events associated with synoptic class 3.....	184
4.7	Time evolution of meso- α forcing during SB, MAR, and NSB events associated with synoptic class 4.....	188
4.8	Time evolution of meso- α forcing during NSB events associated with synoptic class 5.....	191
4.9	Time evolution of meso- α forcing during SB, MAR, and NSB events associated with synoptic class 6.....	194
5.1	Sea-breeze system.....	212
5.2	Study area.....	217
5.3	Case-study events as a function of their associated cross-shore potential temperature gradients ($\delta\theta/\delta x$) and geostrophic wind components (u_G)	221
5.4	Study area topography and reference points..	226
5.5	Elongate S, Coastal S, CSP-Wland, Split S, ISP, and Lowlands isentropic patterns.....	229

5.6	KNWWSW, KNWWSE, CSP-Kland, CSP-Wland, KE, and KN isentropic patterns.....	233
5.7	CICP, LWWP, MWN Drainage, and KWK isentropic patterns.....	236
5.8	“Trough” kinematic pattern.....	238
5.9	SWX and SWP kinematic patterns.....	239
5.10	SWM kinematic patterns.....	241
5.11	NE kinematic patterns.....	243
5.12	NW kinematic patterns.....	245
5.13	COL kinematic patterns.....	247
5.14	Comparison of KWK isentropic patterns occurring with SWM2 kinematic patterns in two separate events.....	255
5.15	Most developed sea-breeze isentropic pattern reached as a function of peak meso- α forcing.	264
5.16	Time of onset and depth of inland penetration.....	266
6.1	Study area.....	276
6.2	Case-study events as a function of their associated cross-shore potential temperature gradients ($\delta\theta/\delta x$) and geostrophic wind components (u_G)	284
6.3	Study area topography and reference points..	288
6.4	Split S isentropic pattern and bifurcated thermodynamic sea-breeze front.....	298
6.5	Peak sea-breeze related meso- β isentropic gradients and wind divergence values as a function of peak meso- α forcing.....	303
6.6	Peak meso- β convergence and rotational frontogenesis with sea-breeze and marginal events, as a function of peak meso- α forcing..	307
7.1	Ozone recorded at Isles of Shoals (ISON3) and Thomson Farm (UNH) site on 23 July 2002.....	327
7.2	Air temperature recorded during ferry trips between Portsmouth and the Isles of Shoals on 23 July 2002.....	329
7.3	C-10 Research and Education Foundation meso- γ environmental monitoring network....	332

ABSTRACT

THE CENTRAL NEW ENGLAND SEA BREEZE STUDY

by

Samuel T. K. Miller

University of New Hampshire, December, 2003

The synoptic and mesoscale environments conducive to the formation of sea breezes were examined, as well as the spatial and temporal evolution of sea-breeze circulations, gravity currents, and fronts along the central New England coast. Sea breeze events were defined as occurring when the observed surface wind direction began the day outside the southeast quadrant, shifted to southeast by afternoon, then shifted back out of the southeast quadrant in the evening, driven by mesoscale, insolation-induced cross-shore temperature gradients.

The meso- α (200 - 2000 km) sea-breeze forcing in the study area was defined as a combination of the cross-shore potential temperature gradient ($\delta\theta/\delta x$) that may drive sea breezes inland, and the cross-shore geostrophic wind component (u_G) that may resist the landward movement of sea breezes. It was found that the peak

values and temporal evolution of the meso- α forcing were dependent on the locations and relative dominance of synoptic-scale surface pressure systems in the eastern United States. These conclusions can often be used to accurately predict sea-breeze events, and their time of onset, using surface observations recorded in the early morning. The forecasting technique is adaptable to any coastal location in the world.

Meso- β (20 - 200 km) horizontal variations in the sea-breeze circulation, gravity current, and front were compared to $\delta\theta/\delta x$ and the cross-shore wind component at 925 hPa (u_{925}) in the study area. The latter was substituted for u_G because it also accounts for the synoptic-scale temperature gradient between the surface and 925 hPa via the thermal wind relation. Near-surface potential temperature (isentropic) fields were used to examine the sea-breeze gravity current, and the wind (kinematic) fields were used to examine the sea-breeze circulation. Isentropic gradient fields were used to examine the thermodynamic sea-breeze front, and convergence fields were used to examine the kinematic sea-breeze front. It was found that the most developed pattern the sea-breeze gravity current achieved, the time of the sea-breeze circulation's

first contact with the coast and its most advanced inland distance,
and the peak meso- β strength of the sea-breeze frontal components
were all functions of the meso- α forcing.

CHAPTER 1

INTRODUCTION

CHAPTER I

INTRODUCTION

Forecasting the sea breeze in coastal areas throughout the world is a standard problem for operational meteorologists. Atmospheric scientists in academia, regulatory agencies, and industry are concerned with its impact on air quality. Aircrews must compensate for wind shear and other hazards to flight created when the sea breeze affects airports near the coast, and sailors must adapt to changes in wind direction and the sea surface caused by the sea-breeze system. For these reasons, the sea breeze has been a subject of human inquiry for more than 2500 years. The purpose of this dissertation was to study the sea breeze of the central New England coast in various synoptic and mesoscale meteorological environments, and develop improved methods for forecasting occurrences, time of onset, depth of inland penetration, and other important parameters. The work was completed for the Atmospheric Investigation, Regional Modeling, Analysis And

Prediction (AIRMAP) program, whose goals include improving weather and air-quality forecasts in New England.

The sea breeze is a complex system (Figure 1.1) that develops when insolation and differential heating of the land and sea surfaces create a mesoscale pressure gradient force pointing toward land.

The sea-breeze circulation (SBC) is a vertically-rotating cell in which a shallow layer of marine air flows inland and converges with continental air. Vertical currents develop in the convergence zone between the sea breeze and the ambient flow – called the kinematic sea-breeze front (SBFkn) -- which creates a raised sea-breeze head (SBH). Fair weather cumulus (Cu) may develop in convective updrafts landward of the front. The circulation is usually closed by seaward return flow near 900 hPa, and weak sinking currents over a broad area several tens of kilometers offshore. The horizontal wind field associated with the sea-breeze circulation is often characterized by local-scale variations in direction and speed, which can create wind-shear hazards at airports, and complicate the problem of predicting the downwind movement and dispersion of air pollution plumes.

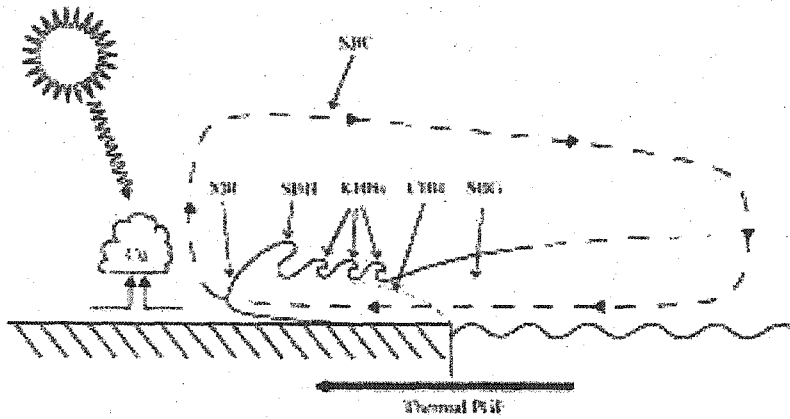


Figure 1.1: Sea-breeze system.

The sea-breeze gravity current (SBG) is the landward flow of cool, moist marine air in the lower half of the SBC, and can provide moisture for morning fog and afternoon thunderstorms. The leading edge of the SBG - called the thermodynamic sea-breeze front (SBFth) - is beneath the SBH, and is usually associated with a strong cross-shore temperature gradient. Kelvin-Helmholtz Billows (KHBs) may develop over land in the shear zone between the upper boundary of the SBG and the seaward return flow, creating a turbulent wake behind the SBH. A Convective Internal Boundary Layer (CIBL) may develop in the SBG, landward of the coast, trapping pollutants near Earth's surface and reducing air quality.

This dissertation research focused on the behavior of the sea-breeze system (SBS) in east-central New England (Figure 1.2). The

study area was characterized by a relatively straight coastline, bound by seaward projections of land at the northern and southern edges. The mean elevation ranged from near sea level at the coast to a maximum height of about 275 meters on the western edge of the study area. The White Mountain Presidential Range (including Mount Washington) was just beyond the northwestern corner.

Centered in the middle latitudes, the study area is subject to wide variations in synoptic-scale temperature and pressure gradients over the course of the year. During summer, when sea breezes are most likely, near-surface air temperatures over land may reach as high as 40 degrees Celsius. Sea surface temperatures in the Gulf of Maine range from about 2 degrees Celsius in the early spring to about 25 degrees Celsius in late summer [*Brown and Irish, 1993*].

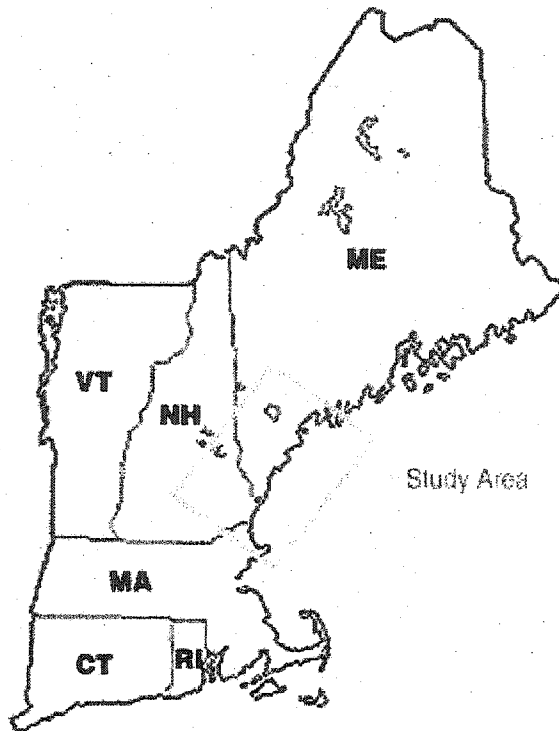


Figure 1.2: Study area and location map. Gray line indicates edges of the study area.

Several aspects of SBS behavior in the study area were studied under a wide range of differing synoptic-scale (>2000 km) environments, including the peak and time-dependent behavior of the thermally-created meso- α (200 - 2000 km) pressure gradient force that drives the sea breeze, variations in the meso- β (20 - 200 km) horizontal behavior of the sea-breeze circulation cell and gravity current, and the spatial and temporal variations in the characteristics of the sea-breeze front. Year-2001 near-surface

temperature, pressure, and wind observations from eastern New England and the Gulf of Maine were used in a variety of ways to accomplish the goals of this research project.

This dissertation contains seven chapters. Chapter 2 is a thorough review of sea-breeze literature extending back more than 2500 years, and Chapters 3 through 6 describe original research accomplished for AIRMAP. Chapter 7 summarizes the entire work. Chapters 2 through 6 were written as individual papers for publication in peer-reviewed journals. Chapter 2 has been accepted to *Reviews of Geophysics* and will be published before the end of 2003. Chapter 3 was submitted to *Weather and Forecasting* in 2002, and was published in the summer of 2003. Chapter 4 was submitted to *Weather and Forecasting* in August, 2003, and is currently under review. Chapters 5 and 6 will be submitted to *Boundary-Layer Meteorology* during the fall of 2003.

The specific objectives addressed in this research were:

1. Determine the synoptic-scale environments that are conducive to the occurrence of the sea breeze along the central New England coastline. While previous studies of the New England sea breeze concluded it occurs under the influence of large-scale anticyclones, specific forecast guidance based on the

locations and relative influence of synoptic-scale surface pressure systems and airmass boundaries was not available. Chapter 3 groups the synoptic-scale environment into six general classes, and documents the conditions when the sea breeze is most likely to occur.

2. Determine the meso- α forcing conditions conducive to the onset of the sea breeze along the central New England coastline. Previous researchers have developed indices for forecasting sea breeze events at specific locations, based on the cross-shore temperature gradient that drives the sea breeze inland, and the cross-shore wind component that resists its inland movement. Chapter 3 presents the sea breeze Nowcast Diagram, a principal tool developed in my work for forecasting the sea breeze. It includes both of the key cross-shore variables. My results show that their values at the time of onset of the sea breeze are a function of synoptic class. In Chapter 4, I show that the *time-evolution* of both variables on the Nowcast Diagram is also a function of synoptic class. Guidance for forecasting sea breeze events at a point 10 kilometers inland using the diagram was also developed in these chapters.

3. Quantify the spatial (horizontal) and temporal evolution of the wind field and marine airmasses over land during sea-breeze events. Previous studies have quantified variations in the behavior of the low-level wind field associated with the sea-breeze circulation along specific coastlines in different large-scale environments. In Chapter 5, I accomplished this task for the sea breeze of the central New England coast. Because of its association with Convective Internal Boundary Layers, and unlike previous studies, my work quantified the spatial and temporal distribution of marine airmasses associated with the sea-breeze gravity current. Specific forecast guidance for the sea breeze is presented for estimating the time of onset at the coast, its peak inland penetration, and the horizontal distribution of marine air at the time of its peak inland penetration.

4. Quantify the characteristics and time-evolution of the sea-breeze front. Previous researchers have studied the sea-breeze and found that, like the sea-breeze circulation and gravity current, the behavior of sea-breeze front is strongly dependent on the specific physical characteristics of the local coastline. In Chapter 6, I document the meso- β sea-breeze frontal behavior along the central New England coast, and develop forecast guidance for

estimating several of its characteristics utilizing meso- α variables. It is shown that the peak meso- β wind convergence, potential temperature gradient, and kinematic frontogenesis at the front can be predicted using easily calculated meso- α variables.

CHAPTER II

THE SEA BREEZE: STRUCTURE, FORECASTING, AND IMPACTS.

This chapter has been accepted for publication in *Reviews of
Geophysics*.

CHAPTER II

THE SEA BREEZE: STRUCTURE, FORECASTING, AND IMPACTS.

ABSTRACT

The sea-breeze system (SBS) occurs at coastal locations throughout the world, and consists of many spatially and temporally nested phenomena. Cool marine air propagates inland when a cross-shore mesoscale (2 - 2000 kms) pressure gradient is created by daytime differential heating. The circulation is also characterized by rising currents at the sea-breeze front, diffuse sinking currents well out to sea, and is usually closed by seaward flow aloft. Coastal impacts include relief from oppressive hot weather, development of thunderstorms, and changes in air quality. This chapter provides a review of SBS research extending back 2500 years, but focuses primarily on recent discoveries. Sea-breeze forcing mechanisms, structure and related phenomena, life cycle, forecasting, and impacts on air quality are discussed.

Introduction

The sea breeze is a local circulation that occurs at coastal locations throughout the world [*Masselink and Pattiaratchi, 1998*]. It has been observed from polar regions to the equator, can provide relief from oppressive hot weather, trigger thunderstorms, provide moisture for fog, and may result in either improved or reduced air

quality near Earth's surface [*Barbato, 1975; Kozo, 1982; Hsu, 1988; Simpson, 1994; Camberlin and Planchon, 1997; Silva Dias and Machado, 1997*]. It is important to continue improving our understanding of the sea breeze because a large part of the human population lives in major cities in coastal areas.

The large-scale environment in which the sea breeze occurs has been understood for thousands of years, and the broad outlines of the sea breeze's behavior have been understood for at least a hundred years. It occurs under relatively cloud-free skies, when the surface of the land heats up more rapidly than the sea. The thermal contrast creates a local-scale pressure gradient force (PGF) directed from sea to land, and a shallow layer of marine air moves inland in response. Some of the components of the SBS (Figure 2.1) are:

- Sea-breeze circulation (SBC): A vertically-rotating mesoscale cell, with shoreward flow near Earth's surface, rising air currents inland, diffuse sinking currents several kilometers out to sea, and (usually) seaward return flow near 900 hPa.
- Sea-breeze gravity current (SBG): The landward flow of cool, moist marine air in the lower horizontal arm of the SBC.

- Sea-breeze front (SBF): The landward edge of the SBG and the SBC, often associated with sharp changes in temperature, moisture, and wind. Its approach may be marked by the development of fair-weather cumulus clouds (Cu).
- Sea-breeze head (SBH): Raised head above and immediately behind the SBF, created by updrafts within both the continental and marine airmasses. It is about twice as high as the following "feeder" flow behind the SBF.
- Kelvin-Helmholtz Billows (KHBs): Waves that develop along the upper boundary of the SBG, during periods of low static stability (mid-day).
- Convective Internal Boundary Layer (CIBL): An unstable region within the marine airmass, appearing at the coast and growing in depth with distance inland, in which low-level pollutants may become trapped and concentrated.

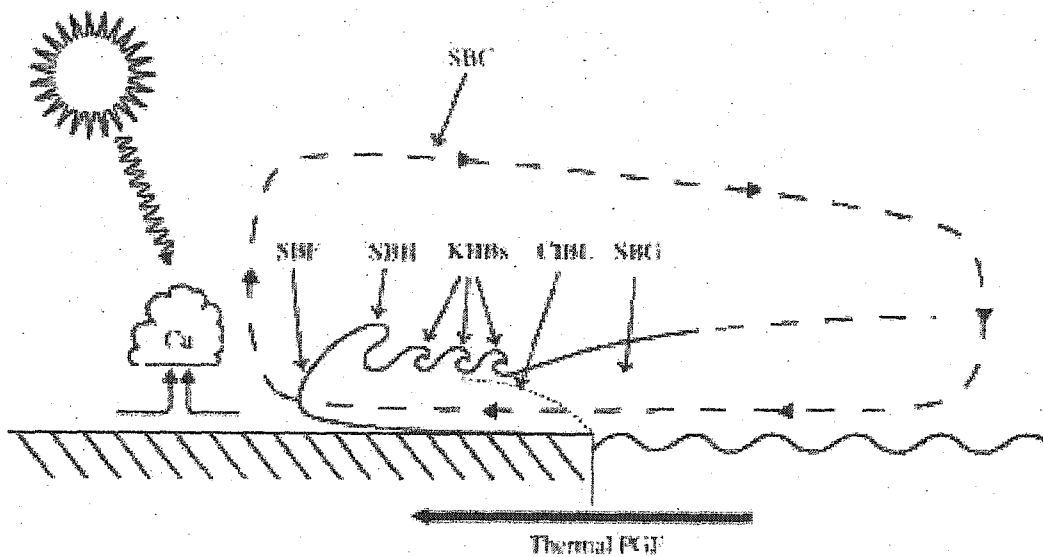


Figure 2.1: Sea-breeze system (SBS). Details are discussed in the text.

The details of the sea breeze's behavior along specific coastlines can be surprising, even to experienced meteorologists. For example, while the sea breeze is initiated during the daytime, it may persist at any time during the day or night. The leading edge of the sea breeze may separate from the feeder flow behind the front, and move hundreds of kilometers inland as an independent entity.

A great deal of new knowledge has been gained over the last 15 years, and an updated overview is needed, tying together our improved understanding of the sea breeze. This paper will fill that need, focusing on sea-breeze forcing mechanisms, structure, life cycle, forecasting, and the ways in which the sea breeze impacts

local air quality. Appendix I contains a glossary of key terms and symbols.

Ancient History

Given their dependence on the wind and tides, it seems likely that early sailors and fishermen understood the diurnal cycle of the sea breeze long before natural scientists began writing about it. Military personnel, particularly those that fought battles at sea, would also have been keenly interested in the sea breeze. *Simpson* [1994] discusses the story of Athenian military leader Themistocles, commander of the Greek forces in a naval battle with the Persians in 480 B.C.E. The battle took place in a narrow channel between the island of Salamis and the Greek mainland. Themistocles chose to begin his battle with the Persians at the moment when the sea breeze began flowing into the narrow channel. The low, solid design of the Greek ships gave them the advantage in the choppy waters caused by the sea breeze, and they defeated the Persians.

The first scientist to write about the wind in general was Aristotle. In *Meteorologica*, written 150 years after Themistocles' victory at Salamis, Aristotle stated that "as a rule a considerable area may be expected to be similarly affected, because neighboring

places lie in a similar relation to the Sun, unless they have some local peculiarity" [Lee, 1952, pg. 169]. He noted that the prevailing wind in Athens is from the north or south, and the *Etesian* wind -- a persistent, northerly or northeasterly wind -- occurs after the Summer Solstice. Aristotle attributed local-scale winds to the unequal distribution of Earth's moist and dry "exhalations" and variations in local topography [Lee, 1952, pg. 165].

Theophrastus' *De Ventis* was written about 300 B.C.E., approximately 30 years after *Meteorologica*, and discusses a) the importance of the Sun in driving the wind, and b) a distinct sea breeze from the south or southwest that occurred during the period of the Etesian wind. According to Theophrastus, "at about the time of the Etesians, winds arise counter to the north wind because of a circling back so that ships move in the opposite direction... These winds are called reverse north winds" [Coutant and Eichenlaub, 1975, pg. 29]. This may be the first written reference to an onshore wind opposing a synoptic (continental)-scale offshore wind.

Theophrastus also noticed that "everywhere at noon the winds die down because of the Sun's actions, and arise again with the late afternoon. It happens that the reversing wind [the seabreeze] blows against the land winds and the Etesians rise at the same time again" [Coutant and Eichenlaub, 1975, pg. 31]. This observation can be

explained as opposing forces reaching equilibrium at about noontime, and Theophratus correctly attributed the developing equilibrium to the Sun's influence. During mid-afternoon, when the land-sea temperature contrast reaches its maximum, the sea breeze moves inland as a southwesterly wind, while well offshore the northeasterly Etesian wind reaches its diurnal maximum [*Coutant and Eichenlaub, 1975*].

As far as we know, there is little documented to demonstrate major advances in the understanding of the sea breeze from about 300 B.C.E. to the 17th Century A.D. This gap in research is a subject best addressed by historians. Over the past several centuries, there has been an increasing interest in the sea breeze, which is documented in *Jehn's* [1973] bibliography of sea breeze research from the 17th century to 1972. He lists 16 references on the sea breeze written before 1800, 113 written between 1800 and 1899, and 407 from between 1900 and 1972. Among *Jehn's* references are a brief article by Francis Bacon, written in 1664, and another by Immanuel Kant from 1755 [*Jehn, 1973*]. A recent search reveals more than 500 new articles published on the subject since 1990 alone.

Modern Understanding

Contemporary studies of the sea-breeze system have been motivated by its influence on local wind velocity and air quality [e.g. *Angell and Pack*, 1965; *Yu and Wagner*, 1970; *Barbato*, 1975; *Neumann*, 1977; *Shair et al.*, 1982; *Kalthoff et al.*, 2002], convective activity [e.g. *Pielke*, 1985; *Pielke et al.*, 1991; *Rao and Fuelberg*, 2000; *Lericos et al.*, 2002], as well as by an interest in the more esoteric aspects of its dynamics and structure [e.g. *Smith*, 1982; *Kraus*, 1992; *Reible et al.*, 1993; *Tijm and van Delden*, 1999]. Some have even studied SBS influence on the coastal ocean [*Schoellhamer*, 1996; *Gibbs*, 2000] and beach morphology [*Masselink and Pattiaratchi*, 1998].

These researchers have found that the SBS, often thought to be easily understood, is actually a very complicated phenomenon, producing associated phenomena or non-linear interactions on several scales, from the meso- β scale (20 - 200 km) through the inertial subrange (where turbulent motions are approximately homogeneous, isotropic, and inviscid) [*Stull*, 1988; *Finkele et al.*, 1995; *Cenedese et al.*, 2000]. Some of the phenomena are the raised head of the advancing sea breeze [e.g. *Craig et al.*, 1945; *Simpson*, 1994]; interactions between the sea breeze or sea-breeze front and

synoptic-scale or other mesoscale circulations [e.g. *Zhong and Takle, 1992; Atkins et al., 1995; Brümmer et al., 1995*], as well as between multiple sea-breeze fronts [*Clarke, 1984*]; the turbulent wake composed of Kelvin-Helmholtz Billows seaward of the sea-breeze front and along the upper boundary of the shallow marine layer [e.g. *Chiba et al., 1999*]; and, the Convective Internal Boundary Layer (CIBL) that forms within the stable marine layer as it moves over the hot land surface [e.g. *Hsu, 1988*].

In the following sections, each of the areas summarized in Table 2.1 will be explored in detail.

Table 2.1: Summary of subjects discussed in sea breeze literature.

General subject	Specific topics included
<i>Forcing</i>	<ul style="list-style-type: none"> • The role of sound waves • Development of the sea-breeze circulation from the mesoscale pressure gradient • More complete physical models
<i>Structure</i>	<ul style="list-style-type: none"> • Pre-frontal phenomena • Sea-breeze's response to the prevailing wind • Sea-breeze gravity current and its response to Kelvin-Helmholtz Billows • Sea-breeze front and associated phenomena
<i>Life-cycle</i>	<ul style="list-style-type: none"> • Sequence of development stages
<i>Interactions with external meteorological phenomena</i>	<ul style="list-style-type: none"> • Separate sea-breeze systems • Convective updrafts • Urban heat islands • River breezes • Temperature inversions • Horizontal convective rolls • Synoptic-scale cold fronts
<i>Forecasting</i>	<ul style="list-style-type: none"> • Occurrence of a sea breeze • Wind speed and direction • Extent of inland penetration
<i>SBS-related air quality impact mechanisms</i>	<ul style="list-style-type: none"> • Pollutant transport mechanisms • Convective internal boundary layers • Sea breeze in complex air pollution scenarios

Forcing.

The role of sound waves. The sea breeze is caused by the temperature difference between the hot land and cool sea surfaces. As the difference increases during the day, a pressure gradient is

produced at low levels in the atmosphere, initiating the sea breeze near Earth's surface [*Simpson*, 1994]. The appearance of the mesoscale pressure gradient force (PGF) that drives the SBS may seem relatively simple to explain, but *Tijm and van Delden* [1999] carefully examined three different variations found in the literature, and concluded that all three are physically inconsistent.

The first is the "upward" theory [*Tijm and van Delden*, 1999], wherein a seaward flow (sometimes called return flow) develops aloft first, due to the vertical expansion of the warmer air over land. Landward flow near Earth's surface then develops in response to the seaward flow aloft. The second is called the "sideways" theory [*Simpson*, 1994], wherein the low-level onshore flow develops first, in response to the horizontal expansion of the warmer air over land. Seaward (return) flow aloft then develops in response to the low-level onshore flow. The third is called the "mixed" theory [*Godske et al.*, 1957], in which the warmer air over land expands both vertically and horizontally, causing the simultaneous development of the surface sea breeze and the return current aloft [*Tijm and van Delden*, 1999].

All three versions, in spite of some evidence in the synoptic surface observations to support them, neglect the process of hydrostatic adjustment. This occurs in the developing SBS, and is

accompanied by the creation of sound (compression) waves, which are generated over land when the air expands due to diabatic heating, and then propagate at 300 ms^{-1} in all directions [*Tijm and van Delden, 1999*]. Utilizing a non-hydrostatic computer model, *Tijm and van Delden* [1999] concluded that sound waves play a critical role in establishing the mesoscale pressure gradient. *Walsh* [1974] concluded earlier that simulations of the sea-breeze circulations using non-hydrostatic models differ very little from those produced by hydrostatic models, but the *Tijm and van Delden* [1999] results indicate that the small difference between the two model schemes is important, because the hydrostatic models do not incorporate sound waves, and therefore do not include the correct mechanism for establishing the mesoscale pressure gradient.

Within a few minutes, sound waves traveling upward induce an increase in pressure through the entire atmosphere above the heated land surface. Waves propagating horizontally induce pressure falls over land and surface pressure increases over the sea. The resulting horizontal pressure gradient initiates the landward movement of the marine airmass associated with the SBS. The surface pressure decrease over land is first seen at the coast, but locations more than 1000 kilometers inland experience a decline in pressure within an hour. These results are supported by a careful

analysis of the synoptic surface record in Europe, and represent a more physically consistent version of the mixed theory [Tijm and van Delden, 1999].

Sea-breeze circulation (SBC) and the Bjerknes circulation theorem. Mathematical models, when used in conjunction with field observations, are a powerful means for exploring physical mechanisms. The Bjerknes circulation theorem is a relatively simple model that begins with the presence of a cross-shore mesoscale PGF, and reproduces the SBC from an initially stationary atmosphere. Circulation is a scalar quantity that represents a macroscopic measure of rotation over a finite area of fluid in two dimensions [Holton, 1992]. Mathematically, circulation about a closed contour in a fluid is defined as the line integral about the contour of the component of the velocity vector that is locally tangent to the contour [Holton, 1992]. The Bjerknes circulation theorem is given by:

$$\frac{D_a C_a}{Dt} = - f \frac{dP}{\rho} \quad (2.1)$$

where D_a/Dt indicates the material derivative in the fixed reference frame, C_a is circulation, P is pressure [Pa], and ρ is density [kg m^{-3}].

The application of the circulation theorem to the SBC begins with (2.1), and substitutes $\rho = P/RT$ (from the Ideal Gas Law), where T is temperature [K], and R is the gas constant for dry air ($287 \text{ J kg}^{-1} \text{ K}^{-1}$). By integrating around the closed path beginning on the land surface (Figure 2.2; lower left), and using the fact that the line integral about a closed loop of a perfect differential is zero, one obtains:

$$\frac{DC_a}{Dt} = R \ln \left(\frac{P_0}{P_1} \right) (\bar{T}_2 - \bar{T}_1) \quad (2.2)$$

where \bar{T} indicates the average temperature through the vertical column [*Holton, 1992*].

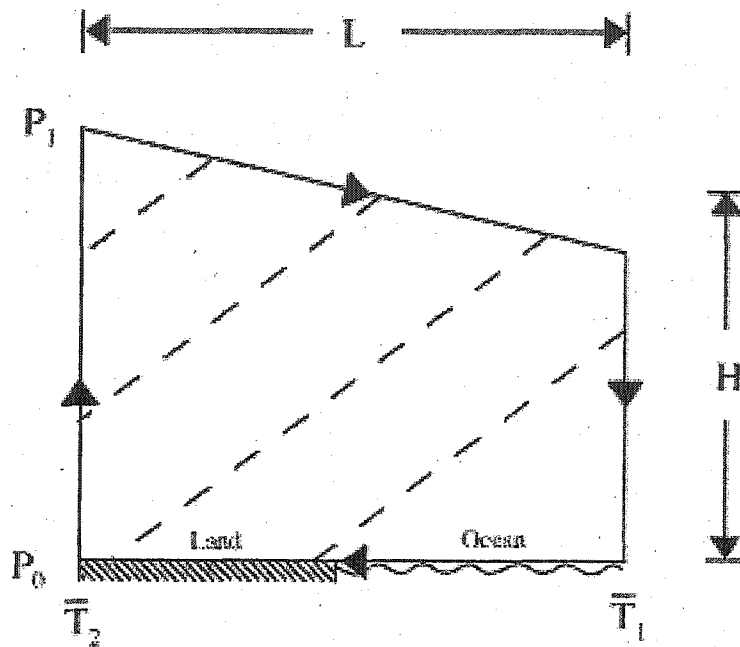


Figure 2.2: Sea breeze and the Bjerknes circulation theorem. Land is on the left, ocean is on the right. The integration path for (2.1) is indicated by arrows along the perimeter. \bar{T} indicates the average temperature through the vertical columns over the land or ocean surfaces. Broken diagonal lines are isopycnals, with denser air at lower right. p_0 and p_1 are the pressure on the surface and at the top of the circulation cell, respectively. [After Holton, 1992.]

To extract the mean wind speed (\bar{U}) associated with the SBS, one uses:

$$\bar{U} = \frac{C_a}{2(H + L)} \quad (2.3)$$

where H is the height of the circulation, and L is its cross-shore length (Figure 2.2). Combining (2.2) and (2.3) yields:

$$\frac{D\bar{U}}{Dt} = \frac{R \ln \left(\frac{p_0}{p_1} \right) (\bar{T}_2 - \bar{T}_1)}{2 (H + L)} \quad (2.4)$$

which is an expression for the mean acceleration of the wind over time, as a result of the SBC. Realistic values for the RHS of (2.4) are:

$$p_0 = 1000 \text{ hPa}$$

$$p_1 = 900 \text{ hPa}$$

$$(\bar{T}_2 - \bar{T}_1) = 10 \text{ K}$$

$$L = 20 \text{ kilometers}$$

$$H = 1 \text{ kilometer}$$

which yields an acceleration of $7.2 \times 10^{-3} \text{ ms}^{-2}$. Beginning at rest, after one hour the mean wind speed around the perimeter is 25.9 ms^{-1} , or about 50 knots [Holton, 1992].

Wind speeds actually produced by the SBS are generally much lower than those suggested by the circulation theorem. *Simpson*

[1994] suggested that surface wind speeds of 6 or 7 ms⁻¹ can reasonably be expected. Other authors [e.g. *Masselink and Pattiaratchi*, 1998] have suggested that speeds as high as 10 ms⁻¹ are common. The main reason for this overestimate is that in the initial formulation, the Bjerknes circulation theorem assumes friction (in its various forms) is too small to be of importance. Another weakness of this application, perhaps just as important, is that it ignores the along-shore dimension.

More complete models, and topography. The following factors affecting the SBS should be included in a complete physical model [*Simpson*, 1994]:

- Diurnal variation of the ground temperature.
- Diffusion of heat.
- Static stability.
- Coriolis force(s).
- Diffusion of momentum.
- Topography.
- Prevailing wind.

The first two are essential for the sea breeze to occur, and the third is a factor in its inland movement [*Simpson*, 1994]. The Coriolis force, while unimportant for the first six hours, is responsible for producing the horizontal rotation of the SBS over time, and thus limits the extent of its inland penetration [*Pearce*, 1955; *Neumann*, 1977; *Anthes*, 1978; *Simpson*, 1996]. Momentum diffusion is important for producing the observed near-surface wind profile, is the most important brake on the developing circulation, and prevents the SBS from producing the very high wind speeds predicted by the Bjerknes circulation theorem [*Anthes*, 1978; *Simpson*, 1994]. SBS response to prevailing (synoptic-scale) wind is discussed below.

Topography -- including the size and shape of the landmass, and the details of the coastline -- is another important factor in the SBS. Many early models investigating SBS behavior assumed straight coastlines and flat topography [e.g. *Estoque*, 1962], but included terms corresponding to the other six items on the list. More recent authors discuss the behavior of the SBS in more realistic physical settings. Most of their conclusions are necessarily specific to the geographical region examined, although some important general conclusions are obtained.

Seaward facing slopes. If a hill is located just inland of a flat coastal plain, with its slope facing the sea, the influence of the hill on the SBS is determined by the hill's surface temperature cycle. When the temperature of the slope varies with the same diurnal period as that of the coastal plain, the SBS is amplified and occurs earlier than it would if the hill were not present. If the slope acts as a barrier only (i.e., is enshrouded in fog or clouds), the SBS is confined to the coastal plain. *Asai and Mitsumoto* [1978] originally described this effect with a computer model, and *Banta et al.* [1993] observed it on the west coast of the United States using a pulsed doppler lidar.

Bays. When a bay is located on an otherwise straight, east-west coastline with the ocean to the south, the bay causes the sea breeze to bow landward relative to the straight sections of coastline on either side. Within the convergence zone between the sea breeze and the seaward synoptic-scale flow, there are regions of enhanced upward and downward vertical motion related to the position of the bay, but distributed asymmetrically. In the Northern Hemisphere, enhanced convergence and vertical motion occur to the west of the bay, where the pressure gradient force (PGF) and Coriolis force act in opposition to each other, and weakened

convergence and vertical motion occur on the east side of the bay, where the two forces act in the same direction [McPherson, 1970].

Narrow landmasses. When two sea-breeze systems form on opposite sides of a narrow landmass, the interactions that result when they converge at the center of the landmass are partially determined by the width of the landmass [Xian and Pielke, 1991]. The thermal forcing over a narrow peninsula or island (width less than 100 km) is insufficient for developing a deep, well-organized mesoscale circulation, and both sea-breeze systems are weak. For landmasses with widths between 100 and 150 km, the thermal forcing is strong enough to develop deep systems, and the landmass is still narrow enough so that the two opposite systems converge at the center and produce a region of deep convection. Landmasses more than 150 km across are too wide for the two opposing systems to reach each other before sunset, and the associated convergence region in the center of the landmass is weakened [Xian and Pielke, 1991]. When the two opposing sea-breeze systems reach each other during the evening hours (when the ambient atmosphere is stable), undular bores may result [Clarke, 1984].

Complex terrain. Complex terrain, with or without non-zero synoptic-scale flow, may produce several separate sea-breeze systems along different portions of the coastline. The appearance of these independent systems may not be simultaneous, and they may not ultimately reach the same intensities. Inland topographic features channel the low-level flow, creating areas of enhanced convergence and upward vertical motion. Upward vertical motion is also enhanced where different sea-breeze systems converge at points inland [*Melas et al.*, 1998; *Melas et al.*, 2000].

Temperature characteristics of land and sea surfaces.

Stronger SBS-associated wind speeds occur with stronger cross-shore temperature gradients. *Schumann et al.* [1991] noted this effect in the sea breeze of Alcoa Bay, South Africa, where the strongest sea breeze occurs in areas with nearby dune fields. During the daytime, the sand dunes create a region of superheated air immediately overhead, setting up a very strong land-sea temperature difference. Coastal upwelling, which brings colder water to the surface, also enhances the cross-shore temperature gradient. On the east coast of a continent in the northern hemisphere, upwelling (driven by Ekman pumping) occurs when there is an along-shore wind component, with low pressure to the

west and high pressure to the east [Apel, 1987]. *Franchito et al.* [1998] observed that the SBS of coastal Brazil is stronger during periods of upwelling, and weaker when there is no upwelling.

Structure.

The SBS consists of phenomena occurring on several spatial scales (Figure 2.1). A summary of these includes the initiating sound waves discussed by *Tijm and van Delden* [1999], the sea-breeze forerunner and similar pre-frontal waves [*Geisler and Bretherton*, 1969; *Sha et al.*, 1993], the closed cell of circulation predicted by the Bjerknes circulation theorem [*Holton*, 1992], the sea-breeze gravity current and all of its associated phenomena [e.g., *Simpson*, 1997], the sea-breeze front and all of its associated phenomena [e.g. *Kraus et al.*, 1990; *Kraus*, 1992; *Reible et al.*, 1993], and smaller-scale phenomena -- such as a Convective Internal Boundary Layer (CIBL) -- within the landward-moving marine airmass [*Hsu*, 1988; *Zhong and Takle*, 1992; *Rao and Fuelberg*, 2000]. One must also include interactions between all of these phenomena, and with phenomena originating from other processes in both the atmosphere and ocean [e.g. *Brümmer et al.*, 1995; *Gibbs*, 2000].

Prefrontal phenomena. In addition to the sound waves that initiate the cross-shore mesoscale PGF, another type of transitory wave precedes the arrival of the sea-breeze front on land. The sea-breeze forerunner is actually a cluster of waves that is initiated when the cross-shore thermal contrast appears above the land-sea interface. The waves with the largest amplitude arrive at points inland first, moving at speeds much faster than the sea-breeze front. Over time, progressively smaller-scale waves arrive inland. Observers on Earth's surface will experience a wind from the direction of the sea consisting of local (continental) air, before the arrival of the sea-breeze front. The model results from *Geisler and Bretherton* [1969] indicate that, with reasonable values of internal (eddy) viscosity and surface friction, the forerunner reaches as far inland as 60 kilometers.

Another type of prefrontal wave may occur in the late evening, when the sea-breeze front interacts with an inland nocturnal stable layer. These waves consist of small overturning cells with a characteristic wavelength of approximately 10 kilometers, propagate inland at approximately 3.5 ms^{-1} , and rapidly dissipate in the ambient flow field [*Sha et al.*, 1993].

SBC response to the synoptic-scale wind. The SBC begins when a landward component is added to the net low-level wind vector in response to the mesoscale thermal PGF, resulting in a divergence in the cross-shore wind component over the sea. The shore-parallel zone in which the new wind component is added grows horizontally in the cross-shore direction, expanding more rapidly seaward than landward [*Finkele et al.*, 1995]. A shallow layer of marine air begins flowing toward the land, converging with continental air and creating a region of upward vertical air currents (Figure 2.1).

A seaward return flow usually develops aloft, above the upper boundary of the marine air, creating a shear zone where the flow changes directions from landward to seaward [*Finkele et al.*, 1995; *Camberlin and Planchon*, 1997; *Tijm et al.*, 1999; *Oliphant et al.*, 2001]. This return flow is required if the SBC is to be considered closed, i.e., mass conservative. Several authors, however, report either the complete absence of this return flow, or its insufficiency at counter-balancing the low-level onshore flow, implying that the SBC may not be a closed system under some circumstances [*Estoque*, 1962; *Intrieri et al.*, 1990; *Banta et al.*, 1993]. The upper limit of the circulation varies from a few hundred meters to one or two kilometers, depending on synoptic conditions [*Frizzola and Fisher*, 1963; *Barbato*, 1975; *Intrieri et al.*, 1990; *Xian and Pielke*, 1991].

On the other hand, *Tijm et al.* [1999] found that the seaward return flow may over-compensate for the low-level landward flow by as much as 30 percent (with respect to mass), creating a landward "return-return" flow above about four kilometers. Weak sinking currents have been observed in situ and in model results over a broad area several tens of kilometers offshore, supporting a closed SBC with at least partial mass conservation [*Estoque*, 1962; *Neumann and Mahrer*, 1971; *Elliott and O'Brien*, 1977; *Asimakopoulos et al.*, 1999; *Chiba et al.*, 1999].

The prevailing wind (PW) plays a large role in determining the shape and shore-relative location of the SBC. The PW is important in determining whether or not a sea breeze will be detectable on land (a very strong offshore PW will prevent the SBC from reaching the coast), as well as exerting an influence on its behavior [e.g. *Finkele et al.*, 1995]. *Mizuma's* [1995, 1998] observational studies of SBC behavior on the coast of Japan include descriptions of several manually-identified sea-breeze modes, which are dependent on the shape of the local coastline and the direction and strength of the PW. Several other studies have examined SBC response to the PW both generically and along specific coastlines [e.g. *Fisher*, 1960; *Estoque*, 1962; *Pearson et al.*, 1983; *McKendry and Roulet*, 1994; *Planchon and Cautenet*, 1997; *Melas et al.*, 1998; *Asimakopoulos et*

al., 1999; Clappier et al., 2000; Melas et al., 2000; Laird and Kristovich, 2001; Oliphant et al., 2001; Lericos et al., 2002].

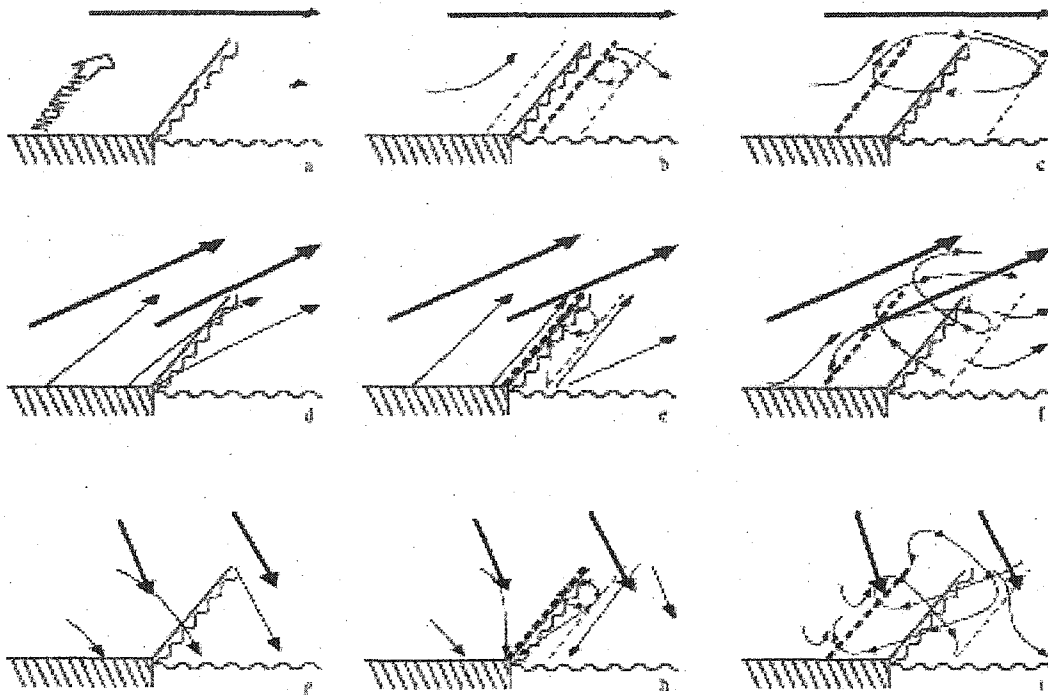


Figure 2.3: Development of pure, corkscrew, and backdoor sea breezes. Land is on the left; ocean is on the right. North is into the page. Heavy red arrows indicate wind at the top of the planetary boundary layer. Narrow red arrows indicate near-surface wind not related to SBC. Blue arrows indicated SBC-related near-surface wind. Heavy broken blue line indicates inland limit of SBC; thin broken blue line indicates seaward extent. Panels a, b, and c illustrate development of pure sea breeze. Broken red line indicates inland extend of calm region that extends offshore to the first broken blue line. Panels d, e, and f illustrate development of corkscrew sea breeze. Panels g, h, and i illustrate development of backdoor sea breeze. [After Adams, 1997.]

Generic categories of sea-breeze circulation. The SBC falls into four PW-dependent categories: *Pure, corkscrew, backdoor,* and *synoptic* [Adams, 1997]. The fourth stretches the definition of

the sea breeze from a locally-driven circulation to any wind blowing from sea to land, and therefore, this category will not be addressed here. The remaining three are described below in the context of the east coast of a Northern Hemisphere continent.

A pure sea breeze [Adams, 1997] occurs under light PW conditions, when the existing geostrophic forcing points seaward at a right angle to the coastline, and closely matches the general description given above (Figure 2.3; a, b, and c). This type of sea breeze is preceded by calm conditions, when the synoptic-scale pressure gradient force (PGF) is briefly in equilibrium with the locally-created thermal PGF. Ohashi and Kida [2002] noted its presence in Japan, ahead of an advancing sea breeze gravity current (SBG) and below 800 m AGL. Chiba *et al.* [1999], using an instrumented helicopter, observed that the calm region extends to about 10 kilometers offshore. The SBC expands throughout the day, with the landward extreme reaching as far inland as about 130 kilometers [Adams, 1997].

The corkscrew sea breeze [Adams, 1997] occurs when the PW has both along-shore and cross-shore components (Figure 2.3; d, e, and f). The along-shore component is *northward* on the east coast of the hypothetical Northern Hemisphere landmass. According to Buys Ballot's Law, a northward wind component implies lower

pressure over land and higher pressure over water [Lutgens and Tarbuck, 2001]. When differences in the coefficient of surface friction are taken into account, a northward wind component and lower pressure over land imply an area of low-level divergence near the coast. Air from aloft sinks into the divergence zone and assists with the initiation of the sea breeze. Since the thermal PGF and the synoptic-scale PGF are not entirely oriented along the same dimension, the former does not have to overcome the full magnitude of the latter, and therefore, there is no calm period prior to the onset of the sea breeze. This also implies that a corkscrew sea breeze can reach the coast with a weaker thermal PGF, relative to a pure sea breeze. The arrival of the corkscrew sea breeze is marked by a gradual backing (rotation in the counter-clockwise direction) of the wind from southwest to southeast. Like the pure sea breeze, the corkscrew sea breeze circulates in a vertical cell, but the along-shore component of the synoptic wind causes the circulation to take on a helical shape rather than a simple loop [Adams, 1997].

The backdoor sea breeze [Adams, 1997] also occurs when the PW has along-shore and cross-shore components (Figure 2.3; g, h, and i). In this case, the along-shore component is *southward* on the east coast of the hypothetical Northern Hemisphere landmass. Buys

Ballou's law implies that lower pressure is over the ocean, and higher pressure is over the land [Lutgens and Tarbuck, 2001]. This, combined with the cross-shore variation in the coefficient of surface friction, results in an area of low-level convergence near the coast. This surface convergence prevents air from sinking from aloft, and inhibits the sea breeze's progress toward land. This also implies that a backdoor sea breeze can only reach the coast with a stronger thermal PGF, relative to a pure or corkscrew sea breeze. As with the corkscrew sea breeze, arrival of a backdoor sea breeze is marked by a gradual shift in wind direction from northwest to northeast. In this case, the wind veers (rotates in a clockwise direction) rather than backs. The backdoor sea breeze also rotates helically rather than in a simple loop, although in this case, the along-shore geostrophic wind component causes the helix to spiral southward rather than northward. The other important differences between the corkscrew and backdoor sea breezes are that the latter is much weaker, arrives on land later in the day, and may manifest in pulses rather than strong, steady flow [Adams, 1997].

Examples of sea-breeze circulation. A series of case studies carried out on the coast of New England provide real-world comparisons to the idealized sea-breeze scenarios described above.

The study area shown in Figure 2.4 is nearly ideal for comparison to the hypothetical sea breezes shown in Figure 2.3, because the central 90 percent of the coastline is reasonably straight, and can be approximated by a straight line rotated 30 degrees clockwise from true north. These sea breeze events were observed during the New England Air Quality Study (NEAQS), 2002 summer campaign, which involved researchers from the U.S. National Oceanic and Atmospheric Administration (NOAA), the University of New Hampshire (UNH), and others [AIRMAP, 2001]. For NEAQS, researchers at UNH's Climate Change Research Center created a mesoscale surface weather network by adding a series of small, automated stations to NOAA's existing network surface stations (Figure 2.4). The enhanced network of stations permits the resolution of meteorological features as small 10 kilometers across, particularly over land. Hourly reports from the combined network were interpolated onto a rectangular grid using standard techniques [Barnes, 1964], and the regrided data were examined for patterns of wind flow near Earth's surface.

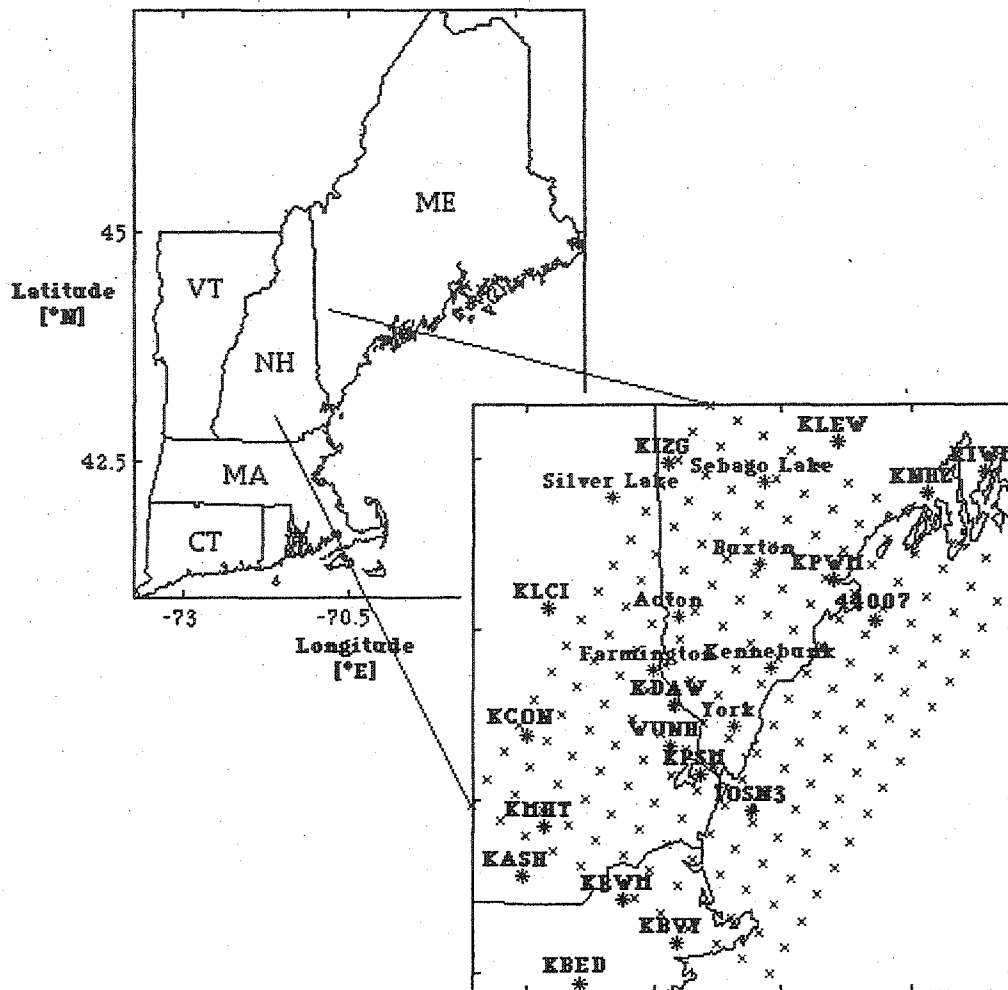


Figure 2.4: New England Air Quality Study, 2002, sea breeze study area. The sea breeze was closely studied along the relatively straight section of coastline from Lawrence, Massachusetts (KLWM) through north of Portland, Maine (KPWM; see inset, lower right). Standard NOAA surface weather observing sites are labeled in black lettering with their International Civil Aviation Organization Identifiers. Stations added by UNH to improve the spatial resolution are shown in red. Data from all stations were combined and interpolated onto the 10-km rectangular grid shown in blue.

The 3 August 2002 event (Figure 2.5) most closely resembled the pure sea breeze. A high pressure center was approaching southern New England from the west, setting up a shore-perpendicular ambient flow. At 1200 (UTC; subtract 4 hours to convert to LDT), the flow throughout most of the study area was northwesterly (Figure 2.5a). At 1600, a region of light winds, cyclonic rotation, and low-level convergence developed in the southern half, approximately 10 kilometers offshore (Figure 2.5b). By 1900, there was a well-developed sea breeze with a clearly-defined inland convergence zone in the southern half, and wind flow crossing the coast at a right angle (Figure 2.5c). The sea breeze was beginning to develop in the north as well. By 2300, the wind direction within the SBC veered to a more southerly direction, causing the system to take on characteristics of the corkscrew sea breeze (Figure 2.5d). At latitudes where Coriolis is important, the sea breeze evolves to take on corkscrew characteristics under the influence of rotational forces.

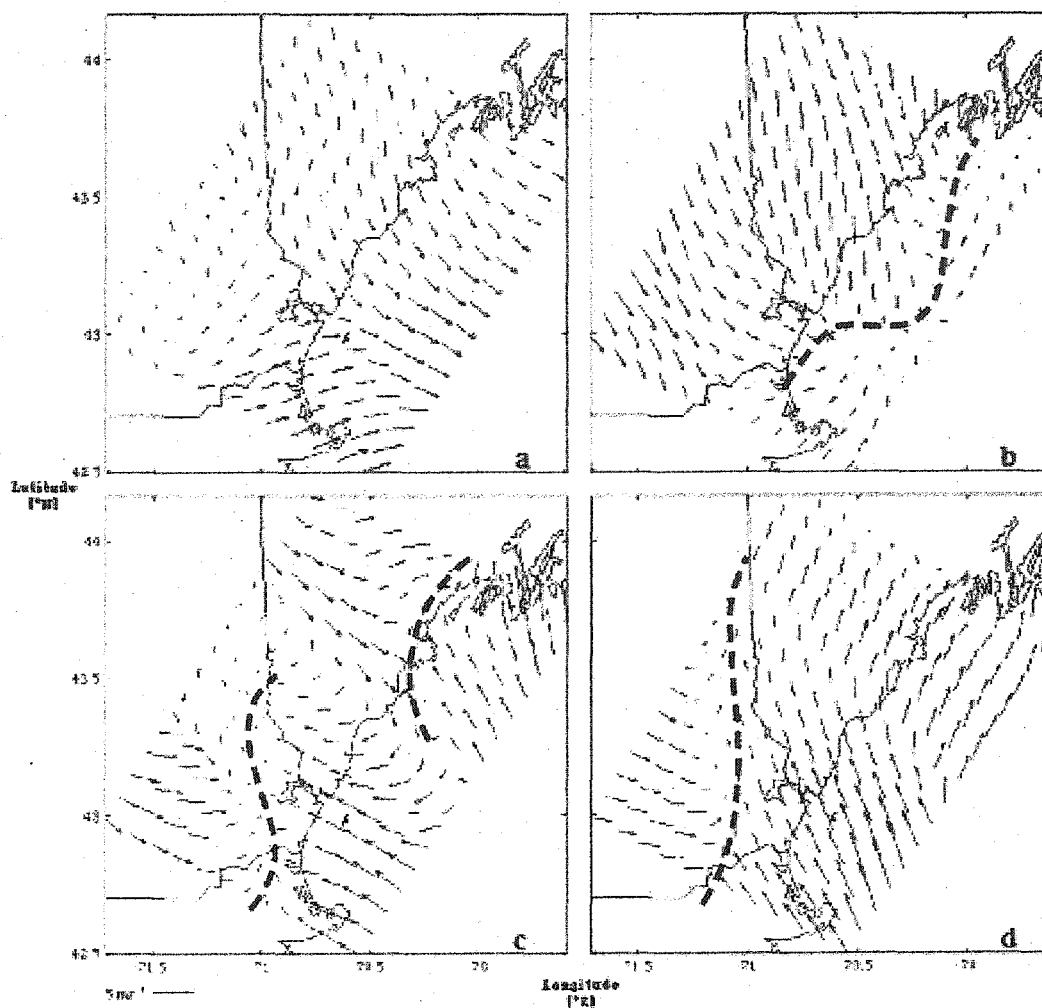


Figure 2.5: Pure sea breeze event, 3 August 2002. a) 1200 UTC (0800 LDT). b) 1600 UTC. c) 1900 UTC. d) 2300 UTC.

The 21 July 2002 event (Figure 2.6) most closely resembled the corkscrew sea breeze from its inception. A cold front was approaching New England from the west, and a high was to the south, setting up shore-parallel, southwesterly flow. At 1300 UTC, the wind throughout the study area was southwesterly and shore-

parallel (Figure 2.6a). By 1400, the wind in the offshore area backed from southwest to southeast, developing a noticeable shoreward component, and creating a pronounced convergence zone at the coast (Figure 2.6b). The SBC reached its peak at 2100, when the leading edge of the SBC extended inland nearly 65 kilometers (Figure 2.6c), and thereafter began to diminish. By 0300 on 22 July, veering wiped out the convergence zone, and the SBC was no longer readily identifiable (Figure 2.6d).

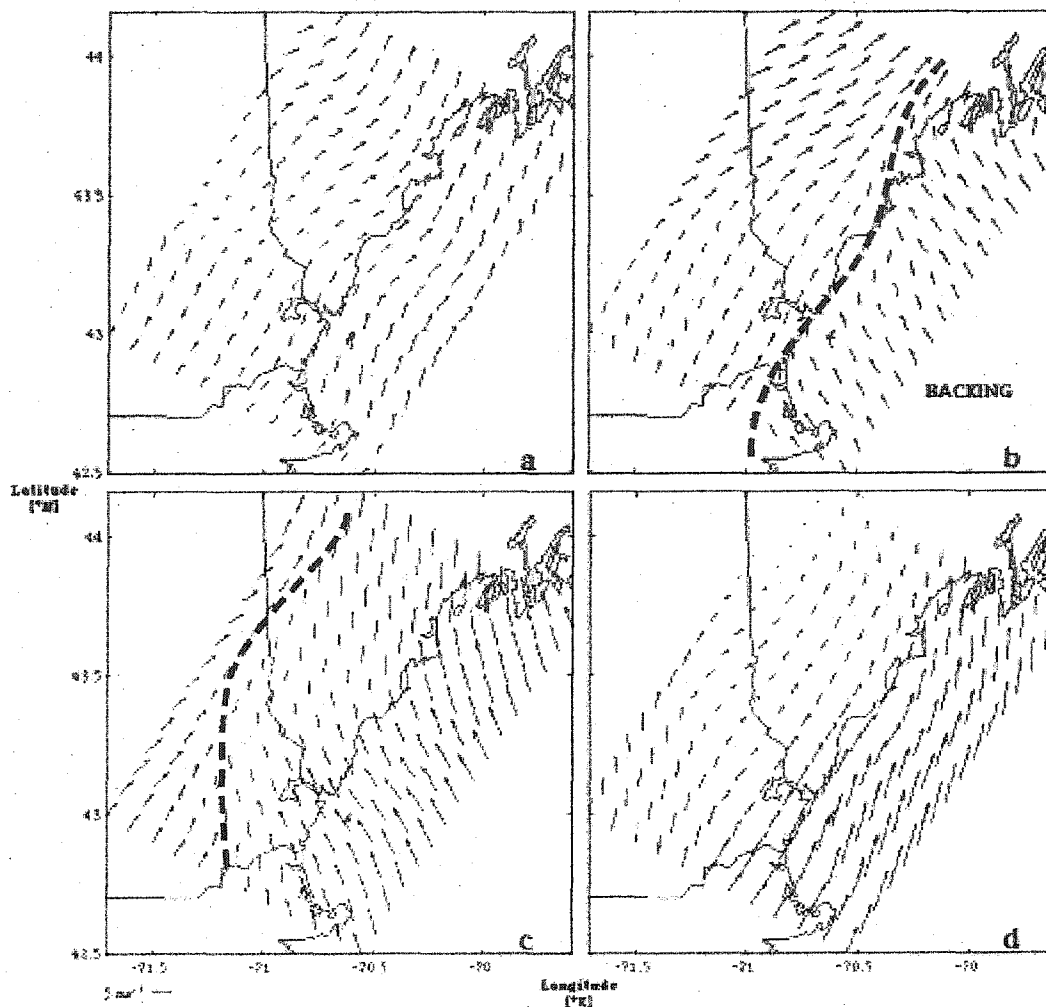


Figure 2.6: Corkscrew sea breeze event, 21 July 2002. a) 1300 UTC (0900 LDT). b) 1400 UTC. c) 2100 UTC. d) 0300 UTC on 22 July.

The 24 July 2002 event (Figure 2.7) most closely resembled the back door sea breeze described in the previous section. A high pressure center was approaching northern New England from the west, setting up shore-parallel, northeasterly flow. At 1200 UTC, the

wind throughout most of the study area was northeasterly and shore-parallel (Figure 2.7a). By 1500, veering added a shoreward component throughout the southern half, therefore there was no well-defined line of convergence between the ambient flow over the continent, and the flow within the developing SBC (Figure 2.7b). Continued veering rotated the wind from northeast to southeast by 2000, resulting in shore-perpendicular flow throughout the study area (Figure 2.7c). By 2300, the demise of the SBC was marked by the collapse of organized flow on the this scale (Figure 2.7d).

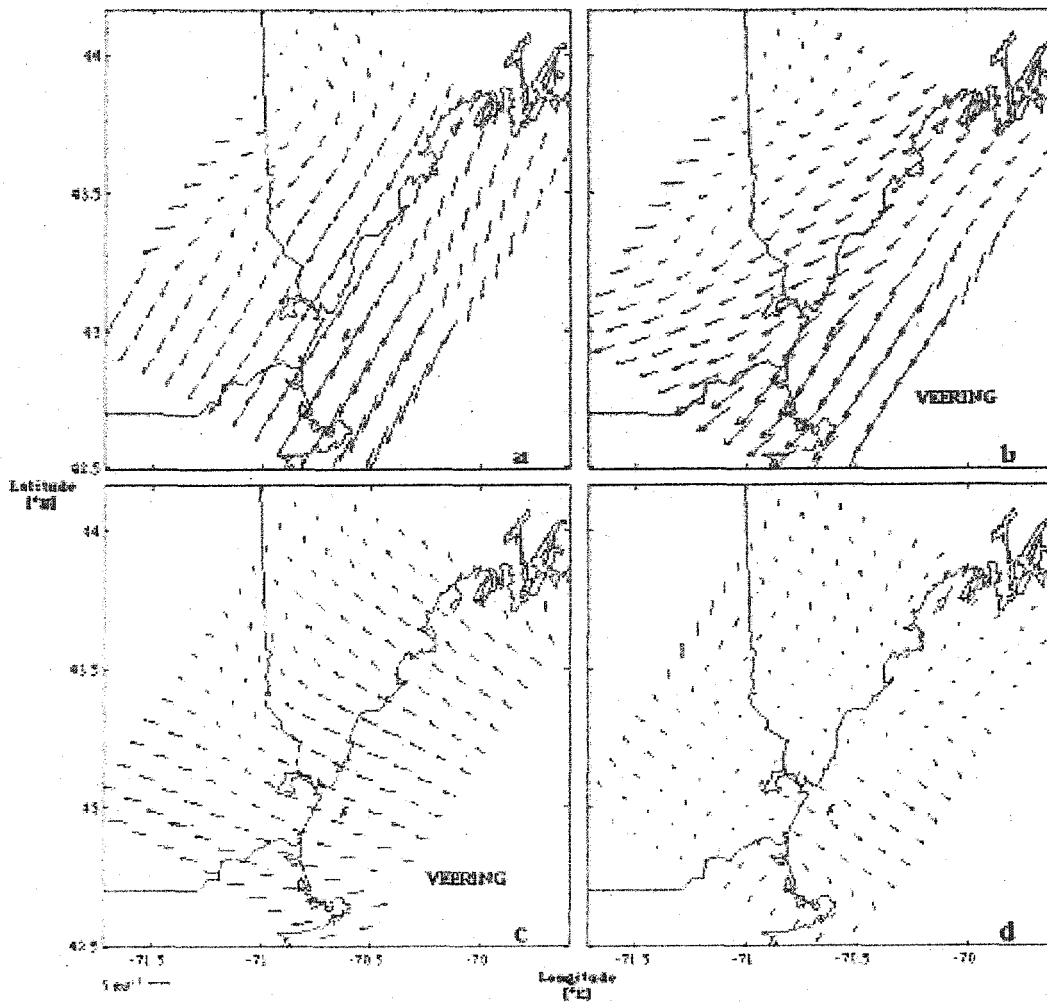


Figure 2.7: Backdoor sea breeze event, 24 July 2002. a) 1200 UTC (0800 LDT). b) 1500 UTC. c) 2000 UTC. d) 0000 UTC on 25 July.

These case studies indicate that the generic models introduced in the previous section are probably too simple for use other than in teaching basic concepts. In addition to along-shore variations, such as differing times of onset of the sea breeze, entire sea breeze events evolve in ways not predicted by the generic models. The

Coriolis force, which favors veering, is a dominant factor. In the 3 August (pure) sea breeze case, veering induced by the Coriolis force transformed the SBC from a pure into a corkscrew system. In the 21 July (corkscrew) case, backing occurred early in the life of the SBC, before Coriolis had time to become an important factor. (The Coriolis force requires several hours to become an important factor -- a fact that can be derived by scaling the equations of motion.) The corkscrew sea breeze was terminated when the Coriolis force wiped out the cross-shore wind component. In the 24 July (backdoor) case, veering (driven by thermodynamic differences between land and sea) initiated the sea breeze, but the Coriolis force prevented backing from destroying it. Instead, the wind direction became random at the end of the SBC's life, driven by smaller-scale, local forces. The Coriolis force's influence on the SBS is discussed in greater detail below.

Sea-breeze gravity current (SBG) and Kelvin-Helmholtz Billows.

The low-level landward flow of marine air is one example of a large class of phenomena called gravity- or density currents. Gravity currents are primarily horizontal flows in fluids that can be generated by a density difference of only a few percent. Other

examples of gravity currents are thunderstorm outflows, turbidity currents, avalanches, and pyroclastic flows [*Simpson, 1997*].

The microscale (< 2 km) horizontal thermal contrast across the boundary between marine and continental airmasses can be very sharp, and the boundary often takes on a frontal nature similar to a synoptic-scale cold front [*Chiba, 1993; Finkele et al., 1995; Simpson, 1997*]. The leading edge of the marine airmass develops a raised head, due to the updraft created by low-level convergence between the marine and continental airmasses [*Finkele et al., 1995*]. The height of the sea-breeze head (SBH) is approximately twice that of the feeder flow originating offshore [*Simpson et al., 1977*], but a headwind (the ambient offshore flow) flattens the SBH [e.g. *Frizzola and Fisher, 1963*]. The depth of the onshore flow behind the front ranges between about 300 and 2500 meters [e.g. *Barbato, 1975*]. *Simpson* [1969] noted that its average depth in Great Britain was about 700 meters.

The speed with which a density current advances into the ambient fluid has been studied extensively in the laboratory and the field [e.g. *Kuelegan, 1957; Simpson, 1969; Physick, 1980; Chiba, 1993*]. *Kuelegan's* [1957] interest was the flow of salt water through locks and into fresh water channels, for which he established the relationship:

$$|U| = k \sqrt{\frac{\Delta\rho}{\rho} g d} \quad (2.5)$$

where $|U|$ is the speed at which the denser fluid front advances into the less-dense fluid [ms^{-1}], k is a constant (taken as 0.78), ρ is the density of the denser fluid [kg m^{-3}], $\Delta\rho$ is the density difference between the two fluids [kg m^{-3}], g is the gravitational acceleration (9.81 m s^{-2}), and d is the height of the SBH [meters].

Simpson [1969] adapted (2.5) to describe the rate at which the SBG propagates inland. To calculate the constant k , he replaced the height of the SBH (d) with its mean height \bar{d} , taken as 700 meters (from a climatology of 54 sea breezes recorded over a six-year period in Britain). He also replaced $\Delta\rho/\rho$ with $\Delta T/T$ [ΔT and T in Kelvin]. This work yielded a k -value of 0.62, which *Schoenberger* [1984] reported is equally effective when compared to radar observations of the propagation speed of a *land* breeze on the lower peninsula of Michigan.

Later, *Simpson and Britter* [1980] determined that the SBG's rate of inland progression is slowed by about 3/5's of the opposing component of the PW, or:

$$|U| = k\sqrt{\frac{\Delta T}{T} g d} - 0.59u_g \quad (2.6)$$

where u_g is the cross-shore geostrophic wind component [ms^{-1}] resulting from the synoptic-scale PGF.

A shear zone develops on the upper boundary of the marine airmass, between the low-level onshore flow and the seaward return flow aloft. Kelvin-Helmholtz Billows (KHBs) develop in the shear zone over land (and are further enhanced by thermodynamic instability induced by insolation during the middle part of the day), causing mixing between marine air and continental air, and creating a turbulent wake behind the SBH [Simpson, 1969; Atkins *et al.*, 1995; Chiba *et al.*, 1999]. The development of KHBs in late morning causes a friction-like force on the upper boundary of the airmass that slows the sea breeze's inland progression [e.g. Sha *et al.*, 1991]. KHBs appear as vortex rolls in regions of strong shear when the Richardson Number (Ri) -- the ratio of static stability to kinetic energy of shear -- is less than 0.25. This may be calculated by:

$$Ri = \frac{\frac{g}{\theta} \frac{\partial \theta}{\partial z}}{\left(\frac{\partial u}{\partial z}\right)^2} \quad (2.7)$$

where g is the gravitational acceleration (9.81 ms^{-2}), θ is the potential temperature [K], u is the horizontal flow component [ms^{-1}], and z is the vertical dimension [m]. It can be seen from (2.7) that regions where the vertical temperature gradient vanishes, such as in a well-mixed layer resulting from convective overturning, are prone to the development of KHBs. *Simpson and Britter* [1980] suggested that the KHBs along the upper boundary of the sea-breeze marine layer may be 500 to 1000 meters in length. *Nielsen* [1992], using aircraft, observed KHBs with wavelengths between 1000 and 2000 meters on the upper boundary of a New England coastal front, a mesoscale phenomenon that closely resembles a sea breeze.

Simpson [1994, 1997] conducted experiments that documented the three-dimensional structure of gravity currents, using laboratory tanks and two bodies of water of slightly different densities. His work reproduced several aspects of the SBG, including the SBH, front, and KHBs. Field studies have confirmed that analogs of the Simpson's laboratory gravity-current features

(Figure 2.8) are also present in the SBG [e.g. *Craig et al.*, 1945; *Chiba et al.*, 1999; *Wood et al.*, 1999].

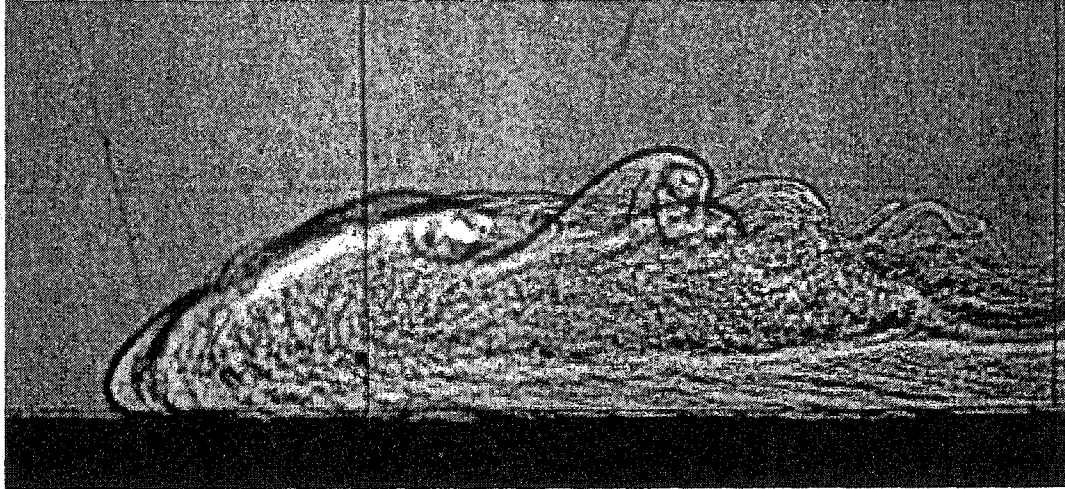


Figure 2.8: Simpson's [1997] shadowgraph of a laboratory gravity current. Pure water is on the left, and slightly salty (denser) water enters from the right. Visible in the photograph are the current's nose (slightly elevated leading edge), raised head, and trailing Kelvin-Helmholtz Billows (as described in text).

Sea-breeze front (SBF). The leading edge of the SBG is often associated with a strong cross-shore temperature contrast, and it can take on characteristics similar to those of a synoptic-scale cold front. As a front, the SBF is subject to frontogenesis and frontolysis, bifurcation (separation of the regions of maximum temperature gradient and maximum low-level convergence), variations in intensity (in terms of cross-shore width and the magnitude of the

various gradients involved), and variations in slope. Strong vertical velocities and the SBH are associated with the SBF (Figure 2.9). The region of the SBG behind the SBF and beneath the SBH can sometimes separate from the feeder flow and propagate inland as a cutoff vortex or undular bore. Sea-breeze fronts vary in intensity in the along-shore direction, even along nearly homogeneous coasts.

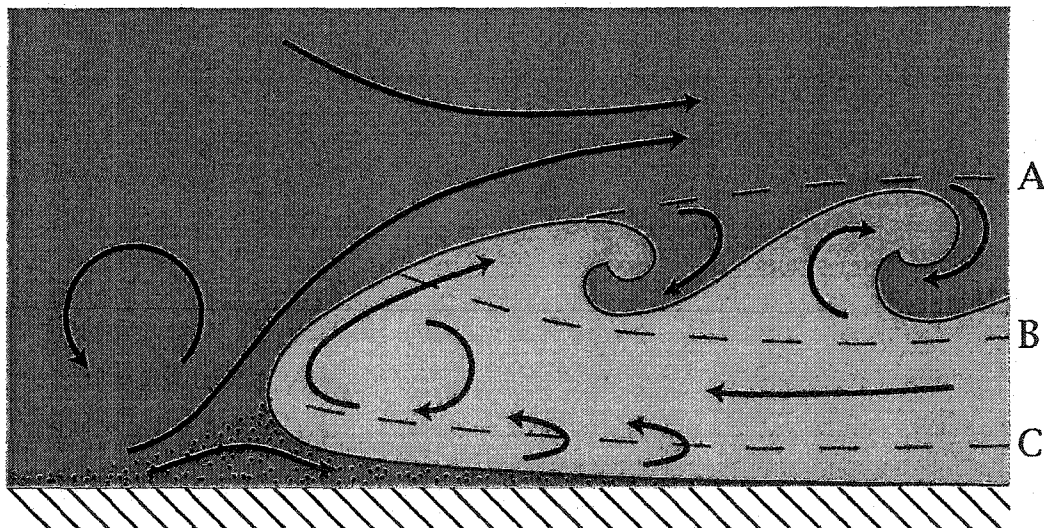


Figure 2.9: Simplified two-dimensional flow associated with a gravity current in presence of surface friction. Ambient fluid (red) is on the left and above. Denser fluid (blue) is invading from the right. Black arrows indicate direction of fluid flow. Mixing between the two fluids occurs both beneath the "nose" of the denser fluid (stippled; below line C) and in turbulent wake region behind the head of the gravity current (between lines A and B). [After Simpson, 1997, and Sha et al., 1993]

Frontogenesis function. Sea-breeze frontogenesis (the formation or intensification of the sea-breeze front) can be defined

as an increase in the magnitude of the cross-shore potential temperature gradient. A secondary set of processes involves the cross-shore water vapor gradient [e.g. *Kraus et al.*, 1990]. A kinematic function describing the processes (not including the release of latent heat) that contribute to the thermal frontogenesis can be derived by beginning with the 3-D diffusion relation:

$$\frac{\partial Q}{\partial t} + u \frac{\partial Q}{\partial x} + v \frac{\partial Q}{\partial y} + w \frac{\partial Q}{\partial z} = K_x \frac{\partial^2 Q}{\partial x^2} + K_y \frac{\partial^2 Q}{\partial y^2} + K_z \frac{\partial^2 Q}{\partial z^2} \quad (2.8)$$

where Q is the heat content (energy) per unit volume [J m^{-3}], the first term on the left-hand side (LHS) is the time-dependent (Eulerian) term, and the remaining three on the LHS describe the horizontal and vertical advection of heat via wind components u , v , and w [m s^{-1}]. The three terms on the right-hand side (RHS) describe the turbulent diffusion of heat in three dimensions, with coefficients K_x , K_y , and K_z [$\text{m}^2 \text{s}^{-1}$] [*Anderson et al.*, 1984]. All seven terms have overall units of power per unit volume [W m^{-3}].

By assuming:

- A north-south coastline with ocean on the right,
- A weak north-south temperature gradient,
- A wind primarily from the west ($v \sim 0$), and,
- $K_x \approx K_z$,

relation (2.8) can be rewritten as:

$$\frac{\partial Q}{\partial t} + u \frac{\partial Q}{\partial x} + w \frac{\partial Q}{\partial y} = K \left[\frac{\partial^2 Q}{\partial x^2} + \frac{\partial^2 Q}{\partial z^2} \right] \quad (2.9)$$

From here, one may follow a line of reasoning similar to that of *Miller* [1948], and derive a function describing sea-breeze frontogenesis. Since (2.9) describes heat, not heat gradient, the first logical step is to take the partial derivative in the cross-shore (x) direction. Assuming that K is approximately constant, and following the chain rule for derivatives, (2.9) becomes:

$$\frac{\partial Q_x}{\partial t} + \frac{\partial u}{\partial x} Q_x + u \frac{\partial Q_x}{\partial x} + \frac{\partial w}{\partial x} Q_z + w \frac{\partial Q_x}{\partial z} = K \nabla^2 Q_x \quad (2.10)$$

where ∇^2 is the second-order derivative in the x-z plane, and subscripts (e.g. Q_x) indicate the partial derivative of the function (Q) in the direction indicated (x,z).

By noting that the first, third, and fifth terms on the LHS of (2.10) constitute the material derivative of the quantity Q_x in the x-z plain, and moving the remaining LHS-terms to the RHS, the relation can be written as:

$$\frac{dQ_x}{dt} = - \frac{\partial u}{\partial x} Q_x - \frac{\partial w}{\partial x} Q_z + K \nabla^2 Q_x \quad (2.11)$$

Reible et al. [1993] began with (2.11) and then introduced scaling arguments to approximate the values of the terms on the RHS. *Kraus et al.* [1990] carried the argument further by using $Q_x = -c_p \rho_a \theta_x$ and $Q_z = -c_p \rho_a \theta_z$, where c_p is the coefficient of specific heat at constant pressure [$J \text{ kg}^{-1} \text{ K}^{-1}$], ρ_a is the density of air [kg m^{-3}], and θ_x and θ_z are the derivatives of the potential temperature field

[K m⁻¹] in the x- and z-directions [Halliday et al., 1993]. These substitutions and algebraic manipulation lead to:

$$\frac{d\theta_x}{dt} = - \frac{\partial u}{\partial x} \theta_x - \frac{\partial w}{\partial x} \theta_z + K \nabla^2 \theta_x \quad (2.12)$$

which is the kinematic frontogenesis function. Term 1 on the RHS describes cross-shore confluence (or deformation); term 2 describes rotation of vertical temperature gradients into the horizontal plane; and term 3 describes cross-shore variations in turbulent heat diffusion [Kraus et al., 1990].

With the ocean to the right (toward positive x-values), sea-breeze frontogenesis is indicated if the sum of the RHS is less than zero, and frontolysis (the destruction or weakening of the sea-breeze front) is indicated if the sum of the RHS is greater than zero. In the former case, the cross-shore potential temperature gradient is tending toward more negative values with time, and in the latter, it is tending toward more positive values with time.

There are two ways to improve this result. First, Neumann [1977] noted that within a few hours, even a system that begins with exclusively cross-shore flow will develop important flows and

gradients in the along-shore direction, due to the rotation of the SBS under Coriolis and other forces. An improved kinematic frontogenesis function will account for horizontal rotation. Second, the assumption that the coefficient of turbulent diffusion is the same in both the horizontal and vertical dimensions may not be correct [e.g. *Anderson et al.*, 1984]. An improved kinematic frontogenesis function will permit anisotropic coefficients. Both of these points indicate a need for a 3-D thermal frontogenesis function, even if the front initially forms parallel to the coastline.

If one begins with (2.8) and follows a derivation similar to that shown above, keeping all three spatial dimensions and allowing $K_H \neq K_V$ (horizontal and vertical coefficients, respectively), one arrives at the following:

$$\begin{aligned} \frac{d\theta_x}{dt} = & - \frac{\partial u}{\partial x} \theta_x - \frac{\partial v}{\partial x} \theta_y - \frac{\partial w}{\partial x} \theta_z \\ & + \frac{\partial}{\partial x} \left[K_H \frac{\partial^2 \theta}{\partial x^2} \right] + \frac{\partial}{\partial x} \left[K_H \frac{\partial^2 \theta}{\partial y^2} \right] + \frac{\partial}{\partial x} \left[K_V \frac{\partial^2 \theta}{\partial z^2} \right] \end{aligned} \quad (2.13)$$

which is similar to (2.12). In (2.13), the RHS terms correspond to:

- Term 1: Cross-shore confluence (or deformation; as in 2.12).

- Term 2: Rotation of along-shore temperature gradients into the cross-shore direction resulting from a cross-shore variation in the along-shore wind component. Along-shore gradients can result from rotation of the entire SBC, interactions between the advancing SBF and convective cells in the continental airmass, and the lobe and cleft structures observed on the front itself [*Neumann, 1977; Simpson, 1997; Stephan et al., 1999*].

- Term 3: Rotation of vertical temperature gradients into the horizontal plane (as in 2.12).

- Terms 4 and 5: Cross-shore variation in cross- and along-shore eddy-driven heat diffusion.

- Term 6: Cross-shore variation in eddy-driven diffusion of heat in the vertical dimension.

Kraus [1992], using data recorded by instrumented aircraft, computed the contribution to overall frontogenesis resulting from

terms 4, 5, and 6, and determined that their contributions are of the same order of importance as the convergence and shear terms, at least in very sharp fronts. These terms can be either frontolytic or frontogenetic.

Frontal bifurcation. The sea-breeze frontogenesis function (2.13) is a diagnostic tool, but there are a number of problems with attempting to use it for practical meteorology. Among them are the absence of a term for variations in along-shore gradients (which come into play in term 2), the absence of a term for shear due to along-shore variation in the cross-shore wind component (which will result in the rotation of horizontal temperature gradients), and the implicit assumption that the strongest temperature gradients and convergence zones associated with sea-breeze fronts occur in the same place. The latter assumption is often not correct.

More than one SBF may develop in a single SBS [e.g. Kraus *et al.*, 1990; Atkins *et al.*, 1995; Lapworth, 2000]. A field study of the SBF in eastern Florida, using Doppler radar stations and an instrumented aircraft, discerned a difference between the thermodynamic and kinematic fronts [Atkins *et al.*, 1995]. The thermodynamic front is the location within the planetary boundary

layer (PBL) where the mean thermodynamic properties of the air begin to differ from those of the ambient (continental) air, and it is created by interactions between the SBC and horizontal convective rolls (HCRs). The kinematic front is the location of maximum near-surface (100 meters AGL) wind convergence. In an ideal case, the two features are in the same place, and (2.13) diagnoses strong frontogenesis. In cases of onshore ambient flow, the thermodynamic front may be as much as 15 kilometers ahead of the kinematic front. The region between the two fronts (called the thermodynamic zone) is the analog of frontal transition zones in synoptic-scale cold fronts, and it is widest where the SBF has merged with HCRs [Atkins *et al.*, 1995].

Atkins et al. [1995] noted that only those cases with an offshore ambient wind exhibited the kinematic front. The lack of a clearly defined kinematic front may also be responsible for the apparent absence of a front in some of the sea-breeze events noted elsewhere [e.g. *Helmis et al.*, 1995].

Strength of the SBF. Strong sea-breeze fronts are those with a) a significant temperature contrast between the two airmasses, b) a sharp temperature gradient (occurring over a narrow horizontal distance), or c) both. The strongest fronts, most

clearly identified by the frontogenesis function, will also be those where the thermodynamic and kinematic fronts are in the same place. At its simplest level, these are the *narrowest* fronts. For narrow fronts to occur, strong low-level convergence is needed. Strong low-level convergence can occur with a) strong, opposing offshore winds, b) strong onshore winds within the marine airmass, or c) both.

Helmis et al. [1987] conducted a field study of the SBF in Athens, Greece, utilizing surface observations, an acoustic mini-sounder, and an atmospheric turbulence probe. They classify fronts into two groups -- narrow and wide -- that are dependent on the synoptic-scale wind direction. Narrower fronts with stronger temperature gradients occur when the synoptic-scale wind is offshore, and wider fronts with weaker temperature gradients occur when the synoptic-scale wind is parallel to the coast.

Chiba [1993] studied the SBF in Japan through a full annual cycle, and reports the width of the front as a function of the ratio U_C/U_M . U_C is the offshore wind speed in the continental airmass (observed before frontal passage), and U_M is the onshore wind speed within the marine airmass (observed after frontal passage). The wind speeds are recorded on a 21-meter tower, two kilometers inland from the coast. During the cold season (October through

March), the ratio has typical values between 0.2 and 0.8, and during the warm season (April through September), it has values between 0.7 and 1.3. As the ratio increases from 0.7 to 2, the width of the SBF increases from 130 to 1120 meters, with an overall average of 560 ± 230 meters. This indicates that, in the study area in *Chiba* [1993], the width of the front is inversely proportional to the relative strength (magnitude) of the onshore wind within the marine airmass, and directly proportional to the offshore wind within the continental airmass.

SBF slope. The advancing SBF slopes backwards over the marine air at an angle of between 10 and 60 degrees from the horizontal [Wood *et al.*, 1999; Lapworth, 2000]. Theoretical studies indicate the slope should be 60 degrees near Earth's surface, with smaller values aloft [Xu, 1992]. These findings are mirrored in the laboratory tank experiments carried out by Simpson [1994, 1997]. Friction on Earth's surface reduces the forward momentum of the advancing front in the lowest few hundred meters -- forcing the frontal surface toward the vertical -- but aloft, in the absence of surface friction, the front moves inland more quickly, resulting in a leading nose with a much shallower slope above (Figure 2.8).

Wood *et al.* [1999], from measurements made of the SBF in instrumented aircraft, reported a slope of 30 degrees from the horizontal between 200 and 500 m AGL in one case, but only 15 - 20 degrees in another. They speculated that the latter front had a shallower slope because it was moving across flat terrain, while the former was moving up a shallow incline, which reduced the front's forward momentum. An ambient opposing wind has a similar effect on the SBF. *Helmis et al.* [1987] observed that when the sea breeze advances into stronger opposing synoptic-scale winds, it exhibits a shallower slope (smaller angles from the horizontal), and a sea breeze moving into ambient shore-parallel wind regimes exhibits a steeper slope (larger angles from the horizontal).

Vertical velocities at the SBF. A scale analysis of the frontogenesis function reveals that the vertical shear term (involving cross-shore variations in the vertical component of velocity) is of the same approximate magnitude as the horizontal terms. Vertical currents initiated or enhanced by the SBF can cause convective clouds, including thunderstorms. (For more about the initiation of thunderstorms and other convective activity by the sea-breeze front, see *Pielke* [1985]; *Pielke et al.* [1991]; *Rubes et al.* [1993]; *Atkins et al.* [1995]; *Weckwerth et al.* [1996]; *Silva Dias and*

Machado [1997]; Weckwerth et al. [1997]; Carbone et al. [2000]; and Rao and Fuelberg [2000].) Vertical currents are also a factor in the dilution of pollutants in the PBL, and are therefore of interest to air pollution meteorologists and engineers. Aviators are concerned about low-level wind shear resulting from sudden changes in vertical velocity. Therefore, there are ample theoretical and practical reasons for studying the changes in the atmosphere's vertical motions brought about by the SBF.

Figure 2.9 illustrates a simplified two-dimensional flow structure in a gravity current with bottom friction, representing a situation analogous to the sea-breeze [*Sha et al., 1993; Simpson, 1997*]. Arrows indicate the direction of the fluid flow. The primary updraft is in the warm air immediately adjacent to the SBF. This updraft is caused by the physical wedge of the denser marine air undercutting the lighter continental air. Another updraft is in the cold air, immediately behind the SBF. This updraft is caused by low-level convergence and mass conservation, with thermal instability adding additional lift, and is the updraft responsible for the SBH. Additional, smaller-scale updrafts are visible behind the SBF, beneath the landward-moving marine airmass, caused by surface friction and thermal instability. A prefrontal downdraft is visible inland of the primary updraft, and is associated with prefrontal

gravity waves [Sha et al., 1993]. This landward downdraft is part of a repeating pattern of up- and downdrafts in the continental airmass, associated with convective activity on a horizontal scale of about two kilometers [Stephan et al., 1999]. Another downdraft is visible immediately seaward of the cold updraft within the sea-breeze head, and together these form a closed vertical circulation [Kitada, 1987]. Pollutants can become trapped within this post-frontal roll vortex and be transported for great distances inland [Kitada, 1987]. Numerous updrafts and downdrafts are also visible in the turbulent mixing region associated with the KHBs.

Before sea-breeze frontal passage (fropa), downdrafts occur 60 percent of the time, while updrafts dominate after fropa [Chiba, 1993]. Observed downdrafts have had average magnitudes of about 0.5 ms^{-1} , while updrafts were between 0.5 and 1.0 ms^{-1} [Chiba, 1993; Stephan et al., 1999]. The magnitude of the vertical velocities is also dependent on the strength of the frontal zone and the rate at which the SBF advances inland [Helmis et al., 1987]. Vertical velocities of 1.0 to 1.5 ms^{-1} have been observed with sharp frontal zones, while weaker fronts produced updrafts and downdrafts only one third as large [Helmis et al., 1987]. Fast-moving fronts produce greater vertical velocities than slow-moving fronts [Helmis et al., 1987]. The direction of the ambient flow is also important, with

updrafts as large as 2.0 ms^{-1} occurring at the SBF when the ambient flow is offshore [*Helmis et al.*, 1987]. When the SBF interacts with horizontal convective rolls (HCRs), the largest upward vertical currents at the front occur where the frontal surface intersects an HCR rotating in the same sense as the post-frontal roll vortex [*Atkins et al.*, 1995]. Regions of enhanced vertical velocities are marked by cumulus cloud development [*Atkins et al.*, 1995].

Formation of undular bores. During the late evening hours, the SBF, SBH, and post-frontal roll vortex can separate from the feeder flow and continue moving inland independently as an undular bore or cutoff vortex [*Kitada*, 1987; *Simpson*, 1994]. The cutoff vortex is a solitary wave that propagates along the top of a low-level maritime or nocturnal radiation inversion [*Smith et al.*, 1982], and is about one kilometer high and about 20 kilometers across in the cross-shore direction [*Sha et al.*, 1993]. At ground level, the approach of a cutoff vortex is marked by an abrupt increase in atmospheric pressure and temperature, and a change in the wind speed and direction. Its arrival may or may not be followed later by the arrival of the sea-breeze proper [*Simpson et al.*, 1977; *Simpson*, 1996]. It often continues moving inland after

the low-level onshore flow has ended, and it therefore is no longer part of a gravity current [Abbs and Physick, 1992].

Simpson et al. [1977] suggest that a cutoff vortex sometimes forms in southern England, shortly before sunset, but the most dramatic example of the phenomenon is the Morning Glory, in the Gulf of Carpentaria region of northern Australia [e.g. *Smith et al.*, 1982]. The Morning Glory occurs around sunrise, during the latter half of the Austral dry season (mid-August through mid-November), and is associated with the sea breeze of the previous day. In addition to an abrupt pressure increase (sometimes exceeding 1 hPa in a few minutes) and shift in wind direction, it is usually accompanied by one or more roll clouds roughly one kilometer in height and many kilometers long (Figure 2.10), as well as intense wind squalls at the Earth's surface [*Smith et al.*, 1982].



Figure 2.10: Australian Morning Glory, as seen from the wing of a glider about one kilometer AGL. (Photograph courtesy of Russell White.)

Numerical model studies have determined two methods by which the sea breeze may contribute to the formation of undular bores. When two SBFs collide, or when one is overtaken by another, a hump of marine air is generated eventually resulting in the conditions favorable for the formation of bores. In this case, two undular bores are created that move with approximately the same velocities as the original SBFs [Clarke, 1984]. Undular bores may also be created when the sea breeze penetrates inland and interacts with a nocturnal temperature inversion [Sha et al., 1993]. The interaction causes the SBH to detach and move inland, cutoff from the low-level feeder flow. Eventually the cutoff vortex dissipates from inertial damping and radiative energy loss [Sha et al., 1993]. Air pollutants emitted from ground sources within the marine layer can become trapped within the closed circulation behind the leading edge of the cutoff vortex [Kitada, 1987]. The vortex then serves as a mechanism that transports the pollutants inland. Downward vertical currents at the rear of the vortex move pollutants from the top of the PBL to the points closer to Earth's surface, even in thermally stable conditions [Kitada, 1987]. (The sea breeze's influence on air quality is discussed in greater detail below.)

Along-shore variations in the SBF. The cross-shore gradients of potential temperature, water vapor, and wind components associated with the SBF usually vary in magnitude in the along-shore direction. On a nearly homogeneous coast, these variations are about ten times smaller than the variations in the cross-shore direction. Along-shore variations in the SBF increase as the coastline becomes more complex. One cause of these variations is collisions between the SBF and convective elements in the continental airmass [Stephan et al., 1999]. The interaction between sea-breeze fronts and convective activity is discussed in greater detail in the next section.

Interactions with external meteorological phenomena.

The SBS interacts with external meteorological phenomena at all stages of its life cycle. Within a short period of time following sunrise on days conducive to the formation of the SBS, cellular convection begins over land in response to surface insolation and low-level destabilization [Mitsumoto et al., 1983]. The cells have an aspect ratio of 1:1 and horizontal scales of 1 - 4 kilometers, and are sometimes visible as fair-weather cumulus [Lyons, 1972; Mitsumoto et al., 1983; Stephan et al., 1999]. A mixed layer of uniform

thickness forms over land as a result of the convection, and the smaller cells merge into larger ones and attenuate [Mitsumoto *et al.*, 1983]. The SBG moves into the well-mixed layer and interacts with the onshore convective disturbances, which in turn contribute to variations in the SBF's shape and speed [Stephan *et al.*, 1999].

The SBS may also interact with horizontal convective rolls (HCRs) that develop in the convectively unstable continental airmass [Atkins *et al.*, 1995]. During periods of ambient offshore flow, the HCR rotation axes are nearly perpendicular to the SBF. As an HCR collides with the SBF, its axis of rotation is lifted upward from updrafts associated with the front. During periods of ambient onshore flow, the HCR rotation axes are approximately parallel to the SBF. In this case, collisions between HCRs and the SBF constitute the merging of the two like-sign vortices, and result in the strengthening of the SBF. Both scenarios result in the enhancement of cumulus clouds at the points of collision [Atkins *et al.*, 1995].

If the SBS develops near a coastal city, it will interact with the city's urban heat island (UHI). The presence of the UHI increases the sea-breeze velocity during its growing stages [Yoshikado, 1992], and the acceleration increases as the size of the inland urban area increases [Ohashi and Kida, 2002]. The UHI also causes the SBC to last longer [Ohashi and Kida, 2002], and the interaction may result

in unusually regular and persistent lines of clouds, such as the Kampachi Street Cloud Line in downtown Tokyo [*Kanda et al.*, 2001].

The SBS may interact with other thermally-driven breezes, generated at points inland. *Zhong and Takle* [1992] conducted an observational study of SBS interactions with river breezes in eastern Florida. The Indian River is a shore-parallel feature about 10 kilometers inland, and produces the largest of the river breezes in their study area. These authors found that the collision of the Indian River Breeze (spreading outward perpendicular to the river's axis) with the Atlantic sea breeze creates areas of enhanced low-level convergence on both sides of the river. Smaller water features nearer the coastline produce minor atmospheric circulations that interact with the sea breeze, enhance low-level convergence, and speed up the inland movement of the SBF [*Zhong and Takle*, 1992].

The low-level landward flow associated with the SBS interacts with the offshore temperature inversion separating the marine boundary layer from the air above it [*Barkan and Feliks*, 1993]. A field study in a harbor south of Tel Aviv, Israel found that the marine inversion moved downward approximately adiabatically during the day, when the SBC was operating, and upward during the night, when the land breeze was in effect [*Barkan and Feliks*, 1993]. Model studies have shown that the portion of the marine inversion

that varies diurnally extends more than 100 kilometers offshore [Feliks, 1993].

The SBS also interacts with synoptic-scale features. Brümmer et al. [1995] observed the interaction between the SBS and a synoptic-scale cold front (SSCF) that approached the northern coast of Germany from the North Sea. Before the relatively weak, shore-parallel SSCF arrived at the coast, the SBC was initiated between the marine airmass ahead of the SSCF and the continental airmass on shore. At about noon, as the SSCF approached the shore from the northwest, the SBF moved inland ahead of it. The onshore wind behind the SBF and ahead of the SSCF was so strong that the SSCF was subjected to a divergent wind field, resulting in the forward transfer of the thermal contrast associated with the SSCF to the SBF. At points inland later in the day, a single very-strong frontal passage was observed [Brümmer et al., 1995].

Daily life-cycle.

The life-cycle of the SBS consists of five stages: *Immature*, *early mature*, *late mature*, *early degenerate*, and *late degenerate* [Clarke, 1984; Buckley and Kurzeja, 1997]. These five stages apply to all three of the sea breeze categories described above. The land

breeze, a near mirror of the sea breeze, evolves through a similar sequence of stages [Holmer and Haeger-Eugensson, 1999].

During stage one, immature, the SBC begins as a divergence in the cross-shore wind component over the sea, in response to the local-scale thermal PGF [Clarke, 1984]. The SBC expands more rapidly seaward than landward [Finkele et al., 1995]. Marine air moves onshore as a gravity current [Simpson, 1997], and the leading edge takes on frontal characteristics [e.g., Kraus et al., 1990; Reible et al., 1993]. Convergence in the cross-shore wind component develops over land, and the gravity current develops a raised head [Finkele et al., 1995].

During stage two, early mature, insolation begins to decline and the KHBs decay, removing the top friction and allowing the inland progression of the sea breeze to accelerate [Clarke, 1984; Sha et al., 1991; Buckley and Kurzeja, 1997]. During stage three, late mature, insolation drops toward zero, the land-sea thermal difference driving the SBC vanishes, the magnitude of the resulting landward force vector drops to zero, and supply of new marine air to the head of the sea breeze is cut off. But the SBF remains sharp, and the center of the SBC cell shifts from a point near the coast to the landward edge of the marine airmass [Clarke, 1984]. After sunset, radiational cooling increases, which reduces vertical mixing

and the associated updrafts, and reduces the height of the SBH. The SBH continues to move inland [Clarke, 1984].

During stage four, early degenerate, the SBH, now separated from the feeder flow and continuing to move inland independently, may interact with a nighttime radiational inversion or other low-level features and form a sea-breeze cutoff vortex or undular bore [Clarke, 1984]. The most noted example of this phenomenon is the Morning Glory, which is discussed above [Smith *et al.*, 1982; Simpson, 1994]. Kitada [1987] found that the undular bore can act as a pollutant transport mechanism, with descending currents at the rear of the cutoff vortex moving pollutants aloft down to Earth's surface.

In the final stage, late degenerate, the circulation in the SBH is no longer closed [Clarke, 1984]. The leading edge flattens out, and Coriolis force rotates the flow and limits further penetration inland. At this stage the remnant of the sea breeze may also interact with developing nocturnal features, such as low-level jets and other gravity flows [Clarke, 1984; Garratt and Physick, 1985; Buckley and Kurzeja, 1997].

Forecasting.

The sea breeze is a standard forecast problem in coastal locations. Weather forecasters usually work under rather severe time constraints and therefore prefer simple, straightforward methods to complicated methods. There are several SBS forecasting techniques in the literature for specific locations that rely on meteorological variables included in standard surface and upper-air observations. Unfortunately, local irregularities in the coastline and inland topography can have a strong effect on the SBS, so techniques developed for use in one location may not work well in another [e.g., *McPherson, 1970; Simpson, 1994*].

Forecasting the sea breeze consists of at least three major components: 1) A simple yes/no (on whether or not it will occur), 2) the wind speed and direction, and 3) the distance of inland penetration during the day. The first question -- whether or not a sea breeze will be observed at a given location -- is also a function of the last question. All three are discussed separately below.

Occurrences. A number of empirical studies examined the occurrence of the sea breeze as a function of land temperature, land-sea temperature difference, the strength of the opposing

background (synoptically-driven) wind, or some combination of these. The simplest approach uses the temperature information only. For example, *McKendry and Roulet* [1994] reported that all sea breezes observed on the western shore of James Bay were associated with inland temperatures greater than 20 °C.

For it to be detected inland, the sea breeze must often blow upwind in opposition to the ambient flow. *Biggs and Graves* [1962] developed an early lake-breeze forecasting index that compares the background wind to the land-sea temperature contrast:

$$\varepsilon = \frac{|U|^2}{C_p \Delta T} \quad (2.14)$$

where ε is the L-B [lake-breeze] Index and represents the ratio of the inertial force ($\rho U^2/2$) and buoyancy force ($\rho g \beta \Delta T$; β is the coefficient of expansion of air). $|U|$ is the near-surface wind speed [ms^{-1}], C_p is the specific heat coefficient of dry air at constant pressure ($1.004 \text{ J g}^{-1} \text{ K}^{-1}$), and ΔT is the difference between the inland air temperature and the temperature of the water surface ($T_{\text{land}} - T_{\text{water}}$) [°C]. Both $|U|$ and ΔT are determined by using a point far enough inland so that it is not affected by the sea breeze

[Simpson, 1994]. If ϵ is large, then the inertial force is large, and there will not be a lake (sea) breeze. If ϵ is small, then the buoyant force is relatively large, and the lake (sea) breeze can move inland. Using a site on the west end of Lake Erie, the authors found that the critical ϵ value is 3.0. If a transition zone between 2.7 and 3.2 is permitted, the L-B Index correctly predicts the occurrence/non-occurrence of the lake breeze 97 percent of the time [Biggs and Graves, 1962].

Lyons [1972] recalibrated the L-B Index for Chicago, Illinois (on the southwest shore of Lake Michigan) using a climatological record obtained during ten summer months over a two-year period (1966 - 1968). Rather than using an observed wind recorded at an inland surface site for the value of $|U|$, Lyons [1972] calculated the geostrophic wind speed using the 1200 UTC surface analysis. The author reports a critical ϵ of 10.0, above which the lake breeze does not occur, which accurately forecasts the lake breeze 90 to 95 percent of the time. The difference between the critical value in Lyons [1972] and that reported by Biggs and Graves [1962] is attributed to the method used to determine $|U|$.

Lake breezes and sea breezes are driven by the same mesoscale, thermally-induced pressure gradients. Simpson [1994]

repeated the L-B Index calculations for the sea breeze at Thorney Island, Britain, and found a critical value of 7. Once again, the difference between Simpson's critical value and that reported by previous authors is attributed to the method used for obtaining $|U|$. In this case, rather than an observed surface wind or calculated geostrophic wind speed, *Simpson* [1994] used the 1000-meter wind speed obtained with a pilot balloon ascent.

About 60 percent of the forecast error by the L-B Index is associated with the failure of the expected lake breeze to occur, i.e., it over-predicts the lake breeze [*Biggs and Graves*, 1962; *Lyons*, 1972]. *Laird et al.* [2001] examined this and related problems with the index using a 15-year climatology of the region surrounding Lake Michigan. The authors tested three variations on the L-B Index, by computing it as originally described by *Biggs and Graves* [1962] (using $|U|$, the wind speed irrespective of wind direction), by substituting the observed cross-shore wind component U_x for U , and by substituting $|U_x|$ -- the magnitude of U_x , -- for $|U|$. The best results are obtained using U_x , and the worst results with $|U|$.

Laird et al. [2001] also reported three additional important findings. The first is that, although the lake breeze is driven by land-lake temperature differences (ΔT), large values of ΔT are not

required, and in 70 percent of the lake-breeze events in their climatology, daytime maximum ΔT values were less than 12 °C. *Simpson* [1994] reports that temperature differences as small as 5 °C are sufficient. A related result is that the lake breeze is always associated with relatively light ambient wind conditions, e.g., for 95 percent of all lake-breeze events, the average daytime wind speed for the unaffected inland station was $\leq 5 \text{ ms}^{-1}$. Three quarters of all lake-breeze events occurred when the cross-shore wind component had a magnitude ($|U_x|$) of 2 ms^{-1} or less. The third additional finding is that, in agreement with *Walsh* [1974], changes in location alone do not significantly affect the critical value of the index, meaning that, for locations with similar topography and coastline shape, the same critical L-B Index value applies.

Surface wind. Once the forecaster has decided a sea breeze will occur, the next questions are of speed and direction. There are relatively straightforward methods for quantitatively estimating both of these in the literature. Speed and direction are considered separately below.

Speed. One method of estimating the wind speed associated with the sea breeze is the Bjerknes circulation theorem, but it has already been shown that this greatly overestimates the surface wind (see above). An alternative approach is to develop climatological records of the strength of the sea breeze and the temperature contrast between the inland air and the sea-surface, and then fitting a regression line relating the two data sets. This is very straightforward, although it obviously must be repeated for each forecast site. *Mathews* [1982] developed a forecast rule for a Royal Australian Naval Air Station (RANAS) using this method. From a climatology of surface observations recorded over two summers at the Nowra RANAS, southeastern Australia, *Mathews* [1982] selected those days when the only important contribution to the 10-meter wind was from the sea breeze. Wind speed was plotted as a function of the difference between the air temperature at the RANAS and temperature of the nearby ocean surface. A regression line resulted in:

$$|U| = \frac{1}{2}\sqrt{\Delta T} \quad (2.15)$$

where $|U|$ is the magnitude of the sea-breeze component [knots], and ΔT is the land-sea temperature difference [$^{\circ}\text{C}$].

Another approach is to relate wind speed within the marine airmass to the speed of an advancing of SBG [e.g. *Simpson and Britter*, 1980]. *Kuelegan's* [1957] relation (2.5) describes the rate at which a gravity current advances into the ambient fluid. *Simpson* [1969] adapted this for forecasting the rate at which the SBG advances inland, and *Simpson and Britter* [1980] modified the relation to account for the opposing prevailing wind (2.6), and determined the relationship between the speed of the advancing sea-breeze front and the wind velocity ahead of and behind it:

$$u_{\text{FRONT}} \approx 0.87u_{\text{SB}} - 0.59u_{\text{g}} \quad (2.16)$$

where u_{FRONT} is the speed at which the sea breeze advances inland, u_{SB} is the wind speed within the marine airmass, and u_{g} is the cross-shore geostrophic wind component resulting from the synoptic-scale pressure pattern [*Reible et al.*, 1993]. The two constants in (2.16) were determined by *Simpson and Britter* [1980] in laboratory studies using tanks of water.

Finkele [1998], from a model study compared with *in situ* observations from aircraft, reported average speeds for the growth of the SBC of 1.6 ms^{-1} in the landward direction (slowing somewhat in the middle of the day), and compares this to a typical value of 3.4 ms^{-1} in the seaward direction. The former is comparable to u_{FRONT} . *Simpson et al.* [1977], from field studies, reported that a typical value for u_{FRONT} in England is about 3 ms^{-1} , and *Clarke* [1955] reported u_{FRONT} values as high as 7 ms^{-1} in Australia. Several studies have reported variations in the speed of the front's inland propagation -- slowing during the mid-day hours, and regaining speed towards late afternoon -- which is attributed to the development of Kelvin-Helmholtz Billows along the top of the inland marine airmass, and variations in soil moisture [*Physick*, 1980; *Sha et al.*, 1991].

Assuming that (2.16) represents the scalar speed at which the SBF moves inland, one can combine (2.6) and (2.16) to obtain:

$$u_{\text{SB}} \approx \frac{k}{0.87} \sqrt{\frac{\Delta\rho}{\rho} g d} \quad (2.17)$$

where k is a constant equal to 0.62, and d (the height of the SBH) can be replaced by a climatological mean (\bar{d}) without the loss of significant accuracy [Simpson, 1969].

Direction. Two preliminary questions of interest are 1) how does the surface wind direction change from the synoptically-driven direction to the sea-breeze direction? and 2) what is the initial direction of the sea breeze once it is established? McKendry and Roulet [1994] addressed the first question in a field study conducted on the southwest shore of James Bay, where the coastline is fairly straight, and oriented from south-southeast to north-northwest. They report that, with a synoptic-scale wind that has a southerly component, the sea breeze is associated with backing (counter-clockwise rotation) of the wind direction from the southern to the eastern quadrant. For a synoptic-scale wind with a northerly component, the sea breeze is associated with veering (clockwise rotation) of the wind from the northern to the eastern quadrant.

McKendry and Roulet's [1994] results are logical when considered in the context of simple vector addition. Assuming that the Coriolis force is unimportant (at least initially) in the sea breeze, then the mesoscale flow will be parallel to the thermally-induced

pressure gradient, toward lower pressure. In the case of a relatively uncomplicated coastline, this implies a sea-breeze wind vector directly perpendicular to the coast. For the net wind direction at any location, one must add the sea-breeze wind vector to the synoptically-produced wind vector to determine the net wind. In the case of a northerly synoptic-scale wind, the growing sea-breeze vector will gradually deform the net wind vector seen by a stationary observer in such a way that the net appears to rotate in a clockwise direction. With a southerly synoptic-scale wind, the opposite is true.

Mathews [1982] discussed vector addition in a practical technique for forecasting the direction of the sea breeze once it is established. The strength of the cross-shore sea-breeze component is calculated by one of the methods discussed above, and its direction is assumed to be directly perpendicular to the local coastline, with some small degree of variation. Then the sea-breeze vector components are added to the gradient wind components, and the resultant wind is determined.

Once the sea breeze is established, the associated wind direction may continue to rotate as the day progresses. Several field studies report a diurnal rotation in the sea breeze [e.g. *Pearce*, 1955; *Fisher*, 1960; *Zhong and Takle*, 1992; *McKendry and Roulet*, 1994].

Within the same hemisphere north or south of the equator, the sense of the rotation may be either clockwise or the reverse, and therefore cannot be accounted for by the Coriolis force alone.

Neumann [1977] derived an expression describing the time-evolution of the wind direction associated with the sea breeze for a north-south oriented coastline. The x- and y-axes correspond to the cross- and along-shore dimensions respectively, and the expression takes the following form:

$$\frac{\partial \alpha}{\partial t} = -f + \frac{1}{|U|^2} \left[\frac{v}{\rho} \frac{\partial p_m}{\partial x} + f(u u_g + v v_g) \right] \quad (2.18)$$

where the LHS describes the rate and sign of the rotation [s^{-1}], and the three terms on the RHS are associated with (from left) 1) the Coriolis force, 2) thermally-induced mesoscale PGF, and 3) synoptic-scale PGF. The angle between the wind vector and x-axis is represented by α [radians], f is the Coriolis parameter ($= 2\Omega \sin\phi$; Ω is the rotational velocity of Earth, and ϕ is latitude) [s^{-1}], $|U|$ is the scalar wind speed (net) [$m s^{-1}$], u and v are the cross- and along-shore components of the total wind vector [ms^{-1}], u_g and v_g are the cross- and along-shore components of the geostrophic wind vector

[ms⁻¹], ρ is density [kg m⁻³], and $\partial p_m / \partial x$ is the mesoscale pressure gradient resulting from the cross-shore temperature contrast [Pa m⁻¹]. Note that the third term on the RHS of (2.18) can also be written as:

$$\frac{f(u u_g + v v_g)}{|U|^2} = \frac{1}{\rho |U|^2} \left(\frac{\partial p_L}{\partial x} v - \frac{\partial p_L}{\partial y} u \right) \quad (2.19)$$

where $\partial p_L / \partial x$ and $\partial p_L / \partial y$ represent the synoptic-scale pressure gradients in the cross- and along-shore dimensions, respectively. A scale analysis reveals that the three terms on the RHS of (2.18) are within an order of magnitude of each other. Using data recorded in Nova Scotia, Southern Australia, Washington State (U.S.A.), Scotland, and Great Britain, *Simpson* [1996] concluded that Terms 1 and 2 are of comparable importance, but that topographical influences can often be responsible for completely reversing the rotation imposed by all three terms.

If the synoptic-scale pressure field is non-zero at the forecast location, then the best approach for determining the rotation imposed on the wind is to calculate the values of all three terms on

the RHS of (2.18). For a few special cases, however, the solution is somewhat simpler.

Consider the east coast of a continent in the Northern Hemisphere with no important variations in the shape of the coastline and no significant topography. If Coriolis clearly dominates, (2.18) becomes:

$$\frac{\partial \alpha}{\partial t} = -f \tag{2.20}$$

and the wind direction rotates clockwise (anticyclonically). This rotation has been well-documented in field studies (noted above). Once rotation begins, then v (the along-shore component of the net wind vector) is non-zero. If the synoptic-scale pressure field is exceedingly weak, then the two components of the geostrophic wind are approximately zero, and (2.18) becomes:

$$\frac{\partial \alpha}{\partial t} = -f + \frac{v}{\rho|U|^2} \left[\frac{\partial p_m}{\partial x} \right] \tag{2.21}$$

With the ocean on the right, one can assume that, in a sea-breeze environment, $\partial p_m / \partial x$ is positive. Therefore, ignoring the Coriolis force for the moment, a positive (northward) along-shore component (v) implies counter-clockwise (cyclonic) rotation, and a negative along-shore component implies clockwise (anti-cyclonic) rotation. Put another way, if the locally-induced wind has a southward component, then the rotation imposed on the wind direction will be counter-clockwise, but, if the locally-induced wind has a northward component, then the two terms in the RHS of (2.21) are at odds, and the net rotation imposed on the wind direction will depend on their relative magnitudes. Given that density (ρ) is nearly constant ($\sim 1.2 \text{ kg m}^{-3}$; [List, 1968]), and f is constant for a fixed latitude, the terms that one must determine are v , $|U|$, and $\partial p_m / \partial x$.

Extent of inland penetration. Forecasting whether the sea breeze will occur at an inland location is a problem of combining guidance from an index, such as (2.14), with an additional estimate of how far inland the sea breeze will penetrate during the day. Field studies have documented the extent of the sea breeze's inland penetration in different parts of the world (Table 2.2), but

determining a set of generic governing principles is a very complex problem. By combining the results of several studies, *Simpson* [1994] found that the magnitude of the ambient cross-shore wind component is an important control. With onshore synoptic-scale winds, inland penetration is limited to 30 or 40 kilometers, possibly because the associated land-sea temperature contrast is weak. Conversely, an offshore wind of 7ms^{-1} at 1000 meters AGL limits inland movement to 20 kilometers [*Simpson*, 1994].

Table 2.2: Varying extent of the sea breeze's inland penetration in different parts of the world.

Where	Distance inland [km]	Reference
Beaufort Sea coast, Alaska	15	<i>Kozo</i> , 1982
Chicago, Illinois (lake breeze)	40	<i>Lyons</i> , 1972
Indonesia	60 - 80	<i>Hadi et al.</i> , 2002
Southern England	100	<i>Simpson et al.</i> , 1977
James Bay, Ontario, Canada	100	<i>McKendry and Roulet</i> , 1994
Southeastern United States	150	<i>Buckley and Kurzeja</i> , 1997
Southeastern Spain	150	<i>Kottmeier et al.</i> , 2000
Australia	200	<i>Simpson</i> , 1994

Chiba et al. [1999] conducted a field study utilizing an instrumented helicopter, and expanded on *Simpson's* [1994] general

principles. From the results of several sea-breeze case studies in Japan, *Chiba et al.* [1999] determined that the inland intrusion distance at mid-day is between 10 and 25 kilometers, depending on the magnitude of the cross-shore synoptic-scale flow, atmospheric stratification, and geographical features in the area. Specifically, they noted that:

- With a strong offshore gradient and an unstable coastal layer, the sea breeze's inland penetration is limited to 10 kilometers,
- When the atmosphere is stably stratified and the ambient flow is onshore at 6 ms^{-1} , the sea breeze reaches as far as 15 kilometers inland, and
- With high pressure and light, offshore 850-hPa winds overhead, the sea breeze reaches as far as 25 kilometers inland.

Field studies produce excellent results on the local behavior of the sea breeze, but computer models are better able to differentiate the many overlapping physical phenomena in the SBS, and therefore, are a better tool for determining the generic principles governing

the sea breeze's inland extent. Some model studies focus on various phenomena that reach inland prior to the arrival of the sea-breeze proper. *Tijm and van Delden's* [1999] sound waves reach over 1000 kilometers inland. *Geisler and Bretherton's* [1969] sea-breeze forerunner may reach as far inland as 60 kilometers. Most modelers have focused on the SBC or the SBG.

Estoque [1962], in a model study assuming a straight coastline and a hydrostatic atmosphere, concluded that an ambient offshore wind of 5 ms^{-1} limits SBC inland penetration to 18 kilometers, while similar thermal forcing with calm ambient winds permits SBC inland penetration of 32 kilometers. The former result closely parallels *Simpson's* [1994] observation-based conclusions. In a comprehensive series of model studies, *Arritt* [1992] noted that an offshore ambient wind of approximately 1 ms^{-1} was conducive to the deepest inland penetration, peaking at more than 60 kilometers. *Finkele* [1998] reported that the inland extent of the sea breeze is greater under light (2.5 ms^{-1}) ambient offshore wind conditions than in moderate (5 ms^{-1}) ones, but the seaward extent is similar in both situations. For strong offshore geostrophic winds (7.5 ms^{-1}), the SBC is entirely over the sea.

Pearce [1955], using an early 3-D numerical model, determined that inland motion of the sea breeze is ultimately limited by Coriolis-induced rotation. *Rotunno* [1983] expanded on this, stating that where:

$$f \geq \omega \quad (2.22)$$

the sea breeze is confined to a finite distance from the coast determined by the vertical scale of heating and the static stability. Conversely, where:

$$f < \omega \quad (2.23)$$

the sea breeze is in the form of internal waves that extend an "infinite" distance inland. In (2.22) and (2.23) f is the magnitude of the local Coriolis parameter ($= 2\Omega\sin\phi$), and ω is the cycle of heating and cooling ($= 2\pi/\text{day}$). Ω is the angular rotation of Earth, and ϕ is the latitude. It follows that the dividing line is where $4\pi\sin\phi/\text{day} \geq 2\pi/\text{day}$, or $\sin\phi \geq 1/2$, which is true if $\phi \geq 30$ degrees. For regions at and above 30 degrees latitude, *Rotunno* [1983] concluded that the

range of sea breeze's inland extent (L) near the ground is defined by:

$$L = \frac{Nh}{\sqrt{\omega^2 - f^2}} \quad (2.24)$$

where N is the Brunt-Väisälä frequency ($= \sqrt{(g/\theta)(\partial\theta/\partial z)}$) [s^{-1}] [Rogers and Yau, 1989], and h is the vertical scale of the heating [m]. Dalu and Pielke [1989] stated that friction limits both intensity (speed) and the inland extent. At the equator, where the Coriolis force is zero, the sea breeze is entirely limited by friction. Within 30° of the equator, the "infinitely propagating" waves suggested by Rotunno [1983] may not appear because friction limits the sea breeze.

By combining conclusions of the studies noted above with results of McPherson [1970], Asai and Mitsumoto [1978], Mitsumoto et al. [1983], Sha et al. [1991], Zhong and Takle [1992], Arritt [1992], and Melas et al. [1998], one can construct a summary of the controls on SBC inland propagation, shown in Table 2.3.

Table 2.3: Summary of controls on the inland penetration of the sea breeze.

Control	Description
<i>Magnitude and direction of the synoptic-scale cross-shore wind component</i>	<ul style="list-style-type: none"> • Seaward wind component of 7 ms⁻¹ will limit inland penetration to 10 kilometers or less. • Light seaward wind component or calm ambient wind is most favorable for deep penetration. Seaward ambient wind component of 1 ms⁻¹ may result in inland propagation of more than 60 kilometers. • Strong shoreward ambient wind is associated with weaker land-sea temperature contrasts; limits inland propagation to about 40 kilometers.
<i>Land-sea temperature contrast</i>	<ul style="list-style-type: none"> • Must have positive land-sea temperature difference. • Very strong temperature differences are not required. • Minimum of 5° C required for "deep" penetration.
<i>Coriolis</i>	<ul style="list-style-type: none"> • Prevents SBC from extending inland "to infinity" by rotating associated wind until it is parallel to the coast.
<i>Surface friction</i>	<ul style="list-style-type: none"> • Slows rate of inland movement and therefore extent SBC may reach before sunset, when thermal forcing is removed.
<i>Top friction (KHBs)</i>	<ul style="list-style-type: none"> • Slows rate of inland movement. • KHBs form on SBH in low-stability conditions, and propagate backwards (toward sea) along top of SBG.

Table 2.3 (Continued): Summary of controls on the inland penetration of the sea breeze.

<p><i>Thermodynamic stability in the continental airmass</i></p>	<ul style="list-style-type: none"> • Sea breeze may initially advance more readily into a well-mixed ambient airmass (often marked by fair-weather cumulus). • Instability also gives rise to KHBs which slow sea breeze's inland movement, and therefore reduces the degree of penetration. • Complex relationship between stability and penetration is discussed in <i>Rotunno</i> [1983]: predicts greater inland penetration in high stability atmospheres, but also in atmospheres with large vertical heating scale.
<p><i>Shape of coastline</i></p>	<ul style="list-style-type: none"> • Inland bays along an otherwise straight coastline provide low-friction pathways for sea breeze to advance inland.
<p><i>Topography</i></p>	<ul style="list-style-type: none"> • Terrain features can either assist or obstruct sea breeze's inland movement. • If sea-facing hillside is relatively close to coast, and is heated on the same diurnal cycle as adjacent coastal plain, resulting uphill wind current can assist the sea breeze's inland movement. If hill is in shadows, or shrouded in fog or clouds, it acts as an obstruction. • Valleys funnel sea breeze, accelerating associated wind speeds, which carries marine air further inland than over comparatively featureless terrain.

Table 2.3 (Continued): Summary of controls on the inland penetration of the sea breeze.

<p><i>Interactions with other mesoscale systems</i></p>	<ul style="list-style-type: none"> • If sea breeze encounters other small-scale circulations, it is modified, and extent of its inland penetration may be either increased or reduced. • For very weak sea or lake breeze, collision with thunderstorm downdraft may be enough to completely stop inland progression. • Sea breeze's speed and direction of movement (and therefore its inland penetration) may be modified by collisions with other sea-breeze systems, lake breezes, or river breezes generated at points inland.
---	--

Air quality impact mechanisms.

Meteorological and topographical features in coastal regions create complex low-level wind circulations. High concentrations of air pollutants are released into these circulations by industrial facilities (e.g., petro-chemical plants, nuclear power stations, etc.), which are typically in or near urban areas, and are often located near coastlines. Understanding the downwind behavior of these pollutants could assist in mitigating significant health problems [e.g. *Shearer and Kaleel, 1982; Clappier et al., 2000*]. The sea breeze has been implicated as either a direct control [e.g. *Kitada, 1987; Hsu, 1988; Physick and Abbs, 1992*] or as one contributing factor to

more complex air-quality scenarios [Gaza, 1998; Seaman and Michelson, 2000; Gangoiti et al., 2002].

One example of a direct control is *Kitada's* [1987] inland transport of pollutants by the post-frontal roll vortex. Another example is the Convective Internal Boundary Layer (CIBL), also known as the Thermal Internal Boundary Layer (TIBL). Cool, stable marine air encounters a thermodynamically unstable situation when it advects over a hot land surface. As the marine airmass moves inland and conducts heat from the land surface, convective currents begin to develop, and modified air is transported vertically. As the air moves further inland, convective currents reach progressively greater heights. The vertical overturning results in a CIBL near Earth's surface, whose upper limit increases non-linearly with distance from the coast. Above the CIBL, the remaining unmodified marine air acts as a cap that prevents mixing between destabilized marine air below and the continental air above [Hsu, 1988; Stull, 1988; Prabha et al., 2002].

The CIBL is frequently the cause of persistent air pollution problems in coastal cities. The onset of the CIBL results in a dramatic reduction of the atmosphere's mixing depth, and locally-generated pollutants trapped in the shallow surface layer can quickly reach unhealthy levels (Figure 2.11) [e.g., Barbato, 1975].

Pollutants such as sulfur dioxide (SO₂) and ozone (O₃) can be rapidly mixed to the surface when they encounter the convective currents within the CIBL [Barbato, 1975; Gangoiti et al., 2002]. Fumigation occurs when air pollution plumes emitted in stable regions of the marine airmass encounter the top of the CIBL, and are rapidly mixed down to the surface (Figure 2.12) [Lyons et al., 1981; Hsu, 1988; Abbs and Physick, 1992; Sawford et al., 1998]. Plumes mixed to the surface may be vertically transported hundreds of meters aloft in updrafts associated with convection or lines of low-level convergence, then divided into multiple branches which move in many different directions. Some may eventually be caught up in the seaward return flow, transported many tens of kilometers offshore, and recirculated landward within the SBC cell. The pollutant concentration within the SBC can grow throughout the day as fresh emissions are fumigated downward into the CIBL, adding to older pollutants already in the SBS [Shair et al., 1982; Panel of Coastal Meteorology, 1992; Abbs and Physick, 1992].

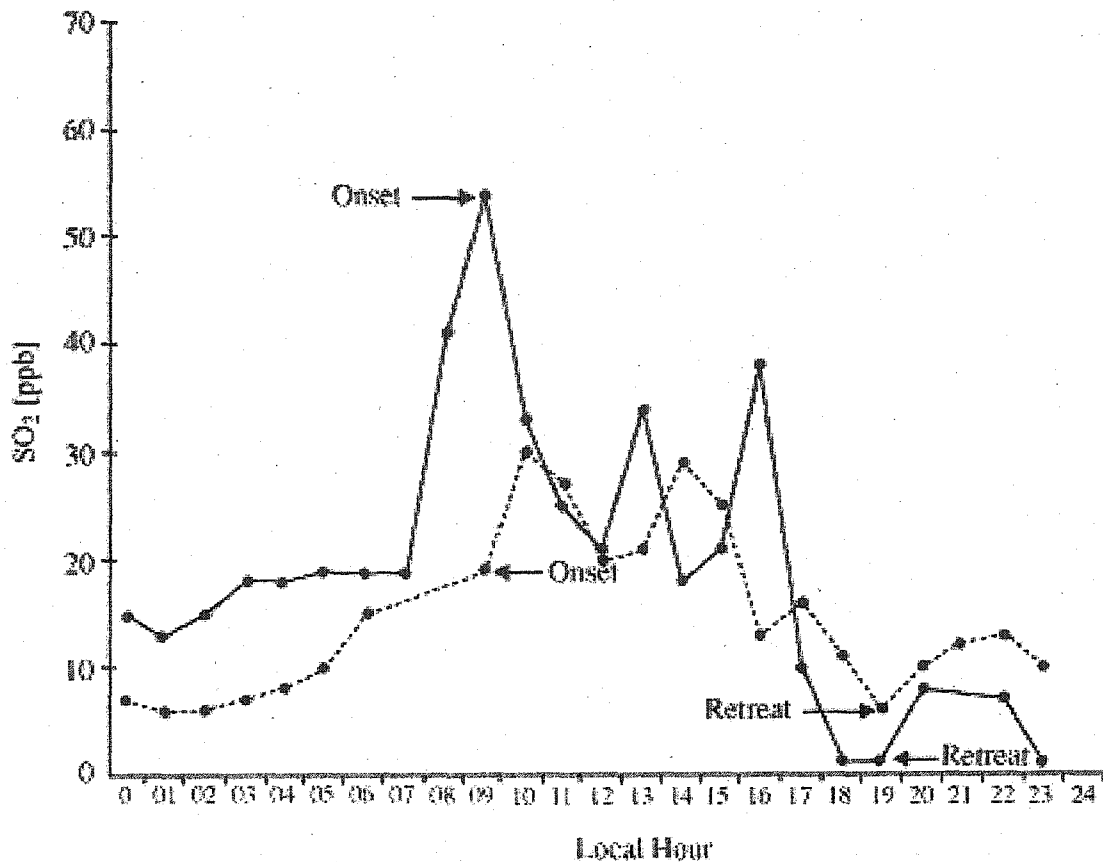


Figure 2.11: Atmospheric SO₂ concentration levels at two stations in Boston, Massachusetts. The concentration of SO₂ jumps dramatically following the passage of the SBF (indicated by "onset") due to CIBL-induced fumigation. Based on hourly SO₂ observations, September, 1972. [After Barbato, 1975].

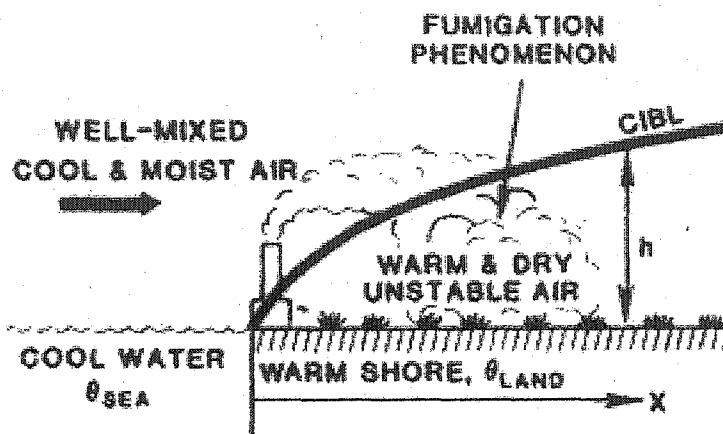


Figure 2.12: Convective Internal Boundary Layer (CIBL) formed by advection of cool marine air over a warm land surface. "h" is the depth of the CIBL, and varies as a function of distance from the coast (eqns. 2.25 and 2.26). Details in text [Hsu, 1988].

The variation in the height of the CIBL with distance from the coast is the subject of several field studies. Raynor *et al.* [1979] studied the CIBL over Long Island, New York under a variety of prevailing wind and stability conditions. They found that the height of the CIBL (as a function of cross-shore distance) increases sharply near the coast, but more gradually inland. Druilhet *et al.* [1982], using an instrumented aircraft, found that height of the CIBL increased as a power of 0.4 of the cross-shore distance along the French Mediterranean coast. Melas *et al.* [2000] conducted a study of sea-breeze behavior on the island of Sardinia, and reported CIBL

heights of about 50 meters near the coastline, which increase gradually to over 500 meters, several kilometers inland. *Prabha et al.* [2002] reported CIBL heights between 150 and 200 m AGL, measured by a mini-SODAR positioned five kilometers inland in the tropics. *Liu and Chan* [2002] studied internal boundary layers over Hong Kong, and reported CIBL heights of up to 700 meters AGL, reaching almost to the top of mountains in the complex terrain of the island.

In general, CIBL heights (h) grow as a function of the square-root of distance from shore (x), but there are many modifying factors that scale the rate of growth. From first principles, *Venkatram* [1977] derived:

$$h = \sqrt{\frac{2 C_D (\theta_{\text{land}} - \theta_{\text{sea}}) x}{\gamma (1 - 2F)}} \quad (2.25)$$

where h and x are in meters, C_D is the drag coefficient ($\approx 12 \times 10^{-3}$), γ is the lapse rate above the boundary layer or over the water surface [K m^{-1}], F is the entrainment coefficient (0 to 0.22), and θ_{land} and θ_{sea} are the potential temperatures over the land and sea surfaces [K]. *Hsu* [1988] evaluated the effectiveness of (2.25) by

utilizing data from several field studies, and reported that the observed CIBL heights and the theoretical predictions are in substantial agreement.

Melas and Kambezidis [1992] evaluated (2.25) and several alternative models using data observed in Athens, Greece. They reported that the following relation, based on *Gryning and Batchvarova [1990]*, is the most accurate predictor of CIBL height:

$$h = (1 - 0.002L_a) \sqrt{2 C_D C_T (1 + 2A)} \times \sqrt{\frac{x\Delta\theta}{\gamma}} + 11 \ln(-L_a) \quad (2.26)$$

where C_T is heat flux coefficient ($\approx C_D$), and A is a constant approximately equal to 2. L_a is given by:

$$L_a = - \frac{(C_D u_h)^2}{k \frac{g}{T_0} C_T \Delta\theta} \quad (2.27)$$

where u_h is the cross-shore wind component at the upper part of the CIBL [ms^{-1}], k is the von Kàrmàn constant (0.40), g is the gravitational acceleration (9.81 ms^{-2}), T_0 is the surface temperature

[K], and $\Delta\theta$ is $\theta_{\text{land}} - \theta_{\text{sea}}$ [K] [Melas and Kambezidis, 1992]. Luhar et al. [1998] evaluated (2.26) using data recorded on the east coast of Australia. They found that it effectively predicted the observed CIBL height unless the atmosphere was neutrally stable, when a more complex model was needed.

A number of additional studies have advanced the understanding of how the CIBL evolves. For example, Raynor et al. [1979], using an instrumented aircraft, found that the time-rate of growth of the CIBL was initially slower with stable lapse rates over the sea than with neutral or unstable lapse rates. They also found that the height (h) of the CIBL does not grow to infinity with distance inland (as suggested by the equations shown above), but reaches an equilibrium height that is dependent on downwind (inland) conditions. A higher CIBL is associated with low wind speeds and stronger land surface heating [Raynor et al., 1979]. Federovich et al. [2001], combining wind-tunnel and numerical models, reported that the sign of the wind shear at the top of the CIBL affects the CIBL's rate of growth. Positive shear -- where the wind momentum above the top of the CIBL is greater than within the CIBL -- impedes the growth of the CIBL, when compared to the case when no wind shear is present. Negative shear -- where the wind

momentum within the CIBL is greater than above it -- enhances the growth of the CIBL.

A third example of a direct control on air quality by the sea breeze was studied by *Physick and Abbs* [1992]. These authors observed the behavior of pollutants released by power stations in the Latrobe Valley, southeastern Australia, over a five-day period. The east-west Latrobe Valley extends more than 130 kilometers inland, and is bordered by mountains as high as 2000 meters. An easterly sea breeze regularly penetrates more than 100 kilometers up the valley, where it collides with an SBC moving inland from the south in the late afternoon. Observations indicated that the associated marine layer was about 1500 meters deep. Westerly winds prevailed above 3000 meters AGL during the study.

The power stations are located about 90 kilometers up the valley. The easterly SBG reaches this point by late afternoon, and the polluted valley air is lifted aloft and into the westerly return flow above the SBG. The marine air behind the SBF is cleaner than the valley air because a) there are no additional pollution sources closer to the coast, b) the top of the CIBL within the marine air is well below the top of the easterly SBG preventing the downward convective mixing of pollutants, and c) the combination of wind velocities aloft and offshore distances traveled makes recycling of

the pollutants from the subsiding end of the SBC impossible [*Physick and Abbs*, 1992].

The SBS can also become a factor in more complex air-pollution scenarios. One of these occurs regularly on the east coast of the United States. *Pagnotti* [1987] describes the Appalachian Lee Trough (APLT), which forms along the eastern seaboard when the 700 - 500 hPa flow is southwesterly to northwesterly. The APLT causes the winds below 850 hPa to turn southwesterly, resulting in shore-parallel flow along the East Coast, which in turn results in long-distance transport of O₃ and its precursors from the Northeast urban corridor to rural areas further up the coast [*Pagnotti*, 1987].

The role played by the SBF in this scenario is documented in a case study of a July, 1995 O₃ pollution event [*Gaza*; 1998]. *Gaza* [1998] used hourly observations of ground-level O₃ concentrations at three locations on a line running north from New York City. O₃ concentrations spiked at each location as the SBF passed through (Figure 2.13). A horizontal contour analysis of O₃ concentrations revealed a front-parallel region of highly polluted air moving inland with the SBF. From additional case-studies in the same region it became apparent that higher ground-level O₃ levels occurred on days when the SBF was associated with well-defined low-level

convergence. The *highest* O₃ levels occurred when the SBF moved inland and merged with the APLT [Gaza, 1998].

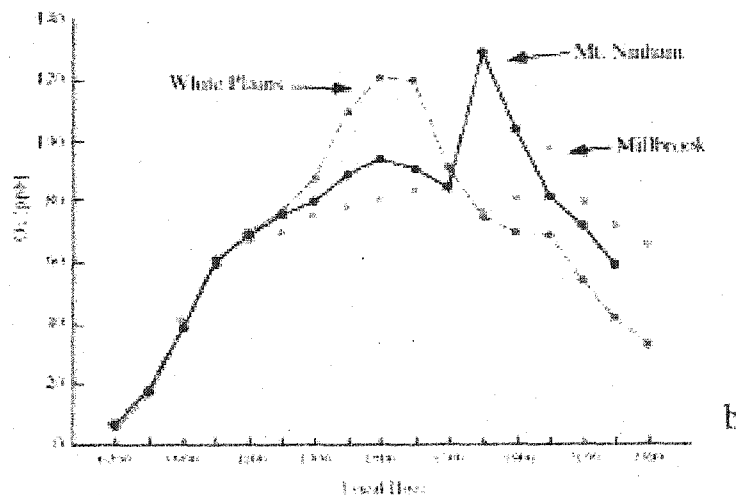
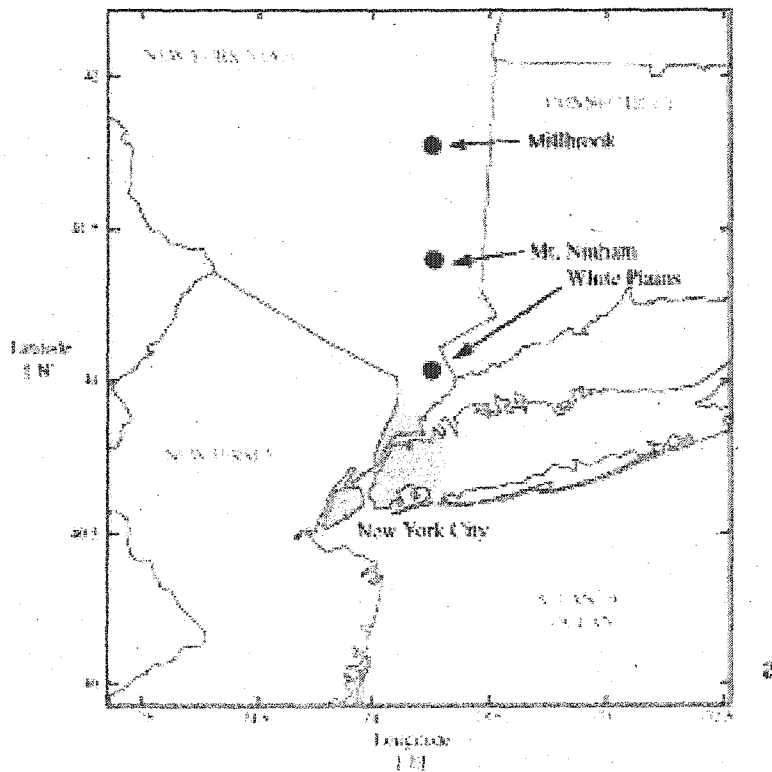


Figure 2.13: Ground-level O₃ concentration levels at three stations north of New York City. a) Locations of O₃ monitors in southern New York State ; b) Time-series of O₃ concentrations -- note "spikes" as the SBF passes successively further inland. Based on hourly O₃ observations, July, 1995. [After Gaza, 1998.]

Summary

The sea breeze is a mesoscale wind that occurs at many coastal locations throughout the world. It develops when solar radiation and the differing rates at which land and water change temperature create a mesoscale pressure gradient force pointing toward the land. Cool marine air moves toward the land as a gravity current, is lifted vertically at the sea-breeze front, and often forms a closed circuit via a return flow aloft and a diffuse region of descending currents several tens of kilometers out to sea.

There are historical records documenting human understanding of the sea-breeze system going back almost 2,500 years, and it is still a rapidly evolving field. The SBS has been intensely studied since the beginning of the 20th Century, and more than 500 new papers have been published on the subject since 1990 alone, describing research using surface observations, balloon soundings of various kinds, aircraft, radar, lidar, and computer models. Modern researchers have been motivated by its influence on local wind velocity and air quality, convective activity, and other aspects of its dynamics and structure. Others have studied the sea breeze's influence on the coastal ocean and beaches. These authors have found that the SBS is a highly complex collection of nested

phenomena, ranging in size from near-synoptic to microscale. The SBS consists not only of the mesoscale sea-breeze circulation (SBC), crudely described by the Bjerknes circulation theorem, but sound waves and other transitory wave-like phenomena that either initiate or are initiated by non-linear responses of the atmosphere to diabatic heating. The SBC itself, sometimes called the sea breeze proper, is distorted by non-zero ambient flow, forming helical circulations with both cross- and along-shore components. The SBC may not be a closed (mass-conservative) circulation.

The sea-breeze gravity current (SBG) is the low-level landward flow of cool, moist marine air. The leading edge of the SBG is usually marked by a sea-breeze frontal zone (SBF) that resembles a synoptic-scale cold front. The SBF may be bifurcated into a thermodynamic front and a kinematic front, where the former is the leading edge of the marine air's influence, and the latter is the point of maximum low-level convergence between the marine and continental airmasses. Strong vertical currents are associated with the front, creating a raised sea-breeze head (SBH) above the SBF that may reach twice the height (up to 2200 meters) of the feeder flow behind the SBF. The SBF and a vertically-rotating post-frontal vortex within the marine airmass can sometimes separate from the

feeder flow, and move inland independently as an undular bore.

The most dramatic example of this is the Australian Morning Glory.

Along the upper boundary of the SBG, Kelvin-Helmholtz Billows (KHBs) develop when the Richardson number is smaller than about 0.25. Sea-breeze related KHBs have wavelengths between 500 and 1000 meters, and are responsible for mixing the two airmasses in the turbulent wake zone behind the SBH. KHBs also generate a friction-like force along the top of the SBG that slows its inland progression during mid-day. A number of other instability phenomena can interact with the SBS, including vertical convection cells and horizontal convective rolls within the continental airmass.

Forecasting the sea-breeze is a three-part problem, consisting of 1) a simple yes/no for the shoreline, 2) determining the wind speed and direction behind the SBF, and 3) determining how far inland the sea breeze will penetrate. A simple index comparing the offshore wind component within the continental airmass to the magnitude of the cross-shore temperature gradient is very effective at answering the first question. The wind speed associated with the sea breeze can be calculated by a number of different methods, all of which are also dependent on the cross-shore temperature gradient, and the wind direction can be determined by an equation that accounts for rotation of the SBC under the Coriolis force, net

along-shore wind component, and synoptic-scale PGF. In the absence of the latter two, the entire SBC, and therefore the wind direction, will rotate anticyclonically over time. Determining the extent of the SBC's inland penetration is a complex problem, dependent on land-sea temperature contrast, the Coriolis force, surface and top friction, stability, and other factors. While theoretical relationships exist to determine the maximum possible inland penetration, accurate forecasts are still dependent on a field study for the site in question.

The sea breeze exerts both direct and indirect controls on the fate of pollutants released into the coastal atmosphere. Examples of direct controls are the landward transport of pollutants by elements of the SBS, trapping and concentration of pollutants in shallow Convective Internal Boundary Layers, and replacement of polluted continental air with relatively clean marine air. The east coast of the United States is the site of a more complex air pollution problem, involving the sea breeze and a larger mesoscale trough that forms east of the Appalachian Mountains. A significant portion of the world's population resides in coastal areas, often side by side with industrial sites, ensuring that the sea breeze will be the subject of increasingly sophisticated research for some time to come.

CHAPTER III

SYNOPTIC-SCALE CONTROLS ON THE SEA BREEZE OF THE CENTRAL NEW ENGLAND COAST

This chapter has been published in *Weather and Forecasting*.

CHAPTER III

SYNOPTIC-SCALE CONTROLS ON THE SEA BREEZE OF THE CENTRAL NEW ENGLAND COAST

ABSTRACT

Using routinely-available hourly surface observations and United States surface analyses for 2001, a method was developed for predicting sea-breeze events. The method is adaptable to any coastal region in the world where surface data are available. Specific prediction guidelines were developed using Portsmouth, New Hampshire as the forecast site. Using the Portsmouth METAR, 167 days were determined to have conditions favorable for the occurrence of a sea breeze. Each of these 167 days were classified as either sea-breeze, marginal, and non-sea-breeze events. Sea breezes were defined as insolation-driven local on-shore winds. Marginal events were weak sea breezes. Non-sea-breeze events were those days where sufficient insolation was present, but failed to produce a seabreeze at Portsmouth. The surface analyses for these 167 days were used to define a set of synoptic classes based on the arrangement of large-scale pressure systems, and meaningful interpretations resulted. For example, sea breezes and marginals account for almost 80 percent of one class, while two other classes produced no seabreeze events. Standard surface observations were used to calculate the meso- α -scale cross-shore potential temperature gradient ($\delta\theta/\delta x$) and the cross-shore geostrophic wind component (u_G) for the hour of onset (sea-breeze and marginal events) or of peak heating (non-sea-breeze events). Stronger negative $\delta\theta/\delta x$ values were needed to develop a sea breeze in the presence of stronger positive u_G values. The six well-defined synoptic classes were plotted as a function of $\delta\theta/\delta x$ and u_G , and occupy specific regions of the resulting diagram.

Introduction

The sea breeze is an important influence on New England's weather, climate, and air quality. The associated moisture can be responsible for creating fog near dawn, and for fueling afternoon convection at points well inland of the coast. Furthermore, the thermal internal boundary layer (TIBL) that forms within the marine airmass often traps pollutants in a shallow layer near Earth's surface, reducing air quality in the coastal zone [Hsu, 1988]. In New England, sea breezes have been shown to foster high tropospheric ozone [Gaza, 1998; Seaman and Michelson, 2000] and high sulfur dioxide episodes [Barbato, 1975]. For these reasons it would be useful to understand the meteorological conditions conducive to sea breeze development in New England, and how these conditions vary with the synoptic-scale meteorological environment.

Research on the New England sea breeze was carried out as part of the Atmospheric Investigation, Regional Modeling, Analysis, and Prediction (AIRMAP) project. AIRMAP's goal is to understand factors influencing New England's climate and air quality. The goal of the Central New England Sea Breeze Study is to understand (and therefore be able to predict) the physical behavior of the sea breeze on the central New England coast, including its inland extent,

vertical depth, and frontal characteristics. This chapter focuses on the synoptic-scale surface environment in which the sea breeze develops.

Pertinent Literature

Some of the early work with New England sea breezes was carried out by *Craig et al.* [1945]. They used psychrometric data recorded by balloons and aircraft along an east-west transect in Massachusetts Bay, and were able to document the characteristic raised-head wave structure later shown in much greater detail by *Simpson* [1994; 1997]. *Fisher* [1960] used vertical profiles along a cross-shore transect near Block Island, Rhode Island, to document the rotation of sea breezes by the Coriolis force. The Coriolis-induced rotation was later studied analytically by *Neumann* [1977]. *Frizolla and Fisher* [1963] used pilot balloons to study sea breezes in the New York City area, finding that the opposing (continental) flow caused the leading edge of sea breezes to take on frontal characteristics, and that the associated marine airmass was shallower in events with stronger opposing winds. *Simpson and Linden* [1989] showed that frontogenesis was a general feature in horizontal density currents such as sea breezes, and a number of

subsequent studies [e.g. *Kraus et al.*, 1990; *Reible et al.*, 1993] specifically examined sea-breeze frontogenesis. All of the latter referenced earlier theoretical work by *Miller* [1948].

Perhaps the most comprehensive observational study of sea breezes in New England was completed by *Barbato* [1975], who focused on forty 1972 sea-breeze events in the Boston, Massachusetts area. *Barbato* determined that sea breezes penetrated as far as 29 kilometers inland, but were usually restricted to the bowl-shaped Boston basin region closer to the coastal zone. Using radiosonde data from eight sea-breeze events, it was found that the marine airmass varied in depth from 330 to 2230 meters. He also found that sea-breeze events often significantly reduced air quality, particularly with respect to sulfur dioxide (SO₂).

Gaza [1998] identified the sea breeze as an important factor in a July, 1995 tropospheric ozone (O₃) pollution event in southern New England and New York State. *Pagnotti* [1987] identified the Appalachian Leaside Trough (APLT) as a contributor to high ozone concentrations in the northeastern United States, and *Seaman and Michelson* [2000] discussed the interaction of the APLT, the sea breeze, and several synoptic-scale features during high ozone events documented in NARSTO-Northeast 1995.

The Kennedy Space Center, in east-central Florida, has also been the site of numerous sea breeze studies. Of interest to this work are the numerical studies carried out by *Zhong and Takle* [1993], who modeled the effects of large-scale (synoptic) wind flow on meso- and micro-scale aspects of the sea breeze. They grouped sea breezes into two types, where the first corresponded to large-scale flow that was either perpendicular (eastward) or anti-parallel (southward) to the east Florida coastline, and the second corresponded to large-scale flow that was either anti-perpendicular (westward) or parallel (northward) to the east Florida coastline. The two general classes of sea breezes differed in many respects, including the associated maximum vertical velocities.

Methods

It would be particularly useful to identify days when sea breezes occurred, and compare them to synoptically-similar days when sea breezes did *not* occur. The comparison might include general groupings of the arrangement of synoptic-scale pressure systems in the Northeast, and the resulting cross-shore potential temperature gradients and cross-shore geostrophic wind components. The cross-shore potential temperature gradient is a

measure of the density contrast driving the sea breeze, and the cross-shore surface geostrophic wind component is a measure of the synoptic-scale movement of mass that opposes the sea breeze's inland propagation. For this comparison to be possible, a relatively simple and accurate means of identifying the dates of sea breeze events is needed.

Pease Air National Guard Base's (KPSM; see Figure 3.1) weather observations were used to identify sea-breeze events. Pease is in Portsmouth, New Hampshire. Pease also happens to be in a relatively central location on the study area's coastline, is equipped with top-of-the-line weather equipment, and is operated 24/7 by a human weather observer -- not an Automated Surface Observing System (ASOS). Because of these points, it was assumed that Pease's hourly observation records are satisfactory for identifying sea-breeze events throughout the study area's coastal zone. It was also assumed that the influences of the Great Bay, which surrounds Pease on two sides, and the Piscataqua River, to the north of the airfield, are small compared to that of the Atlantic Ocean.

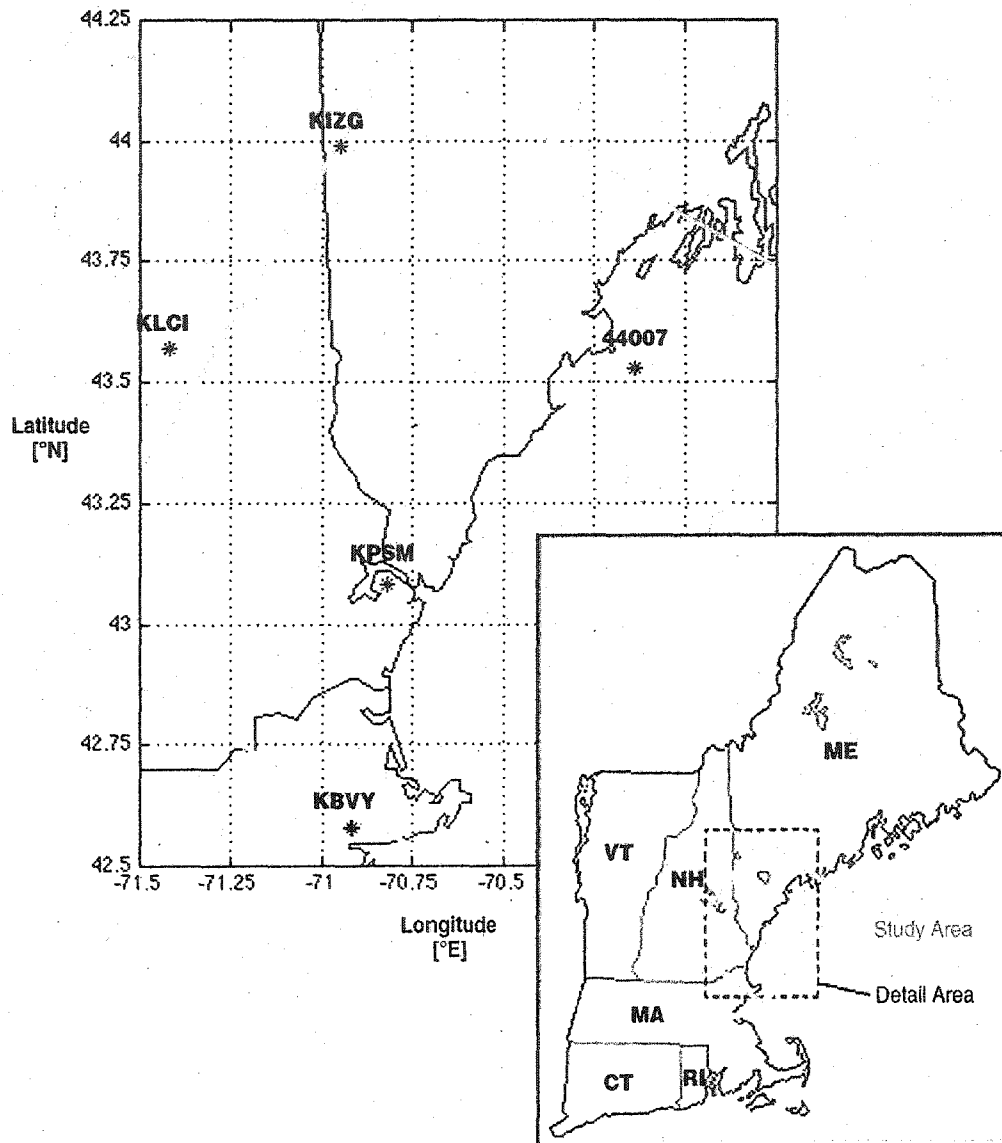


Figure 3.1: Study area and location map. Gray line indicates edges of the study area. Surface weather observing stations shown are Fryeburg, Maine (KIZG); the Portland, Maine Buoy (44007); Portsmouth, New Hampshire (KPSM); Beverly, Massachusetts (KBVY); and Laconia, New Hampshire (KLCI).

While the sea breeze is often easily identifiable by sharp wind, temperature and humidity changes marking its arrival, experience in

weather observation has shown that it is occasionally an ambiguous event. One kind of ambiguity is the initial occurrence of a southeasterly wind that has nothing to do with a sea breeze, to which a sea breeze is added later in the day. Other kinds of ambiguity are a very weak seabreeze developing late in the afternoon, or of very short duration, or lacking one or more of the defining characteristics noted above.

With this in mind, nomenclature for three different "event" definitions was developed:

- A *sea-breeze event* occurs when the surface wind in the study area is from some direction other than the southeast at the beginning of the day, shifts to the southeast during mid-day, then shifts to another direction in the evening. (Any wind between 95 degrees and 174 degrees is considered southeasterly, although the sea breeze at Pease generally comes from 130 degrees.) The shift to a southeasterly wind must not be associated with a synoptic-scale pressure system. The observed sky conditions should be characterized by less than "broken" (BKN; 5/8 sky cover or more) cloud coverage in the low (surface to 1981 meters above ground level) and middle (1981 to 7010 meters) etages, on the assumptions that the local temperature contrast driving the seabreeze cell is

powered by insolation, and that high-etape (higher than 5029 meters) clouds are generally thin and do not significantly reduce insolation. (Sky cover contractions are defined in AFM 15-111, 1998; see *WMO*, 1956 for cloud etages.)

- A *non-sea-breeze event* is one where the background conditions resemble those of seabreeze event, except that the daytime windshift to the southeast does not occur.
- A *marginal event* is one where the sea breeze occurs at Portsmouth, but is either very short-lived (two hours or less), is marked by very light wind speeds, or merely manifests as a short interval of "light and variable" winds during a period of sustained wind from a non-southeasterly direction.

Days when the wind was already from the southeast at sunrise were excluded from this study. While it seems likely that the sea breeze can supplement a synoptically-driven southeasterly wind, it was decided to reserve this kind of event for later studies.

Event Identification

The KPSM Surface Weather Observations form was used to provisionally identify all sea-breeze, marginal, and non-sea-breeze events for the calendar year 2001 (January - December). Sea breezes and marginal events were identified using the following tests:

1. Surface wind at Pease was from the northwest, northeast, southwest or "variable" (only if associated with "light" winds) for the majority of the early morning hours prior to the onset of the seabreeze. (Light winds are defined as "6 knots or less" in AFM 15-111, 1998.)
2. Wind direction changed to southeast (usually 130 degrees true, but any direction between 95 and 174 degrees was allowable) after onset, lasting more than two hours. (Two hours or less was classified as a "marginal" event.) Sea-breeze-associated southeasterly winds were differentiated from synoptically-driven southeasterly winds using the following criteria:

2.1. Sea breezes manifest at Pease as either a "sudden" shift (occurring over a period of several minutes) in wind direction to the southeast, or, as a prolonged transition from steady winds out of the synoptically-driven wind direction (e.g. northwest), followed by a one-two hour period of light and variable winds (speed less than seven knots, possibly with direction reported as "variable" by the observer), then shifting to a steady southeasterly direction.

2.2. Onshore winds not associated with sea breezes were identified as those where the wind direction gradually shifted to a southeasterly direction over a period of several hours, coincident with an observed sky condition (cloud cover) and/or other weather phenomena indicative of an approaching synoptic-scale system, such as shields of "invading" high cloud, systematically increasing middle-etaage or low-etaage clouds, or non-showery precipitation. (See *WMO*, 1956, for descriptions of low-, mid-, and high-etaage clouds.)

3. The wind direction returned to northwest, northeast, southwest or variable following the end of the seabreeze event.

4. There was less than BKN cloud cover in both the low and middle etages prior to onset. This was chosen because the physical mechanism driving the sea breeze is insolation and differential surface heating in the coastal zone, and BKN or greater coverage in the low and middle etages was assumed to significantly reduce surface insolation. Total high cloud coverage was excluded because of the assumption that high clouds are generally thin and do not usually reduce insolation significantly.

5. There was no "significant" precipitation (one or two brief, light showers, encoded -SHRA, were permissible) within the six-hour period prior to onset of the seabreeze. (We relied on the observer's assigned intensity to identify "light" rainshowers; see AFM 15-111 for a precise description of how these intensities are assigned. "Brief " means "minutes rather than hours.") In the event that the southeasterly wind might have been synoptically-driven by a fast-moving system that was undetected by the checks listed in 1 - 4, significant precipitation prior to onset of the southeasterly wind could serve as an additional indication that it is not necessarily associated with local-scale differential heating.

Once the sea-breeze and marginal events were provisionally identified from the KPSM observations, the National Weather Service (NWS) United States surface analyses charts for 1200 UTC (0700 LST) on these days were downloaded from either the National Virtual Data System (NVDS) webpage (January - October; see http://nndc.noaa.gov/?http://ols.ncdc.noaa.gov/cgi-bin/nndc/buyOL-006.cgi?FNC=chart_Ancep_get_chart_htm) or the NWS Fax FTP site (November and December; see <ftp://weather.noaa.gov/fax/>). These were then examined for the direction of the geostrophic wind in the study area. If the surface analysis for the event in question suggested that the southeasterly wind was caused by synoptic-scale circulation, the event was removed from consideration altogether, *i.e.*, not classified as a sea-breeze, marginal, or non-sea-breeze (see below) event.

"Non-sea-breeze events" were identified using tests 1, 4, and 5, above. Surface analyses for 1200 UTC on these days were also downloaded from either the NVDS website or the NWS FTP site. If the event "passed" the sea breeze tests outlined in tests 1, 4, and 5, but no sea breeze occurred, it was classified as a non-sea-breeze event.

A total of 59 sea-breeze events, 10 marginal events, and 98 non-sea-breeze events were identified. (For a complete list of these, see Appendix 4.)

Definition of Synoptic Classes

Zhong and Takle [1993], among others, demonstrate that the arrangement of synoptic-scale features, and the resulting geostrophic wind are important controls on sea-breeze behavior. For example, a synoptically-driven northwesterly wind would probably cause very different sea-breeze behavior in our study area (Figure 3.1) than would a shore-parallel southwesterly wind.

The 1200 UTC surface charts for the 167 sea-breeze-favorable days were parsed according to the general direction of the geostrophic wind over the study area, as implied by surface isobars:

Group A. Northwesterly (271 through 360 degrees true), *i.e.*, having a significant component perpendicular to the coastline.

Group B. Southwesterly (180 through 270 degrees true), *i.e.*, the largest component of the wind is parallel to the coastline.

Group C. Northeasterly (001 through 090 degrees true), *i.e.*, the largest component of the wind is anti-parallel to the coastline.

Any days with synoptic-scale geostrophic winds from the southeast quadrant would have by definition been excluded from the analysis (see above), though no cases occurred.

A second screening was made that further refined groups A and B. This led to three sub-categories for the group A cases (total of 93), called classes 1, 2, and 3:

Class 1 (Figure 3.2). An areally large, well-defined high pressure cell is generally located somewhere to the west of the study area. The curvature of the isobars over the study area is anticyclonic, meaning that the lower atmosphere is dynamically stable. (25 cases.)

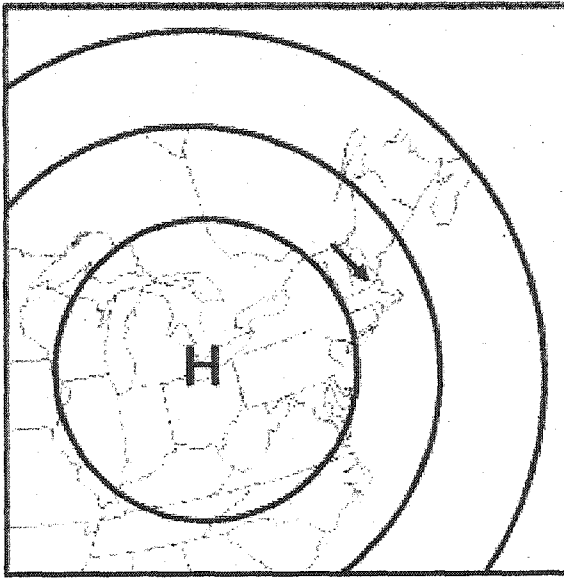


Figure 3.2: Synoptic Class 1. Westerly to northerly geostrophic wind over the study area. A large high (or open ridge) dominates the region. Surface isobars are anticyclonically curved.

Class 2 (Figure 3.3). A somewhat weaker high pressure cell (or open surface ridge) is generally to the south or west of the study area, and a weak low pressure area (cell or trough) is to the north or east. Neither system dominates, and the resulting isobaric curvature is either very slight or neutral. (51 cases.)

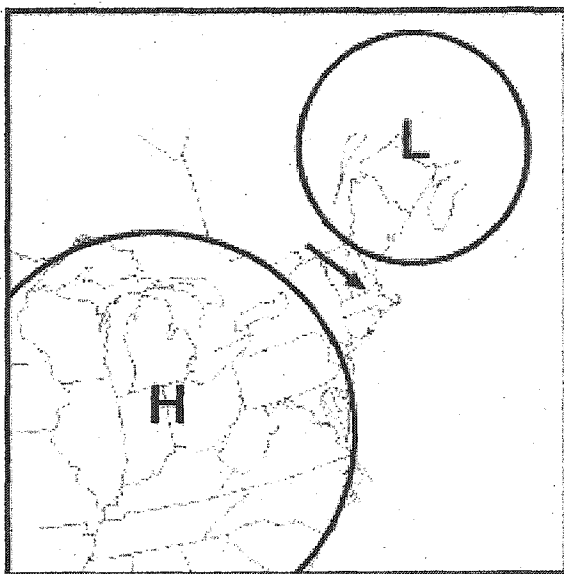


Figure 3.3: Synoptic Class 2. Westerly to northerly geostrophic wind over the study area. A weak high (or open ridge) shares dominance of the region with a weak low (or open trough). Surface isobars have no significant curvature.

Class 3 (Figure 3.4). A strong low pressure cell is located to the northeast, and dominates the study area. The surface isobars are cyclonically curved, meaning that the lower atmosphere is dynamically unstable. (17 cases.)

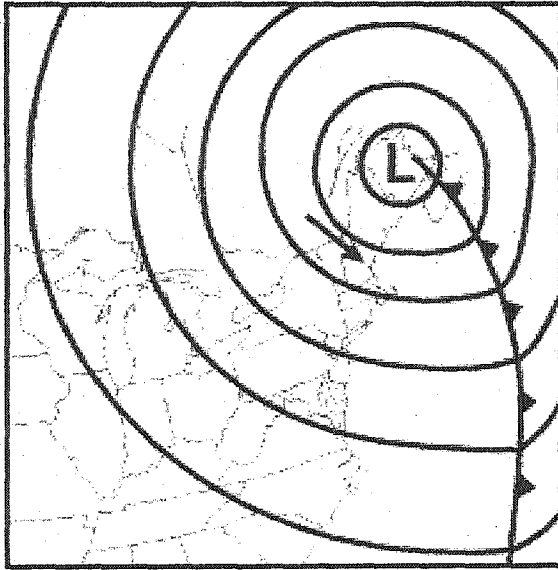


Figure 3.4: Synoptic Class 3. Westerly to northerly geostrophic wind over the study area. A large low dominates the region. Surface isobars are cyclonically curved.

All three of these resulted in a northwesterly geostrophic wind in the study area. Group B (38 cases) was sub-divided into two smaller groups, called classes 4 and 5:

Class 4 (Figure 3.5). A large high pressure cell is located in the southeastern United States, and a low is located either in the upper midwest, Great Lakes, or the southern Hudson Bay region, with or without a front extending into the central part of the United States. The isobars over the study area are either anti-cyclonically or cyclonically curved, but the former tends to dominate. This class

includes two situations which are similar in appearance on a surface chart, but dynamically quite different. These are described below.

(31 cases.)

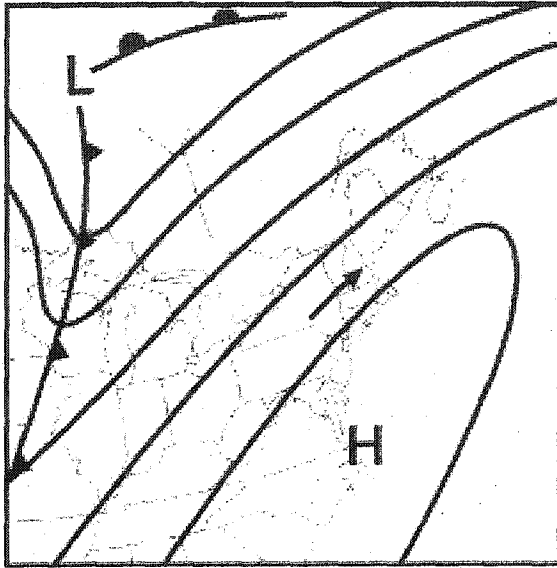


Figure 3.5: Synoptic Class 4. Pre-frontal southerly to westerly geostrophic wind over the study area. A high (or open ridge) is located south of the study area, and a low with associated trough (or front) is to the west. This class also includes the circumstance where the isobar closest to the high center in the southeast does not wrap back around the eastern side of the high. (See text for additional details).

Class 5 (Figure 3.6). A southwesterly geostrophic wind follows the passage of a mature frontal system, with a low to the west of the study area and a weak ridge immediately to the east (and immediately behind a cold or occluded front). (7 cases.)

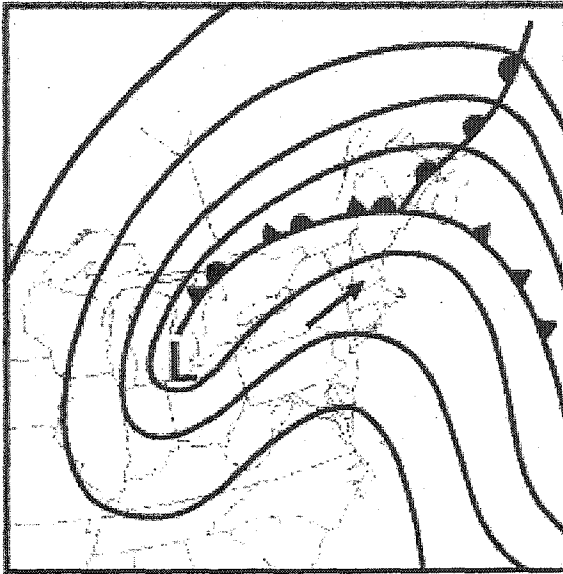


Figure 3.6: Synoptic Class 5. Post-frontal southerly to westerly geostrophic wind over the study area. A low with associated trough (or front) is to the west, a weak ridge is immediately to the east, and a front is further east.

Group C, renamed class 6 for consistency, tends to be fairly uniform in terms of the arrangement of synoptic features, and is not further subdivided. In general, synoptic class 6 (Figure 3.7) is associated with a high (or northeastward tilting ridge) to the northwest and a low (or frontal system) to the southeast of the study area. (31 cases.)

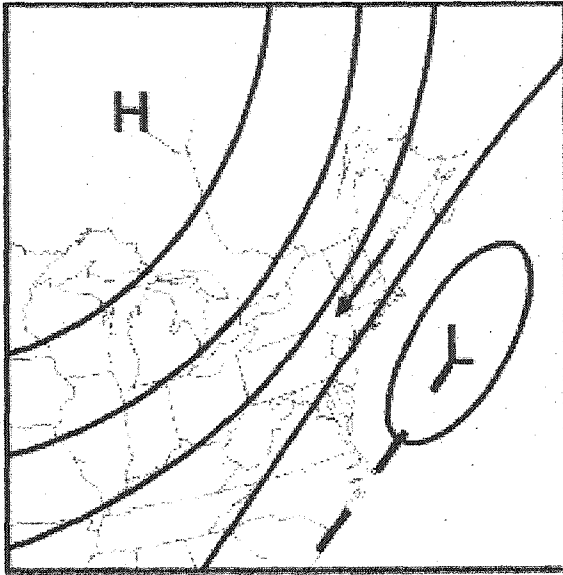


Figure 3.7: Synoptic Class 6. Northerly to easterly geostrophic wind over the study area. A high (or northeastward-tilting open ridge) is located to the northwest, and a low (or open trough) is to the southeast.

There were five cases that did not fit any of the above classes, and these were grouped together into class 7 -- miscellaneous. No further breakdown was made of this class.

Table 3.1 summarizes the occurrences of the synoptic classes and their associated percentages of the total. Figs. 3.2 - 3.7 illustrate the general configuration of surface synoptic pressure systems associated with each class.

Table 3.1: Occurrences of synoptic classes and associated percentages of all occurrences.

Group	Synoptic Class	Number of cases	Percentage of total
A	1	25	15.0
	2	51	30.5
	3	17	10.2
	1, 2, and 3 combined	93	55.7
B	4	31	18.6
	5	7	4.2
	4 and 5 combined	38	22.8
C	6	31	18.6
Miscellaneous	7	5	3.0
	All	167	

Synoptic Classes Associated With Sea-Breeze, Marginal, And Non-Sea-Breeze Events

The occurrences of the sea-breeze, marginal, and non-sea-breeze events were compared to the synoptic classes described in Figs. 3.2 - 3.7 (Table 3.2). A χ^2 calculation indicates rejecting the null hypothesis ($p < 0.05$). Rejecting the null hypothesis indicates that the distribution of events in the table is non-random, and is therefore associated with synoptic class. (For more about the χ^2 , see Johnson [1992], or Clark and Hosking [1986].)

Table 3.2: Comparison of sea-breeze, marginal, and non-sea-breeze events to synoptic classes.

Synoptic Class	Sea-Breeze Events	Marginal Events	Non-Sea-Breeze Events	All Events
1	15	2	8	25
2	9	3	39	51
3	0	0	17	17
4	12	2	17	31
5	0	0	7	7
6	21	3	7	31
7	2	0	3	5

The sea-breeze/non-sea-breeze event distribution evolves gradually over the first three classes. Out of the 25 class 1 cases, 60 percent resulted in the occurrence of a sea breeze. Class 2 (the largest of the seven) is distributed between sea breezes, marginals, and non-sea breezes, with non-sea breezes dominating (76 percent). Class 3 cases are exclusively associated with non-sea breezes. It is proposed that this distribution arises from a combination of the cross-shore geostrophic wind component (u_G) and the magnitude of the cold-air advection associated with the low-level flow. Large values of either are likely to prevent a seabreeze. (This is examined in somewhat more detail below.)

If marginal events are grouped with sea-breeze events, the distribution is almost evenly divided in class 4. A possible reason for this bifurcation is that class 4 includes two situations that are

superficially similar in appearance, but quite different in origin. In the first situation, the high to the south of New England is a migratory anticyclone associated with a modified continental polar airmass. (Southwesterly flow in the study area precedes the passage of a frontal system.) In the second situation, the high is an extension of the semi-permanent subtropical ridge, and is associated with a maritime tropical airmass. (Southwesterly winds in the study area result from the flow around the western extent of the Bermuda High.) The cross-shore temperature gradient, and therefore the density contrast that drives the seabreeze in the study area, would be different in these two situations. In the former, cool, dry air would be on the land side, and -- given a relatively cool sea-surface temperature -- the land-sea temperature gradient would be weak. In the latter, warm, moist air would be on the land side, and the driving force for a sea breeze would be strong.

As with class 3, class 5 is exclusively non-sea breezes. Once again, this distribution probably arises from the magnitude of u_g and cross-shore cold-air advection associated with the synoptic-scale systems. Almost 70 percent of class 6 cases (21 of 31 total cases) are sea-breeze events, with the remaining 30 percent distributed among the marginal and non-sea-breezes events. The

class 7 cases probably do not represent any meaningful physical information, as this is a miscellaneous category.

Meso- α -Scale Temperature Gradients And Geostrophic Wind

To explain the distribution of synoptic-scale forcing and sea-breeze events described above, the cross-shore potential temperature gradient ($\delta\theta/\delta x$) that gives rise to the sea breeze was compared to the cross-shore geostrophic wind component (u_G) that resists the inland penetration of the sea breeze. This method is similar to one developed by *Simpson* [1994] for Thorney Island, in the United Kingdom.

Meso- α -scale (200 - 2000 kms; *Fujita* [1986]) calculations were completed for all 167 events, using reported sea-level equivalent pressures (SLP) and air temperatures reported by four widely separated stations (Figure 3.1). The four stations were chosen to represent the thermal and pressure forcing near the edges of "the box" defining the study area in the north-south and east-west directions. It was assumed that the Fryeburg-Beverly (KIZG-KBVY) differences sufficiently represented the north-south gradients, and

the Portland-Laconia (44007-KLCI) differences sufficiently represented the east-west gradients.

Sea-level pressures and the mean latitude of the four stations (43.4175 °N) were used to calculate the two components of the geostrophic wind. Reported air temperatures were converted to potential temperatures using station elevations and an exponential vertical pressure function (to estimate the station pressure from SLP), then the potential temperature gradients were estimated using first-order finite differences [Carnahan *et al.*, 1990]. These gradients were deliberately estimated using a linear method, and could no doubt be improved with more sophisticated techniques. Equivalent geostrophic wind and potential temperature gradient components were then determined for a coordinate system rotated 30 degrees. This rotation was introduced because the coastline in the study area, if estimated by a straight line, is approximately 30 degrees clockwise from north. Rotating the vector components results in a cross-shore component x' that points toward 120 degrees true, and an along-shore component y' that points toward 30 degrees true. The result was a set of meso- α cross-shore and along-shore geostrophic wind (u_G, v_G) and potential temperature gradients ($\delta\theta/\delta x, \delta\theta/\delta y$).

The date and synoptic class associated with each event were cross-referenced with $\delta\theta/\delta x$ and u_G (the cross-shore components) for either the hour closest to the onset of the event (for sea-breeze and marginals) or 1400 LST (for non-sea-breeze events). The choice of 1400 LST was chosen for the latter group because this approximately coincides with the time of peak surface heating and maximum diurnal land-sea temperature contrast. Figures 3.8 through 3.14 illustrate results of these comparisons.

General Discussion. Figure 3.8 (called the Nowcast Diagram) shows that it takes stronger $\delta\theta/\delta x$ to overcome stronger u_G , and initiate a sea breeze detectable at Pease. Line A shows the critical limits that are needed for both independent variables to prevent a sea breeze from overcoming an opposing synoptically-driven wind. In the region above or to the right of A, $\delta\theta/\delta x$ is too weak to overcome the opposing u_G . Line B defines the critical limits below which a sea breeze will always occur. In the region below or to the left of B, u_G is either *onshore* or too weak to prevent $\delta\theta/\delta x$ from initiating a sea breeze. Most of the marginal events (with three exceptions) lie in the cross-over region between A and B. Line C defines what appears to be a cutoff value in the geostrophic wind:

No sea-breeze events occurred with u_g greater than about 12 ms^{-1} ,
or 25 knots.

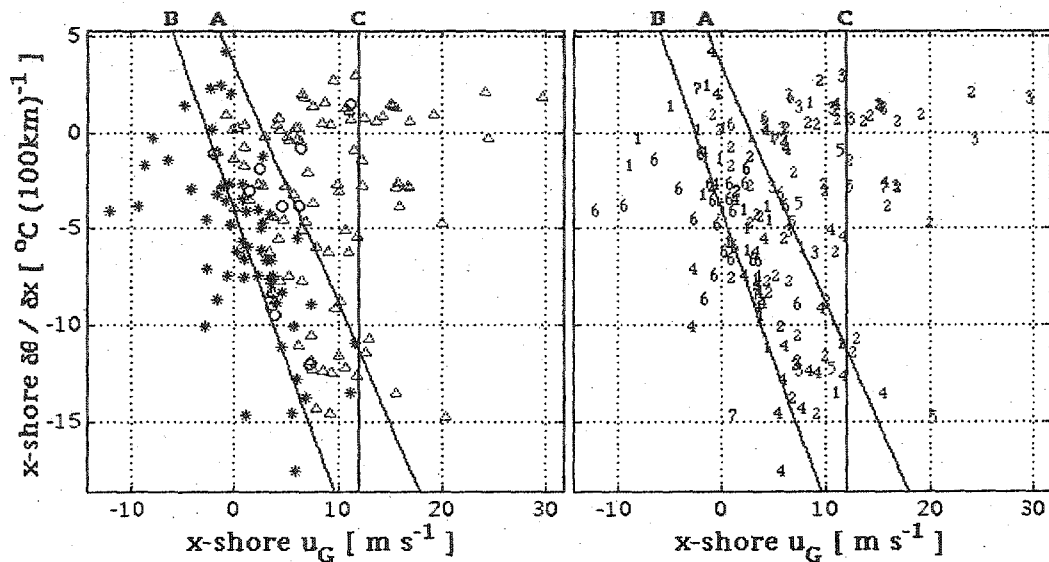


Figure 3.8: Nowcast Diagram. Left-hand panel: All sea-breeze, marginal, and non-sea-breeze events as a function of their associated cross-shore meso- α potential temperature gradients and geostrophic wind components. Events are plotted using the meso- α temperature gradients and geostrophic wind components present at either the time of onset (for sea breezes and marginals), or 1400 LST (for non-sea breezes). Sea-breeze events are depicted with a blue star (*), marginal events with a black circle (o), and non-seabreezes with a red delta (Δ). Right-hand panel: Synoptic classes of sea-breeze, marginal, and non-sea-breeze events. Sea-breeze events are depicted with a blue text, marginal events with black text, and non-sea breezes with red text.

Note that along line A, u_G is 3 ms^{-1} where $\delta\theta/\delta x$ is zero. This indicates that, in the absence of a favorable meso- α cross-shore potential temperature contrast, the sea breeze can still overcome a "light" opposing wind (as defined in AFM 15-111, 1998). A related

observation is that sea-breeze events can occur even if $\delta\theta/\delta x$ is in the wrong direction, *i.e.*, indicating warmer air offshore rather than on land. This suggests that, under certain circumstances, favorable cross-shore temperature gradients develop in the immediate coastal zone that are not detected by this meso- α -scale calculation.

Figure 3.8 (right-hand panel) also shows the synoptic classes associated with the sea-breeze, marginal, and non-sea-breeze events. Beginning with the lower left, it is apparent that the strongest sea breezes are associated with synoptic classes 4 and 6. This is entirely reasonable given that these two were initially defined as situations where the isobars indicated a relatively weak u_G . In the upper right corner, one finds that the strongest non-sea-breeze events are mostly associated with synoptic classes 2 and 3, with 3 marking the extreme limit. Once again, this is reasonable because class 3 was defined as a scenario where the study area is dominated by northwesterly winds on the cold side of an intense low pressure system. Such a location is subject to very strong northwesterly winds and strong cold air advection, neither of which are conducive to the formation of a sea breeze. Similar arguments hold for the scenario defining class 2.

Classes 1, 2, and 3. Figure 3.9 (left-hand panel) shows that most of the sea-breeze and marginal events associated with synoptic classes 1 and 2 lie within the cross-over region between lines A and B. Very few occur to the left side of the diagram, where u_G is -5 ms^{-1} or less, and none of them reach as far toward the lower left corner as do the class 4- and 6-associated sea-breeze events noted in Figure 3.8. Because of the associated $\delta\theta/\delta x$ and u_G values, class 1- and 2-associated sea-breeze events should range from slow-moving, thermally-strong systems (bottom center) to relatively fast-moving, thermally-weak systems (upper left). The large span of these three synoptic classes on the $\delta\theta/\delta x$ axis indicates that these classes, and their associated sea-breeze and marginal events, can occur over a very wide range of temperature regimes, and therefore, over a wide seasonal range.

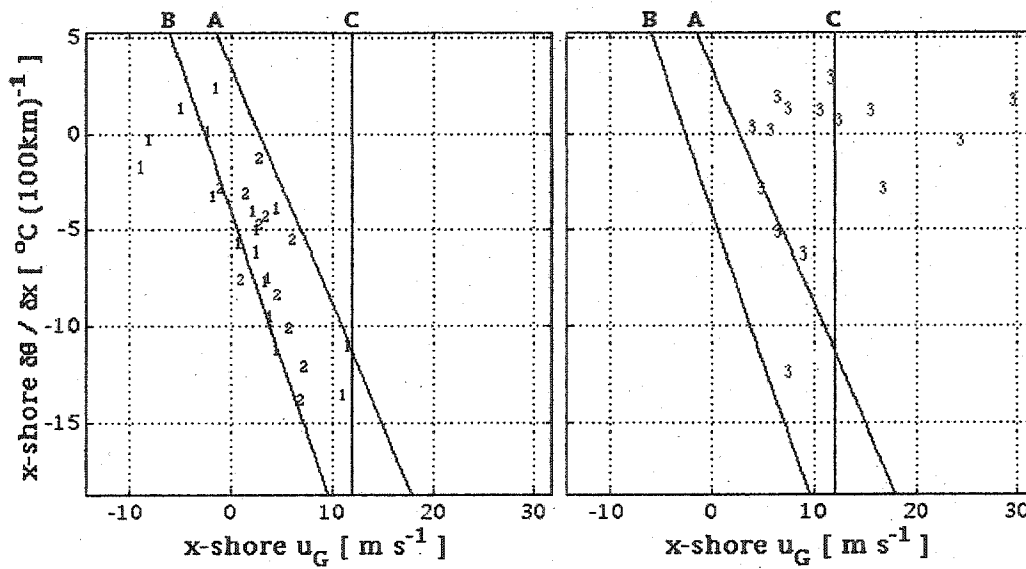


Figure 3.9: Nowcast Diagram for Synoptic Classes 1, 2, and 3. Left-hand panel: Sea-breeze and marginal events associated with class 1 and class 2 cases. Right-hand panel: Non-sea-breeze events associated with class 3 cases. Axes and color-coding of events are as described for Figure 3.8.

Non-sea-breeze events extend in a triangle-shaped region from the left edge of the cross-over region to the upper right corner of the diagram, indicating that the highest values of u_G are associated with positive $\delta\theta/\delta x$, *i.e.*, with colder air over land and warmer air over the sea-surface, and therefore not favorable for the formation of a sea breeze. Figure 3.9 (right-hand panel) shows that most of the class 3 cases (all associated with non-sea-breeze events) occur in the upper right quadrant of the diagram, where the temperature gradient and geostrophic wind conditions are least favorable for

sea-breeze formation. One would expect that the class 3 cases would primarily occur during winter, when the long wave trough and Polar Jet over the eastern half of the country have a high amplitude, rendering the New England region subject to the passage of intense baroclinic cyclones.

Figure 3.10 (left-hand panel) shows the dates associated with sea-breeze and marginal events coincident with synoptic classes 1 and 2. Note that the dates span the calendar from mid-February through late November. A seasonal pattern also emerges, with most summer events appearing in the lower half of the diagram -- in the region of highly-favorable $\delta\theta/\delta x$ -- and all of "non-summer" events appearing in the upper half -- in the region of weak or reversed $\delta\theta/\delta x$. This indicates that, in general, sea breezes can occur with larger opposing u_G in summer than during other seasons. Of particular interest are two February events, one October event, and one November event toward the upper left, with unfavorable $\delta\theta/\delta x$ values, but weak to negative u_G values. There are (at least) two possible explanations for this: 1) these events were mischaracterized as sea-breeze events, or, 2) the sea breezes were driven by local-scale temperature gradients that were too small (confined within a narrow zone immediately adjacent to the

shoreline) to register in the meso- α -scale calculation used here. The second possibility will be examined in subsequent research.

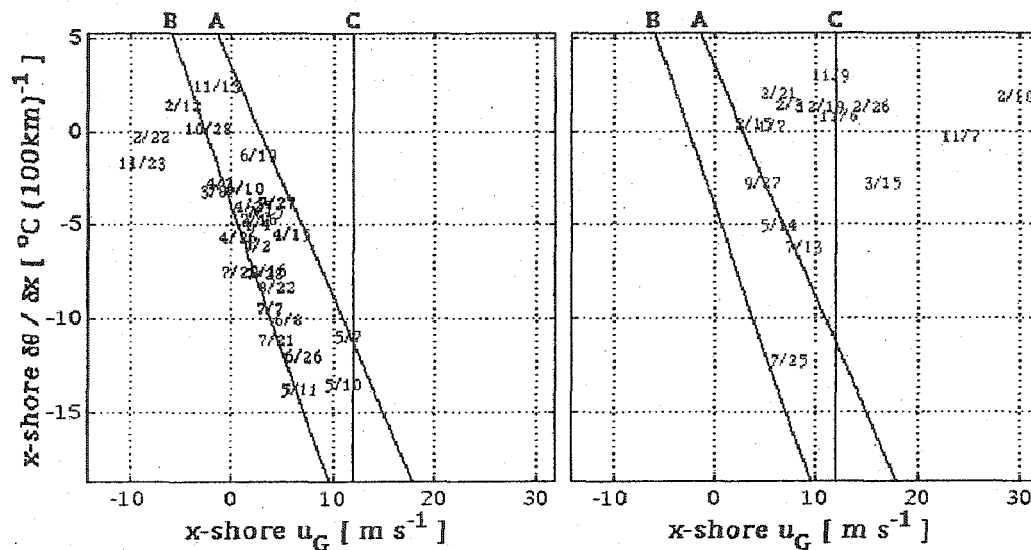


Figure 3.10: Nowcast Diagram for Synoptic Classes 1, 2, and 3. Left-hand panel: Dates of sea-breeze and marginal events associated with class 1 and class 2 cases. Date format is MM/DD. Right-hand panel: Dates of non-sea-breeze events associated with class 3 cases. Axes are as described for the above figures.

Figure 3.10 (right-hand panel) shows the dates associated with the synoptic class 3 cases -- all non-sea-breeze events. As expected, those cases occurring during winter are located near the upper boundary of the diagram, where $\delta\theta/\delta x$ is weak or unfavorable, *i.e.*, where the sea-surface temperature is the same as or warmer than land. More than half of the class 3 occurred in November,

December, January, and February, and the strongest non-seabreeze event, located near the upper right corner (where a strong positive u_G opposes the sea breeze), occurred on February 10.

Classes 4 and 5. Of all the synoptic classes, class 4 cases have the widest range of $\delta\theta/\delta x$ (Figure 3.11). This probably reflects the wide annual range over which this class occurs, as well the two superficially similar but dynamically different scenarios included in class 4 (described above). With the largest part of the geostrophic wind vector parallel (rather than perpendicular, by definition) to the coastline, the sea-breeze and marginal events occur further towards the lower left corner than do the same types of events associated with classes 1 and 2. Values of u_G for all types of events are generally biased further toward the negative than are those associated with classes 1 - 3. The u_G overlap between sea-breeze and non-sea-breeze events essentially disappears toward the lower boundary of the diagram, where $\delta\theta/\delta x$ is most favorable, but becomes more pronounced nearer the middle region and upper boundary of the diagram, where $\delta\theta/\delta x$ is less favorable for a seabreeze. This means that forecasting the occurrence/non-occurrence of the seabreeze in the lower half of the diagram is a

straightforward endeavor, but is somewhat more uncertain toward the upper half. The former cases (where $\delta\theta/\delta x$ is most favorable) are probably associated with the semipermanent Bermuda High and maritime tropical airmass in the southeast United States, and the latter cases (where $\delta\theta/\delta x$ is less favorable) are probably associated with migratory anticyclones and modified continental polar airmasses.

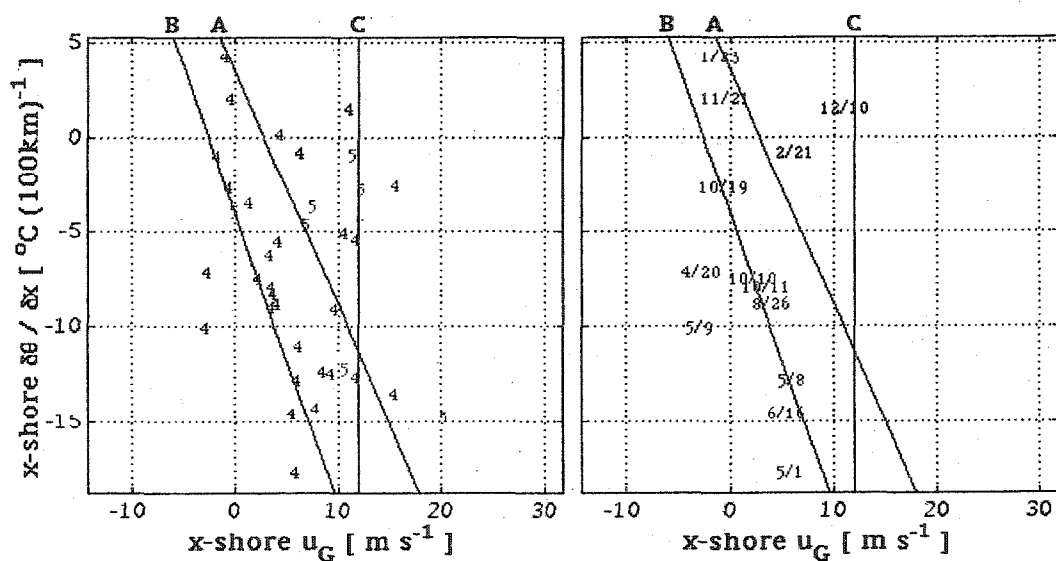


Figure 3.11: Nowcast Diagram for Synoptic Classes 4 and 5. Left-hand panel: All events associated with class 4 and 5 cases, by synoptic class. Right-hand panel: Dates associated with class 4 sea-breeze and marginal events. Axes and color-coding of events are as described for the above figures.

Sea-breeze and marginal events associated with class 4 span a wide range of $\delta\theta/\delta x$ values, and they tend to cluster closer to the lower boundary than the upper, where $\delta\theta/\delta x$ values are more favorable. (See Figure 3.11.) All of the sea-breeze and marginals are clustered between u_G values of -3 and +12 ms^{-1} . Some remnant of the (diagonal) marginal cross-over region remains, although the region is somewhat more vertical in this coordinate system, because of the assumptions defining class 4 (wind parallel to the coast), which force the sea-breeze event region into a more vertical position. Note also that there are no sea-breeze or marginal events associated with class 5 cases.

Figure 3.11 (right-hand panel) shows the dates associated with class 4 sea-breeze and marginal events. A general picture emerges that is similar to the class 1 - 3 picture, with summer events appearing nearer the lower boundary of the diagram and non-summer events appearing nearer the upper boundary. Of particular interest is the January 23 sea-breeze event near the upper boundary. This event is associated with an unfavorable $\delta\theta/\delta x$, but an essentially non-existent opposing u_G . It is likely that an extremely narrow band of warm surface temperatures developed on the coastal plain immediately adjacent to the shore. A very narrow

band of relatively warm air on the land side of the coast is not conducive to "strong" sea breezes -- any landward intrusion of the marine airmass would quickly extinguish the favorable $\delta\theta/\delta x$ and shut down the driving force.

Figure 3.12 shows the dates associated with class 4 and 5 non-sea-breeze events. The seasonal pattern described above is again evident, with the exception of several mid-autumn events near the center of the diagram. It is not surprising that several non-sea-breeze events occur toward the lower half of the diagram. During late summer and early autumn, the warmest conditions along the central New England coast occur with a southwesterly wind, when warm-air is advected from the southern United States and the Gulf of Mexico. This sets up warmer air temperatures on the land-side of the coast. There are two mechanisms responsible for cooling the surface waters of the Gulf of Maine in late autumn, and thus setting up the cooler air temperatures on the sea-side of the coast: Local heat loss due to vertical heat fluxes [*Brown and Irish, 1993; Miller, 1999*], and Ekman pumping. The former begins to take effect in early October. The latter occurs any time there is a southwesterly surface wind along the coast, which sets up surface Ekman transport toward the east, and net ocean mass transport toward the southeast [*Apel, 1987*]. Surface flow away from the coast, coupled with mass

conservation, forces upwelling in the coastal zone, and upwelling brings cooler water to the ocean surface [Feng, 1996]. The combination of southwesterly warm-air advection over land and cool sea-surface temperatures places the $\delta\theta/\delta x$ in a seabreeze-favorable range, but the sea breeze is prevented from reaching Pease because of the relatively strong southwesterly winds.

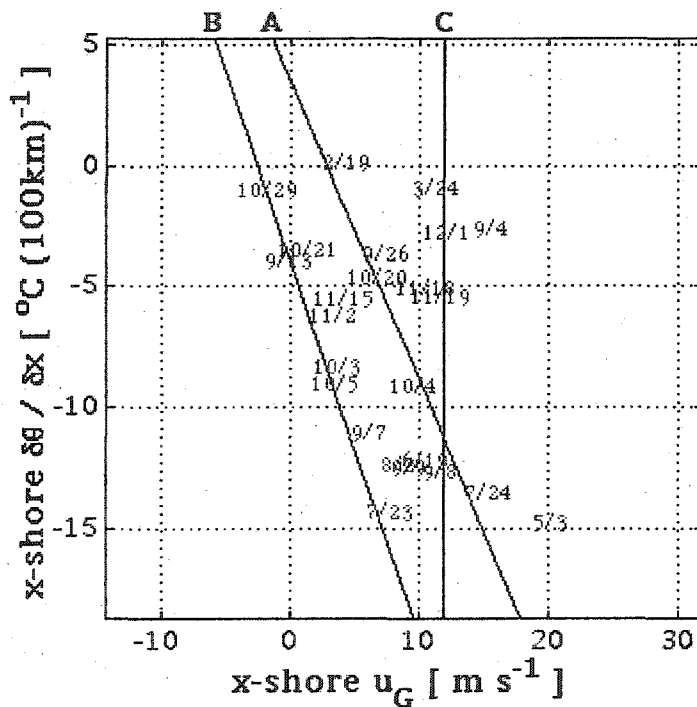


Figure 3.12: Dates associated with class 4 and 5 non-sea-breeze events. Axes are as described for the above figures.

Class 6. Like the class 1-, 2-, and 3-related sea-breeze events, synoptic class 6 seabreeze events seem to occupy a fairly coherent

region of the diagram (Figure 3.13), but the cross-over area between sea breezes and non-sea breezes is narrower than it is for the former events. A forecaster can therefore use the diagram to predict sea-breeze events in class 6 cases with a high degree of confidence.

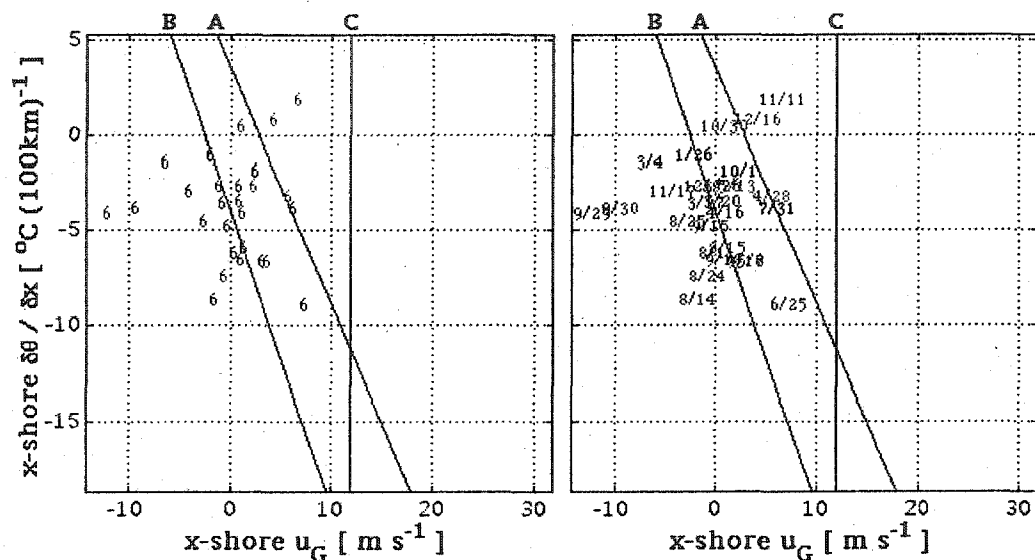


Figure 3.13: Nowcast Diagram for Synoptic Class 6. Left-hand panel: All sea-breeze, marginal, and non-sea-breeze events associated with class 6. Right-hand panel: Dates of class 6 seabreeze, marginal, and non-seabreeze events. Axes and color-coding of events are as described for the above figures.

Ignoring the marginals and the non-sea-breezes, late summer/early fall appear to cluster toward the lower left of the class 6 grouping (where u_G is on-shore), winter and late fall toward the upper boundary (where $\delta\theta/\delta x$ is least favorable), and summer

toward the center of the diagram (where $\delta\theta/\delta x$ is more favorable) (Figure 3.13, right-hand panel). The latter two observations are relatively simple to explain with the expected seasonal variations. The first of the three observations may be an artifact of the relatively small sample (31 cases spread out over a single year), and two objectives of future work should be to increase the total number of cases observed, and to extend the database of events from one to several years.

Hour of Onset. Figure 3.14 shows the hour [UTC] closest to the time of onset of the sea-breeze at Pease, as best as could be determined using the KPSM observations. Hours that are greater than 24 correspond to the early-UTC hours of the following day: Subtract 24 to convert to a 24-hour clock. The conversion from UTC to local standard time (LST) is -5. (For example, "26" should be understood as "02" UTC, or 2100 LST.)

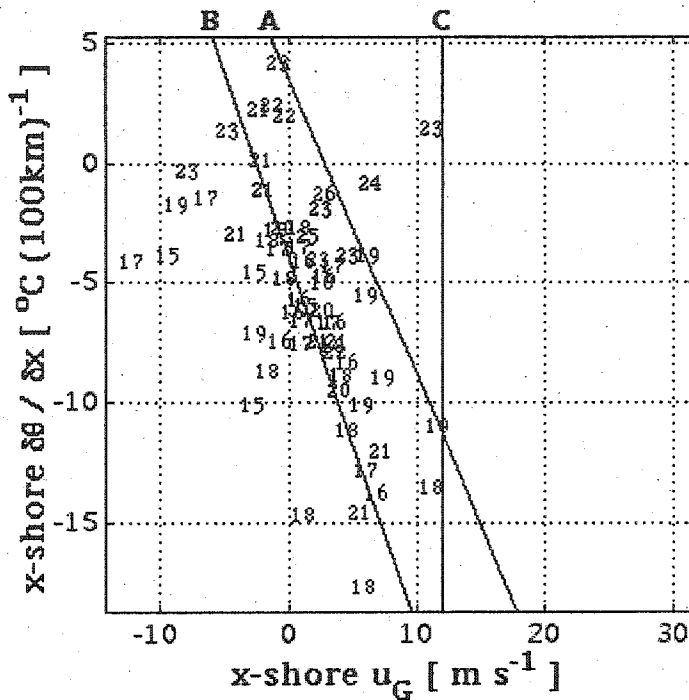


Figure 3.14: Onset hour [UTC] of sea-breeze and marginal events, all synoptic classes. Axes are as described for the above figures.

Sea-breeze events near the top left of the diagram occur relatively late in the day, which is not surprising, since this is a region on the diagram where the land-sea temperature forcing is weak, and a sea breeze is only possible when the opposing u_G is weak. There are three cases in this region where the sea breeze did not arrive at Pease until 2300 UTC, or 1800 LST. Toward the bottom center of the diagram, where $\delta\theta/\delta x$ is highly favorable and the opposition from u_G is still relatively weak, the latest onset time is

2100 UTC (1600 LST) with 1800 UTC (1300 LST) more common, and one case as early as 1600 UTC (1100 LST).

Some, but not all, of the earliest onset times occur toward the lower left, where both $\delta\theta/\delta x$ and u_G are favorable. Some of these cases are those with onset times as early as 1500 UTC (1000 LST). But there are other events with equally early onset times in the cross-over region, toward the center of the diagram. All of the marginal events occur at 1900 UTC (1400 LST) or later, although there are definite seabreeze events that begin later than the latest marginal event.

In short, while there appears to be some weak tendencies toward (1) later onset periods for marginals than for seabreeze events; (2) later onsets toward the upper left (where $\delta\theta/\delta x$ is either very weak or unfavorable) than toward the bottom center; and (3) earlier onsets toward the lower left (where $\delta\theta/\delta x$ and u_G are both highly favorable), these are fairly weak tendencies and can hardly be considered conclusive. It appears that the one-way "strong => early" formulation is valid from this diagram, but proving the two-way formulation will require looking at an average onset time over the entire 120-kilometer long coastline in the study area. These

results suggest that this generally unclear picture would arise if the seabreeze were nonhomogeneous in the along-shore direction.

Summary and Conclusions

Using routinely-available hourly surface observations and United States surface analyses for the year 2001, a method was developed for predicting sea-breeze events. The method is adaptable to any coastal region in the world where surface data are available. Specific prediction guidelines were developed using Portsmouth, New Hampshire as the forecast site.

Using the Pease Air National Guard Base, Portsmouth, New Hampshire weather observation records, 167 days in 2001 were identified that had conditions favorable for the formation of a sea breeze on the central New England coastline. Favorable conditions were defined as the absence of significant cloud-cover in the low and middle etages, and the non-occurrence of significant precipitation, thereby permitting insolation to establish a cross-shore potential temperature gradient. Days when synoptic-scale forcing was responsible for on-shore flow were excluded from the study. These 167 days were grouped into sea-breeze, marginal, and non-sea-breeze events. Sea-breeze events were those days when the

wind direction shifted from southwest, northwest, or northeast to southeast during mid-day, then back to southwest, northwest, or northeast in the evening. Non-sea-breeze events were those days that the windshift did not occur, in spite of relatively cloud-free skies. Marginal events were those days when the sea-breeze occurred, but was short-lived (lasting two hours or less) or exceptionally weak (characterized by very light wind speeds, with or without a highly variable wind direction). A total of 59 sea-breeze events, 10 marginal events, and 98 non-sea-breeze events were identified for 2001.

The 1200 UTC surface synoptic situations for all 167 event days were evaluated using NWS United States surface analyses. These situations were grouped into seven different general classes, where classes 1, 2, and 3 corresponded to northwesterly geostrophic winds, classes 4 and 5 corresponded to southwesterly winds, and class 6 corresponded to northeasterly winds over the study area. Class 7 was a miscellaneous grouping. We found that sea breezes occurred about 60 percent of the time with class 1, about 20 percent of the time with class 2, and never with class 3. Sea breezes or marginal events were almost as likely as non-sea breezes with class 4, but never occurred with class 5. Sea breezes and marginals accounted for almost 80 percent of the class 6 cases.

Four stations -- one each near the northern, eastern, southern, and western boundaries of the study area -- were used to calculate meso- α -scale cross-shore potential temperature gradients ($\delta\theta/\delta x$) and cross-shore geostrophic wind components (u_G). The former is a measure of the force driving the sea breeze, and the latter is a measure of the force opposing the sea breeze. A Nowcast Diagram was set up with u_G on the horizontal axis and $\delta\theta/\delta x$ on the vertical axis. Synoptic classes and the dates of all three types of events were plotted on these axes, as well as the hour-of-onset for sea-breeze and marginal events. (See Figures 3.8 through 3.14.)

In general, it was found that stronger negative $\delta\theta/\delta x$ values were needed to develop a sea breeze in the presence of stronger positive u_G values (Figure 3.8). Sea-breeze events associated with synoptic classes 4 and 6 were toward the lower left corner of the diagram, in the region of strongly-negative $\delta\theta/\delta x$ and weak or negative (landward) u_G . These events showed a tendency to be "early-onset," but more detailed study at the mesoscale is required to resolve this question satisfactorily (Figure 3.14). Sea-breeze events associated with classes 1 and 2 were confined to a relatively narrow diagonal region, running from the center bottom boundary of the diagram (highly favorable $\delta\theta/\delta x$, and weak u_G) to the upper

left corner (unfavorable $\delta\theta/\delta x$, and near-zero or negative u_G) (Figure 3.9), and sea-breeze events associated with class 6 were confined to almost circular region in the upper left part of the diagram (weakly favorable $\delta\theta/\delta x$, near-zero or negative u_G) (Figure 3.13). Non-sea-breeze events associated with classes 2 and 3 were toward the upper right corner of the diagram (highly unfavorable $\delta\theta/\delta x$, and strongly opposing u_G) (Figure 3.9), with class 3 exhibiting the most extreme case, and non-sea-breeze events associated with class 5 were divided between a large circular region in the central part of the diagram (weakly favorable $\delta\theta/\delta x$, weak u_G), and a narrower area stretching from the center toward the lower right corner (highly favorable $\delta\theta/\delta x$, but strongly opposing u_G) (Figure 3.11).

The Nowcast Diagram (Figure 3.8) is a useful tool for predicting sea-breeze events. Using the synoptic class, the sea-surface temperature in the coastal zone (to act as a proxy for offshore air temperature), some idea of the daily temperature curve for some point well inland, and the magnitude of the cross-shore geostrophic wind component, one can decide -- often with a high degree of confidence -- whether or not a sea breeze will occur in the study area. This method is similar to one developed by *Simpson*

[1994, ch. 4] for Thorney Island, in the United Kingdom, and is in principle adaptable to any coastal region of the world.

CHAPTER IV

SYNOPTIC-SCALE CONTROLS ON THE SEA BREEZE OF THE CENTRAL NEW ENGLAND COAST, PART II: TIME-EVOLUTION OF MESO-ALPHA FORCING

This chapter has been submitted for publication in *Weather and
Forecasting*.

CHAPTER IV

SYNOPTIC-SCALE CONTROLS ON THE SEA BREEZE OF THE CENTRAL NEW ENGLAND COAST, PART II: TIME-EVOLUTION OF MESO-ALPHA FORCING

ABSTRACT

The time-evolution of net mesoscale forcing of the sea breeze along the central New England coast was examined for 32 case studies spanning the year 2001. The net forcing, consisting of the cross-shore geostrophic wind component (u_G) that may resist the inland movement of the sea breeze, and the mesoscale cross-shore potential temperature gradient ($\delta\theta/\delta x$), responsible for the thermal pressure gradient that may drive the sea breeze inland, is shown to be a function of six well-defined synoptic classes. Synoptic classes are based on the relative locations and dominance of surface pressure systems in the Northeast United States. The diurnal variation of $\delta\theta/\delta x$ is dominated by differential land-sea diabatic heating, cold-air advection, and the transport of haze into the study area. The diurnal variation of u_G is dominated by the orientation of the geostrophic wind and the strength of the pressure gradient associated with synoptic-scale pressure systems. Forecast guidance for the sea breeze is developed for the time of onset in Portsmouth, New Hampshire, using 1200 UTC values of u_G and $\delta\theta/\delta x$. In a pair of the synoptic classes, u_G and $\delta\theta/\delta x$ are sufficient to determine if the sea breeze will occur at Pease. In another pair, additional information is required to differentiate the net forcing in sea-breeze and non-sea-breeze events at Pease. Sea breezes do not occur in Portsmouth in two of the synoptic classes, because of cold-air advection and strong cross-shore wind components.

Introduction

The seabreeze is an important influence on New England's weather, climate, and air quality. The associated moisture can be responsible for creating fog near dawn, and for fueling afternoon convection at points well inland of the coast [Chapter 2]. The convective internal boundary layer (CIBL) that forms within the marine airmass may trap pollutants in a shallow layer near Earth's surface, reducing air quality in the coastal zone [Hsu, 1988]. In New England, sea breezes have been shown to foster high surface ozone [Gaza, 1998; Seaman and Michelson, 2000] and high sulfur dioxide episodes [Barbato, 1975]. For these reasons it would be useful to understand the meteorological conditions conducive to sea breeze development in New England, and how these conditions vary with the synoptic-scale meteorological environment.

Research on the New England sea breeze was carried out as part of the Atmospheric Investigation, Regional Modeling, Analysis, and Prediction (AIRMAP) project. The primary goal of AIRMAP is to understand the factors influencing climate and air quality in New England. The goal of the Central New England Sea Breeze Study is to understand the physical behavior of the sea breeze on the central New England coast, and aid in its prediction.

Background

The sea breeze is a mesoscale wind that occurs at coastal locations throughout the world. It develops when insolation and differential heating of the land and sea surfaces create a mesoscale pressure gradient force pointing toward the land. If the low-level cross-shore wind component created by the synoptic-scale pressure pattern is relatively weak, cool marine air moves toward the land as a gravity current [*Simpson*, 1994]. The sea breeze is usually a closed circulation cell, with a front on the landward extreme marking the boundary between the marine and continental airmasses. Landward-moving marine air is lifted to a height of between 300 and 2200 meters at the sea-breeze front [*Barbato*, 1975]. The circuit is usually closed by seaward return flow near 900 hPa, and a diffuse region of descending currents several tens of kilometers out to sea [Chapter 2].

Chapter 3 documented year-2001 sea-breeze (SB), marginal (MAR), and non-sea-breeze (NSB) events on the coast of New England, using surface weather observation records from the Pease airport (in Portsmouth, New Hampshire; 10 km inland). SB events were defined as occurring on days when there was sufficient sunlight (cloud-free sky conditions) to create a negative cross-shore

potential temperature gradient in the coastal zone near Portsmouth, which in turn creates a landward-pointing mesoscale pressure gradient force (PGF), bringing the sea breeze inland to the Pease airport (KPSM; Figure 4.1). Its arrival at Pease is typically marked by a wind shift to approximately 130 degrees azimuth, decreasing temperatures, and increasing dew points. MAR events were defined as those when the sea breeze occurred at Pease, but was either very short-lived (two hours or less), was marked by very light wind speeds, or merely manifested as a short interval of "light and variable" winds during a period of sustained wind from a non-southeasterly direction. NSB events were those in which there was sufficient insolation to establish a strong cross-shore potential temperature gradient, but the sea breeze failed to reach Pease.

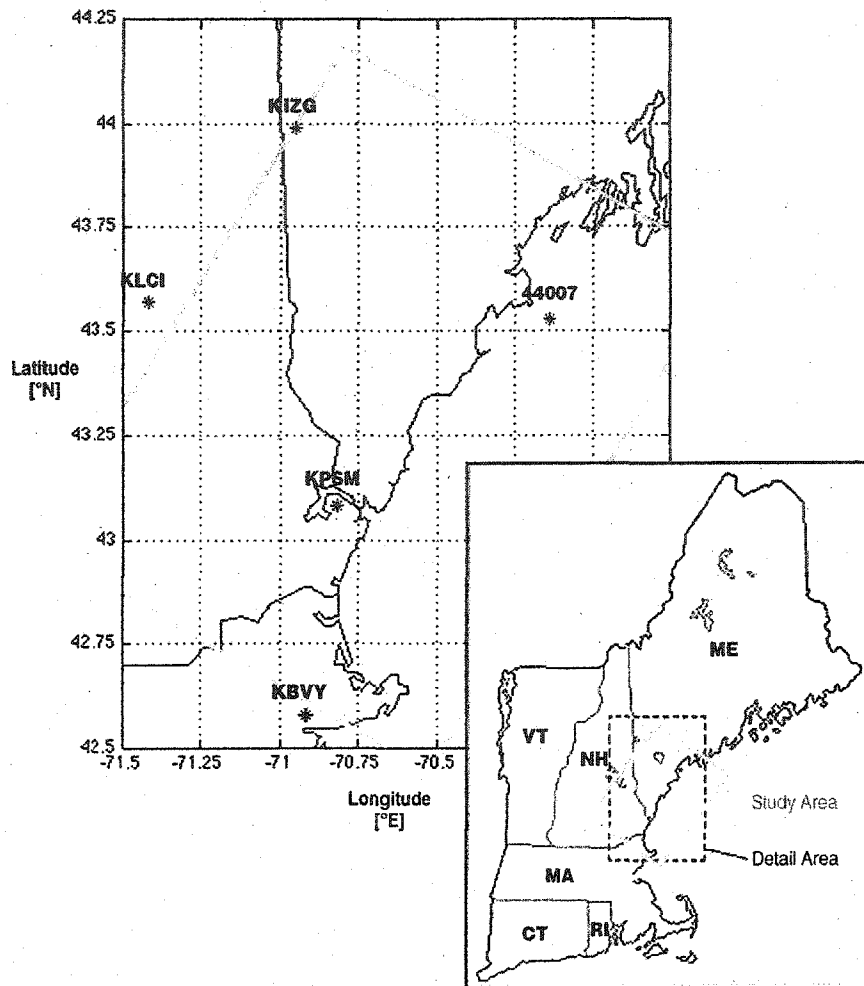


Figure 4.1: Study area and location map. Gray line indicates edges of the study area. Surface weather observing stations shown are Fryeburg, Maine (KIZG); the Portland, Maine Buoy (44007); Portsmouth, New Hampshire (KPSM); Beverly, Massachusetts (KBVY); and Laconia, New Hampshire (KLCI).

The occurrence of SB, MAR, and NSB events at Pease was compared to the United States surface analysis on the morning of the event, and the meso- α (200 - 2000 kms; [Fujita, 1986]) forcing in the coastal zone. The net forcing consists of the cross-shore

geostrophic wind component (u_G) that may resist the inland movement of the sea breeze, and the cross-shore potential temperature gradient ($\delta\theta/\delta x$) that may drive the sea breeze toward land [Chapter 3]. The surface analyses were grouped into six well-defined classes (Table 4.1 and Figure 4.2), and both sea-breeze forcing parameters were calculated for the hour of sea-breeze onset at Pease, using four widely separated surface weather stations. It was found that different synoptic classes resulted in different meso- α forcing patterns, and that sea breezes were more likely in some synoptic situations than in others [Chapter 3].

Table 4.1: Description of synoptic classes defined in Chapter 3.

Synoptic Class	Description of near-surface synoptic-scale features	Resulting flow over study area	Sea breeze possible in Portsmouth ?
1	Migratory high centered from midwestern United States through southern Ontario.	Anticyclonic; northwesterly	Yes
2	Migratory high in midwestern United States or Great Lakes region, and migratory low in northern New England through Canadian Maritimes Provinces.	Weak to neutral curvature; northwesterly	Yes
3	Strong migratory low in northern New England through Canadian Maritime Provinces, with trough or front extending southward from low center into Gulf of Maine.	Cyclonic; northwesterly	No
4	Low over Great Lakes or south-central Canada, with trough or front extending from low center southward; High centered in southeastern United States. High in Southeast may be migratory, or an extension of the Subtropical Ridge.	Southwesterly	Yes
5	Low in midwest or south-central Canada, with front extending from low center east to northern New England. May include an open ridge over northeastern United States.	Southwesterly	No
6	High in Great Lakes region or Ontario; low southeast of New England, over Atlantic Ocean, with front or trough extending southwest from low center.	Northeasterly	Yes

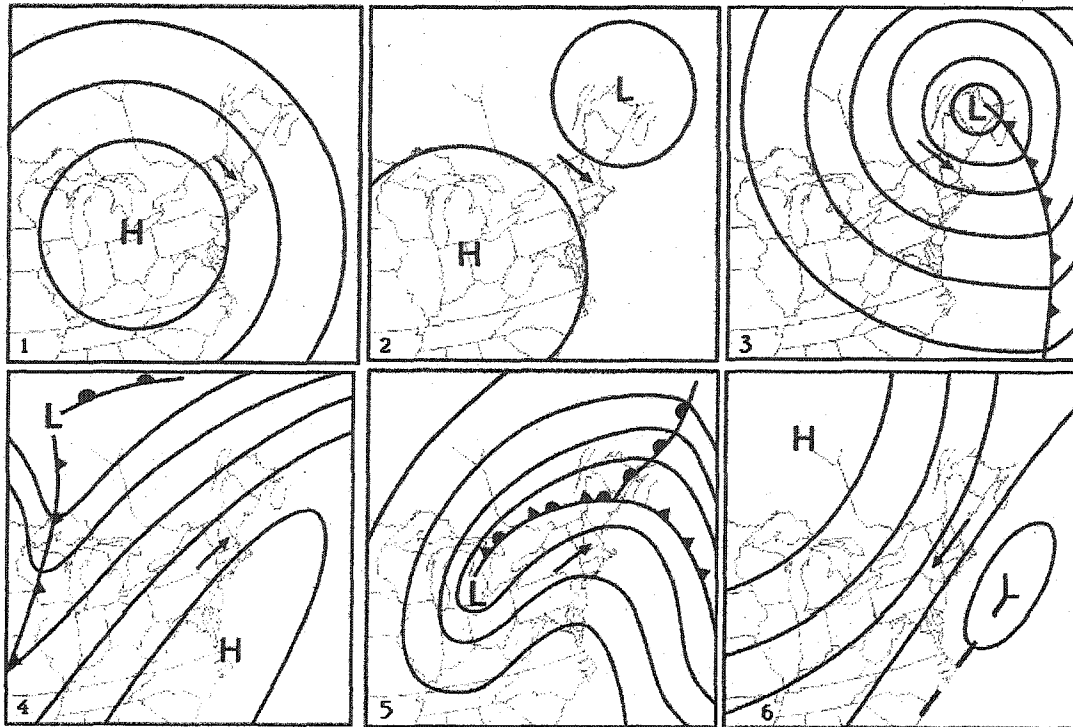


Figure 4.2: Synoptic classes. Classes 1, 2, and 3 are associated with northwesterly geostrophic wind (indicated by arrow) in study area. Classes 4 and 5 cause a southwesterly geostrophic wind. Class 6 results in a northeasterly geostrophic wind.

This chapter focuses on the time-evolution of the net forcing that controls sea breezes in the coastal zone of east-central New England. The specific objectives are to 1) quantify the time-evolution of the cross-shore geostrophic wind component and the cross-shore potential temperature gradient, 2) relate the behavior of the sea-breeze forcing to the synoptic-scale environments, and 3) quantify the relationship between the sea breeze's time of onset at a single forecasting point (Pease) and the time-dependent behavior of

the mesoscale forcing. Because this method may be adapted to any coastal location in the world, this will assist in the forecasting of sea breezes throughout coastal New England and beyond.

Methods

This chapter examines the hourly time-evolution of the sea breeze's meso- α forcing along the central New England coast (Figure 4.1), using 32 case-studies during the year 2001 (Table 4.1 and Figure 4.3). Chapter 3 examined Pease airport's hourly surface weather observations for 2001, and identified 167 days where there was potential for the development of a sea breeze. Sea-breeze favorable conditions were defined as the absence of significant cloud-cover below 7 km AGL, and the non-occurrence of significant precipitation, thereby permitting insolation to establish a cross-shore potential temperature gradient. These 167 days were cross-checked with the corresponding 1200 UTC (0700 LST) United States surface analysis for the occurrence of synoptically-driven southeasterly winds to eliminate them from the dataset.

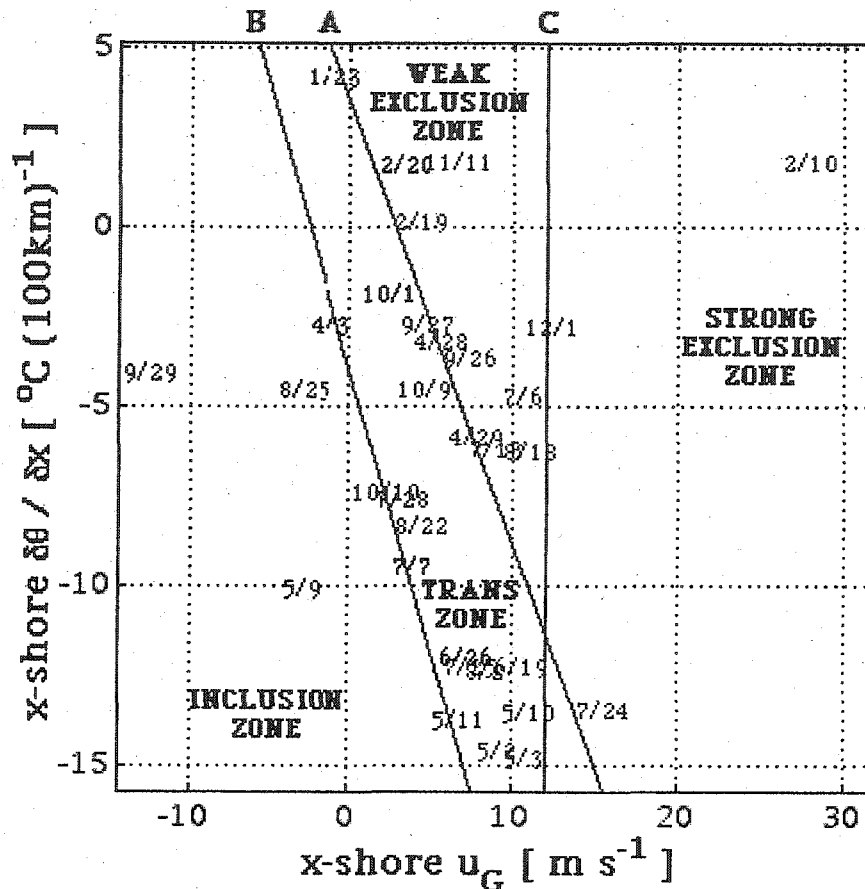


Figure 4.3: Summary of 32 case-studies selected from 2001. SB and MAR events (blue and black, respectively) are plotted for the hour of onset at Pease airport, in Portsmouth, New Hampshire. NSB events (red) are plotted for 1900 UTC (1400 LST). The inclusion, transition, and exclusion zones are discussed in the text.

For this chapter, 32 events were selected (Table 4.1) from the 167 days in Chapter 3 using the following three criteria: First, these events span the full length of the year, and therefore represent all four seasons. Second, they represent most of the range of variation in the two meso- α forcing variables ($-18^{\circ}C (100km)^{-1}$ to $+5^{\circ}C (100$

km)⁻¹ for $\delta\theta/\delta x$; -15 ms⁻¹ to +30 ms⁻¹ for u_G) associated by SB, MAR, and NSB events. Third, they cover the three types of events associated with the six well-defined synoptic classes. Figure 4.3, called the Nowcast Diagram, shows the net forcing associated with the 32 events chosen. For SB events (plotted in blue) and MAR (plotted in black) events, the forcing is diagnosed for the approximate moment that the sea breeze arrived at the Pease airport. For NSB events, the forcing is diagnosed at 1900 UTC (1400 LST) -- the time of day when the landward-pointing mesoscale PGF should be at its peak.

The Nowcast Diagram contains three important lines, separating the it into four zones. These zone were determined by comparing the net forcing diagnosed by the diagram with the resulting sea-breeze behavior in Portsmouth. In the *Strong Exclusion Zone*, to the right of line C ($u_G = 12 \text{ ms}^{-1}$), sea breezes never reach Portsmouth regardless of the magnitude of the mesoscale thermal PGF (diagnosed by the parameter $\delta\theta/\delta x$), because u_G is too strong. In the *Weak Exclusion Zone*, to the right of line A and to the left of line C, sea breezes occasionally reach Portsmouth as MAR events, but $\delta\theta/\delta x$ is too weak to overcome the opposing u_G , which prevents well-developed sea breezes from reaching Pease. The region between

lines A and B represents ambiguity in the diagram's diagnosis of the forcing, and is called the *Transition Zone*. Sea-breeze, marginal, and non-sea-breeze events all occur in the Transition Zone. In the *Inclusion Zone*, below and to the left of line B, the sea breeze usually reaches Portsmouth, because u_G is too weak to stop the landward-movement of the sea breeze initiated by the mesoscale PGF [Chapter 3].

For this chapter, hourly values of $\delta\theta/\delta x$ and u_G were calculated using reported sea-level equivalent pressures and air temperatures reported by four stations (Figure 4.1). The Fryeburg-Beverly (KIZG-KBVY) differences were chosen to capture the north-south gradients, and the Portland-Laconia (44007-KLCI) differences were chosen to represent the east-west gradients relevant to sea breezes in Portsmouth (KPSM). After calculating north-south and east-west components of the geostrophic wind and potential temperature gradient, the components were transformed into a coordinate system rotated 30 degrees clockwise from north, resulting in cross- and along-shore components. The time interval between 1200 UTC (0700 LST) and 0000 UTC (1900LST) is of primary interest because that is the time of day when the sea-breeze system is initiated and evolves through the majority of its life-cycle.

Results

In this section, the evolution of the net sea-breeze forcing during SB, MAR, and NSB events occurring in the six well-defined synoptic classes is discussed. The net forcing is described in terms of time-evolving nowcast vectors (TENVs), which consist of hourly values of $\delta\theta/\delta x$ and u_G plotted on the Nowcast Diagram. Unless otherwise noted, all times are UTC. The conversion to LST is UTC - 5 hours, and the conversion to DST is UTC - 4 hours.

Synoptic Class 1 (SC1). The TENVs associated with five SC1 cases were examined (Figure 4.4). In SC1 SB events, the TENV either began inside the TZ at 1200, or moved into the TZ almost immediately after 1200. In the MAR and NSB events, the TENV began to the right of line A and moved into the TZ at 1500 or later. In all cases, u_G remained weakly offshore and relatively constant throughout the day. The MAR case occurred when the weak-gradient region near the center of the high approached the study area, u_G diminished from about 10 ms^{-1} to less than 5 ms^{-1} , and the mesoscale PGF drove the sea breeze inland. Most of the TENV's evolution was on the $\delta\theta/\delta x$ axis, reflecting the diurnal temperature cycle. The relatively large span of variation on the $\delta\theta/\delta x$ axis (in

excess of $8 \text{ }^\circ\text{C (100 km)}^{-1}$) indicates the absence of significant cold-air advection into the study area.

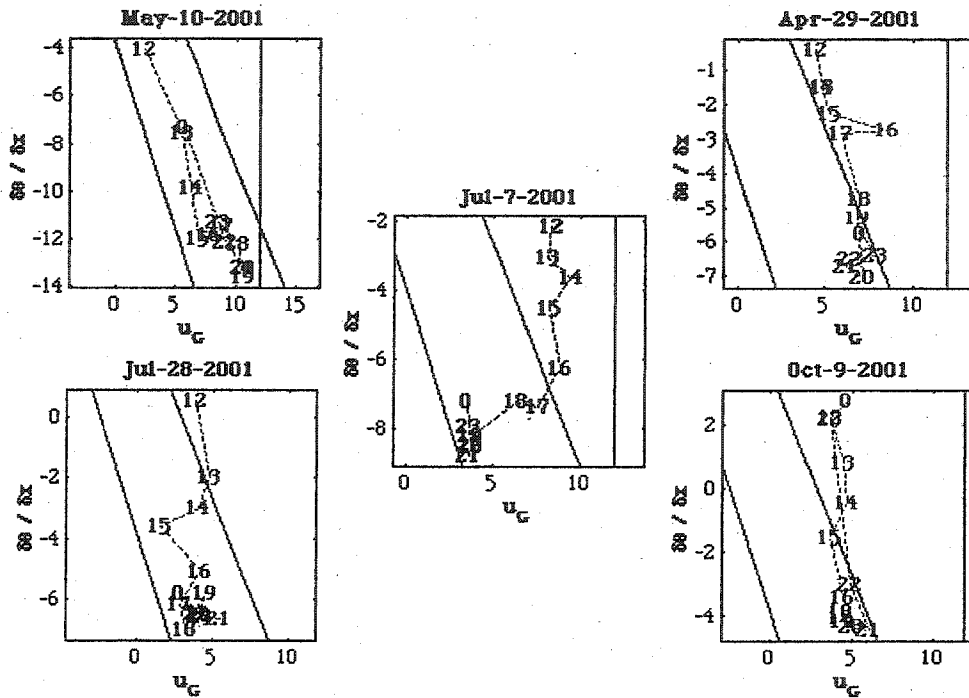


Figure 4.4: Time evolution of meso- α forcing during SB, MAR, and NSB events associated with synoptic class 1. Horizontal axis (u_G) is the cross-shore geostrophic wind component [ms^{-1}]. Vertical axis ($\delta\theta/\delta x$) is the cross-shore potential temperature gradient [$^\circ\text{C (100 km)}^{-1}$]. Plots indicate hour (UTC), beginning with 1200 and ending with 0000. Three reference lines are the same as in Figure 4.3. SB events are shown in blue; MAR event is shown in black; NSB events are shown in red.

Synoptic Class 2 (SC2). The TENVs associated with seven SC2 cases were examined (Figure 4.5). Five of the case-studies exhibited either 1) time-evolution primarily on the $\delta\theta/\delta x$ axis, or 2)

diminishing u_G as the day progressed, and therefore resembled SC1 cases. The remaining two showed significant evolution along the u_G axis toward more positive values, and therefore resembled SC3 cases (see below).

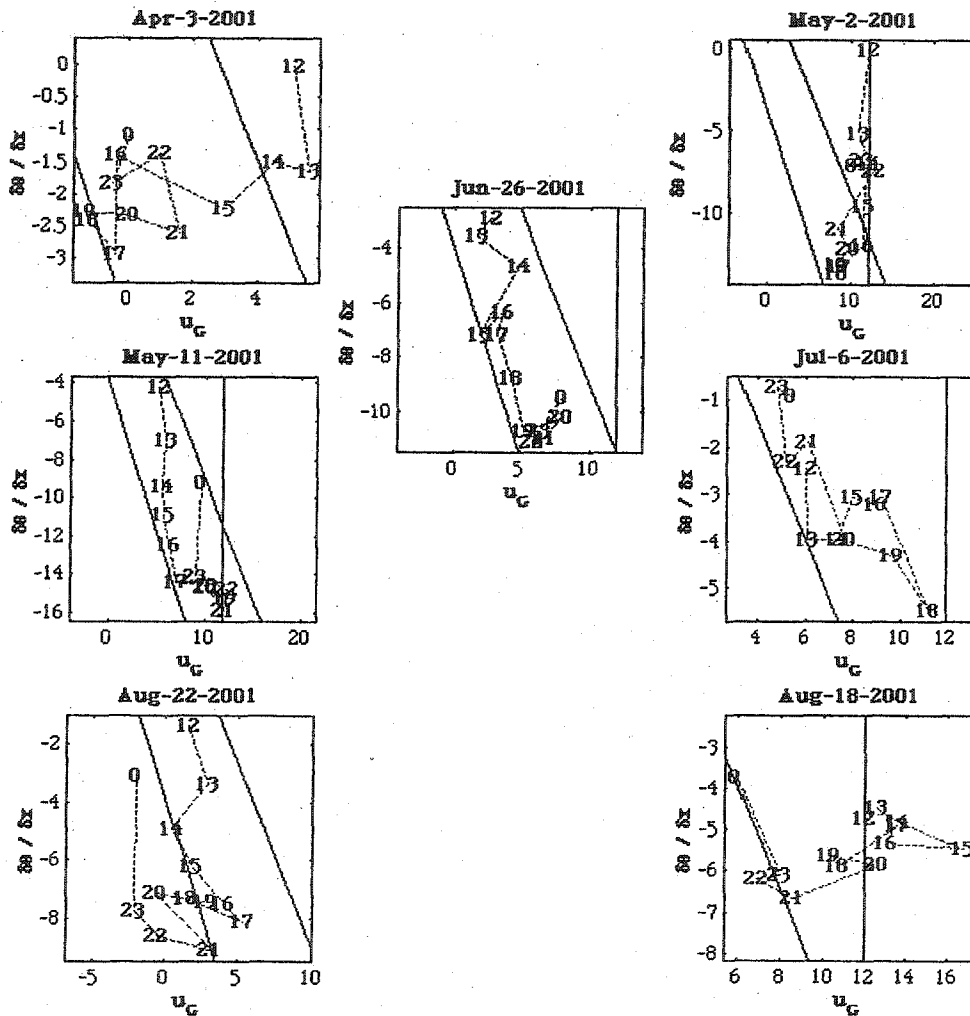


Figure 4.5: Time evolution of meso- α forcing during SB, MAR, and NSB events associated with synoptic class 2. Axes, reference lines, and color coding are the same as in Figure 4.4.

In the May 11 and August 22 SB events, the TENV began inside the Transition Zone and evolved downward along the $\partial\theta/\partial x$ axis, as daytime land-sea differential heating created a landward mesoscale PGF. In the April 3 SB event, the TENV began in the Weak Exclusion Zone, but evolved to the left as the weak gradient region near the center of the synoptic anticyclone approached the study area, and the opposing geostrophic wind component diminished. This resembles the June 7 SC1 MAR event, except that the TENV moved into the Transition Zone by about 1400, rather than after 1600. SC2 SB events may therefore be initiated by either 1) developing a strong mesoscale PGF that overcomes a relatively steady opposing u_G , or by 2) a diminishing u_G that allows an already-established, relatively weak mesoscale PGF to drive the sea breeze inland. This is similar to SC1 sea-breeze behavior.

The June 26 SC2 MAR event closely resembles both the May 11 SC2 and May 10 SC1 SB events, which indicates that a third physical factor prevented the sea breeze from becoming well established at Pease. This factor must therefore be accounted for to accurately differentiate the net forcing in SB and MAR events. This will be explored in a future paper.

Of the three SC2 NSB events, one (May 2) exhibited SC1 behavior, with strong evolution along the $\delta\theta/\delta x$ axis driven by daytime land-sea differential heating in the absence of significant cold-air advection. The sea breeze did not reach Pease because, for much of the day, the TENV was in the Weak Exclusion Zone, indicating that the landward forcing was too weak to overcome the opposing u_G . The TENV moved into the Transition Zone after 1500, so this case supports the previous observation that the sea breeze does not reach Pease in this circumstance.

In the NSB events of July 6 and August 18, the TENVs began in the Weak Exclusion Zone, and exhibited an increasing u_G early in the day, as the synoptic-scale flow between the anticyclone to the southwest and the cyclone to the northeast increased or reoriented into the cross-shore direction. Some early land-sea differential heating was also indicated by the evolution of $\delta\theta/\delta x$ toward more negative values, but rapid cooling after 2000, enhanced by cold-air advection on the west side of the synoptic cyclone, quickly weakened the landward mesoscale PGF (as indicated by the evolution of $\delta\theta/\delta x$ toward positive values). With the exception of one hour (2200) on August 18, the TENVs in both of these events remained to the right of line A for the entire period between 1200 and 0000.

Synoptic Class 3 (SC3). The TENVs associated with four SC3 NSB events were examined (Figure 4.6). SB and MAR events do not occur with SC3 [Chapter 3]. In two of the case studies the TENV began in the Weak Exclusion Zone, and in the other two cases the 1200 TENV began in the Strong Exclusion Zone, indicating a strong opposing synoptic-scale wind component.

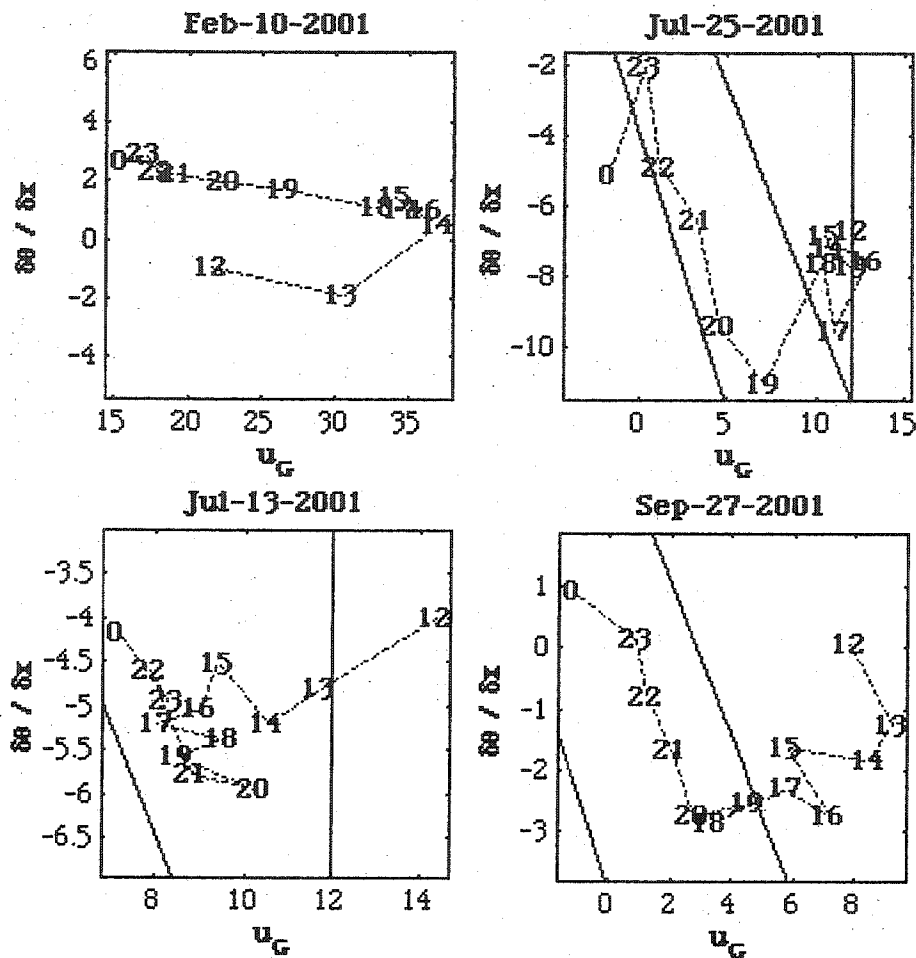


Figure 4.6: Time evolution of meso- α forcing during NSB events associated with synoptic class 3. Axes, reference lines, and color coding are the same as in Figure 4.4.

On February 10, the most extreme case, u_G increased early in the day as the synoptic-scale flow associated with cyclone to the northeast of the study area increased or reoriented into the cross-shore dimension, then diminished after 1400 as the cyclone moved

away and the associated PGF over the study area began to weaken. Cold-air advection on the west side of the cyclone was indicated, as $\delta\theta/\delta x$ evolved toward positive values throughout the day, in spite of the presence of insolation due to the absence of significant cloud cover. (In the absence of cold-air advection, strong insolation should cause $\delta\theta/\delta x$ to evolve toward more negative values.)

September 27 was somewhat less extreme: The opposing wind component only increased for the first hour, then began to diminish as the synoptic-scale PGF rapidly weakened, and the higher sun angle resulted in weak TENV evolution toward negative $\delta\theta/\delta x$ values. The TENV crossed into the Transition Zone at about 1800, three hours after 1500, and the sea breeze did not reach Pease.

The July 13 case began in the Strong Exclusion Zone, and the opposing wind component diminished throughout the day as the synoptic-scale cyclone moved away. As in the previous case, weak development toward negative $\delta\theta/\delta x$ values occurred as insolation and cold-air advection on the west side of the cyclone competed for dominance. The sea breeze never reached Pease because the opposing wind component remained too strong, and the mesoscale thermal PGF remained too weak. The July 25 case exhibited an increasing opposing wind component for the first hour, which then began to rapidly diminish as the cyclone moved away (toward the

northeast) from the study area. As in the previous two cases, the net result of daytime land-sea differential heating and cold-air advection was weak evolution toward negative $\delta\theta/\delta x$ values. The combination of the weakening synoptic-scale PGF and the development of a weak landward mesoscale PGF caused the TENV to cross into the Transition Zone after 1800 - too late for the sea breeze to reach the Pease airport.

Synoptic Class 4 (SC4). Of the seven SC4 cases examined, three were SB events, one was a MAR event, and three were NSB events (Figure 4.7). In the May 9 SB event, the TENV was inside the Transition Zone at 1200, indicating that a sufficient meso- α thermal PGF was already present for the sea breeze to reach Pease. Daytime land-sea differential heating (and the absence of cold-air advection into the study area) resulted in strong evolution toward negative $\delta\theta/\delta x$ values, and the TENV crossed into the Inclusion Zone by 1300. The cross-shore geostrophic wind component was fairly constant (near zero) until 2000, then drifted into slightly negative values, as the synoptic-scale flow backed to a more southerly direction. In the October 10 SB event, the TENV began in the Weak Exclusion Zone, and a combination of differential heating and a diminishing u_G moved the TENV into the Transition Zone after 1600. In the January

23 SB event, the TENV began in the Weak Exclusion Zone and crossed into the Transition Zone after 2000. The cross-shore geostrophic wind component increased from near zero at 1200 to about 8 ms^{-1} by 1900, then dropped back to zero again by 2200. Neither of the latter two events crossed into the Inclusion Zone.

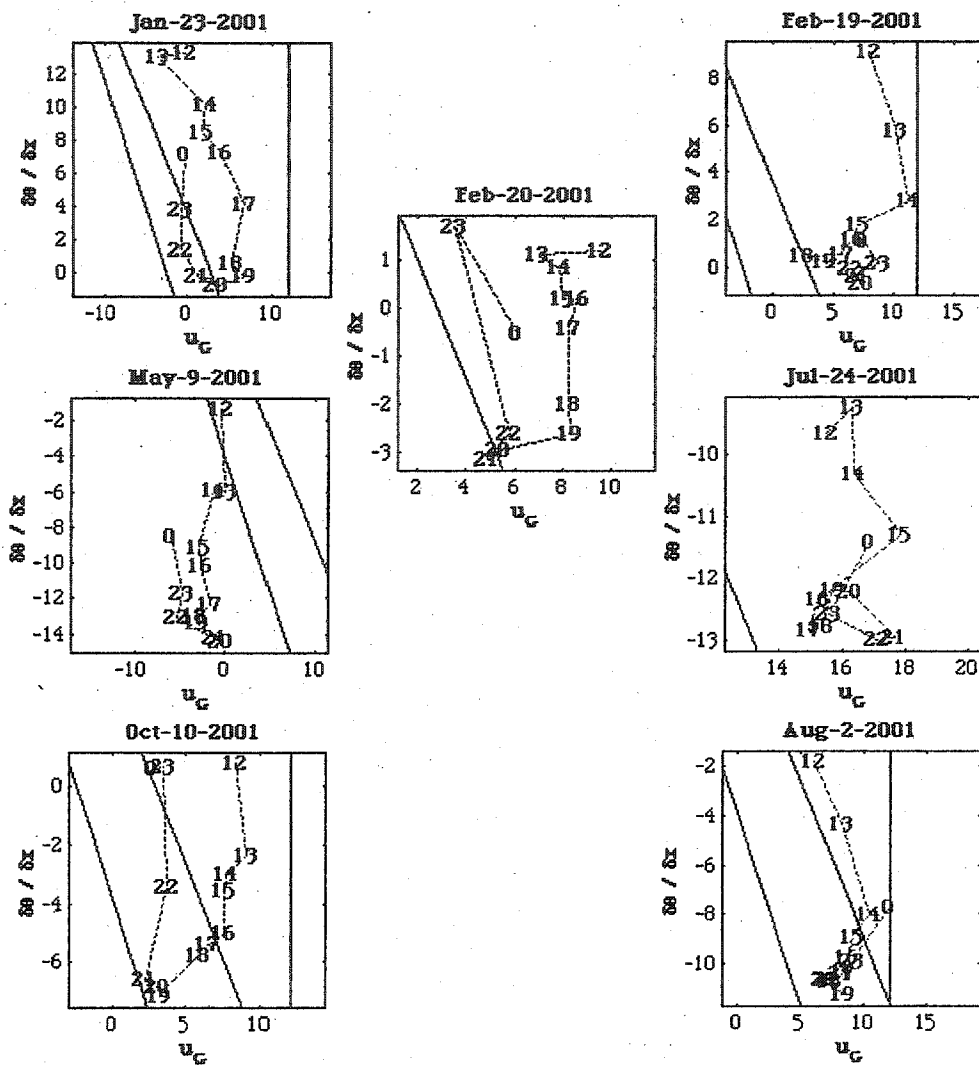


Figure 4.7: Time evolution of meso- α forcing during SB, MAR, and NSB events associated with synoptic class 4. Axes, reference lines, and color coding are the same as in Figure 4.4.

The February 20 MAR event began in the Weak Exclusion Zone, in the positive $\delta\theta/\delta x$ range, and evolved toward negative $\delta\theta/\delta x$ values

as insolation set up a sea-breeze favorable mesoscale PGF. The cross-shore geostrophic wind component diminished after 1900 as the geostrophic wind backed from the southwest toward the south, becoming more closely aligned in the along-shore dimension. The net result was that the TENV briefly crossed into the Transition Zone at 2000.

Two of the three NSB events (February 19 and August 2) also showed a great deal of diurnal variation on the $\delta\theta/\delta x$ axis. The same two events were marked by increasing u_G in the early part of the day that kept the TENV out of the Transition Zone. This was probably caused by an increase in the magnitude of the synoptic-scale PGF, as a cyclone and frontal system approached from the west. In the February 19 event, the net TENV briefly crossed into the Transition Zone at 1800, and in the August 2 event, it crossed into the Transition Zone between 1400 and 1500, and remained there until after 2300.

The third NSB event (July 24) exhibited a relatively steady u_G throughout the day (varying by only about 3 ms^{-1}), and a weak diurnal $\delta\theta/\delta x$ evolution toward negative values between 1200 and 0000 (and magnitude increase of only about $4 \text{ }^\circ\text{C} (100 \text{ km})^{-1}$, versus $8 \text{ }^\circ\text{C} (100 \text{ km})^{-1}$ or more in other cases), indicating the presence of an offsetting (cooling) factor. Examination of the Pease hourly

metar reports for July 24 indicates the presence of fog and haze that restricted visibility to 5 or 6 statute miles. Haze increases albedo over dark surfaces (Salby, 1996), and less radiation is absorbed by the solid Earth, so it is assumed that haze was the offsetting factor that prevented stronger development of negative $\delta\theta/\delta x$ values. The sea breeze did not occur on July 24 because u_G values remained too high for the entire day.

Synoptic Class 5 (SC5). The four SC5 cases examined are exclusively associated with NSB events at Pease (Figure 4.8). SB and MAR events do not occur with SC5 [Chapter 3]. The May 3 and December 1 events closely resembled SC1 NSB events. The June 19 and September 26 events resembled both SC3 and a SC4 events.

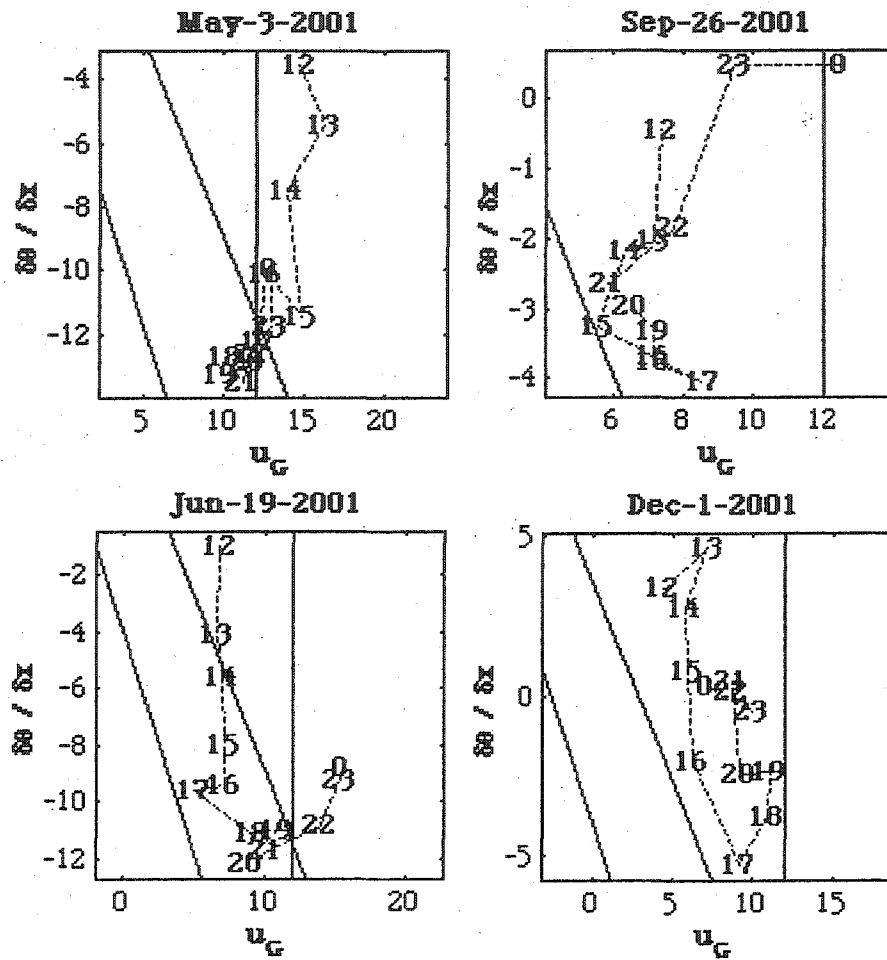


Figure 4.8: Time evolution of meso- α forcing during NSB events associated with synoptic class 5. Axes, reference lines, and color coding are the same as in Figure 4.4.

The May 3 and December 1 cases resembled SC1 NSB events, in that they exhibited weak variation in the u_G dimension ($\sim 5 \text{ ms}^{-1}$), and great variation in the $\theta\theta/\delta x$ dimension, indicating a consistent synoptic-scale PGF and the absence of significant cold-air advection. On May 3, daytime land-sea differential heating resulted in an

increasingly negative $\delta\theta/\delta x$, and the TENV crossed into the Transition Zone after 1600 and remained there until after 2300. On December 1, u_G was stronger and the TENV remained in the Weak Exclusion Zone for the entire period.

June 19 resembled both SC3 and SC4 NSB events. The TENV began in the Weak Exclusion Zone at 1200, then, driven by daytime land-sea differential heating and the absence of significant cold-air advection, $\delta\theta/\delta x$ fell by more than $10\text{ }^\circ\text{C (100 km)}^{-1}$ (as in some SC4 cases). The TENV crossed into the Transition Zone by about 1400. The cross-shore geostrophic wind component showed little variation until after 2100, when the synoptic-scale wind rotated further into the cross-shore dimension, resulting in an increase of about 10 ms^{-1} , and moving the TENV back to the right and out of the Transition Zone. Increases of this magnitude in u_G are often associated with SC3 cases.

September 26 also resembled both SC3 and SC4 NSB events. As in an SC3 event, significant cold-air advection was present, limiting land-sea differential heating to a $\delta\theta/\delta x$ change of only about $5\text{ }^\circ\text{C (100 km)}^{-1}$. As in an SC4 event, the TENV drifted toward positive u_G values as the cross-shore component of the synoptic-scale wind increased from 6 to 12 ms^{-1} – an increase of only about 6 ms^{-1} .

Synoptic Class 6 (SC6). Of the five SC6 cases studied, two were SB events, one was an MAR event, and two were NSB events (Figure 4.9). The TENVs associated with the two SB events are similar, in that they both began in the Inclusion Zone. A landward cross-shore geostrophic wind component over the study area is a common outcome of the arrangement of synoptic-scale pressure systems associated with SC6 (Figure 4.2). Both events exhibited evidence of relatively weak daytime land-sea differential heating -- a change in both cases of only about $6\text{ }^{\circ}\text{C}\text{ (100 km)}^{-1}$ (discussed below). In both events, u_G values began in the negative and evolved toward positive u_G values. This reorientation of the large-scale flow resulted when the cyclone to the southeast of the study area moved further away and the anticyclone to the north or northwest approached. In the August 25 event, u_G increased by almost 10 ms^{-1} , reaching about $+5\text{ ms}^{-1}$ by 2000, as the geostrophic wind associated with approaching anticyclone backed from a northeasterly (crossing the shore toward land) direction to a more northwesterly (crossing the shore toward sea) direction. In the September 29 event, u_G increased by about 10 ms^{-1} , but remained in the negative, as the weak gradient region near

the center of the synoptic anticyclone moved closer to the study area.

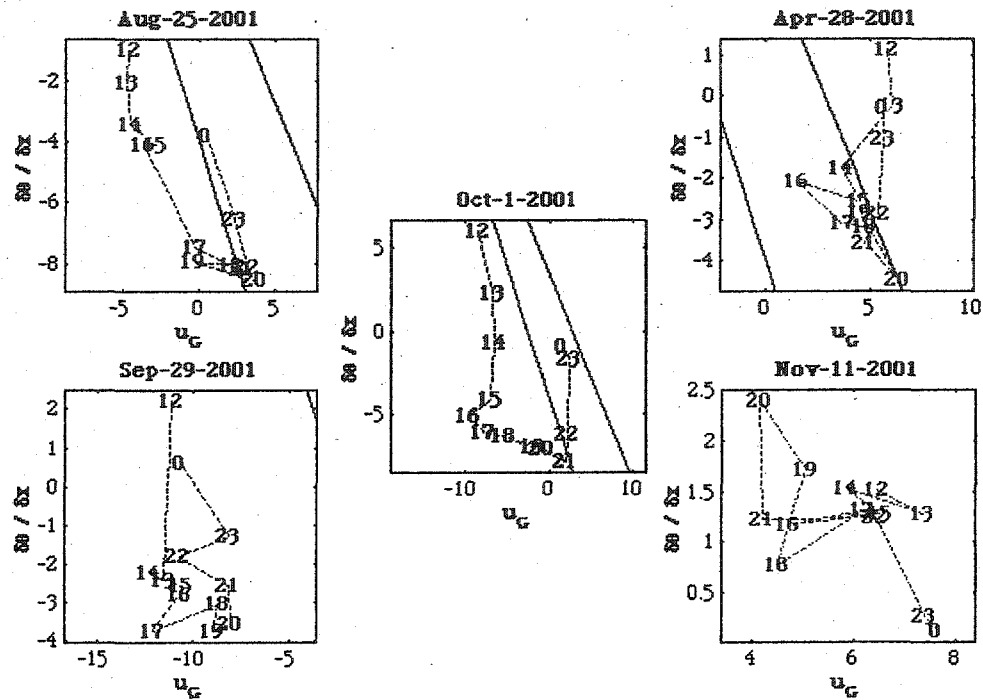


Figure 4.9: Time evolution of meso- α forcing during SB, MAR, and NSB events associated with synoptic class 6. Axes, reference lines, and color coding are the same as in Figure 4.4.

The October 1 MAR event differs from the SC6 SB events in that $\delta\theta/\delta x$ exhibited evidence of stronger daytime land-sea differential heating. The cross-shore potential temperature gradient changed by more than $10\text{ }^\circ\text{C (100 km)}^{-1}$ during the day. As in the August 25 SB event, u_G increased by more than 10 ms^{-1} during the

day, reaching weak positive values by 2100. The evolution of the TENV indicates that u_G moved to the right because the synoptic-scale wind was backing (becoming more shore-parallel), and diminishing as the weak-gradient region of the anticyclone approached the study area.

As in the SC6 SB events, both of the SC6 NSB events exhibited evidence of weak land-sea differential heating. The April 28 event changed, somewhat erratically, by about $6\text{ }^\circ\text{C (100 km)}^{-1}$, and the November 11 event changed by less than $3\text{ }^\circ\text{C (100 km)}^{-1}$. One may be tempted to attribute the latter to the late time of year and a resulting low Sun angle, but this should be compared to the December 1 SC5 NSB event, when $\delta\theta/\delta x$ changed by more than $10\text{ }^\circ\text{C (100 km)}^{-1}$ through the day. The reason for this weak change in the land-sea temperature contrast can be determined by examining the cross-shore geostrophic wind components with the NSB events. In both the April 28 and November 11 cases, u_G began in positive values and remained there throughout the day, indicating an offshore geostrophic wind component. The November 11 event, associated with a somewhat stronger u_G , is also associated with the weaker daytime changes in $\delta\theta/\delta x$. This indicates that cold-air advection on the east side of the anticyclone was an important factor in limiting the daytime land-sea differential heating.

The TENVs with both of the SC6 NSB events began in the Weak Exclusion Zone. The TENV associated with the April 28 event moved into the Transition Zone by about 1400, but the plot associated with the November 11 event remained in the Weak Exclusion Zone for the entire period.

Discussion

In this section, conclusions are presented regarding the observed behavior of the net sea-breeze forcing and sea-breeze system response in Portsmouth. These are discussed in terms of the combined results (Table 4.2), and as a function of the six well-defined synoptic classes. Table 4.3 summarizes the behavior of the meso- α forcing as a function of synoptic class.

Table 4.2: Summary of case studies. SB = Sea breeze; MAR = Marginal; NSB = Non-sea-breeze. Hour of onset of the sea breeze at Pease airport (UTC) shown for SB and MAR events. Synoptic classes are described in Figure 4.2 and Table 4.1. TENV line A crossing determined from Figures 4.4 - 4.9.

Date [MM/DD/YYYY]	Type of event	Synoptic class	Time of Onset [UTC]	Time TENV Crossed left of line A into TZ [UTC]
01/23/2001	SB	4	2300	2000
02/10/2001	NSB	3		Never
02/19/2001	NSB	4		Never
02/20/2001	MAR	4	2300	2100
04/03/2001	SB	2	1800	1400
04/28/2001	NSB	6		1400
04/29/2001	NSB	1		1800
05/02/2001	NSB	2		1500
05/03/2001	NSB	5		1700
05/09/2001	SB	4	1500	(Entire period)
05/10/2001	SB	1	1800	(Entire period)
05/11/2001	SB	2	1600	(Entire period)
06/19/2001	NSB	5		1300
06/26/2001	MAR	2	2100	(Entire period)
07/06/2001	NSB	2		Never
07/07/2001	MAR	1	2000	1630
07/13/2001	NSB	3		Never
07/24/2001	NSB	4		Never
07/25/2001	NSB	3		1800
07/28/2001	SB	1	1800	1300
08/02/2001	NSB	4		1430
08/18/2001	NSB	2		2200
08/22/2001	SB	2	1600	(Entire period)
08/25/2001	SB	6	1500	(Entire period)
09/26/2001	NSB	5		Never
09/27/2001	NSB	3		1730
09/29/2001	SB	6	1700	(Entire period)
10/01/2001	MAR	6	2300	(Entire period)
10/09/2001	NSB	1		1500
10/10/2001	SB	4	2100	1700
11/11/2001	NSB	6		Never
12/01/2001	NSB	5		Never

Table 4.2 indicates that, in cases when the TENV was to the right of line A at 1200, the sea breeze reaches Portsmouth (SB or

MAR events) after the TENV moves into the Transition Zone. The observed mean lead time (the difference between the time the TENV crosses into the Transition Zone and the onset in Portsmouth) is about four hours, with a minimum of two and a maximum of five hours. For all of these cases the mean onset time of the sea breeze (SB or MAR event) in Portsmouth is about 2030, but it occurs as early as 1800 and as late at 2300. In cases where the TENV is already to the left of line A at 1200 UTC, the mean arrival time of the sea breeze (SB or MAR event) in Portsmouth is three hours earlier, at 1730, with the earliest occurring at 1500 and the latest at 2300. This difference is logical because in the cases where the TENV begins to the left of the line A, the cross-shore geostrophic wind component is relatively weak, a weaker meso- α thermal PGF is needed to overcome it, and the sea breeze is able to reach Portsmouth at an earlier time.

Table 4.3: Observed meso- α forcing and sea-breeze response by synoptic class.

Synoptic Class	Meso- α forcing and sea breeze response
1	<p>Sea breezes occur when daytime differential heating of the land and sea-surfaces creates a landward mesoscale PGF that overcomes a relatively constant u_G. If u_G is less than 5 ms^{-1} at 1200 UTC, a well-developed sea breeze can reach Portsmouth.</p> <p>Most of the diurnal variation is on the $\delta\theta/\delta x$ axis. An increase (toward negative values) in $\delta\theta/\delta x$ of at least $8 \text{ }^\circ\text{C} (100\text{km})^{-1}$ after 1200 UTC is common. There is no significant cold-air advection into the study area.</p> <p>Sea breezes will reach Portsmouth if the mesoscale PGF becomes strong enough to overcome the opposing u_G before 1500 UTC (1000 LST). This is indicated by the movement of the TENV into the Nowcast Diagram Transition Zone.</p>
2	<p>Synoptically, SC2 is intermediate between SC1 and SC3, and this is reflected in the behavior of the meso-α forcing:</p> <ul style="list-style-type: none"> • SC2 may be associated with strong cold-air advection into the study area, which limits the development of a sea-breeze favorable $\delta\theta/\delta x$. In the absence of cold-air advection, an increase (toward negative values) in $\delta\theta/\delta x$ of at least $8 \text{ }^\circ\text{C} (100\text{km})^{-1}$ after is common. • SC2 may also exhibit a u_G that increases during the day, and prevents the sea breeze from reaching Portsmouth. If u_G is less than 5 ms^{-1} at 1200 UTC, a well-developed sea breeze can reach Portsmouth. <p>Sea breezes will reach Portsmouth if the mesoscale PGF becomes strong enough to overcome the opposing u_G before 1500 UTC (1000 LST). This is indicated by the movement of the TENV into the Nowcast Diagram Transition Zone.</p>
3	<p>SB events do not occur.</p> <p>The development of a strong landward mesoscale PGF is prevented by cold-air advection on the west side of the cyclone, which offsets daytime land-sea differential heating.</p> <p>Most of the diurnal variation is on the u_G axis, which may vary by more than 20 ms^{-1}. In extreme cases, u_G increases as the wind velocity between the synoptic-scale anticyclone and cyclone increases or reorients.</p>

Table 4.3 (Continued): Observed meso- α forcing and sea-breeze response by synoptic class.

4	<p>SB events exhibit significant evolution toward negative $\delta\theta/\delta x$ values, indicating the absence of cold-air advection. Cold-air advection is unlikely in SC4, since the synoptic-scale flow in the study area is from the south or southwest, which is more likely to produce warm-air advection. If haze is not advected into the study area, $\delta\theta/\delta x$ may increase (toward negative values) by more than $8\text{ }^{\circ}\text{C (100km)}^{-1}$ at 1200 UTC. If haze reduces visibility below 6 miles, diurnal variation in $\delta\theta/\delta x$ will be reduced to less than $4\text{ }^{\circ}\text{C (100km)}^{-1}$.</p> <p>In SB and MAR events, u_G may diminish during the day, which is probably caused by the synoptic-scale flow backing from southwesterly (near-zero to positive u_G values over study area) to southerly (negative u_G values). This occurs as the cyclone (with cold front trailing to the southwest; see Figure 4.2) approaches the study area. Diurnal variation in u_G between 1200 and 0000 is about 5 to 7 ms^{-1}.</p>
5	<p>SB events do not occur. Meso-α forcing with NSB events may exhibit characteristics resembling SC1, SC3 and SC4 NSB events:</p> <ul style="list-style-type: none"> • The arrangement of synoptic-scale pressure centers (and their associated wind fetches) occurring with SC5 should be followed by the arrangement associated with SC1, i.e., a migratory cyclone is usually followed by a migratory anticyclone in the mid-latitudes. • SC5 is characterized by southwesterly synoptic-scale flow following the passage of a cold front, which is often associated with cold-air advection in the study area. • Both SC4 and SC5 are both associated with southwesterly synoptic-scale flow over the study area.

Table 4.3 (Continued): Observed meso- α forcing and sea-breeze response by synoptic class.

6	<p>SB and MAR events occur when u_G is negative (toward the land), and NSB events occurred when u_G was positive (toward the sea). With the coast oriented toward 30 degrees, this indicates that the sea breeze will reach Portsmouth if the geostrophic wind is between 30 and 90 degrees, but not if it has a more northerly component.</p> <p>Differs from SC1 and SC2 in two important ways:</p> <ul style="list-style-type: none"> • The time that the TENV crosses into the Transition Zone cannot be used to predict the occurrence of the sea breeze at Pease. This indicates that a third physical variable (probably associated with the wind aloft) must be quantified for accurate sea-breeze predictions. • It is usually marked by relatively weak land-sea differential heating. There are two possible causes: 1) A landward geostrophic flow component limits the developing warm pool over land by continuously moving in cooler marine air. 2) Cold-air advection on the east side of the anticyclone moves cooler air into study area. Both offset uneven diabatic heating of the land and sea surfaces.
---	---

In SC1 and SC2 cases, forecasters can expect an increase (toward negative values) in the cross-shore potential temperature gradient of at least $8\text{ }^\circ\text{C (100km)}^{-1}$ after 1200, provided there is no significant cold-air advection on the east side of the anticyclone. If the cross-shore geostrophic wind component is less than about 5 ms^{-1} at 1200 (it may vary by $5\text{ to }7\text{ ms}^{-1}$ during the day), it is possible for a well-developed sea breeze to reach Portsmouth. MAR (weak) sea breezes are possible in Portsmouth if u_G is *greater* than about 5 ms^{-1} at 1200, but only if the weak-gradient region near the center of the anticyclone moves into the study area. If the

combination of the evolving $\delta\theta/\delta x$ and u_G values move the TENV into the Transition Zone by 1500, the sea breeze will reach Portsmouth.

SB events associated with SC4 showed significant evolution toward negative $\delta\theta/\delta x$ values, indicating the absence of cold-air advection. Since SC4 is associated with southwesterly geostrophic flow, warm-air advection into the study area, as well as the possible transport of haze, is likely. In at least one instance, haze seems to have reduced the amount of variation in $\delta\theta/\delta x$ from more than $8\text{ }^\circ\text{C (100km)}^{-1}$ (as would be expected in an SC4 SB event) to less than $4\text{ }^\circ\text{C (100km)}^{-1}$. SC4 events may exhibit mean u_G values ranging from -8 to $+16\text{ ms}^{-1}$, varying by 5 to 7 ms^{-1} over the day. SC4 shows a wider range in possible daily-mean values of u_G than SC1 because of the difference in the arrangement of large-scale highs and lows. In the SC1 cases, a migratory anticyclone is west or southwest of the region, moving slowly eastward. The cross-shore geostrophic wind component is relatively light, and grows progressively lighter as the weak-gradient region near the center of the anticyclone approaches. In the SC4 cases, a synoptic-scale front or trough approaches the region from the west, and an anticyclone is to the south or southeast. The geostrophic wind over the study area is southwesterly, but the precise orientation of the isobars varies considerably from one case to another, depending (for example) on

whether the anticyclone to the south is a migratory anticyclone that originated in Canada, or the quasi-stationary subtropical ridge. In the case of a moving anticyclone to the south, the geostrophic wind ahead of the approaching cold front can maintain a significant positive u_G . In the case of quasi-stationary anticyclone to the south, the geostrophic flow ahead of the approaching cold front may become “squeezed” and reoriented into a more southerly configuration. Mainly southerly winds result in negative u_G values over the study area.

Most of the time, forecasters can expect relatively weak land-sea differential heating to occur with SC6, which has two causes. In most cases, cold-air advection on the east and southeast side of the anticyclone offsets uneven heating of the land and sea surfaces via insolation. If there is a significant landward geostrophic wind component, the developing warm pool over land may also be limited by the continuous low-level introduction of cooler marine air from the Gulf of Maine. Forecasters can expect SC6 SB and MAR events to occur when u_G is negative (toward the land), and NSB events to occur when u_G is positive (toward the sea).

Sea breezes do not occur in Portsmouth with SC3 or SC5 [Chapter 3]. In this chapter it is shown that in SC3, cold-air

advection on the west side of the cyclone prevents the development of a strong landward mesoscale PGF. Most of the diurnal variation in SC3 TENVs is in the u_G dimension, which may increase by as much as 20 ms^{-1} as the synoptic-scale PGF between the anticyclone and the cyclone increases or reorients. Chapter 3 showed that u_G values of greater than 12 ms^{-1} prevented the sea breeze from reaching Pease, regardless of the strength of $\partial\theta/\partial x$. In this chapter it is shown that in SC5, cold-air advection behind a passing cold front limits the development of a strong cross-shore potential temperature gradient, and the cross-shore geostrophic wind component is too strong.

SC4 and SC6 cases differ from SC1 and SC2 cases in that the time that TENV crosses from the Weak Exclusion Zone into the Transition Zone cannot be used to predict whether a sea breeze will reach Portsmouth. This suggests the need for additional indices to more rigorously differentiate the net forcing in SB, MAR, and NSB events. There are two synoptic-scale impacts that may suppress the development of the sea breeze. The first is the cross-shore component of the near-surface geostrophic wind (u_G), which is used as one of the indices in this study. The second is the synoptic-scale temperature gradient, a factor preventing sea breezes under SC3 and SC5, that has not been taken into consideration. Therefore,

future research is warranted to account for both the synoptic-scale dynamic and thermodynamic impacts on the sea breeze.

Summary

This chapter extends the work of Chapter 3 by examining the time-evolution of the net meso- α sea-breeze forcing on the central New England coast. The net sea-breeze forcing is diagnosed as a combination of the cross-shore geostrophic wind component and the mesoscale cross-shore potential temperature gradient. These two components form the basis of a time-evolving nowcast vector (TENV), which is plotted with hourly values on the Nowcast Diagram shown in Figure 4.3. The TENVs were examined for 32 sea breeze, marginal, and non-sea breeze events under different synoptic-scale situations at all times of the year. Specific conclusions were drawn for Pease airport, in Portsmouth, New Hampshire.

In cases where the TENV began the day in the Weak Exclusion Zone (between lines A and C), the sea breeze reaches Portsmouth two to five hours after the TENV moved into the Transition Zone (between lines A and B). The mean lead time is about four hours, with a mean sea breeze onset time in Portsmouth of about 2030 UTC (1530 LST) \pm ~ 2 hrs. In cases where the TENV begins the day in the

Transition Zone, the mean arrival time of the sea breeze in Portsmouth is about three hours earlier, at about 1730 UTC (1230 LST). Compared to the latter cases, the cross-shore geostrophic wind component in the former cases more strongly resists inland propagation of the sea breeze, and the mesoscale PGF created by local land-sea differential heating must be stronger to drive the sea breeze 10 km inland to the Pease airport.

In SC1 and SC2 cases, forecasters can expect an increase (toward negative values) in the cross-shore potential temperature gradient of at least $8\text{ }^{\circ}\text{C}\text{ (100km)}^{-1}$ after 1200 UTC (0700 LST), provided there is no significant cold-air advection on the east side of the anticyclone. A sea breeze will reach Portsmouth if the cross-shore geostrophic wind component is less than about 5 ms^{-1} at 1200 UTC (0700 LST), and the combination of the evolving $\delta\theta/\delta x$ and u_G values move the TENV into the Transition Zone by 1500 UTC (1000 LST). Sea-breeze events associated with SC4 also show significant evolution toward negative $\delta\theta/\delta x$ values, indicating the absence of cold-air advection. Because SC4 is associated with synoptic-scale southwesterly flow, warm-air advection into the study area, as well as the possible transport of haze, is likely. In at least one instance, haze seems to have reduced the amount of variation in $\delta\theta/\delta x$ from more than $8\text{ }^{\circ}\text{C}\text{ (100km)}^{-1}$ (observed in SC4 in the absence of haze)

to less than $4\text{ }^{\circ}\text{C (100km)}^{-1}$, limiting the development of a strong landward mesoscale PGF, and preventing the sea breeze from reaching Pease.

Forecasters can usually expect relatively weak land-sea differential heating to occur with SC6, which has two causes: Cold-air advection on the east and southeast side of the anticyclone, which offsets uneven heating of the land and sea surfaces via insolation, and the continuous low-level introduction of cooler marine air over from the Gulf of Maine to the land by the synoptic-scale wind. Forecasters can expect SC6 SB and MAR events to occur when u_G is negative (toward the land), and NSB events to occur when u_G is positive (toward the sea). Sea breezes do not occur at Pease with SC3 or SC5 because cold-air advection on the west side of the cyclone prevents the development of a strong landward mesoscale PGF, and the cross-shore wind component may be greater than 12 ms^{-1} , shown in Chapter 3 to prevent the sea breeze from reaching Pease, regardless of the strength of $\delta\theta/\delta x$.

In SC4 and SC6 cases, the time that TENVs crosses from the Weak Exclusion Zone into the Transition Zone cannot be used to predict whether a sea breeze will reach the Pease airport. Future research will account for both the synoptic-scale dynamic and thermodynamic impacts on sea breeze development, and improve

sea-breeze forecasting in SC4 and SC6. Future research will also examine the meso- β (20 - 200 kms; [Fujita, 1986]) details of sea-breeze response in differing synoptic and meso- α forcing environments, and determine sea breeze influence on ground-level ozone in east central New England.

CHAPTER V

THE SEA BREEZE: MESO-ALPHA FORCING AND MESO-BETA RESPONSE, PART I: CIRCULATION AND GRAVITY CURRENT

CHAPTER V

THE SEA-BREEZE: MESO-ALPHA FORCING AND MESO-BETA RESPONSE, PART I: CIRCULATION AND GRAVITY CURRENT

ABSTRACT

This work compares the meso- β response of the sea-breeze circulation and gravity current to meso- α forcing on the central New England coast, using twelve case-studies from the year 2001. Considerable along-shore variation is documented in both the kinematic (wind circulation) and isentropic (potential temperature) fields. New practical forecasting techniques are developed, enabling operational meteorologists to predict the areas that will be invaded by marine air during a sea-breeze event, the earliest time of onset along the coast, and the maximum inland penetration. These techniques are adaptable to any coastal location, and improve the forecasting techniques proposed in previous studies.

Introduction

The sea breeze is a mesoscale wind that occurs at coastal locations throughout the world, and is an important influence on New England's weather, climate, and air quality. It can provide moisture for early-morning fog and afternoon thunderstorms, at

points ranging from the shore to more than 50 kilometers inland, and may trap pollutants in a shallow layer near Earth's surface, reducing air quality in the coastal zone [*Barbato, 1975; Hsu, 1988; Gaza, 1998; Seaman and Michelson, 2000*]. For these reasons it is important to better understand the local-scale behavior of the New England sea breeze, and how this behavior varies with the larger-scale meteorological environment.

The sea-breeze system (Figure 5.1) consists of many nested phenomena, and develops when insolation and differential heating of the land and sea surfaces create a mesoscale pressure gradient force (PGF) pointing toward the land [*Simpson, 1994; Tijn and van Delden, 1999*]. The sea-breeze circulation (SBC) is a vertically-rotating cell in which a shallow layer of marine air flows inland and converges with continental air. Vertical currents develop in the convergence zone between the sea breeze and the ambient flow -- called the kinematic sea-breeze front -- which creates a raised sea-breeze head (SBH; [*Finkele et al., 1995*]). Fair weather cumulus (Cu) may develop in convective updrafts landward of the front. The circulation is usually closed by seaward return flow near 900 hPa, and weak sinking currents over a broad area several tens of kilometers offshore [e.g. *Estoque, 1962; Elliott and O'Brien, 1977*;

Camberlin and Planchon, 1997; Chiba et al., 1999; Oliphant et al., 2001].

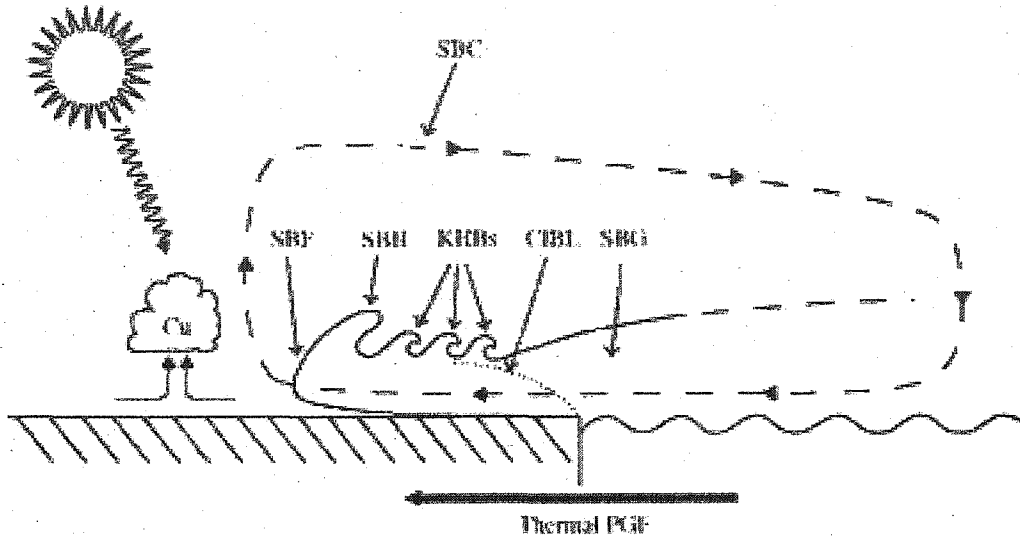


Figure 5.1: Sea-breeze system. See text for discussion.

The sea-breeze gravity current (SBG) is the landward flow of cool, moist marine air in the lower half of the SBC. The leading edge of the SBG - called the thermodynamic sea-breeze front - is beneath the SBH, and is usually associated with a strong cross-shore temperature gradient. Kelvin-Helmholtz Billows (KHBs) may develop over land in the shear zone between the upper boundary of the SBG and the seaward return flow, creating a turbulent wake behind the SBH [Simpson, 1969; Sha, 1991; Atkins et al., 1995; Chiba et al., 1999]. A Convective Internal Boundary Layer (CIBL)

may develop in the SBG, landward of the coast [Hsu, 1988; Stull, 1988; Prabha et al., 2002].

Both the wind and temperature fields associated with the sea-breeze system are subject to distortions created by insolation and local topography. The wind is channeled by topography, which may create regions of convergence that are not associated with the sea-breeze [e.g. Physick and Abbs, 1992]. Topography may also cause distortions to the in situ thermal field: adiabatic cooling of the marine air as it is lifted will create a temperature gradient unrelated to an airmass boundary [Hess, 1959]. The near-surface airmass is subject to uneven local diabatic heating from below, especially during summer and autumn, which rapidly modifies the air near the surface and may mask the marine influence [Atkins et al., 1995]. Diabatic heating may also result in the creation of an additional thermodynamic sea-breeze front immediately on the coast, marking the boundary between the unmodified marine air offshore and the modified marine air inland. Uneven inland heating may create additional convergence lines resulting from microscale (<2 km; [Fujita, 1986]) density flows, such as river and lake breezes, which can also mask the low-level convergence associated with the kinematic sea-breeze front [Zhong and Takle, 1992].

The prevailing wind (PW) plays a large role in determining the shape of the SBC, which can be described as falling into three generic, PW-dependent categories: *Pure*, *corkscrew*, and *backdoor* [Adams, 1997]. A "pure" sea breeze occurs under light PW conditions, when the existing geostrophic forcing is perpendicular to the coastline, pointing seaward. The "corkscrew" sea breeze occurs when the PW has both along-shore and cross-shore components. The along-shore component is northward on the east coast of a Northern Hemisphere landmass, causing the corkscrew SBC to circulate in a helical shape rather than a simple loop. The "backdoor" sea breeze also occurs when the PW has along-shore and cross-shore components, but the along-shore component is southward rather than northward on the east coast of a Northern Hemisphere landmass [Adams, 1997].

Previous studies [e.g. *Biggs and Graves*, 1962; *Simpson*, 1994; Chapters 3 and 4] have compared sea-breeze system response to meso- α (200 - 2000 kms; [*Fujita*, 1986]) forcing in an effort to improve forecasting skill. These studies have generally used the cross-shore temperature gradient as a parameter representing the mesoscale pressure gradient force that drives the sea breeze toward land, and either an observed or calculated cross-shore wind component to represent the force resisting the landward movement

of the sea breeze. Chapters 3 and 4 used the meso- α cross-shore potential temperature gradient ($\partial\theta/\partial x$), and the cross-shore geostrophic wind component (u_G), but noted that this approach results in ambiguous forecasts in some synoptic-scale environments, because it fails to account for the effect of the large-scale temperature gradient on the sea-breeze system. A more complete set of forecast indices would include one parameter corresponding to the meso- α thermal PGF, and another that takes both the the synoptic-scale dynamics and temperature gradient in account.

Mizuma [1995, 1998] utilized near-surface wind data, recorded at fine spatial resolution, to study the behavior of the sea breeze on the coast of Japan. He developed a series of sea-breeze types based on the time of onset at different points on the coast, whether or not sea breezes initiated at different points interacted later in the day, and the interaction between sea breezes and other locally-generated winds. *Mizuma's* [1995, 1998] sea-breeze types focused on the sea-breeze circulation, but did not explicitly examine the behavior of the near-surface potential temperature field, which would have revealed the location and movement of the sea-breeze gravity current.

This chapter addresses means to improve sea breeze forecasting in east central New England by examining the impacts of

synoptic-scale dynamics and thermodynamics, meso- α thermal forcing, and regional topography on the sea-breeze system. The three primary objectives are to 1) improve the forecasting skill of the meso- α sea-breeze Nowcast Diagram presented in Chapters 3 and 4 by substituting the calculated cross-shore geostrophic wind component with an improved parameter; 2) quantify the time-evolving meso- β (20 - 200 kms; [Fujita, 1986]) behavior of the SBC and SBG in the study area (Figure 5.2) in terms of a series of topographically-related patterns; and 3) quantify the relationship between the net meso- α forcing and the meso- β response of the sea-breeze system in the study area. The last objective includes identifying the forcing regimes wherein the SBC and SBG are not closely linked. The SBC and SBG were chosen as the primary sea-breeze components of interest because they are the spatially dominant components of the system, and can be measured in detail with conventional meteorological instruments positioned on Earth's surface.

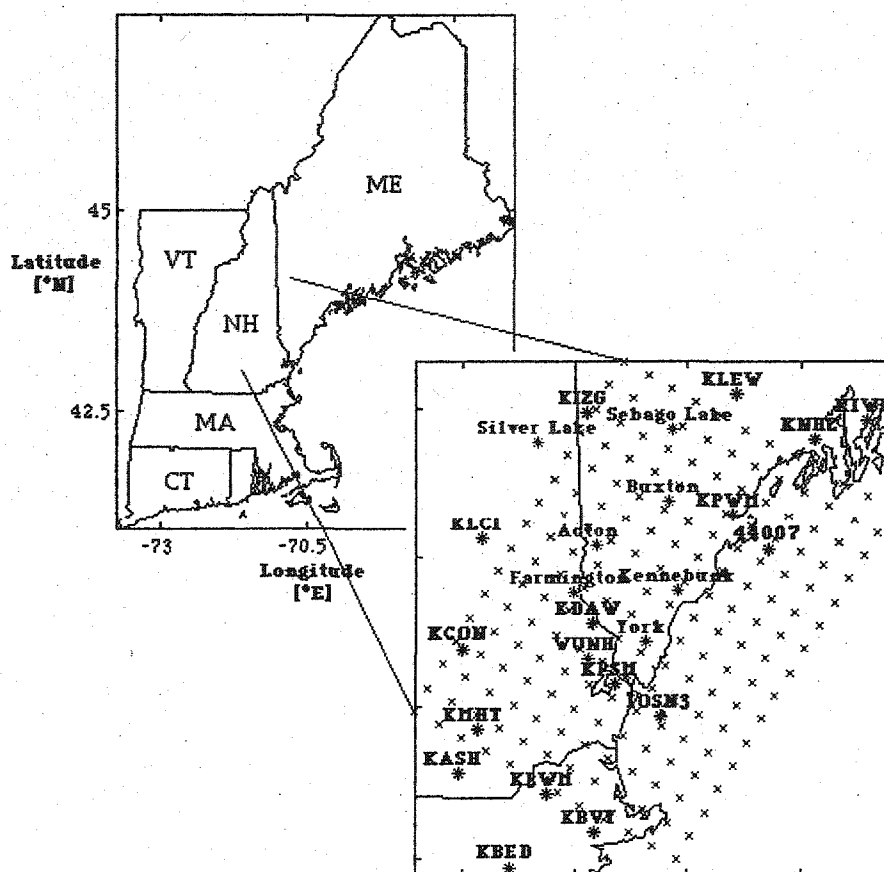


Figure 5.2: Study area. Standard NOAA surface observing stations (black) are identified by International Civil Aviation Organization identifier. UNH stations are plotted in red. Blue “x” indicate grid points used for interpolated scalar fields.

Research on the New England sea breeze was carried out as part of the Atmospheric Investigation, Regional Modeling, Analysis, and Prediction (AIRMAP) project. The primary goal of AIRMAP is to understand the factors influencing climate and air quality in New England. The goal of the Central New England Sea Breeze Study is to

understand the physical behavior of the sea breeze on the central New England coast, and aid in its prediction.

Scope and Methods

The study area includes the relatively straight section of New England's coastline between Cape Ann, Massachusetts, and Wiscasset, Maine (Figure 5.2). This section of coastline was chosen to avoid "edge effects" introduced by seaward projections of land, and simplifying the problem of describing sea-breeze behavior. *Barbato* [1975] noted that the Boston-area sea breeze extends about 30 kilometers inland, and others [e.g., *Hadi et al.*, 2002] have observed that the sea breeze is prevented from further inland penetration by mountain ranges more 60 kilometers from the coast. *Simpson* [1994] noted inland intrusions of more than 200 kilometers in the absence of topographic obstructions. With this in mind, the inland boundary of our study area was set to 65 kilometers, bringing the northwest boundary to the edge of the White Mountains. The offshore boundary was set to the expected limits of land-breeze phase of the circuit -- forty kilometers from shore [*Simpson*, 1994; *Holmer and Haeger-Eugensson*, 1999]. The northeastern and southwestern boundaries correspond to the

straight section of coastline noted above. The southwestern boundary was extended somewhat beyond the straight section of coastline to include a meso- γ scale (2 - 20 kms; [Fujita, 1986]) network of wind recording stations in the vicinity of Newburyport, Massachusetts.

Twelve case-studies were selected from the year 2001 for this analysis. These events were chosen because they collectively span the range of variation in $(\delta\theta/\delta x, u_G)$ meso- α forcing observed in Chapters 3 and 4 during year-2001 sea-breeze (SB) and marginal events (MAR), and borderline non-sea-breeze (NSB) events (Figure 5.3 and Table 5.1). Values of u_G and $\delta\theta/\delta x$ (shown in Figure 5.3) were calculated for the moment of onset (for sea-breeze and marginal events) in Portsmouth, New Hampshire (10 km inland), or 1900 UTC (for non-sea breeze events). Sea breeze events were defined as the occurrence of a local, insolation-driven wind from the southeast in Portsmouth [Chapters 3 and 4]. Marginal events were weak sea breezes, and non-sea breeze events were those when sufficient insolation was available to drive a sea breeze, but it did not reach Portsmouth [Chapters 3 and 4].

Table 5.1: Case study dates, synoptic classes, and event types. Synoptic classes are described in Chapter 3. Types of events are sea-breeze (SB), marginal (MAR), and non-sea-breeze (NSB).

Date [MM/DD/YYYY]	Type of Event ¹	Synoptic Class
01/23/2001	SB	4
04/03/2001	SB	2
05/09/2001	SB	4
05/10/2001	SB	1
05/11/2001	SB	2
06/14/2001	SB	7
07/06/2001	NSB	2
07/07/2001	MAR	1
07/13/2001	NSB	3
07/28/2001	SB	1
08/18/2001	NSB	2
09/29/2001	SB	6

Notes:

1. Type of event determination is based on the occurrence/non-occurrence of the sea breeze at Pease airport, in Portsmouth, New Hampshire.

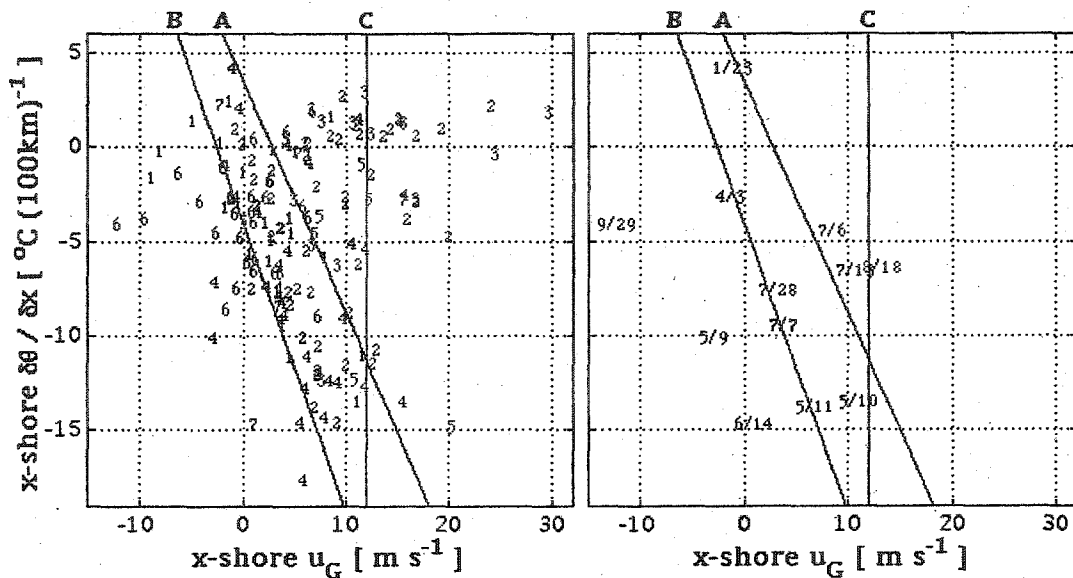


Figure 5.3: Case-study events as a function of their associated cross-shore potential temperature gradients ($\delta\theta/\delta x$) and geostrophic wind components (u_G). Events are plotted using the regional-scale temperature gradients and geostrophic wind components present at either the time of onset (for sea breezes and marginal events), or 1400 LST (for non-seabreeze events). Sea-breeze events are in blue, marginal events are in black, and non-seabreeze events are in red. Left: Synoptic classes of all events in 2001 [Chapter 3]. Right: Dates of case-studies chosen for this work.

Previous sea-breeze forecasting studies have neglected the impact of the synoptic-scale temperature gradient. A single parameter, representing the influence of the synoptic-scale wind and the synoptic-scale temperature gradient in the planetary boundary layer can be derived from the vector form of the thermal wind relation:

$$V_T = V_G(p_1) - V_G(p_0) = - \frac{R}{f} \int_{p_0}^{p_1} (\mathbf{k} \times \nabla_p T) d \ln p \quad (5.1)$$

where V_T is the thermal wind in the layer from p_0 to p_1 ; $V_G(p_0)$ and $V_G(p_1)$ are the geostrophic wind at pressure levels p_1 and p_0 , respectively; R is the universal gas constant; f is the local coriolis parameter; and $\nabla_p T$ is the synoptic-scale temperature gradient on a constant pressure surface [Holton, 1992]. By rearranging (5.1), the geostrophic wind at p_1 can be expressed as:

$$V_G(p_1) = V_G(p_0) - \frac{R}{f} \int_{p_0}^{p_1} (\mathbf{k} \times \nabla_p T) d \ln p \quad (5.2)$$

If u_G is the cross-shore geostrophic wind component near Earth's surface [scalar form of $V_G(p_0)$], and u_{925} is the cross-shore wind component at 925 hPa [scalar form of $V_G(p_1)$], then the difference between them is a function of the vertically-averaged synoptic-scale temperature gradient in the surface - 925 hPa layer. This work improves on the Nowcast Diagram developed in Chapters 3 and 4 by substituting u_{925} for u_G , and therefore accounts for the

two critical synoptic-scale impacts on the sea-breeze system. Values of u_{925} above the study area was interpolated from 1200 and 0000 UTC 925 hPa charts obtained from the Plymouth State College website (<http://vortex.plymouth.edu>).

The spatial and temporal evolution of the SBC and SBG were examined using near-surface meso- β wind and potential temperature fields. These fields were derived from observations of temperature, pressure, and wind in the study area. The surface observations produced by the standard NOAA surface observing network within the study area were supplemented with a series of automated weather stations placed in areas with sparse coverage, creating a surface observing network capable of resolving meso- β features (Figure 5.2). The supplemental weather stations were installed on public buildings and private homes, conforming as closely as possible to World Meteorological Organization (WMO) standards for the positioning of meteorological instrumentation [WMO, 1996].

Observed temperatures were converted to potential temperatures (θ), removing most of the distortion of the temperature field resulting from differences in station altitude, and all distortion due to pressure variations [Hess, 1959]. Observed winds were converted to eastward (u) and northward (v) scalar

components, which were then recalculated for a coordinate system rotated clockwise by 30 degrees, yielding u' and v' . The coastal zone within the study area can be approximated by a straight line, running from 210 degrees to 30 degrees azimuth, so u' and v' represent cross- and along-shore wind components.

A grid system with 10-km grid spacing (Figure 5.2) was generated, with the x-axis oriented in the cross-shore dimension (positive x toward 120 degrees true), and the y-axis oriented in the along-shore dimension (positive y toward 30 degrees true). All three scalars from the observing sites (θ , u' , and v') were interpolated onto the grid by means of a 2-D, anisotropic, adaptive Barnes interpolation routine [Barnes, 1964]. Randomly-chosen contour plots of interpolated temperature fields and vector plots of interpolated wind fields were compared to hand-analyzed plots for corresponding dates and times, and found to be satisfactory.

The surface synoptic situation for each of the twelve case-studies is determined using United States surface analyses archived in the National Virtual Data System, and accessed via the NVSD website (http://nndc.noaa.gov/?http://ols.ncdc.noaa.gov/cgi-bin/nndc/buyOL-006.cgi?FNC=chart_Ancep_get_chart_htm). GOES infrared images (obtained from the NOAA Historical Archive; see

<http://lwf.ncdc.noaa.gov/servlets/GoesBrowser>) are used to determine cloud cover in and around the study area.

Results

The gridded meso- β potential temperature and wind data were used to quantify SBG and SBC behavior in the study area. The behavior of the near-surface isentropic (potential temperature) and kinematic (near-surface wind) fields were classified into a series of horizontal patterns. The word "patterns" was chosen carefully, and preferred over "modes," which implies linear independence. There is no evidence that these patterns are linearly independent.

A set of simplified geographical reference points (Figure 5.4b) -- derived from a 2-km resolution topographic map of the study area (Figure 5.4a) -- were used when examining of the isentropic and kinematic patterns. Two of the reference points are low-lying (below 150 m MSL), scallop-shaped areas in the northern and southern halves of the study area, referred to as the Northern Lowlands Area (NLA) and the Southern Lowlands Area (SLA). The line following the high ground from Mount Agamenticus (York, Maine) to Lake Winnepesaukee (near Wolfeboro, New Hampshire) is referred to as "MALW," and the roughly shore-parallel line

demarking the approximate location of the 200 m MSL topographic contour is referred to as "2ML." The Gulf of Maine (GOM) is the portion of the Atlantic Ocean immediately offshore of Massachusetts, New Hampshire, and Maine. The Great Bay is the inland body of water west and south of Portsmouth, New Hampshire (KPSM).

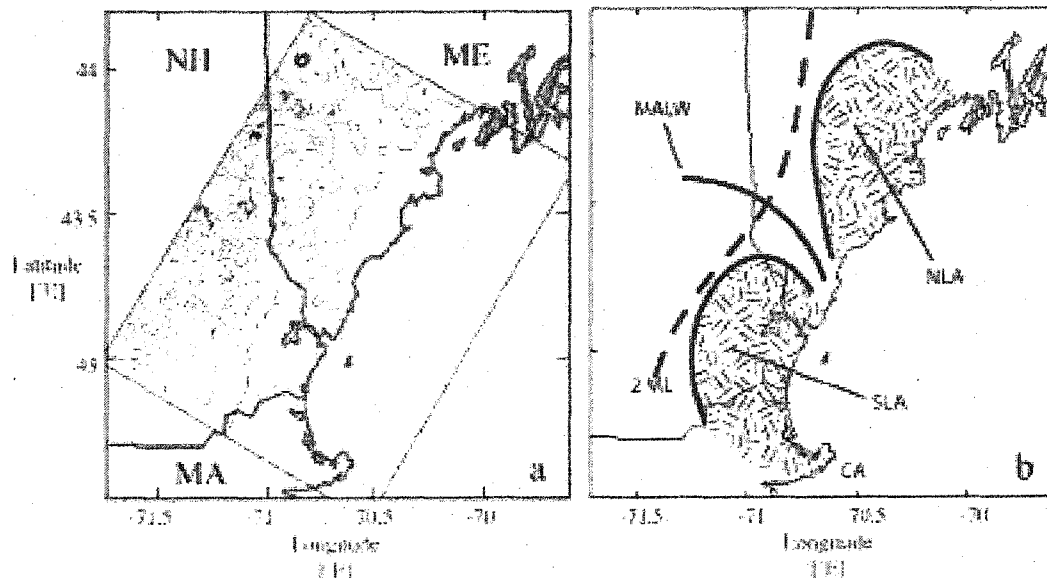


Figure 5.4: Study area topography and reference points. a) Study area (blue box) with topographic contours (green lines). Topo contours are drawn at intervals of 50 m ASL, beginning with 50 m ASL. b) Reference points used in discussion of isentropic and kinematic patterns.

The primary focus was on the relatively straight section of coastline that runs from north of Cape Ann (CA; Figure 5.4) to north

of Portland, Maine (KPWM; Figure 5.2). A shore-parallel wind in this area will result in onshore flow in the complex coastal area south of Brunswick Naval Air Station, Maine (KNHZ; Figure 5.2). This is not classified as a sea breeze. Similar arguments hold for CA. Times are discussed in terms of UTC, unless otherwise noted. The conversion to New England's Local Standard Time (LST) is UTC - 5 hours.

Isentropic Patterns. The isentropic fields observed in the twelve case-studies moved between a series of recurring "patterns." The isentropic patterns (summarized in Table A5.1, Appendix V) were created and modified by local topography, land- and sea-surface temperature fields, and by the advection of heat from outside the study area. Additional explanation of the patterns is included below, with primary focus on the patterns associated with the sea-breeze gravity current.

Most SB events analyzed in this study began in the Elongate S configuration (ES; Figure 5.5a). In NSB events, Elongate S formed by the rotation of the cold-warm-cold (KWK; Figure 5.7d) pattern. The precise physical mechanisms involved in creating Elongate S during SB and MAR events are not entirely obvious, but the following explanation is offered:

- Cold component: The cold air in the northern portion of the study area had two possible sources. The first was the Gulf of Maine's cold, southward along-shore (ocean) current [*Brown, 1998*]. This pattern is typical of the overall pattern of sea-surface temperatures in the GOM, especially in summer and autumn. The second source is MWN Drainage events (discussed below). Both of these sources seemed to contribute to the formation of the Central Inland Cold Pocket (CICP; discussed below) east of the Ossipee formation and west of Sebago Lake, and to cold air east of 2ML (Figure 5.4b) in the northern half of the study area generally.

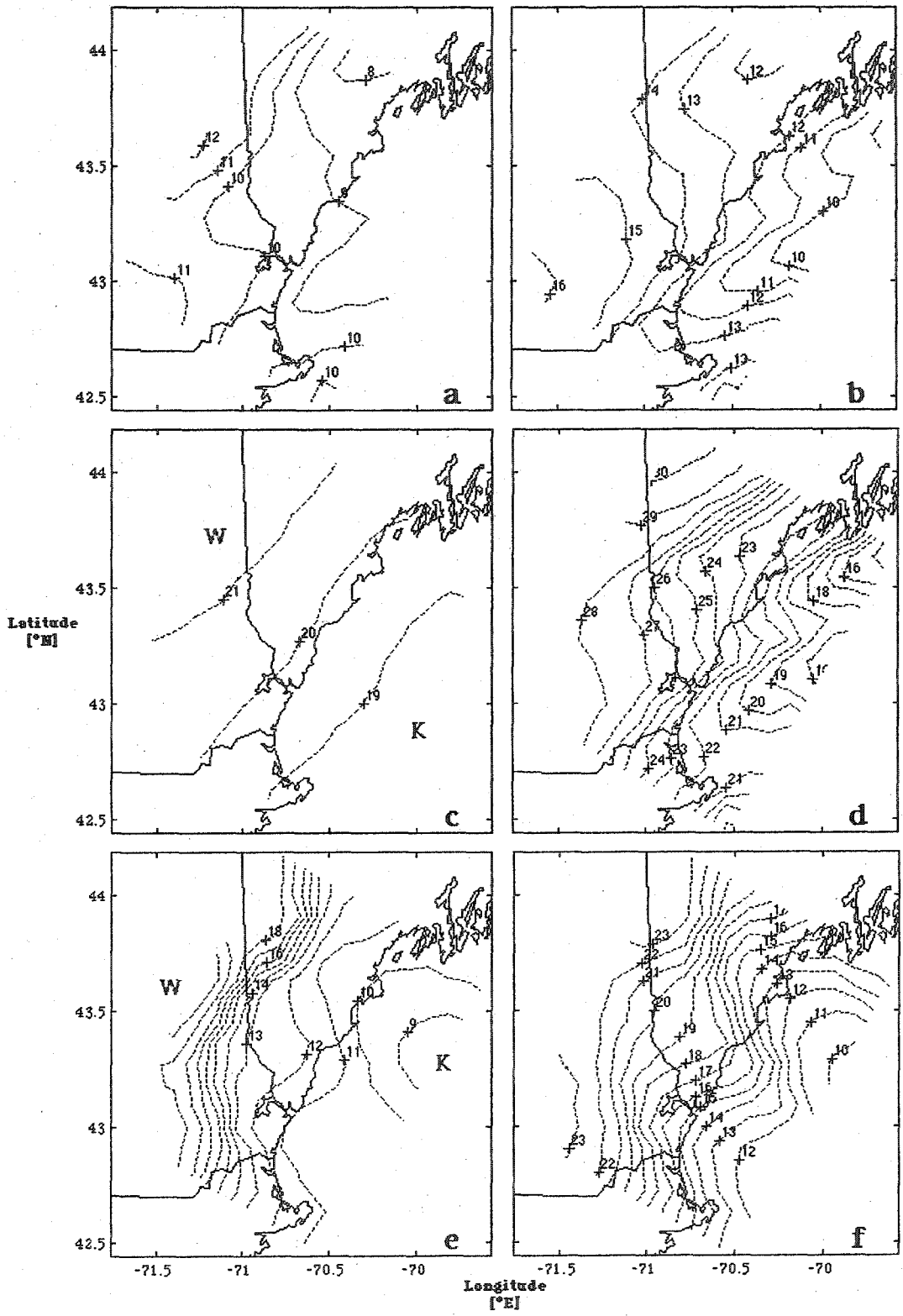


Figure 5.5 (previous page): Elongate S, Coastal S, CSP-Wland, Split S, ISP, and Lowlands isentropic patterns. Broken blue lines are isentropes, in intervals of 1 °C. K = cold areas; W = warm areas. a) Elongate S (example shown is May 10, 2001, 1200 UTC). b) Coastal S (May 9, 2001, 1400 UTC). c) CSP-Wland (July 28, 2001, 1800 UTC). d) Split S (May 11, 2001, 1900v). e) ISP (May 9, 2001, 2300 UTC). f) Lowlands (May 9, 2001, 1800 UTC).

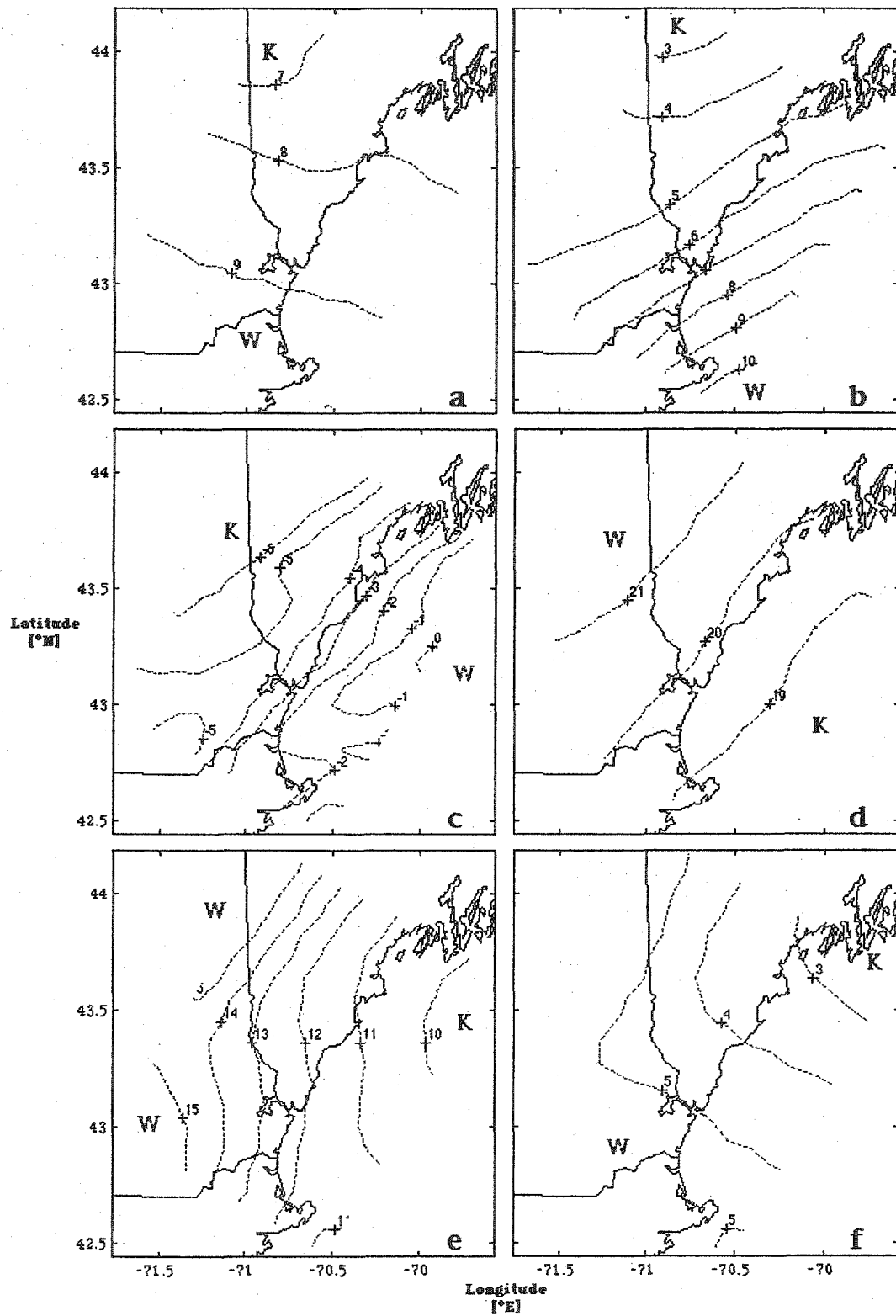
- **Warm component:** The warm air in the southwestern portion of the study area appeared to originate in two ways. The first was advection from further southwest, which only occurred on days when the large-scale flow had a shore-parallel component toward the. The second was probably insolation, which may be more effective in the southern portion of the study area than in its northern portion because of differences in land-use patterns and soil type.

Coastal S (CS; Figure 5.5b) appeared to form by three different methods. In the first, inland diabatic heating depleted the cold component of an Elongate S, enhancing the cross-shore potential temperature gradient at the coast. In the second, generally shore-parallel isentropes (CSP-Wland; Figures 5.5c and 5.6d) were deformed by fine-scale variations in the sea-surface temperature that appeared to be related to either Piscataqua River outflow

(vicinity of Portsmouth, Hampshire), or variations in Ekman-induced cold-water upwelling near the coast [Apel, 1987; Feng, 1996]. The third was similar to the second, except that the pre-Coastal S isentropes were at an oblique angle to the coast.

Split S (SS; Figure 5.5d) commonly formed from Coastal S during SB events, which indicated the presence of a bifurcated thermodynamic sea-breeze front in the northern half of the study area. The inland component of the Split S indicated the landward extent of the marine airmass's influence (or the leading edge of the sea-breeze gravity current), and the coastal component marked the boundary between modified marine air over land, and unmodified marine air over the sea. Split S, and therefore a bifurcated thermodynamic sea-breeze front, were common sea-breeze phenomena. Several authors [e.g. Atkins *et al.*, 1995; Fosberg and Schroeder, 1966] have observed bifurcated sea-breeze fronts in other parts of the world.

Inland Shore-Parallel (ISP; Figure 5.5e) appeared to originate in two ways. In the first, the inland component of Split S separated from its coastal component, followed by the dissolution of the coastal component. This generally happened in the late afternoon, as the Sun descended toward the horizon, which diminished the surface-based airmass modification process (diabatic heating) that



created the Split S. Inland Shore-Parallel also formed when a sea breeze-gravity current that had previously been confined to the SLA and the NLA (Lowlands pattern; discussed below) climbed above the 150-meter ASL topographic contour onto to higher terrain. This also generally occurred later in the afternoon.

The Lowlands pattern (LL; Figure 5.5f) represented either the peak of the marine air's landward push, a state through which it passed on its way to ISP, or a transitory state that occurred as an ISP or SS pattern decayed in the evening. Cold Northwest and Warm Southwest (KNWWSW; Figure 5.6a) was an early morning pattern that generally evolved into Elongate S. Most pattern sequences ended in the Cold Northwest and Warm Southeast pattern (KNWWSE; Figure 5.6b), because of the uneven rate at which land and sea surfaces cool, and the relatively high terrain in the northwest part of the study area. At night, radiational cooling over rugged terrain results in very cold air in the northwest, while the waters in the southeast (removed from the cold, along-shore current) remain relatively warm.

Figure 5.6 (previous page): KNWWSW, KNWWSE, CSP-Kland, CSP-Wland, KE, and KN isentropic patterns. Isopleths and other symbols are as in Figure 5.5. a) KNWWSW (example shown is September 29, 2001, 1200 UTC). b) KNWWSE (September 30, 2001, 0300 UTC). c) CSP-Kland (January 24, 2001, 0000 UTC). d) CSP-Wland, shown in this Figure 5. for contrast with CSP-Kland (July 28, 2001, 1800 UTC). e) KE (May 10, 2001, 1300). f) KN (April 3, 2001, 1700 UTC).

In winter months, a sea breeze developed if sufficient insolation was available to mature a Coastal Shore-Parallel; Cold Air Over Land (CSP-Kland; Figure 5.6c) configuration into an Elongate S configuration. As the Sun set, Elongate S decayed back to CSP-Kland. Elongate S matured into the Cold Air East pattern (KE; Figure 5.6e) if a light offshore wind resulted in the transport of warm air from the land into the southern offshore area.

The Central Inland Cold Pocket pattern (CICP; Figure 5.7a) appeared to originate from two different sources: An influx of cool air from the northeast, making it a cutoff extension of the cold component of an Elongate S; or, as a pool of cold air that collected in the wake of a MWN Drainage event. The Lake Winnepesaukee Warm Pocket (LWWP; Figure 5.7b) resulted from differential cooling over the land and lake surfaces. The Mount Washington Drainage Event (MWN drainage; Figure 5.7c) appeared to be the result of topographic channeling and amplification of a mountain breeze,

flowing down into the arc-shaped valley region southwest of Bartlett, New Hampshire from the Presidential Peaks (which includes Mount Washington), then southeastward past the circular Ossipee formation, through Sanford, Maine (KSFM), and toward the Gulf of Maine.

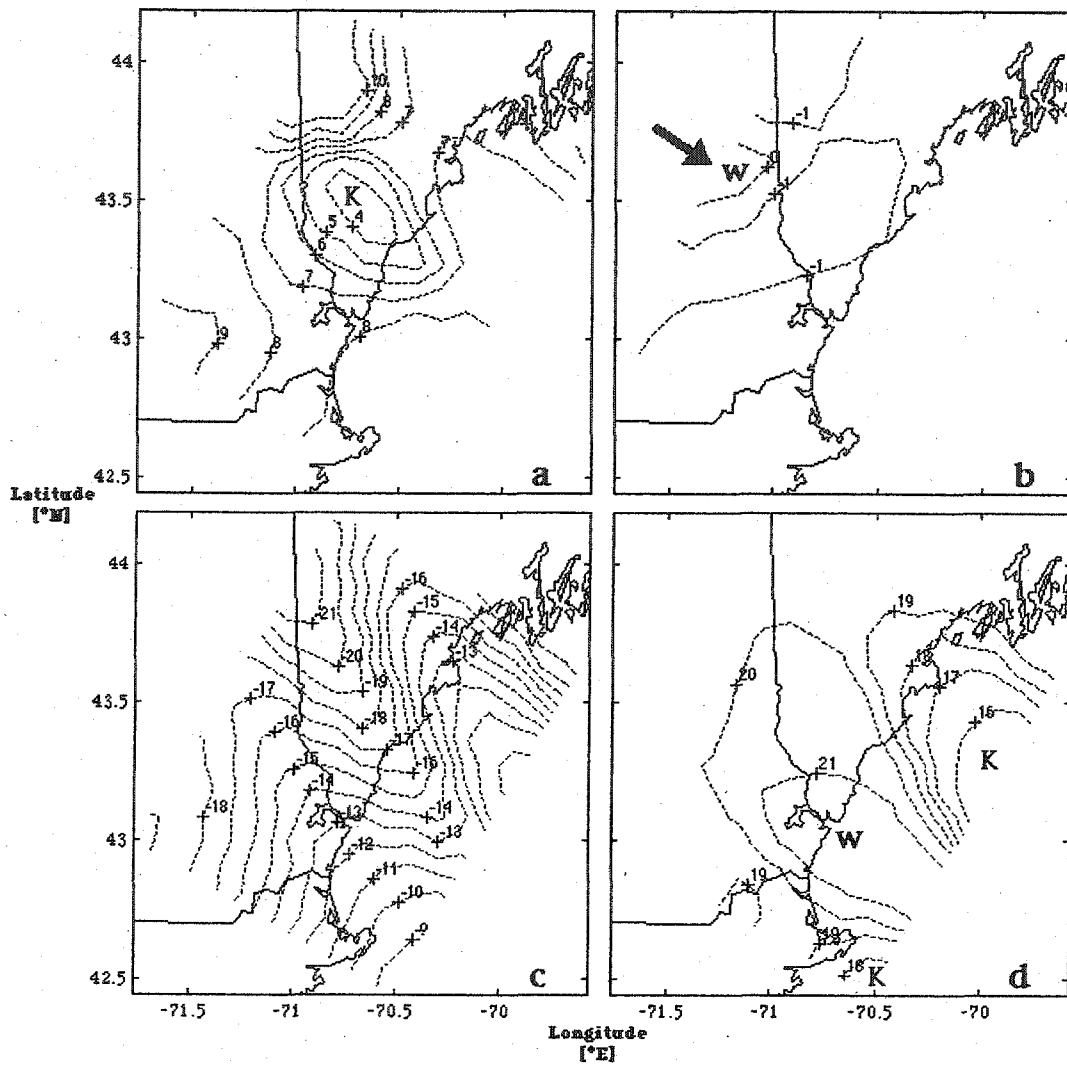


Figure 5.7: CICP, LWWP, MWN Drainage, and KWK isentropic patterns. Isopleths and other symbols are as in Figure 5.8. a) CICP (May 10, 2001, 0400 UTC). b) LWWP, indicated by arrow (April 3, 2001, 1200 UTC). c) MWN Drainage (January 23, 2001, 1200 UTC). d) KWK (July 6, 2001, 1600 UTC).

Kinematic Patterns. The hourly evolution of the kinematic fields observed in the twelve case-studies also moved within a series of recurring patterns. The kinematic patterns (summarized in Table A5.2, Appendix V) resulted from a combination of synoptic-scale (as described by the synoptic classifications), meso- α (as described by the nowcast diagram), meso- β (as described by the isentropic patterns), and smaller-scale forcing. Local effects include topographic channeling and land-sea surface friction changes. Additional explanation of the patterns is included below, with primary focus on the patterns associated with the sea-breeze circulation.

There was no evidence for the existence of a sea-breeze circulation with the Trough (T; Figure 5.8), SWX (Figures 9a,b,c), or NW (Figures 12a,b,c) kinematic patterns, when the ambient flow near the coast was primarily toward the sea. However, with the SWP (ambient flow was primarily shore-parallel; Figures 9d,e,f) kinematic patterns, a weaker thermal PGF was required, and a sea-breeze circulation sometimes developed. The kinematic sea-breeze front usually appeared first as a weak line of convergence along an inland line parallel to the coast, while a weak divergence region (marking the region of descending currents on the seaward edge of the sea-

breeze circulation) appeared along an offshore line parallel to the coast.

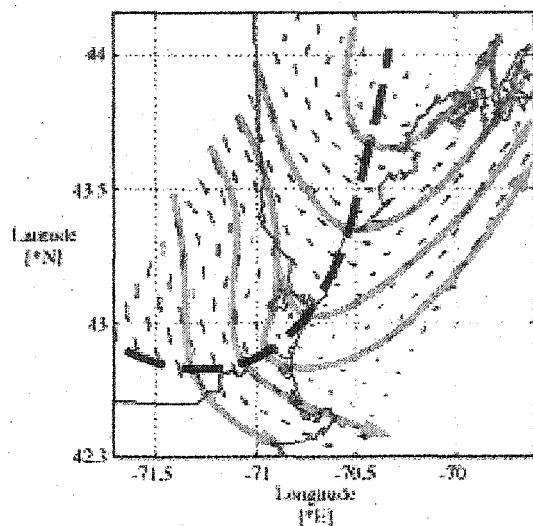


Figure 5.8: "Trough" kinematic pattern. Small arrows indicate wind vectors at grid points shown in Figure 5.3. Gray arrows are streamlines; heavy broken line is trough axis. (Example shown is May 10, 2001, 1500.)

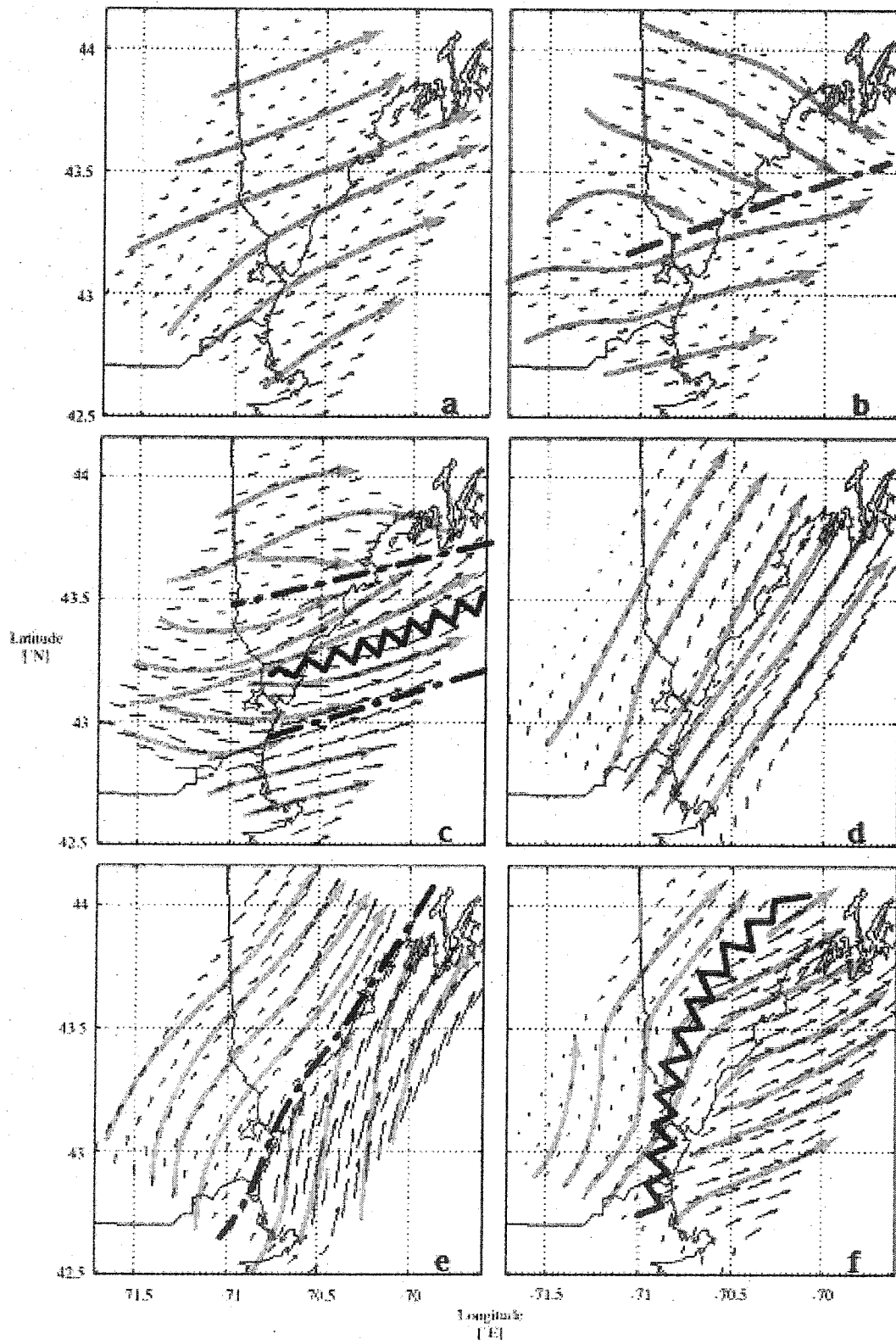


Figure 5.9 (previous page): SWX and SWP kinematic patterns. Small arrows indicate wind vectors at grid points shown in Figure 5.3. Gray arrows are streamlines; dash-dot lines are convergence lines; heavy sawtooth are axes of divergence. a) SWX1 (August 19, 2001, 0000 UTC). b) SWX2 (July 7, 2001, 0000 UTC). c) SWX3 (August 18, 2001, 1500 UTC). d) SWP1 (January 23, 2001, 1500 UTC). e) SWP2 (January 23, 2001, 2200 UTC). f) SWP3 (January 24, 2001, 0300 UTC).

A sea-breeze circulation was also possible with the SWM (Figures 10a,b,c) kinematic patterns. With SWM2 (Figure 5.10b), flow over the northern offshore area was cyclonic, and sometimes became shore-parallel, or even crossed back toward the land at an oblique angle, indicating of the development of a weak sea breeze. The corresponding isentropic fields indicated that the landward flow was associated with a sea-breeze favorable cross-shore isentropic gradient. With SWM3 (Figure 5.10c), landward flow in the northern half of the study area, and convergent shore-parallel flow in the southern half, indicated a complex circulation. A mesoscale cyclonic circulation sometimes developed along the associated kinematic sea-breeze front.

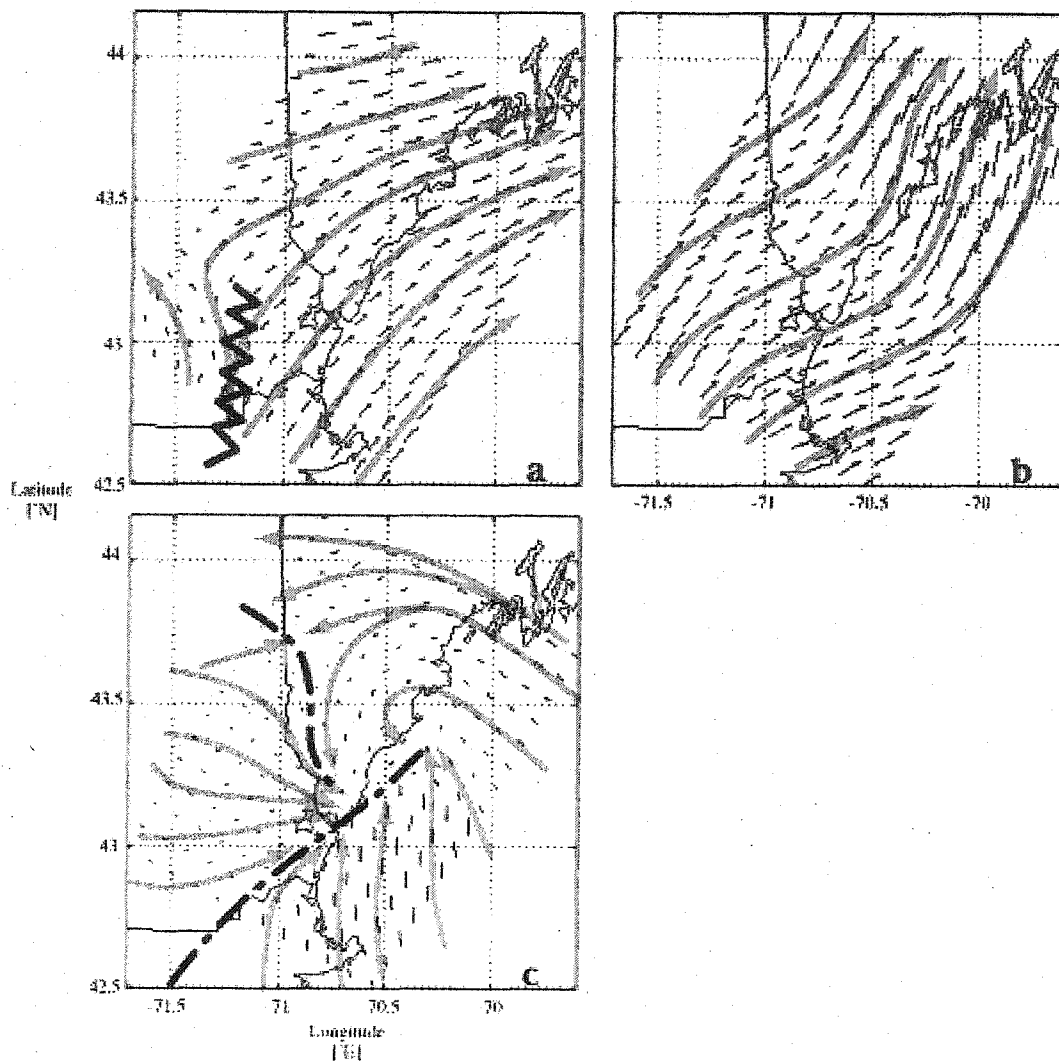


Figure 5.10: SWM kinematic patterns. Small arrows indicate wind vectors at grid points shown in Figure 5.3. Gray arrows are streamlines; dash-dot lines are convergence lines; heavy sawtooth are axes of divergence. a) SWM1 (May 12, 2001, 0300 UTC). b) SWM2 (July 7, 2001, 2100 UTC). c) SWM3 (May 9, 2001, 1400 UTC).

A sea-breeze circulation also developed under northeasterly ambient flow, with the NE (Figures 5.11a through 5.11f) kinematic

patterns. As in the SWP kinematic patterns (Figures 5.9d,e,f), the kinematic sea-breeze front often developed at some point inland (e.g. NE4; Figure 5.11d), rather than forming at the coast and moving inland. In NE6 (Figure 5.11f), the kinematic sea-breeze front traced out the shape of the NLA and SLA. Flow east of the front was landward, crossing the shore at an oblique angle. Flow west of the line was generally shore-parallel, and sometimes followed the topographic contours.

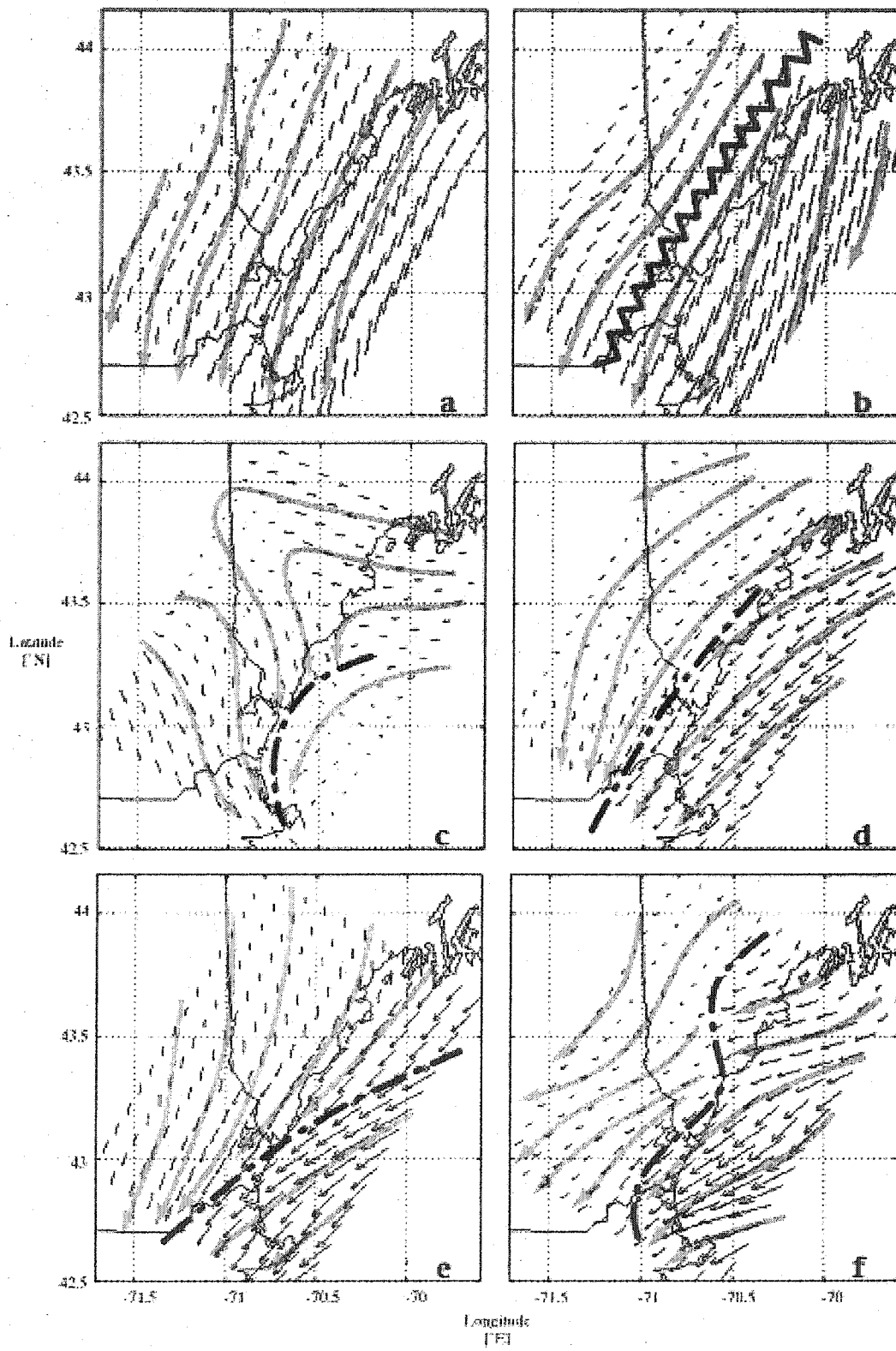


Figure 5.11 (previous page): NE kinematic patterns. Small arrows indicate wind vectors at grid points shown in Figure 5.3. Gray arrows are streamlines; dash-dot lines are convergence lines; heavy sawtooth are axes of divergence. a) NE1 (September 29, 2001, 1200 UTC). b) NE2 (September 29, 2001, 1300 UTC). c) NE3 (May 11, 2001, 1400 UTC). d) NE4 (September 30, 2001, 0100 UTC). e) NE5 (September 30, 2001, 0300 UTC). f) NE6 (September 29, 2001, 2300 UTC).

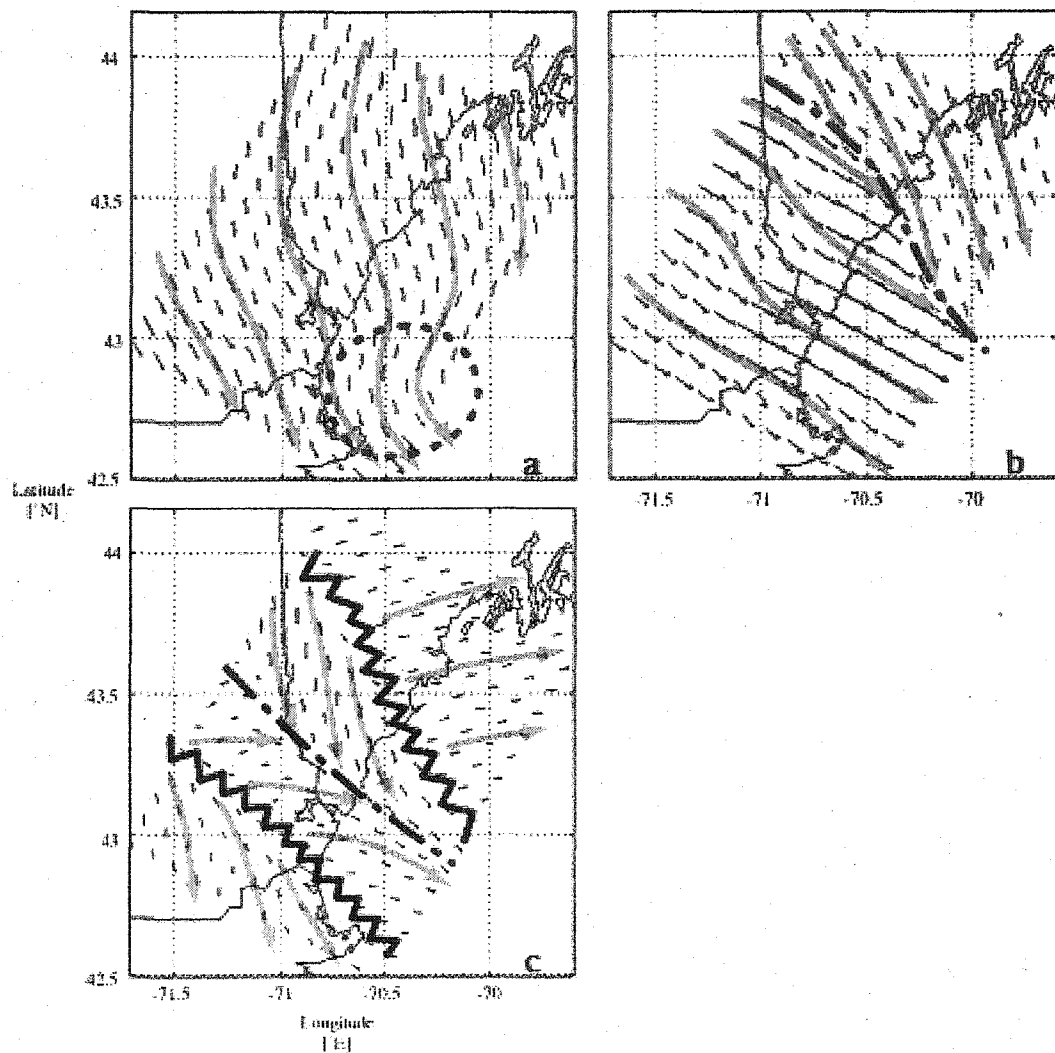


Figure 5.12: NW kinematic patterns. Small arrows indicate wind vectors at grid points shown in Figure 5.3. Gray arrows are streamlines; dash-dot lines are convergence lines; heavy sawtooth are axes of divergence. Circular gray area indicates possible region of calm or very light wind. a) NW1 (April 3, 2001, 1600 UTC). b) NW2 (July 6, 2001, 1500 UTC). c) NW3 (May 10, 2001, 1300 UTC).

The strongest sea breezes developed with the COL kinematic patterns (Figures 5.13a through 5.13e), when northeastward flow near the northeastern boundary, and southwestward near the southwestern boundary, suggested that the study area was in the middle of a broad, diffuse col area. In its initial stage (COL1; Figure 5.13a), the kinematic sea-breeze front developed parallel to and in the immediate vicinity of the coast, with northwesterly flow inland and southwesterly flow over water. In the next stage (COL2; Figure 5.13b), the front rotated so that some portion of it was no longer parallel to the coast. Flow over the water backed toward the east. As the sea-breeze circulation developed further (COL3; Figure 5.13c), the front line traced out the approximate inland limits of the SLA and NLA. Mesoscale cyclonic rotation in the NLA and SLA was often induced by a combination of topographic channeling and convergence at the front. With further development (COL4; Figure 5.13d), the front pushed inland, beyond the limits of the 150 m ASL topographic contour. Calm, very light, or mesoscale cyclonic rotation sometimes developed along the front. At its most developed, the sea-breeze circulation grew in size to meso- α scale (COL5; Figure 5.13e), and the kinematic sea-breeze reached or exceeded the western extreme of the study area.

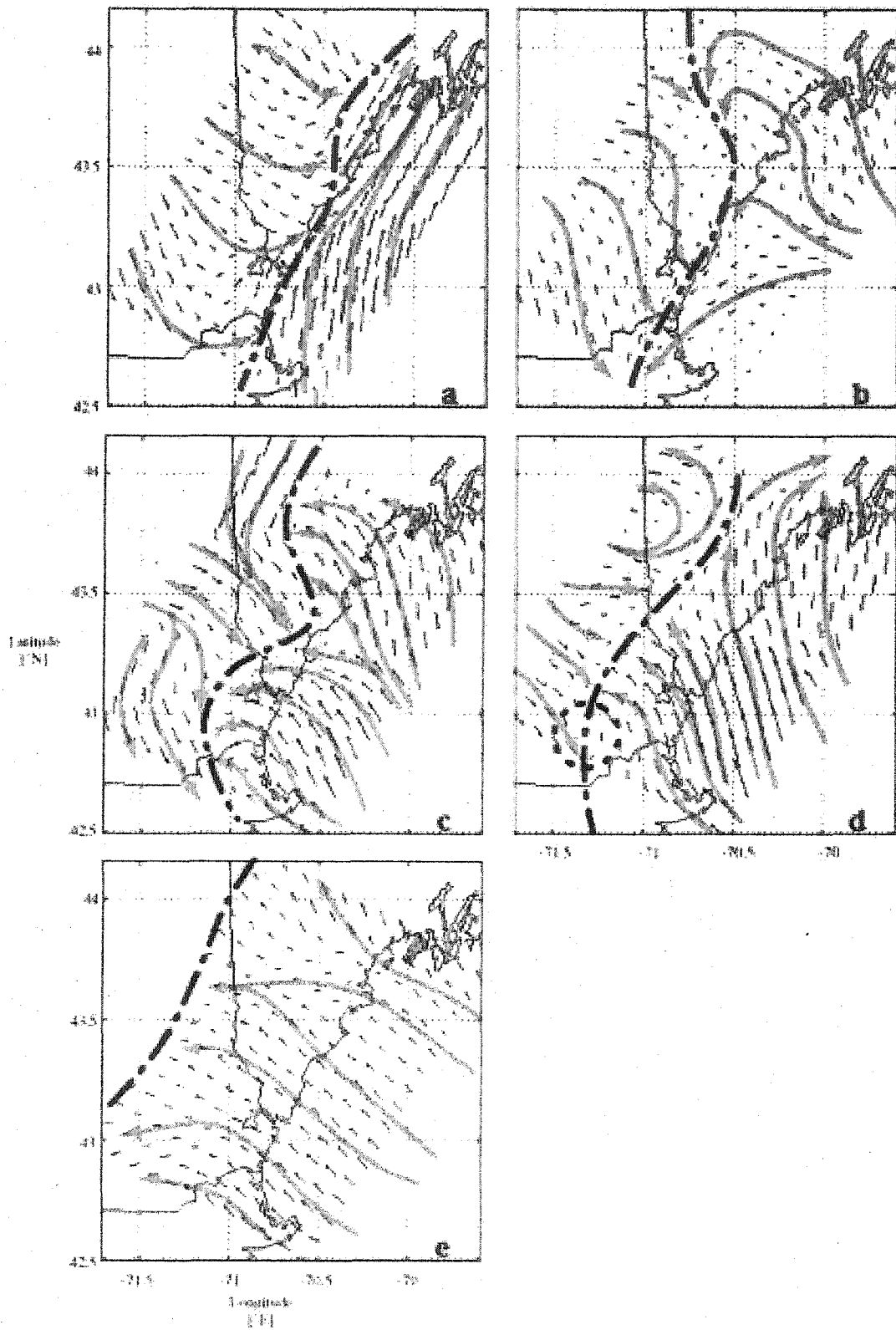


Figure 5.13 (previous page): COL kinematic patterns. Small arrows indicate wind vectors at grid points shown in Figure 5.3. Gray arrows are streamlines; dash-dot lines are convergence lines. Circular gray area indicates possible region of calm or very light wind, or cyclonically-rotating circulation a) COL1 (May 10, 2001, 2300 UTC). b) COL2 (May 11, 2001, 1500 UTC). c) COL3 (May 10, 2001, 1800 UTC). d) COL4 (May 11, 2001, 1900 UTC). e) COL5 (May 9, 2001, 1600 UTC).

Discussion

Table A5.3 (Appendix V) summarizes the behavior of the eight SB and one MAR event in 2001 case studies in terms of the isentropic and kinematic patterns. Isentropic patterns describe the potential temperature field associated with the sea-breeze gravity current, and kinematic patterns describe the near-surface wind field associated with the sea-breeze circulation. All of the isentropic patterns and all but two of the kinematic patterns (SWX1 and SWX3) are required to describe these nine events. The kinematic patterns SWX1 and SWX3 occur only on NSB days, and are not discussed further.

Development of the sea-breeze gravity current. Most SB events begin in the Elongate S isentropic pattern. This pattern places a warm tongue of air in the southern portion of the study

area's coastal plain, adjacent to the cold surface water of the Gulf of Maine, and therefore is ideal for a strong, negative cross-shore potential temperature gradient.

A "strong" SB event then matures from Elongate S to Coastal S, which is indicative of a strengthening (and narrowing) cross-shore potential temperature gradient. From there it reaches Inland-Shore Parallel by passing first through either Lowlands or Split S. Split S is indicative of a sea-breeze gravity current with a shore-parallel bifurcated thermodynamic sea-breeze front, resulting from surface-based diabatic modification of the inland marine airmass in the northern half of the study area. Lowlands is indicative of a relatively unmodified sea-breeze gravity current with a unified thermodynamic sea-breeze front, confined to the two scallop-shaped areas below the 150-meter ASL topographic contour. Inland-Shore Parallel is indicative of a relatively unmodified sea-breeze gravity current with a unified thermodynamic sea-breeze front, and generally occurs in the late afternoon.

Decay of the sea-breeze gravity current. The decaying phase of a sea breeze follows several paths. Inland Shore-Parallel sometimes decays first into Lowlands, representing the seaward retreat of the sea-breeze gravity current after the landward forcing

(insolation) has been removed from the system. Lowlands sometimes then retreats to CSP-Wland, as the gravity current spills back out of the NLA and SLA and toward the sea. This condition in turn decays to either KN and KE, depending on the precise location of the cold reservoir in the offshore waters. Split S, often the end member in a sea-breeze maturation sequence, also decays to Lowlands, as the modified marine air over land in the northern half of the study area retreats into the lower-lying areas. Most sequences end with KNWWSE, which is created by strong radiational cooling over the mountainous terrain in the northwest, and the retention of warm temperatures in the surface waters south of Cape Ann.

Annual variation in most developed state of the sea-breeze gravity current. In periods of very weak forcing (winter), the peak state reached by the sea-breeze gravity current is Elongate S, which is where the majority of non-winter sea-breeze events began in the morning. In spring and autumn, the $\delta\theta/\delta x$ forcing is strong enough to produce Lowlands SB events, with clearly-defined sea-breeze gravity currents. During summer, the final state reached by a sea-breeze gravity current depends on the strength of $\delta\theta/\delta x$ and u_{925} .

Isentropic patterns with winter sea breeze events. In winter, a sea breeze develops if sufficient insolation is available to mature a CSP-Kland into an Elongate S. This evolution indicates the reversal of the cross-shore potential temperature gradient, from positive (not sea-breeze favorable) to negative (sea-breeze favorable), and the development of a mesoscale thermal PGF pointing toward land. As the Sun sets, Elongate S decays back to CSP-Kland, indicating the re-establishment of colder air over land, and an unfavorable cross-shore potential temperature gradient.

Kinematic patterns associated with pure, corkscrew, and backdoor sea-breeze circulation. The kinematic patterns discussed in section 3 are related to the categories of sea breezes discussed in *Adams* [1997] and Chapter 2. The "pure" sea breeze is associated with low-level, landward flow that is primarily perpendicular to the coast, while the "corkscrew" sea breeze has a northward, along-shore flow component (in addition to a cross-shore component), and the "backdoor" has a southward along-shore flow component [*Adams*, 1997].

Pure sea breezes occur in the northern portion of SWM3 (Figure 5.10c), some portion of COL2 (Figure 5.13b), COL3 (Figure 5.13c), part or

all of COL4 (Figure 5.13d), and COL5 (Figure 5.13e). Corkscrew sea breezes occur in SWP2 (Figure 5.9e), the northern coastal half of SWM2 (Figure 5.10b), the southern coastal portion of SWM3 (Figure 5.10c), part or all of COL1 (Figure 5.13a), and part or all of COL4 (Figure 5.13d). Backdoor sea breezes occur in NE3 (Figure 5.11c), NE4 (Figure 5.11d), NE5 (Figure 5.11e), and NE6 (Figure 5.11f). Individual SB events may therefore be described as one or some spatial combination of the three generalized sea-breeze categories in *Adams* [1997].

Sea-breeze events also evolve from one general category to another over time. If one considers the rotation of the sea-breeze circulation cell by background forces, such as Coriolis (Neumann, 1977), it is not difficult to imagine evolution from pure to corkscrew. This was observed in the case studies. Table 5.2 lists the dominant general categories of each of the sea-breeze and marginal events. Two cases occurred when the sea breeze was dominated throughout its life cycle by a direct crossing of the coastline: One on April 3, when it was confined to the SLA only, and the other on May 9, when its kinematic pattern was driven primarily by meso- α scale forcing (discussed in more detail below). In all other cases, it either began with a significant along-shore component, or developed one as time progressed, indicating clockwise rotation of the sea-breeze circulation cell. This confirms

the importance of the Coriolis force in the evolution of the system [Neumann, 1977]. The oscillation between NE4 and NE5 toward the end of the life-cycle of the September 29 backdoor event might also be interpreted as two competing forces: The developing seaward acceleration in the late evening hours (due to the collapse of sea-breeze favorable meso- α scale thermal forcing), and the tendency for clockwise rotation of the remnant SBC imposed by Coriolis.

Table 5.2: General category of sea-Breeze and marginal events observed in case-studies. Kinematic events are described here in terms of the sea-breeze categories described in Adams [1997] and Chapter 2.

Date	Category
January 23	Corkscrew
April 3	Pure (south only)
May 9	Pure
May 10	Pure, evolving into corkscrew
May 11	Pure, evolving into corkscrew
June 14	Corkscrew
July 7	Corkscrew (north only)
July 28	Pure (south) and corkscrew (north), becoming corkscrew throughout.
September 29	Backdoor

Along-shore variation associated with weak sea-breeze events. Given the same meso- α forcing, the sea-breeze circulation sometimes occurs on some parts of the straight section of coastline in the study area, but not on others. This occurs when the SWM2

kinematic pattern appears in conjunction with the KWK isentropic pattern, as in the July 7 marginal event. KWK is associated with cold air offshore of the northern coastline, and warm air offshore of the southern coastline. While the surface flow associated with SWM2 is generally southwesterly (crossing the shore toward the sea), the landward-pointing potential temperature gradient in the north creates a large enough thermal PGF at the meso- β scale for a weak and highly localized corkscrew SBC to occur.

KWK does not always produce these highly localized sea breezes for two reasons. The first is that it was not always associated with the SWM2 kinematic pattern. For example, in the July 6 event, it was associated with kinematic patterns NW1 and NW2, as well as with meso- α scale u_{925} values of about 11 ms^{-1} . (The July 7 u_{925} value was, by contrast, only about 6.7 ms^{-1} .) The second reason is that, even in cases where KWK is associated with SWM2, the landward-pointing meso- β thermal PGF is too weak to overcome the seaward-pointing u_{925} to produce an observable sea breeze in the northern coastal area. In other words, even if the SBC develops, its landward edge may not reach the coast. For example, in the July 13 NSB event (which had a u_{925} value of approximately 6.5, comparable to July 7), KWK occurred along with SWM2, but the

associated meso- β potential temperature gradient was slightly weaker than in the July 7 case (Figure 5.14).

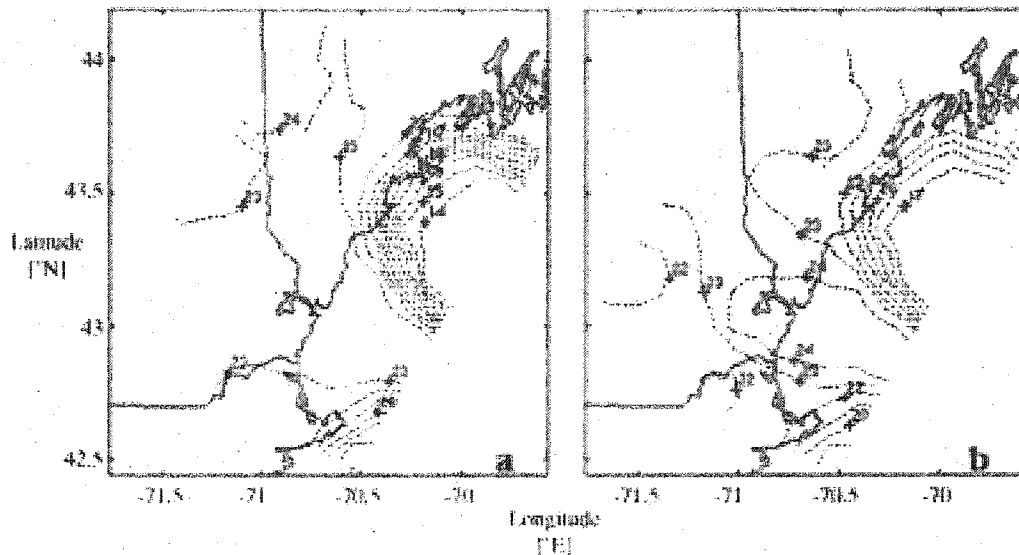


Figure 5.14: Comparison of KWK isentropic patterns occurring with SWM2 kinematic patterns in two separate events. The July 7, 2001 SWM2 kinematic pattern produced weak on-shore flow in the northern coastal area, beginning at about 1700. The potential temperature field is shown (panel a) for the hour that the northern flow began to cross the coast toward land. The July 13, 2001 SWM2 kinematic pattern produced only shore-parallel flow in the north, despite similar meso- α scale forcing. The meso- β potential temperature gradient is slightly weaker in the second case than in the first (shown in panel b at its peak value, at 2100 UTC).

Differing scales of sea-breeze system forcing and response.

Two scales of kinematic (SBC) response to mesoscale forcing are evident in the case studies: One that appears to correspond to the

larger meso- α forcing estimated by the Nowcast Diagram, and another that appears to correspond to the smaller thermal forcing produced by the meso- β potential temperature fields (and is therefore more directly linked to the sea-breeze gravity current). When the meso- α forcing is weak, as indicated when the $(\delta\theta/\delta x, u_G)$ forcing remains within the TZ, details of the wind field appear to correspond to details of the potential temperature field. (Time-evolution of the $[\delta\theta/\delta x, u_G]$ forcing is discussed in Chapter 4.) In this situation, the sea breeze behaves as a true gravity current [*Simpson*, 1994]. When the meso- α forcing is strong, as indicated by the track of the $(\delta\theta/\delta x, u_G)$ forcing to the left of line B, the correspondence of the wind field (defining the sea-breeze circulation) and the potential temperature field (defining the sea-breeze gravity current) appears to weaken considerably.

One illustration of this can be obtained by comparing the behavior of the wind fields on May 9 and 10. In the former, the $(\delta\theta/\delta x, u_G)$ forcing began in the transition zone, and quickly moved to the left of line B, indicating that the meso- α sea-breeze forcing was strong. In the latter, the $(\delta\theta/\delta x, u_G)$ forcing remained inside the transition zone, indicating that the meso- α sea-breeze forcing was much weaker. The resulting meso- β kinematic behavior in the two

sea-breeze events differed markedly. In the May 9 event, once the sea-breeze circulation was initiated, it rapidly progressed inland, and reached the northwestern edge of the study within an hour's time. The sea-breeze gravity current, however, "lagged behind" the kinematic field by several hours. Table 5.3 illustrates the difference in the evolution of the two variables.

Table 5.3: Evolution of May 9, 2001 isentropic and kinematic patterns.

Hour [UTC]	Isentropic Pattern	Kinematic Pattern
1200	ES/LWWP	SWP1
1300	CS/LWWP	SWM3
1400	CS	SWM3
1500	CS	COL5
1600	CS	COL5
1700	IL	COL5
1800	IL	COL5
1900	IL	COL5
2000	IL	COL5
2100	IL	COL5
2200	ISP	COL5
2300	ISP	COL5
0000	ISP	COL5
0100	KN	COL5
0200	KN	COL5
0300	KN	COL5
0400	CICP	COL5

While both the potential temperature and wind fields eventually reached their most developed sea-breeze patterns (Inland Shore-Parallel and COL5, respectively), COL5 occurred early in the

day. If the sea breeze had behaved as a gravity current, the isentropic and kinematic patterns would have evolved in conjunction with each other. Over the course of several hours with southeasterly flow reaching the northwestern edge of the study area, the potential temperature field reflected a very gradual invasion of marine air (the inland movement of the sea-breeze gravity current). By 1700, after three hours of the COL5 kinematic pattern, the isentropic field indicated marine air in the NLA and SLA (Lowlands isentropic pattern). By 2200, after an additional five hours of the COL5 kinematic pattern, the potential temperature field reflected a well-defined, shore-parallel thermodynamic sea-breeze front (Inland Shore-Parallel isentropic pattern) approximately 50 kilometers inland.

One possible explanation for the time-lag in response of the potential temperature field is rapid surface modification. Diabatic heating from Earth's surface could mask the thermal signature of the marine airmass's inland advance. Given the apparent rapidity with which the sea-breeze circulation advanced inland (and the implied wind speeds) surface-based modification would seem an unlikely explanation. For the sea breeze to propagate from the coast to the northwestern boundary in one hour would require wind speeds of at least 65 km h^{-1} , or approximately 18 ms^{-1} . But wind

speeds of this magnitude are not observed in the field file for May 9. This explanation is therefore unsatisfactory.

Another interpretation is that the initial landward thrust consisted of continental air, not modified marine air, which closely matches the description of the "sea-breeze forerunner" [*Geisler and Bretherton, 1969*]. The sea-breeze forerunner is a cluster of waves initiated when the cross-shore thermal contrast appears above the land-sea interface. The waves with the largest amplitude arrive at points inland first, moving at speeds much faster than the sea-breeze front. Over time, progressively smaller-scale waves arrive inland. (In the May 9 case, only one wave was discernable in the gridded wind data.) Observers on Earth's surface will experience a wind from the direction of the sea consisting of local (continental) air, before the arrival of the sea-breeze front. (In this case, the sea-breeze front is defined as the leading edge of the marine airmass.) The model results from *Geisler and Bretherton [1969]* indicate that, with reasonable values of internal (eddy) viscosity and surface friction, the forerunner reaches as far inland as 60 kilometers. Our results show its inland penetration easily exceeding 65 kilometers. For this reason, and because of the absence of additional waves following the first, this hypothesis is rejected as well.

A third interpretation is that the sudden landward rush of air in the May 9 event -- independent of the marine airmass -- was a meso- α response to meso- α forcing. The entire mass of air in the study area reacted at essentially the same moment, when the meso- α forcing reflected in the Nowcast Diagram overcame the opposing synoptic-scale southwesterly flow. In this scenario, the slower evolution of the meso- β potential temperature field was then a reflection of the inland advance of relatively unmodified marine air (the sea-breeze gravity current), occurring on a much longer time-scale than the wind field. The latter seems the most plausible.

The May 10 sea-breeze event evolved quite differently. Table 5.4 summarizes the evolution of the potential temperature and wind fields. It can be seen that, in this event, the kinematic pattern led the isentropic pattern in the beginning. The COL3 kinematic pattern (beginning at 1600) reflected landward flow into the NLA and SLA, while the isentropic pattern reflected either Coastal S (a potential temperature gradient with minor deviations from the shape of the coastline) or KE (a potential temperature gradient closely reflecting the shape of the coast). With weak meso- α forcing reflected on the Nowcast Diagram, a significant component of the forcing driving the marine airmass inland was associated with the meso- β potential

temperature gradient at the thermodynamic sea-breeze front. In other words, given a relatively well-defined potential temperature gradient at the coast, the wind responded by blowing inland and filling the northern and southern lowlands areas. There was no sudden landward rush of air occurring throughout the study area as in the previous case.

By 2000 UTC (1500L), surface diabatic modification began to weaken, and the isentropic pattern indicated that the unmodified marine air was reaching further inland, particularly in the northern portion of the study area. Split S was established -- the precursor to Inland Shore-Parallel. At about the same time, the landward forcing at the meso- α scale began to weaken, and the definable onshore flow in the kinematic fields began to reflect a somewhat weaker inland intrusion (COL2). By 2200, the isentropic pattern indicated that the sea-breeze gravity current was spilling back into the lowlands, towards the coast, and the kinematic pattern indicated that the landward edge of the sea-breeze circulation and was moving back toward the coast. This event is indicative of a much closer association between the potential temperature and wind fields at the meso- β scale, and better fits the gravity current sea-breeze model discussed by *Simpson* [1994] and others.

temperature gradient at the thermodynamic sea-breeze front. In other words, given a relatively well-defined potential temperature gradient at the coast, the wind responded by blowing inland and filling the northern and southern lowlands areas. There was no sudden landward rush of air occurring throughout the study area as in the previous case.

By 2000 UTC (1500L), surface diabatic modification began to weaken, and the isentropic pattern indicated that the unmodified marine air was reaching further inland, particularly in the northern portion of the study area. Split S was established -- the precursor to Inland Shore-Parallel. At about the same time, the landward forcing at the meso- α scale began to weaken, and the definable onshore flow in the kinematic fields began to reflect a somewhat weaker inland intrusion (COL2). By 2200, the isentropic pattern indicated that the sea-breeze gravity current was spilling back into the lowlands, towards the coast, and the kinematic pattern indicated that the landward edge of the sea-breeze circulation and was moving back toward the coast. This event is indicative of a much closer association between the potential temperature and wind fields at the meso- β scale, and better fits the gravity current sea-breeze model discussed by *Simpson* [1994] and others.

Table 5.4: Evolution of May 10, 2001 isentropic and kinematic patterns.

Hour [UTC]	Isentropic Pattern	Kinematic Pattern
1200	ES/LWWP	COL3
1300	KE	NW3
1400	KE	T
1500	KE	T
1600	CS	COL3
1700	CS	COL3
1800	KE	COL3
1900	CS	COL2
2000	SS	COL2
2100	SS	COL2
2200	IL	COL1
2300	IL	COL1
0000	IL	COL1
0100	LL, transitioning	T
0200	KN	T
0300	KN, transitioning	NW2
0400	KNWWSE	NW2

Forecasting the most developed state of the sea-breeze gravity current. The most developed isentropic pattern that the sea-breeze gravity current achieve is a function of the peak meso- α cross-shore potential temperature gradient (which provides landward forcing), and the strength of the cross-shore wind component at the top of the PBL (which resists the gravity current's landward movement). Figure 5.15 shows the most advanced stages of the SB and MAR events discussed above against the peak forcing associated with each event. The time of peak forcing for each event

was determined from the time-evolving nowcast diagrams discussed in Chapter 4.

Stronger meso- α cross-shore potential temperature gradients result in more advanced isentropic patterns, but this is mitigated by the opposing 925 hPa wind component. The sea-breeze gravity current achieves the Inland Shore-Parallel isentropic pattern (advancing out of the low-lying areas near the coast, and extending as far inland as the 200-meter topographic contour) if the thermal forcing is sufficiently strong to overcome the opposition imposed by the cross-shore 925 hPa wind component. Weaker values of $\delta\theta/\delta x$, or stronger values of u_{925} , result in a limiting of the system to the Split S, Lowlands, or Elongate S isentropic patterns. In the first, the sea-breeze gravity current undergoes diabatic modification, especially over the high ground along the MALW line (Figure 5.4), resulting in a bifurcated thermodynamic sea-breeze front. In the second, the sea-breeze gravity current does not escape from the low-lying areas near the coast. The third is associated with the starting point of most of the sea-breeze events studied, and is not associated with a clearly-defined sea-breeze gravity current.

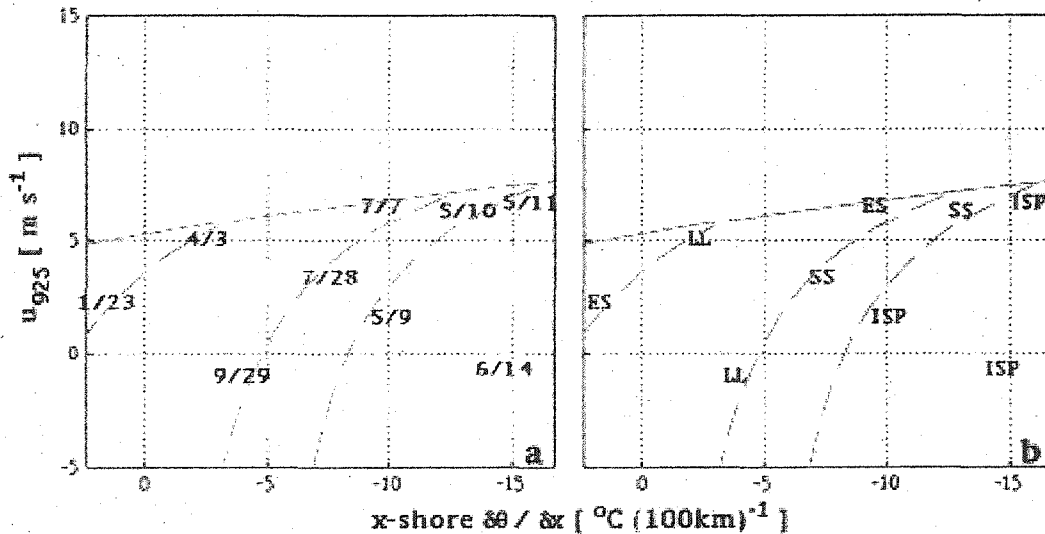


Figure 5.15: Most developed sea-breeze isentropic pattern reached as a function of peak meso- α forcing. Explanation of determination of peak forcing is in the text. Gray broken line indicates approximate boundaries defining peak results. Gray solid line indicates dividing line between sea-breeze and non-sea-breeze events. a) Dates associated with events (MM/DD). b) Peak isentropic pattern (ES = Elongate S; LL = Lowlands; SS = Split S; ISP = Inland Shore-Parallel).

Forecasting time-of-onset and maximum inland penetration of the sea-breeze circulation. The earliest moment that the sea-breeze circulation reaches the coastline in the study area, and the maximum distance the associated convergence line moved inland, are both functions of the peak meso- α isentropic gradient (which provides landward forcing) and the strength of the cross-shore wind component at the top of the PBL (which resists the sea breeze's inland movement). The former resolves a question raised

in Chapter 3, and the latter is similar to the correlation between meso- α scale forcing and the peak isentropic pattern (Figure 5.15). Figure 5.16 shows both the moment of onset and the distance traveled inland for the sea-breeze and marginal events discussed above, against the peak ($\delta\theta/\delta x, u_{925}$) forcing associated with each event.

The earliest time of onset was estimated by visual inspection of the hourly frames describing the wind fields in the case-study field files. Time-of-onset at the coast for corkscrew or backdoor kinematic sea breezes (those crossing landward at a shallow angle; [Adams, 1997]) was interpreted as the approximate time when the wind developed a component that crossed the straight section of coast in the study area. Time-of-onset at the coast for a "pure" sea breeze was interpreted as the approximate time when the landward flow (that initially developed offshore) reached any point on the straight section of coast in the study area.

The maximum distance of inland penetration was also estimated by visual inspection of the wind fields in the field files. The location of the axis of convergence between the sea-breeze related flow (SBC), and the ambient flow reflected in the wind field farther inland, was determined for each of the hourly frames. This line was often not parallel to the coast (as, for example, in the COL2

and COL3 kinematic patterns), so the maximum inland penetration achieved by the kinematic sea breeze may not be a good indicator of its mean inland penetration. In some cases the convergence line was less clearly defined than in others, forcing a somewhat subjective judgment as to its location.

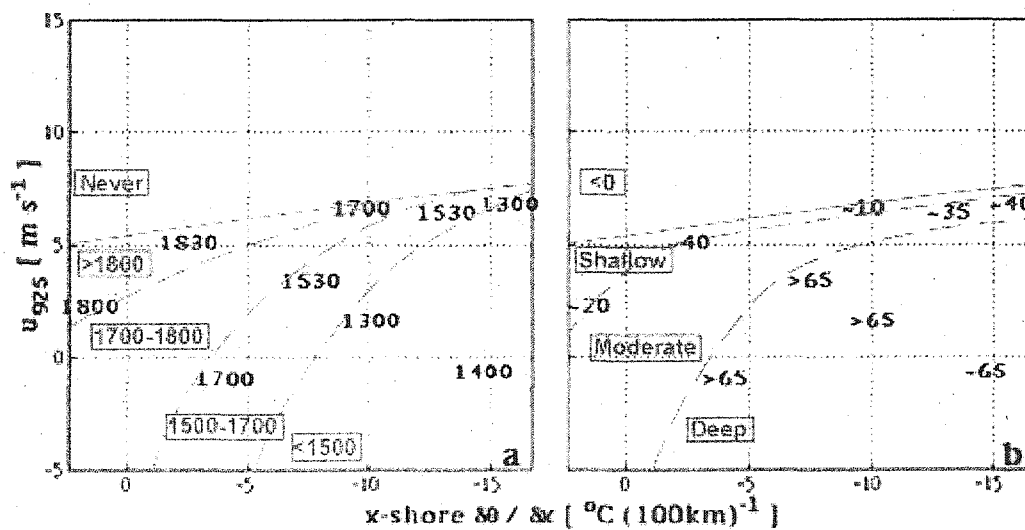


Figure 5.16: Time of onset and depth of inland penetration. a) The approximate earliest time (UTC) that the kinematic sea breeze first reaches the coast in the study area plotted as a function of the peak meso- α cross-shore potential temperature gradient and the estimated cross-shore wind component at 925 hPa. b) Maximum distance the sea breeze reaches inland (km) during its lifetime plotted as a function of the same variables. Events shown in both panels correspond to the dates shown in Figure 5.15a.

The time of onset for the nine case-studies describing SB or MAR events occurred in a range from about 1300 UTC (0800 LST) through about 1830 UTC (1330 LST). It can be seen from Figure 5.16a that stronger negative meso- α $\delta\theta/\delta x$ values generally result in an earlier onset time, and weaker values generally result in a later onset time, but the time of onset is delayed as the magnitude of the opposing 925 hPa wind component increases. In cases with an earlier onset, the meso- α forcing is relatively strong, and the response of the wind field was generalized, i.e., occurring throughout the study area at approximately the same moment. This approximately corresponds to those events that began relatively early in the day. In situations where the meso- α forcing is weak, inland movement of the sea-breeze circulation is dependent on meso- β scale forcing associated with the thermodynamic sea-breeze front, and varies on a local scale. This approximately corresponds to those events that begin relatively late in the day. Similar arguments can be made for maximum inland penetration depth (Figure 5.16b): Stronger negative meso- α scale $\delta\theta/\delta x$ values resulted in greater depths of inland penetration, but this was mitigated by the strength of the opposing 925 hPa wind component.

Summary and Conclusions

This chapter compared local-scale variations in the sea-breeze system to routinely available (or easily calculable) regional-scale forcing variables. Meso- α (regional) forcing ($\delta\theta/\delta x, u_{925}$) and meso- β (local) near-surface potential temperature and wind fields were examined for twelve case-studies from the year 2001. The potential temperature fields were used to explore the response of the sea-breeze gravity current, and the wind fields were used to explore the response of the sea-breeze circulation. The result is the development of new practical weather forecasting techniques, enabling operational meteorologists to predict several aspects of the sea breeze's behavior in the central New England coastal zone. These techniques are adaptable to any coastal location, and represent an increase in the level of detail covered in previous studies. Previous forecasting studies have focused on predicting sea breeze events at single locations [e.g. *Biggs and Graves, 1962; McKendry and Roulet, 1994*].

The potential temperature (isentropic) fields evolves between 15 "patterns," some of which are associated with sea-breeze events. Most of them exhibit considerable along-shore variation. The most developed (mature) patterns associated with the sea breezes are the

Lowlands, Split S, and Inland Shore-Parallel patterns (Figure 5.5). In the first, the sea-breeze gravity current moves inland and fills the low-lying areas (below 150 m ASL) in the northern and southern lowlands areas (NLA and SLA; Figure 5.4). In the second, the gravity current moves up onto the higher ground west of the NLA, and along the Mount Agamenticus-Lake Winnepesaukee line (MALW; Figure 5.4). In the third, the gravity current moves onto the high ground west of the SLA as well, resulting in the formation of a well-defined, roughly linear, shore-parallel thermodynamic sea-breeze front about 40 to 50 kilometers inland. The most developed isentropic pattern the sea-breeze gravity current achieves is a function of the meso- α ($\delta\theta/\delta x, u_{925}$) forcing.

The wind (kinematic) fields evolve between 24 patterns, all but two of which occurred on sea breeze days. Many of them exhibit considerable along-shore variation. In some of them, the kinematic sea breeze occurs along some parts of the coast, but does not occur along other parts of the coast. The strongest sea breezes are associated with the COL1 through COL5 kinematic patterns (Figure 5.13). In COL1, a well-developed kinematic sea-breeze front is on the coast, with southeasterly flow seaward of the front, and westerly or northwesterly flow west of the front. In COL2, the front becomes deformed and begins to move inland. In COL3, the front

traces out the inland limits of the NLA and SLA (Figure 5.4). COL4 occurs when the front moves onto the higher ground along the MALW line, between the NLA and SLA, and COL5 occurs when the front moves further inland, often past the northwestern boundary of the study area, approximately 65 kilometers inland. The time of the sea-breeze circulation's first contact with the coast (in the study area), and its most advanced inland distance, are both functions of the meso- α ($\delta\theta/\delta x, u_{925}$) forcing.

Two scales of meso- β kinematic (SBC) response to mesoscale forcing were evident in the case studies: One that corresponded to the larger meso- α forcing estimated by the Nowcast Diagram (Figure 5.3), and another that corresponded to the smaller thermal forcing produced by the meso- β potential temperature fields associated with the sea-breeze gravity current. When the meso- α forcing is weak, details of the wind field mirror details of the potential temperature field, and the sea breeze behaves as a true gravity current [*Simpson*, 1994]. When the meso- α is strong, the correspondence of the wind field (defining the sea-breeze circulation) and the potential temperature field (defining the sea-breeze gravity current) weakens considerably.

The values of the 925 hPa cross-shore wind component used in this chapter were estimated (via linear interpolation) from the 1200 and 0000 UTC radiosonde observations at nearby stations. At best, the resulting wind component estimates are accurate to within about 2.5 ms^{-1} , and correspond to the value of wind component at 1800 UTC (1300 LST). The conclusions drawn from the use of these data should be considered approximations, and could undoubtedly be improved by using direct observations of the wind aloft in the middle part of the day. Future research will quantify the behavior of the sea-breeze front in different meso- α forcing scenarios, and quantify the influence of the sea breeze on ground-level ozone along the central New England coast.

CHAPTER VI

THE SEA BREEZE: MESO-ALPHA FORCING AND MESO-BETA RESPONSE, PART II: FRONTAL BEHAVIOR

CHAPTER VI

THE SEA BREEZE: MESO-ALPHA FORCING AND MESO-BETA RESPONSE, PART II: FRONTAL BEHAVIOR

ABSTRACT

Behavior of the sea-breeze front along the central New England coast was studied using 12 year-2001 case studies. The front is composed of a convergence zone called the kinematic sea-breeze front, and a zone of maximum isentropic gradient called the thermodynamic sea-breeze front. Both are subject to bifurcation, resulting from diabatic airmass modification over the land surface and surface roughness difference. The magnitudes of both components usually peaked once in mid-afternoon, and once in early evening. The reduction in magnitude between the two peaks is a result of a combination of diabatic heating, changes in surface roughness, and changes in the wind direction seaward of the sea-breeze front.

Weather forecasters can determine if the sea-breeze front will bifurcate using the meso- α cross-shore potential temperature gradient and the cross-shore wind component near the top of the planetary boundary layer. When the meso- α forcing is strong, forecasters can expect multiple sea-breeze frontal passages at a given location. When meso- α forcing is weaker, forecasters can expect a single front causing simultaneous changes in wind velocity and air temperature at a given location. The strongest kinematic and thermodynamic fronts occur when the cross-shore wind component near the top of the planetary boundary layer is about 5 ms^{-1} , and the cross-shore potential temperature gradient is between -10 and $-15 \text{ }^\circ\text{C} (100\text{km})^{-1}$. This is the same range of meso- α forcing that results in the strongest meso- β sea-breeze frontogenesis.

Introduction

The sea breeze is a mesoscale wind that occurs at coastal locations throughout the world, and is an important factor in coastal New England's weather, climate, and air quality. It can provide moisture for early-morning fog and afternoon thunderstorms, at points ranging from the shore to more than 50 kilometers inland, and may trap pollutants in a shallow layer near Earth's surface, reducing air quality in the coastal zone [Barbato, 1975; Hsu, 1988; Gaza, 1998; Seaman and Michelson, 2000]. For these reasons it is important to better understand the local-scale behavior of the New England sea breeze, and how this behavior varies with the larger-scale meteorological environment.

The sea-breeze system (SBS) consists of many components. Among these are the sea-breeze circulation, sea-breeze gravity current, and the sea-breeze front (SBF) [Chapter 2]. Predicting the SBS's effect on climate and air quality requires specific knowledge of the location and behavior of its components, and it would be useful to be able to predict their behavior using routinely-measured meteorological variables. The objective of the work described in this chapter was to quantify the behavior and characteristics of the SBF along the central New England coast (Figure 6.1). The specific

characteristics studied were 1) bifurcation of the front; 2) meso- β (20 - 200 kms; [Fujita, 1986]) horizontal convergence, isentropic gradient, and frontogenesis; and 3) the relationship between the meso- α (200 - 2000 kms; [Fujita, 1986]) forcing and the SBF's meso- β response.

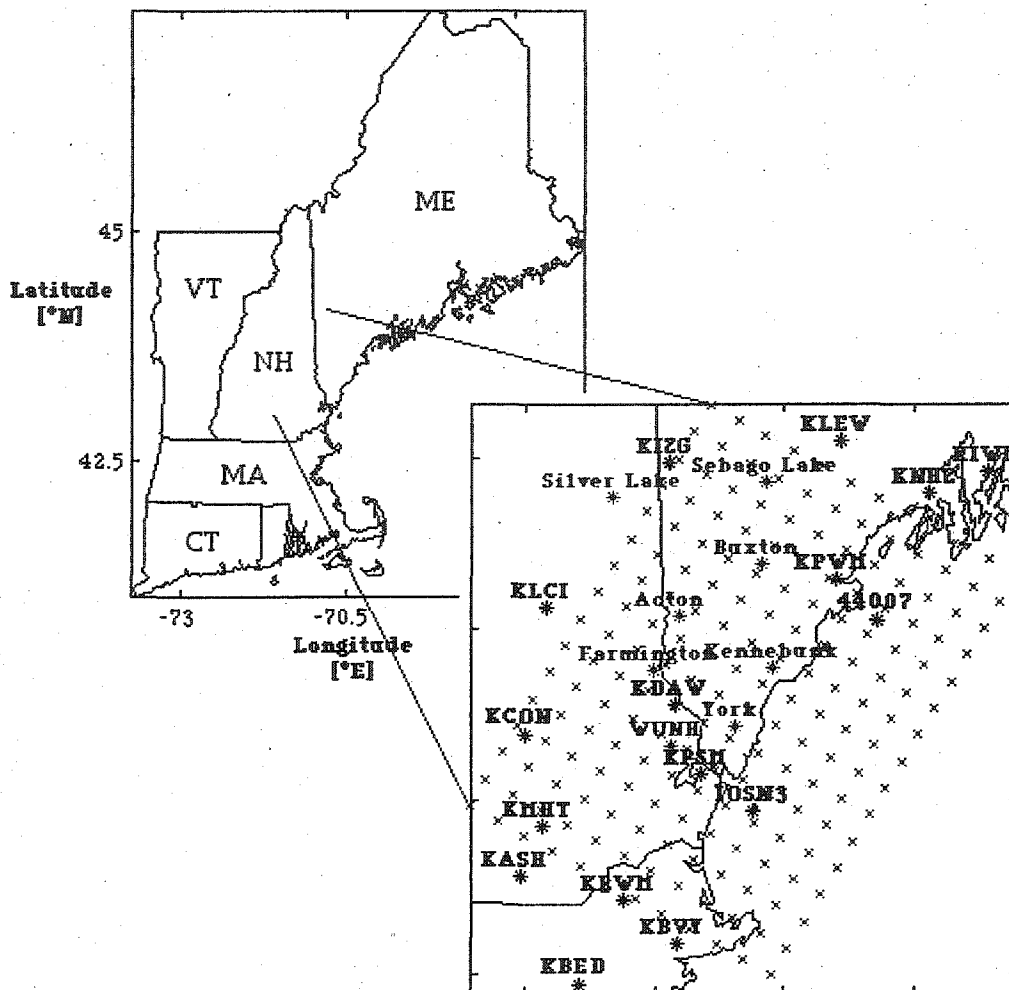


Figure 6.1: Study area. Standard NOAA surface observing stations (black) are identified by International Civil Aviation Organization identifier. UNH's supplemental stations are plotted in red. Blue crosses indicate grid points used for interpolated scalar fields.

Chapters 3 and 4 showed that sea breeze occurrences at a specific location (Portsmouth, New Hampshire, 10 km inland) could

be predicted by comparing the 1200 UTC United States surface chart to six well-defined six synoptic classes (based on the locations and relative dominance of surface pressure systems), and by a simple calculation of the cross-shore geostrophic wind component (u_G) and the meso- α cross-shore potential temperature gradient ($\delta\theta/\delta x$). The cross-shore potential temperature gradient creates the mesoscale pressure gradient force that drives the sea breeze toward land, and the cross-shore geostrophic wind component may resist the sea breeze's inland movement. Chapter 4 showed that the time-dependent behavior of u_G and $\delta\theta/\delta x$ is a function of the synoptic class. Chapter 5 replaced u_G with the cross-shore wind component at 925 hPa (u_{925}), thereby incorporating information about both the synoptic-scale wind and synoptic-scale horizontal temperature gradient, and improving forecasts of sea-breeze events. They also used near-surface potential temperature (isentropic) and wind (kinematic) fields to study the sea-breeze circulation and sea-breeze gravity current, and showed that both the kinematic and isentropic fields in east-central New England evolve between several well-defined patterns. The most developed sea-breeze gravity current patterns, the time of earliest sea-breeze onset in the study area, and

the greatest distance of inland penetration were all found to be functions of the meso- α ($\delta\theta/\delta x$, u_{925}) forcing.

The SBF marks the landward edge of the sea-breeze circulation and the gravity current [Chapter 2]. More than one SBF may develop in a single sea-breeze event [e.g. Kraus *et al.*, 1990; Atkins *et al.*, 1995; Lapworth, 2000]. A field study of the SBF in eastern Florida, using Doppler radar stations and an instrumented aircraft, discerned a difference between the thermodynamic and kinematic sea-breeze fronts [Atkins *et al.*, 1995]. The thermodynamic sea-breeze front (SBF_{th}) is the location within the planetary boundary layer where the mean thermodynamic properties of the air begin to differ from those of the ambient (continental) air, and the kinematic sea-breeze front (SBF_{kn}) is the location of maximum near-surface (100 meters AGL) wind convergence. Chapter 5 showed that if the meso- α forcing is weak in east-central New England, there is a unified SBF, but if the meso- α forcing is strong, the SBF is often bifurcated into the SBF_{th} and the SBF_{kn}. This finding serves as the focal point of this chapter.

The SBF is subject to frontogenesis and frontolysis [e.g. Reible *et al.*, 1993]. Sea-breeze frontogenesis (the formation or intensification of the SBF) is defined as an increase in the magnitude of the cross-shore potential temperature gradient. Chapter 2

derived a kinematic frontogenesis function (KFF) from the 3-D diffusion relation for potential temperature, resulting in:

$$\begin{aligned} \frac{d\theta_x}{dt} = & - \frac{\partial u}{\partial x} \theta_x - \frac{\partial v}{\partial x} \theta_y - \frac{\partial w}{\partial x} \theta_z \\ & + \frac{\partial}{\partial x} \left[K_H \frac{\partial^2 \theta}{\partial x^2} \right] + \frac{\partial}{\partial x} \left[K_H \frac{\partial^2 \theta}{\partial y^2} \right] + \frac{\partial}{\partial x} \left[K_V \frac{\partial^2 \theta}{\partial z^2} \right] \end{aligned} \quad (6.1)$$

where x , y , z , are the cross-shore, along-shore, and vertical dimensions, respectively; u , v , and w are the wind components in the x , y , and z dimensions [$m s^{-1}$]; θ is the potential temperature [K]; K_H and K_V are the diffusion coefficients in the horizontal and vertical directions [$m^2 s^{-1}$]; and subscripts (e.g. x in θ_x) indicate the partial derivative of the function (θ) in the direction indicated (x). The physical interpretations of the terms on the right-hand side of (6.1) are:

- Term 1: Cross-shore confluence (or deformation).
- Term 2: Rotation of along-shore isentropic gradients into the cross-shore direction resulting from a cross-shore variation in the along-shore wind component.

- Term 3: Rotation of vertical isentropic isentropic gradients into the horizontal plane.
- Terms 4 and 5: Cross-shore variation in cross- and along-shore eddy-driven heat diffusion.
- Term 6: Cross-shore variation in eddy-driven diffusion of heat in the vertical dimension.

With ocean on the right (toward positive x-values), sea-breeze frontogenesis is indicated if the sum of the right-hand side is less than zero, and frontolysis (the destruction or weakening of the sea-breeze front) is indicated if the sum of the right-hand side is greater than zero. In the former case, the cross-shore potential temperature gradient is tending toward more negative values with time, and in the latter, it is tending toward more positive values with time [Chapter 2]. Scaling arguments and additional analysis of the KFF are in Appendix III.

Research on the central New England sea breeze was carried out as part of the Atmospheric Investigation, Regional Modeling, Analysis, and Prediction (AIRMAP) project. AIRMAP's goal is to

understand factors influencing New England's climate and air quality. The goal of the Central New England Sea Breeze Study is to quantify the behavior of the sea breeze on the central New England coast and develop improved forecasting techniques.

Scope and Methods

The study area included the relatively straight section of New England's coastline between Cape Ann, Massachusetts, and Wiscasset, Maine (Figure 6.1). This section of coastline was chosen to avoid "edge effects" introduced by seaward projections of land and simplify the problem of describing sea-breeze behavior. *Barbato* [1975] noted that the Boston-area sea breeze extends about 30 kilometers inland, and others [e.g., *Hadi et al.*, 2002] have observed that the sea breeze is prevented from further inland penetration by mountain ranges more 60 kilometers from the coast. *Simpson* [1994] noted inland intrusions of more than 200 kilometers in the absence of topographic obstructions. With this in mind, the inland boundary of the study area was set to 65 kilometers, near the eastern edge of the White Mountains. The offshore boundary was set to the expected limits of land-breeze phase of the circuit -- forty kilometers from shore [*Simpson*, 1994;

Holmer and Haeger-Eugensson, 1999]. The northeastern and southwestern boundaries corresponded to the straight section of coastline noted above. The southwestern boundary was extended somewhat beyond the straight section of coastline to include a meso- γ scale network of wind recording stations in the vicinity of Newburyport, Massachusetts.

The research described in this chapter used twelve case-studies in this domain that collectively span the range of variation in $(u_G, \delta\theta/\delta x)$ meso- α forcing observed in the study area during year-2001 sea-breeze (SB) and marginal events (MAR), as well as borderline non-sea-breeze (NSB) events (Figure 6.2 and Table 6.1). The values of u_G and $\delta\theta/\delta x$ shown in Figure 6.2 were calculated for the moment of onset (for SB and MAR events) in Portsmouth, New Hampshire, or 1900 UTC (for NSB events) [Chapter 3]. Sea breeze events were defined as the occurrence of a local, insolation-driven wind from the southeast in Portsmouth [Chapter 3]. Marginal events were weak sea breezes, and non-sea breeze events were those when sufficient insolation was available to drive a sea breeze, but it did not reach Portsmouth [Chapter 3].

Table 6.1: Case study dates, synoptic classes, and event types. Synoptic classes are described in Chapter 3. Types of events are sea-breeze (SB), marginal (MAR), and non-sea-breeze (NSB).

Date [MM/DD/YYYY]	Type of Event ¹	Synoptic Class
01/23/2001	SB	4
04/03/2001	SB	2
05/09/2001	SB	4
05/10/2001	SB	1
05/11/2001	SB	2
06/14/2001	SB	7
07/06/2001	NSB	2
07/07/2001	MAR	1
07/13/2001	NSB	3
07/28/2001	SB	1
08/18/2001	NSB	2
09/29/2001	SB	6

Notes:

1. Type of event determination is based on the occurrence/non-occurrence of the sea breeze at Pease airport, in Portsmouth, New Hampshire.

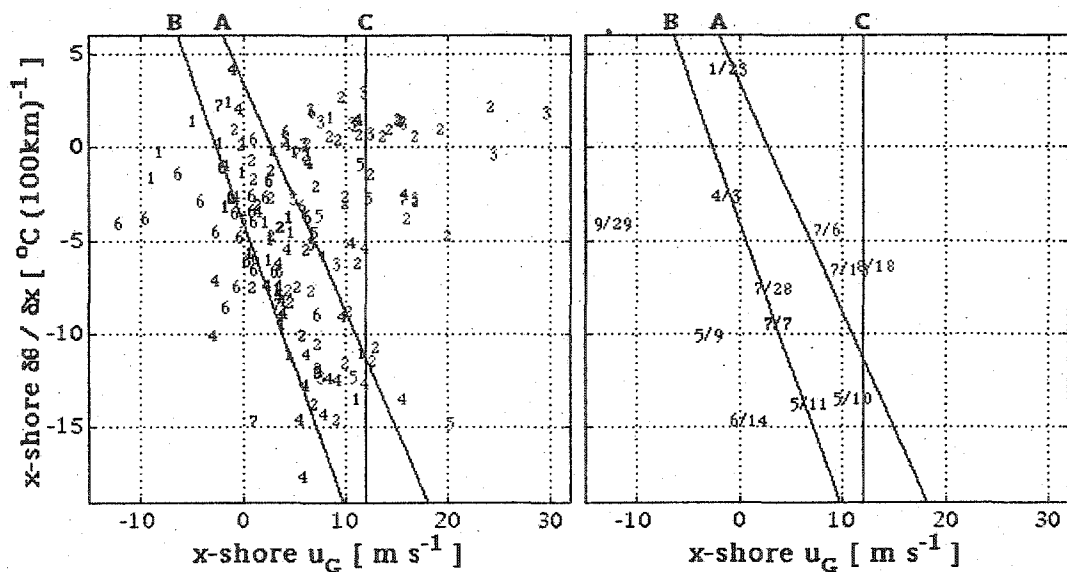


Figure 6.2: Case-study events as a function of their associated cross-shore potential temperature gradients ($\partial\theta/\partial x$) and geostrophic wind components (u_G). Events are plotted using the regional-scale temperature gradients and geostrophic wind components present at either the time of onset (for sea breezes and marginal events), or 1400 LST (for non-seabreeze events). Sea-breeze events are in blue, marginal events are in black, and non-seabreeze events are in red. Left: Synoptic classes of all events in 2001. Right: Dates of case-studies chosen for this work.

The u_{925} field above the study area was interpolated from 1200 and 0000 UTC 925 hPa charts obtained from the Plymouth State College website (<http://vortex.plymouth.edu>). The spatial and temporal evolution of the SBF were examined using near-surface meso- β wind-divergence and isentropic gradient fields. These fields

were derived from observations of temperature, pressure, and wind in the study area. Surface observations produced by the standard NOAA surface observing network (Figure 6.1) within the study area were supplemented with a series of automated weather stations placed in areas of sparse coverage installed by the University of New Hampshire (UNH), creating a surface observing network capable of resolving meso- β features. The supplemental weather stations were installed on public buildings and private homes, conforming as closely as possible to World Meteorological Organization (WMO) standards for the positioning of meteorological instrumentation [WMO, 1996].

Observed temperatures were converted to potential temperatures (θ), removing most of the distortion of the temperature field resulting from differences in station altitude, and all of the distortion due to pressure variations. Observed winds were converted to eastward (u) and northward (v) scalar components, which are then recalculated for a coordinate system rotated clockwise by 30 degrees, yielding u' and v' . The coastal zone within the study area can be approximated by a straight line, running from 210 degrees to 30 degrees on a compass, so u' and v' represent cross- and along-shore wind components.

A grid system with 10-km grid spacing (Figure 6.1) was generated, with the x-axis oriented in the cross-shore dimension (positive x toward 120 degrees true), and the y-axis oriented in the along-shore dimension (positive y toward 30 degrees true). All three scalars from the observing sites (θ , u' , and v') were interpolated onto the grid system by means of a 2-D, anisotropic, adaptive Barnes interpolation routine [Barnes, 1964]. Randomly-chosen contour plots of interpolated temperature fields and vector plots of interpolated wind fields were compared to hand-analyzed plots for corresponding dates and times, and found to be satisfactory. Divergence ($\nabla \cdot \mathbf{V}$), isentropic gradient ($|\nabla\theta|$), and the first two terms of the kinematic frontogenesis function ($-(\partial u/\partial x)\theta_x$; $-(\partial v/\partial x)\theta_y$) calculated at each of the gridpoints were used as the basis of the work described in this chapter.

The surface synoptic situation for each of the twelve case-studies was determined using United States surface analyses archived in the National Virtual Data System, and accessed via the NVSD website (http://nndc.noaa.gov/?http://ols.ncdc.noaa.gov/cgi-bin/nndc/buyOL-006.cgi?FNC=chart_Ancep_get_chart_htm). GOES infrared images (obtained from the NOAA Historical Archive; see

<http://lwf.ncdc.noaa.gov/servlets/GoesBrowser>) were used to determine cloud cover in and around the study area.

Results

Meso- β scale isentropic gradient ($|\nabla\theta|$) and wind divergence ($\nabla \cdot \mathbf{V}$) fields were used to study the behavior of the sea-breeze front in the study area. Only those case-studies involving sea breeze and marginal events are discussed, and only those gradients associated with the sea-breeze gravity current or circulation are discussed in depth.

A set of simplified geographical reference points (Figure 6.3b) -- derived from a 2-km resolution topographic map of the study area (Figure 6.3a) -- were used in the studies of frontal behavior. Two of the reference points are low-lying (below 150 m MSL), scallop-shaped areas in the northern and southern halves of the study area, referred to as the Northern Lowlands Area (NLA) and the Southern Lowlands Area (SLA). The line following the high ground from Mount Agamenticus (York, Maine) to Lake Winnepesaukee (near Wolfeboro, New Hampshire) is referred to as "MALW," and the roughly shore-parallel line demarking the approximate location of the 200 m MSL topographic contour is referred to as "2ML." The

Gulf of Maine (GOM) is the portion of the Atlantic Ocean immediately offshore of Massachusetts, New Hampshire, and Maine. The Great Bay is the inland body of water west and south of Portsmouth, New Hampshire (KPSM). Specific weather stations are generally referred to by their International Civil Aviation Organization identifiers, and are shown in Figure 6.1.

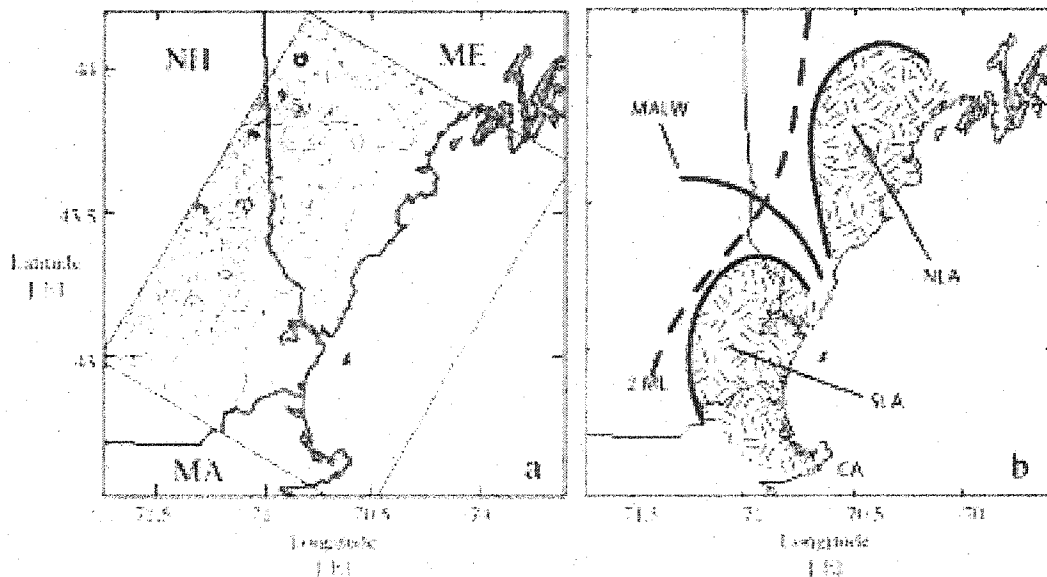


Figure 6.3: Study area topography and reference points. a) Study area (blue box) with topographic contours (green lines). Topo contours are drawn at intervals of 50 m ASL, beginning with 50 m ASL. b) Reference points used in discussion of frontal behavior.

The focus is on the relatively straight section of coastline that runs from north of Cape Ann (CA; Figure 6.3) to north of Portland,

Maine (KPWM; Figure 6.1). It can be seen that a shore-parallel wind in this area will result in onshore flow in the complex coastal area south of Brunswick Naval Air Station (NAS), Brunswick, Maine (KNHZ; Figure 6.1). This was not classified as a sea breeze. Similar arguments hold for CA.

Table A5.4 (Appendix V) summarizes the evolution of the $|\nabla\theta|$ and $\nabla \cdot \mathbf{V}$ fields that occurred during the eight case studies involving SB and MAR events. Additional discussion of these events is included below. Times are discussed in terms of UTC, unless otherwise noted. The conversion to Local Standard Time (LST) is UTC - 5 hours, and to Local Daylight Time is UTC - 4 hours.

The absence of a strong, meso- β isentropic gradient during the January 23, 2001 SB event indicates the absence of a classical sea-breeze gravity current and associated SBFth. Because of the presence of the sea-breeze circulation from 1800 through 2200, and because the meso- α ($\delta\theta/\delta x$, u_G) forcing was not conducive to a sea breeze (Figure 6.2b), it is concluded that a meso- β -scale sea breeze occurred in the immediate coastal area in response to the weak cross-shore potential gradient that appeared at 1600. As the marine air moved onshore, the cross-shore isentropic gradient was destroyed, and the sea-breeze circulation diminished. It is proposed

that the sea-breeze circulation continued until 2200 (two hours after the disappearance of a significant meso- β $|\nabla\theta|$ field) because of the system's momentum.

The magnitude of the convergence (negative divergence) associated with the SBFkn peaked twice during the January 23, 2001 SB event: Once at 2000, when the magnitude of the onshore flow component peaked, and once at 2200. The latter peak occurred because the inland wind began shifting back to a shore-parallel configuration first (as the sea-breeze circulation diminished in size and retreated back toward the sea), while the shoreward component offshore (within the sea-breeze circulation) lasted later into the evening. The maximum convergence was about the same in both peaks.

During the April 3, 2001 SB event, a synoptic-scale cloud shield covered the northern portion of the study area which prevented the sea breeze from developing there. A well-developed sea-breeze circulation (with SBFkn) and gravity current (with SBFth) appeared in the southern half of the study, which was relatively free of cloud cover. As in the January 23, 2001 event, the onset of the sea breeze in the south was preceded by the disappearance of along-shore isentropic gradients. There was an extended period (approximately three hours) when no discernible isentropic

gradients were present, followed by the appearance of a cross-shore gradient. The wind offshore of the SLA began to recurve toward land at 1800, at the same time the cross-shore isentropic gradient appeared. This indicates that the sea-breeze circulation and the sea-breeze gravity current were closely coupled. Eventually, a well-defined SBFth developed that marked out the limits of the SLA, further indicating a close coupling of the sea-breeze circulation and gravity current. The sea-breeze circulation disappeared (at 0000) after the isentropic gradients became indiscernible (at 2200) -- a two-hour time-lag which mirrors the lag noted in the January 23, 2001 event.

The strongest cross-shore isentropic gradients appeared on the north side of Cape Ann, which is a rocky mass projecting out into the Gulf of Maine. The coastal region north of Cape Ann (at the southern extreme of the straight section of coastline in the study area) is a barrier island (Plum Island) and a combination of estuaries and salt marshes. Since bare rock has a much lower specific heat coefficient (c_p) than wet ground (the c_p of granite is about $790 \text{ J kg}^{-1} \text{ K}^{-1}$; seawater's is about $4000 \text{ J kg}^{-1} \text{ K}^{-1}$ [Fofonoff and Millard, 1983; Halliday et al., 1993]), it is proposed that cross-shore isentropic gradients were stronger over Cape Ann because of its relatively low specific heat coefficient.

The May 9, 2001 SB event was associated with strong meso- α ($\delta\theta/\delta x, u_G$) forcing, and as a result, there was weak correspondence between the sea-breeze circulation and gravity current. The primary SBFkn appeared at 1400 along the coast, and moved inland rapidly. By 1600, it was beyond the northwestern edge of the study area. The secondary SBFkn that appeared at 1600 was associated with the inland movement of the SBFth and sea-breeze gravity current, which filled the NLA and SLA at the same time. The temporary weakening of the SBFth that occurred between 2100 and 2300 probably resulted from a combination of 1) increased low-level mechanical turbulence seen by the marine airmass as it crossed onto higher, more rugged terrain, and 2) diabatic heating from below.

Two aspects the evolution of the $|\nabla\theta|$ and $\nabla \cdot \mathbf{V}$ fields in the May 10, 2001 SB event reflect the frontal bifurcation discussed in *Atkins et al.* [1995]. First, the SBFkn and SBFth were not in the same place at the same time. Second, the SBFth was itself bifurcated as a result of diabatic modification of the marine air over land, resulting in an inland SBFth, representing the leading edge of diabatically modified marine air, and a coastal SBFth, representing the boundary between the modified and unmodified marine air.

As in the May 10, 2001 SB event, an inland SBFth developed without a clearly-visible preceding movement of the sea-breeze gravity current through the lowlands during the May 11, 2001 SB event. The weakening of the inland SBFth between 2000 and 2200 occurred as the near-surface wind flow shifted from a directly shore-perpendicular direction to a more southerly direction. This forced the marine air feeding the inland SBFth to travel a longer distance over land before reaching the front. The longer over-land distance resulted in greater airmass modification by diabatic heating. The inland SBFth then reintensified to its previous peak convergence value due the loss of significant insolation and the resulting reduction in diabatic modification to the marine airmass.

Thermodynamically, the June 14, 2001 SB event resembled the previous two sea-breeze events. The secondary inland SBFth developed in the north at 1900, then grew slightly weaker for the following two hours. From 2200 through 2300, it intensified again, but did not regain its original peak values. The coastal SBFth exhibited its peak values at 1600, but then the northern half of the coastal SBFth weakened for the remainder of the day, while the southern coastal SBFth maintained a relatively constant magnitude. Stated another way, unlike the May 10, 2001 SB event, the magnitude of the inland SBFth *did* increase at the expense of the

coastal SBFth in the north. In the south, where there was no inland SBFth, this did not occur. The July 28, 2001 SB event was also thermodynamically similar. The coastal SBFth initially appeared at 1600, and by 2000, the inland SBFth began to appear in the northern half of the study area. By 2100, the northern coastal SBFth began weakening as the inland SBFth continued to intensify, while the southern SBFth maintained a steady magnitude. By 2200, as the inland SBFth reached its peak intensity, the northern coastal front became almost undetectable. The southern SBFth also weakened, but could still be detected in the $\nabla \cdot \mathbf{V}$ field.

The September 29, 2001 SB event was marked by a very weak $|\nabla\theta|$ field over its entire duration, indicating the absence of a well-defined SBFth. The $\nabla \cdot \mathbf{V}$ field was comparable to the other sea-breeze events discussed above. The apparent SBFkn associated with this event did not develop at the landward extreme of the SBC, but rather within the SBC, along a line near the coast where the wind speeds rapidly diminished due to the increase in surface friction.

Discussion

Morning development of cross-shore gradients. Early-morning isentropic gradients are usually quite weak, or oriented in

an along-shore direction. The early-morning convergence field is also often quite weak. The onset of the sea breeze is often preceded by the complete disappearance of early-morning isentropic gradients and convergence axes (resulting in an hour or two of undetectable gradients), followed by the redevelopment of new patterns indicating the presence of cross-shore isentropic gradients and wind convergence.

Kinematic and thermodynamic fronts develop in different locations. Once the sea-breeze circulation begins developing, the SBFkn (which represents the landward edge of the circulation) and SBFth (which represents the landward edge of the sea-breeze gravity current) are usually not in the same place (i.e., the circulation and gravity current are not closely coupled). This is especially true when the meso- α forcing (see Figure 6.2) is strong, as in the September 29, May 9, and June 14 events. When the meso- α forcing is weak, as in the May 10 and May 11 events, the two fronts are closer together (i.e., the circulation and gravity current are closely coupled).

Evening persistence of circulation. The sea-breeze circulation often persists up to two hours after the meso- α scale forcing

vanishes, maintained either by momentum, or by meso- β thermal forcing associated with the SBFth.

Dual peaks in magnitude of thermodynamic front. The magnitude of the SBFth often peaks twice during the life of the sea breeze. Following the first peak, (around 2000 UTC, or 1500 LST), there is a mid-afternoon weakening in isentropic gradients. This is associated with a combination of the SBFth's movement out of the lowlands and up onto the higher ground near ZML, resulting in mechanical turbulence, and diabatic heating, resulting in surface modification of the marine airmass seaward of the front.

Weakening of the SBFth may also occur when veering within the sea-breeze circulation rotates the wind from a southeasterly to a more southerly direction, forcing the marine air feeding the SBFth to travel a longer distance over land (and therefore be subject to more diabatic modification) before reaching the front. After about three hours (at about 2300 UTC, or 1800 LST), the SBFth intensifies again, which is probably the result of the loss of significant insolation (and the subsequent reduction in diabatic modification), and relatively strong radiational cooling in the dryer, continental airmass landward of the SBFth.

Dual peaks in magnitude of kinematic front. The magnitude of the SBFkn often peaks twice during the life of the sea breeze. The first peak occurs when the magnitude of the landward component of the surface wind within the sea-breeze circulation peaks in the mid-afternoon (at about 1900 or 2000 UTC; 1400 or 1500 LST). The second peak occurs when the ambient wind landward of the SBFkn begins to diminish or veers to a shore-parallel direction (at about 2200 or 2300 UTC; 1700 or 1800 LST). Another possible cause of mid-day amplification of the SBFkn is an increase in the seaward component of the ambient wind landward of the front, as occurred in the May 10, 2001 event. Late evening weakening of the SBFkn occurs when the surface wind *within* the sea-breeze circulation veers from southeasterly to a more shore-parallel direction.

Bifurcation of the thermodynamic front. Chapter 4 discusses the behavior of the sea-breeze gravity current in terms of a series of isentropic patterns. From the evidence presented in previous sections of this chapter, it is concluded that the Split S isentropic pattern (Figure 6.4) is associated with a bifurcated thermodynamic sea-breeze front, where the inland SBFth (appearing in the northern half of the study area) represents the leading edge of the marine airmass, and the coastal SBFth represents the boundary between

modified (inland) and unmodified (offshore) marine air. In the south, it has not been determined whether two separate SBFth's develop. The inland SBFth in the north may gain in strength at the expense of the northern coastal SBFth (as in the June 14, 2001 sea-breeze event), or it may not (as in the May 10, 2001 sea-breeze event). More research is required to determine the physical mechanism responsible for this division.

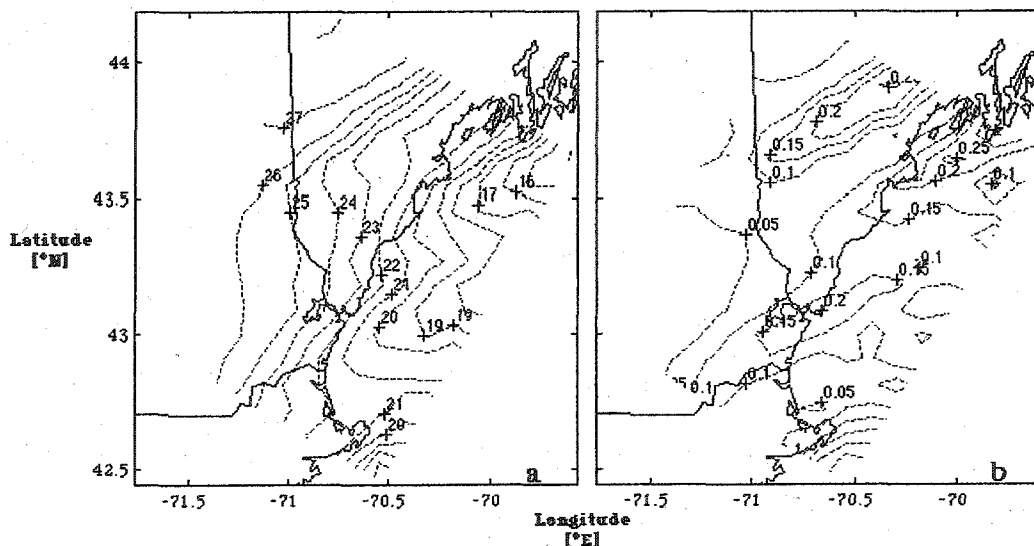


Figure 6.4: Split S isentropic pattern and bifurcated thermodynamic sea-breeze front. a) Isentropic field observed on May 10, 2001, 2100 UTC. Isentropic contours are drawn at interval of 1 °C. b) Magnitude of the isentropic gradient associated with contours in panel a), drawn at intervals of 0.05 °C km⁻¹. Fronts are visible as elongate regions of strong isentropic gradient.

Persistent zone of convergence. A zone of convergence commonly extends along a line from Lawrence, Massachusetts (KLWM; see Figure 6.1), through Portsmouth, New Hampshire (KPSM), and further northeast into the Gulf of Maine. Its appearance in these case studies may be the result of some physical phenomena, or it may be a mirage created by bias in the algorithm that interpolated the raw wind observations onto the grid. The latter possibility has been eliminated with some certainty by comparing the interpolated wind vectors to several hand-analyzed streamline fields that were selected at random. Additional research is therefore needed to determine the physical mechanism causing this regular feature. One indicator of the development of the SBC is when this convergence zone begins to rotate in a counter-clockwise direction, causing the southern half to move toward the coast from the land side, and the northern half to move toward the coast from the ocean side.

Bifurcation of the kinematic front. A weak, secondary convergence zone may develop within the sea-breeze circulation, seaward of the primary SBFkn. Unlike the coastal SBFth, which usually rivals the inland SBFth in magnitude, the secondary SBFkn is usually quite weak and short-lived. In the May 9, 2001 event, this

secondary convergence zone may have been associated with the inland movement of the SBFth, well behind in the SBFkn in an environment of strong meso- α forcing. Another possible cause, which occurred during the same event, is when wind speeds over land within the sea-breeze circulation diminish more rapidly than wind speeds over water, as the SBS weakens toward the end of its life. A similar phenomena occurred during the September 29 sea-breeze event, when strong northeasterly winds in the Gulf of Maine initially encountered the rougher land surface, resulting in a convergence zone either on the coast or halfway into the two lowlands areas.

In one event (June 14, 2001), the new coastal convergence zone appeared to move from the sea into its place on the KLWM-KPSM-GOM line. Later, as the sea-breeze circulation contracted, the original (inland) SBFkn began to weaken and move back toward the sea, while the coastal convergence zone gained in strength. Eventually there was only one SBFkn along the coast.

Distribution and forecasting of peak isentropic and kinematic gradients. Table 6.2 summarizes the peak isentropic gradients and divergence values associated with each sea-breeze

event. Equivalent values for the July 7, 2001 marginal event are added as a point of reference.

Table 6.2: Peak sea-breeze related isentropic gradients and wind divergence values. Isentropic gradients shown are the absolute value of the strongest negative isentropic gradients associated with the sea breeze. (Negative gradients indicate colder air over the ocean to the east.) Negative divergence values indicate regions of convergence. Gradients and convergence values not associated with the sea-breeze system are not included.

Case Study	Peak Neg Isentropic Gradient ($ \nabla\theta $) [$^{\circ}\text{C km}^{-1}$]	Time of Peak [UTC]	Peak Neg Wind Div ($\nabla \cdot \mathbf{V}$) [$\text{m s}^{-1} \text{ km}^{-1}$]	Time of Peak [UTC]
23 Jan	0.16	1600	-0.29	2000
03 Apr	0.14	1800	-0.37	2100
09 May	0.34	2300	$(-0.21)^1$	$(1500)^1$
10 May	0.42	1900	-0.47	1900
11 May	0.38	1700	-0.37^2	2000^2
14 Jun	0.38	1600	-0.39	2200
07 Jul	0.67	1700	-0.32	1700
28 Jul	0.21	1700	-0.39	1900
29 Sep	0.10	1800	-0.37	2300

Notes:

1. The divergence value (and time of peak divergence) for the May 9, 2001 sea-breeze event are shown in parenthesis, because these correspond to the peak wind convergence noted along the SBFkn before the front moved beyond the northwestern boundary of the study area.
2. The May 11, 2001 exhibited a secondary negative peak divergence of -0.36 at 1700.

In all cases (with the exception of the May 9, sea-breeze event), the peak values of both isentropic gradient and negative wind divergence occurred between 1600 and 2300 UTC (1100 and

1800 LST). (The May 9 peak convergence is unreliable because the SBFkn moved beyond the northwestern boundary of the study area early in the day.) The strongest isentropic gradients generally occurred at least an hour prior to the strongest convergence values. The two peaks occurred at the same time during the May 10 sea-breeze event and the July 7 marginal event. In a third event (May 11), there was an additional negative divergence peak (almost equal to the primary peak) that occurred at 1700 UTC, which was at the same time as the strongest isentropic gradient.

Figure 6.5 shows the peak meso- β isentropic gradient and peak negative divergence values as a function of the peak meso- α forcing associated with each event. The vertical forcing axis is the estimated cross-shore wind component at 925 hPa, and the horizontal forcing axis is the meso- α -scale cross-shore isentropic gradient (which is responsible for the thermal PGF that moves the sea breeze onshore).

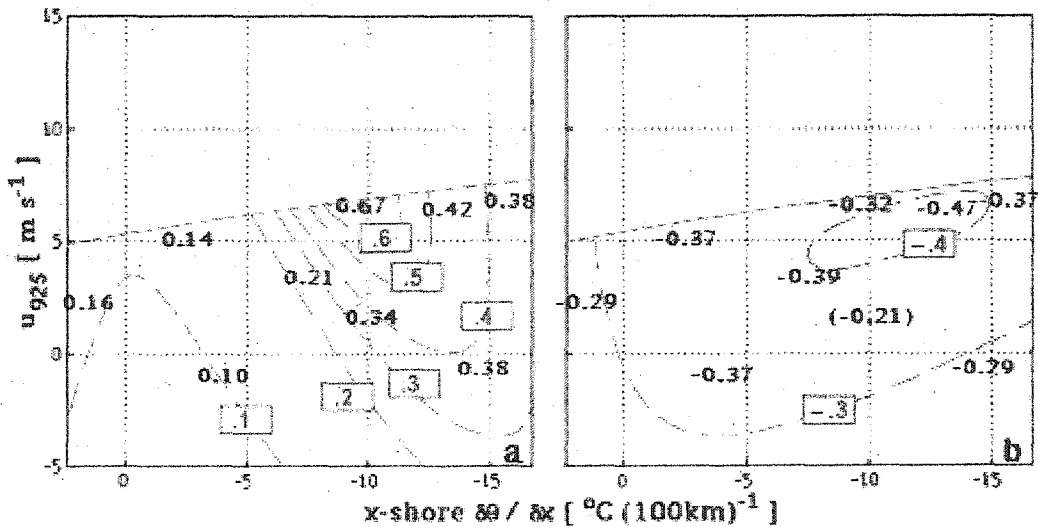


Figure 6.5: Peak sea-breeze related meso-β isentropic gradients and wind divergence values as a function of peak meso-α forcing. Vertical axis is the cross-shore wind component at 925 hPa; horizontal axis is the meso-α cross-shore potential temperature gradient. Sea-breeze events are in blue text; marginal event is in black text. Contours were drawn by inspection. a) Absolute value of peak meso-β isentropic gradient associated with the SBFth. Units of plots and contours are °C km⁻¹. b) Peak meso-β negative divergence (i.e. convergence) associated with the SBFkn. Units of plots contours are m s⁻¹ km⁻¹.

From Figure 6.5a, it is obvious that the strongest sea-breeze-related meso-β isentropic gradients occur when the 925 hPa cross-shore wind component is greater than about 5 ms⁻¹, and the meso-α cross-shore isentropic gradient is about -10 °C (100 km)⁻¹. The offshore wind component near the top of the planetary boundary layer, coupled with a moderate meso-α land-sea temperature difference, results in a well-defined SBFth. The strongest SBFth was

associated with a marginal event, when the marine airmass moved over land for only a brief period, and did not penetrate very far inland. Toward the lower left of the Figure 6.5a, meso- β isentropic gradients are weak because the planetary boundary layer wind has an onshore component (shown to be detrimental to strong continental-marine temperature contrasts by *Simpson* [1994]), and the meso- α thermal difference in the two airmasses is small (or nonexistent) to begin with. Toward the far right side of the same panel, the land temperatures are so high (as indicated by very strong negative land-sea isentropic gradients) that diabatic heating significantly modifies the marine airmass when it comes onshore, weakening the peak meso- β gradient at the SBFth.

Figure 6.5b indicates that the strongest SBFkn's occurred in the same events as the strongest SBFth's. Stronger offshore winds near the top of the planetary boundary layer resulted in stronger meso- β convergence values. In the upper right (where the July 7, May 10, and May 11 events are plotted), meso- β wind convergence is further enhanced by the coupling of the sea-breeze circulation and the sea-breeze gravity current. Figure 6.2 indicates that these three events were within the Nowcast Diagram's transition zone, between lines A and B, where Chapter 4 shows that the sea-breeze

circulation and gravity current are closely coupled. In these cases, net convergence occurred at a unified sea-breeze front. Toward the lower right of the same panel, there is strong meso- α thermal forcing, but an onshore wind near the top of the planetary boundary layer. In this case, such as in the May 9, or June 14 events, the sea-breeze circulation and gravity current were decoupled, and meso- β convergence was divided between the SBFth and SBFkn. On the left side of the panel, meso- α thermal forcing is weak, non-existent, or of the wrong sign, and there was no gravity current. Meso- β convergence is created entirely by a very weak sea-breeze circulation.

Forecasting peak meso- β frontogenesis. The cluster of three strong events in the upper right corners of Figures 6.5a and 6.5b are the same three events in which the peak SBFth and peak SBFkn occurred at the same time (shown in Table 6.2). That these three indicate the conditions for the strongest unified sea-breeze fronts (i.e. that the two peaks occur in the same *place*) is suggested by their proximity on the diagram. This was determined quantitatively by calculating the first two terms of the kinematic frontogenesis function. The first term combines information about the cross-

shore meso- β isentropic gradients and wind divergence. The second term combines information about the along-shore gradients and the horizontal rotation of these gradients into the along-shore dimension induced by the wind curl [$\mathbf{k} \cdot (\nabla \times \mathbf{V})$].

The first term of the kinematic frontogenesis function [KFF_1 ; - $(\partial u / \partial x) \theta_x$] is the convergence term, and the second term [KFF_2 ; - $(\partial v / \partial x) \theta_y$] is the rotation term. In both cases, negative values indicate frontogenesis, and positive values indicate frontolysis. This can easily be illustrated by considering the convergence term: With cold air on the right (over sea), and warm air on the left (over land), frontogenesis is indicated by a negative meso- β isentropic gradient (θ_x). Frontogenesis is also indicated by a negative divergence value, indicating meso- β convergence ($\partial u / \partial x$). If both are negative, their product results in a positive number. Adding the third negative sign reverses the sign of the entire term.

These calculations were applied to the gridded meso- β wind and potential temperature fields discussed in Chapter 5. Following an inspection of the hourly KFF fields, peak values of KFF_1 and KFF_2 associated with sea-breeze system (and subject to the limitations discussed in the appendix) were determined for the sea-breeze and

marginal events. The results are shown in Figure 6.6.

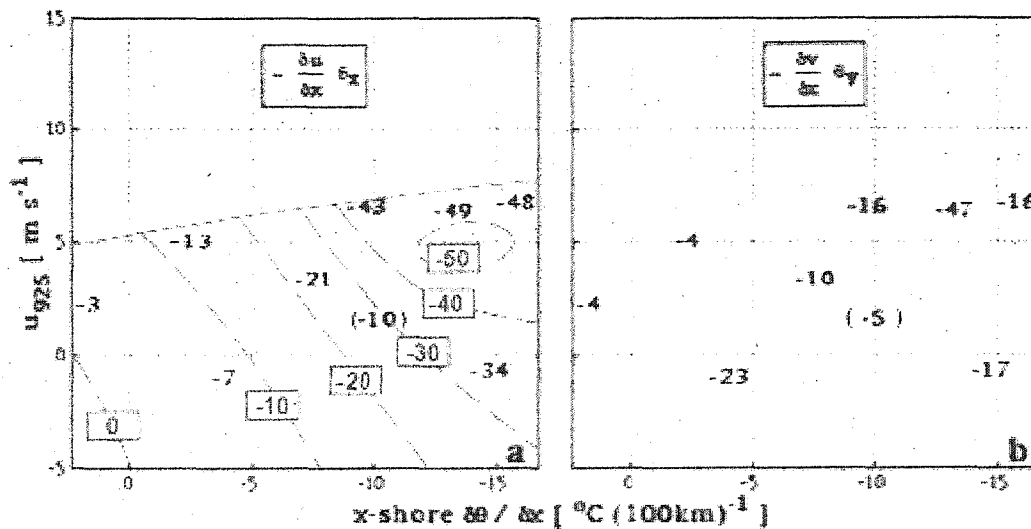


Figure 6.6: Peak meso- β convergence and rotational frontogenesis with sea-breeze and marginal events, as a function of peak meso- α forcing. Axes and color coding are as shown in Figure 6.5. Contours were drawn by inspection. Units of both terms and contours are $(^\circ\text{C s}^{-1} \text{m}^{-1}) \times 10^9$. a) Peak meso- β values of convergence frontogenesis (KFF term 1). b) Peak meso- β values of rotational frontogenesis (KFF term 2). The May 9, 2001 values, shown in parenthesis near $\delta\theta / \delta x = -10$, $u_{925} = 2$ are unreliable for reasons discussed in the text.

The plot shown in Figure 6.6a (KFF₁) reveals structure similar Figure 6.5. (The May 9, 2001 values, near $\delta\theta / \delta x = -10$, $u_{925} = 2$, are unreliable for reasons discussed above.) Strong convergence frontogenesis occurs in the presence of a seaward cross-shore wind component near the top of the planetary boundary layer, and a

moderately negative meso- α cross-shore potential temperature gradient (upper right of Figure 6.6a). The strongest meso- β convergence frontogenesis occurs when the cross-shore wind component near the top of the planetary boundary layer is about 5 ms^{-1} , and the meso- α cross-shore potential temperature gradient is about $-12 \text{ }^\circ\text{C (100 km)}^{-1}$. Toward more negative $\delta\theta/\delta x$ values, strong surface modification of the marine airmass occurs, which weakens the SBFth, and therefore the overall sea-breeze front. Weak to non-existent convergence frontogenesis occurs with shoreward winds near the top of the planetary boundary layer, and a weak meso- α cross-shore potential temperature gradient (in lower left corner of the diagram).

The plot shown in Figure 6.6b (KFF_2) does not reveal meaningful structure. While the Figure 6.6a compares meso- β response to analogous meso- α forcing, the same is not true with Figure 6.6b. A more appropriate coordinate system for the KFF_2 plot would be meso- α values of the vertical component of wind curl (along the vertical axis) and meso- α values of the along-shore potential temperature gradient ($\delta\theta/\delta y$). This is a subject for future research.

Summary

The sea-breeze front is a complex structure with at least two distinguishable components: The convergence zone associated with the landward edge of the sea-breeze circulation, called the kinematic sea-breeze front (SBFkn), and the zone of maximum isentropic gradient separating the marine and continental airmasses, called the thermodynamic sea-breeze front (SBFth). Both the SBFkn and SBFth are subject to bifurcation, resulting from diabatic airmass modification over the land surface, and surface roughness differences between the sea surface, the coastal lowlands and the inland highlands. When bifurcation occurs, there is an inland component (which may or may not be shore-parallel, depending on meso- α forcing and topography) and a coastal component. Both components are generally of equal magnitude, but one may grow in magnitude at the expense of the other. The magnitudes of the two components usually peak twice during the life-cycle of the sea breeze -- once in mid-afternoon, and once in early evening. The reduction in magnitude between the two peaks is a result of a combination of diabatic heating, changes in surface roughness (as one or both fronts move further inland), and changes in the wind direction seaward of the sea-breeze front.

Results presented here are useful to weather forecasters concerned with predicting several aspects of sea-breeze frontal behavior. When the meso- α forcing is strong --as determined by the Nowcast Diagram developed in Chapters 3 and 4 -- decoupling of the sea-breeze circulation and the sea-breeze gravity current results in spatial and temporal separation of the SBFkn and SBFth. In the case, forecasters can expect multiple sea-breeze frontal passages at a given location, associated with temporally-separate changes in wind velocity and air temperature. When meso- α forcing is weaker, the two components are more closely associated, and forecasters can expect a single sea-breeze front causing simultaneous changes in wind velocity and air temperature at a given location.

The strongest SBFkn and SBFth occur when the cross-shore wind component near the top of the planetary boundary layer is about 5 ms^{-1} , and the meso- α cross-shore potential temperature gradient is between -10 and $-15 \text{ }^\circ\text{C} (100\text{km})^{-1}$. (The results presented here show that relatively imprecise estimates of the former will do. The latter is easily determined using four widely-spaced standard surface weather stations.) This is also the same range of meso- α forcing in which the two components of the SBF occur in the same *place* at the same *time*, resulting is the strongest

measurable meso- β sea-breeze frontogenesis.

A zone of convergence commonly extends along a line from Lawrence, Massachusetts through Portsmouth, New Hampshire, and further northeast into the Gulf of Maine, but more research is needed to determine its cause. The SBFkn sometimes develops when this line rotates in a counter-clockwise direction, moving its southern half toward the coast from the land, and its northern half toward the coast from the sea. Weak, secondary convergence zones may develop within the SBC during the afternoon, and eventually replace the primary SBFkn.

Future research will study the fine-scale behavior of the kinematic sea-breeze front in the coastal zone, and the sea-breeze system's influence on ground-level ozone. The first will utilize a meso- γ network of automated surface weather stations in and around Newburyport, Massachusetts. Because the study area for this dissertation was extended to include the Newburyport weather network, it will be possible to correlate the meso- γ kinematic fields with the synoptic, meso- α and meso- β results discussed in this chapter and in Chapters 3, 4, and 5. The second will compare a 14-year record of sea-breeze events to a similar record of hourly ground-level ozone levels in Portsmouth, New Hampshire, with the

objective of determining the synoptic-scale conditions under which the onset of the sea breeze increases ozone levels, decreases ozone levels, and has no effect on ozone levels.

CHAPTER VII

SUMMARY AND CONCLUSIONS

CHAPTER VII

SUMMARY AND CONCLUSIONS

Summary of Research Results

For my dissertation research I examined the synoptic and mesoscale environments conducive to the formation of the sea breeze, as well as the spatial and temporal evolution of the sea-breeze circulation, gravity current, and front along the central New England coast. The first task was to develop a method for predicting sea-breeze events. I accomplished this in Chapters 3 and 4 using routinely-available hourly surface observations and United States surface analyses for the year 2001. While sea-breeze prediction guidance was developed using Portsmouth, New Hampshire as the forecast site, the method is adaptable to any coastal region in the world where surface meteorological data are available.

In Chapter 3, I identified 167 days that had conditions favorable for the formation of a sea breeze. Favorable conditions

were defined as the absence of significant cloud-cover in the low and middle cloud etages, and the non-occurrence of significant precipitation, thereby permitting insolation to establish a cross-shore gradient in potential temperature. Days when synoptic-scale forcing was responsible for on-shore flow were excluded from the study.

The 167 days were grouped into sea-breeze (SB), marginal (MAR), and non-sea-breeze (NSB) events. SB events occurred on days when the wind direction shifted from southwest, northwest, or northeast to southeast during mid-day, then back to southwest, northwest, or northeast in the evening. NSB events were on days when a shift in the winds did not occur, in spite of relatively cloud-free skies. MAR events were present on days when the sea-breeze occurred, but was short-lived (lasting two hours or less) or exceptionally weak (characterized by very light wind speeds, with or without a highly variable wind direction). A total of 59 SB events, 10 MAR events, and 98 NSB events were identified for 2001.

The 1200 UTC surface synoptic situations for all 167 event days were evaluated using NWS United States surface analyses. These situations were grouped into seven different general classes, where classes 1, 2, and 3 corresponded to northwesterly geostrophic winds, classes 4 and 5 corresponded to southwesterly

winds, and class 6 corresponded to northeasterly winds over the study area. Class 7 was a miscellaneous grouping for synoptic situations that did not fit into the first 6 classes. Sea breezes occurred about 60 percent of the time with class 1, about 20 percent of the time with class 2, and never with class 3. SB or MAR events were almost as likely as NSB events with class 4, while class 5 was exclusively associated with NSB events. Sea breezes and MAR events accounted for almost 80 percent of the class 6 cases.

Four stations -- one each near the northern, eastern, southern, and western boundaries of the study area -- were used to calculate meso- α -scale cross-shore potential temperature gradients ($\delta\theta/\delta x$) and cross-shore geostrophic wind components (u_G). The former is a measure of the force driving the sea breeze, and the latter is a measure of the force opposing the sea breeze. A Nowcast Diagram was generated with u_G on the horizontal axis and $\delta\theta/\delta x$ on the vertical axis, calculated for the hour of onset (for SB and MAR events) or 1900 UTC (for NSB events).

My results show that strong negative $\delta\theta/\delta x$ values were needed to develop a sea breeze in the presence of strong positive u_G values (Figure 3.8), and that the net meso- α sea-breeze forcing was related to the synoptic-scale environment present at 1200 UTC on the

morning of the event. SB events associated with synoptic classes 4 and 6 were toward the lower left corner of the diagram, in the region of strongly-negative $\delta\theta/\delta x$ and weak or negative (landward) u_G . These events showed a tendency to be "early-onset" ones (Figure 3.14). SB events associated with classes 1 and 2 were confined to a relatively narrow diagonal region, running from the center bottom boundary of the diagram (highly favorable $\delta\theta/\delta x$, and weak u_G) to the upper left corner (unfavorable $\delta\theta/\delta x$, and near-zero or negative u_G) (Figure 3.9), and SB events associated with class 6 were confined to almost circular region in the upper left part of the diagram (weakly favorable $\delta\theta/\delta x$, near-zero or negative u_G) (Figure 3.13). NSB events associated with classes 2 and 3 were toward the upper right corner of the diagram (highly unfavorable $\delta\theta/\delta x$, and strongly opposing u_G) (Figure 3.9), with class 3 exhibiting the most extreme case, and NSB events associated with class 5 were divided between a large circular region in the central part of the diagram (weakly favorable $\delta\theta/\delta x$, weak u_G), and a narrower area stretching from the center toward the lower right corner (highly favorable $\delta\theta/\delta x$, but strongly opposing u_G) (Figure 3.11).

The work described in Chapter 3 was extended in Chapter 4 by examining the time-evolution of the net meso- α [$\delta\theta/\delta x$, u_G] sea-

breeze forcing on the central New England coast. The two components formed the basis of a time-evolving nowcast vector (TENV), which was plotted with hourly values on the Nowcast Diagram. The TENVs were examined for 32 SB, MAR, and NSB events under different synoptic-scale situations occurring throughout the year.

In cases where the TENV began the day in the Weak Exclusion Zone (between lines A and C; Figure 4.3), the sea breeze reached Portsmouth two to five hours after the TENV moved into the Transition Zone (between lines A and B). The mean lead time was about four hours, with a mean sea breeze onset time in Portsmouth of about 2030 UTC (1530 LST) \pm ~ 2 hrs. In cases where the TENV began the day in the Transition Zone, the mean arrival time of the sea breeze in Portsmouth was about three hours earlier, at about 1730 UTC (1230 LST). Compared to the latter cases, the cross-shore geostrophic wind component in the former cases more strongly resisted inland propagation of the sea breeze, and the mesoscale PGF created by local land-sea differential heating had to be stronger to drive the sea breeze 10 km inland to the Pease airport.

Under conditions of synoptic class (SC) 1 and SC2, forecasters can expect an increase (toward negative values) in the cross-shore potential temperature gradient of at least $8\text{ }^{\circ}\text{C (100km)}^{-1}$ after 1200

UTC (0700 LST), provided there is no significant cold-air advection on the east side of the anticyclone. A sea breeze will reach Portsmouth if the cross-shore geostrophic wind component is less than about 5 ms^{-1} at 1200 UTC (0700 LST), and the combination of the evolving $\partial\theta/\partial x$ and u_G values move the TENV into the Transition Zone (Figure 4.3) by 1500 UTC (1000 LST). SB events associated with SC4 also show significant evolution toward negative $\partial\theta/\partial x$ values, indicating the absence of cold-air advection. Because SC4 is associated with synoptic-scale southwesterly flow, warm-air advection into the study area, as well as the possible transport of haze, is likely. In at least one instance, haze seems to have reduced the amount of variation in $\partial\theta/\partial x$ from more than $8 \text{ }^\circ\text{C (100km)}^{-1}$ (observed in SC4 in the absence of haze) to less than $4 \text{ }^\circ\text{C (100km)}^{-1}$, limiting the development of a strong landward mesoscale PGF, and preventing the sea breeze from reaching inland to Portsmouth.

Forecasters can usually expect relatively weak land-sea differential heating to occur with SC6, which has two causes: Cold-air advection on the east and southeast side of the anticyclone, which offsets uneven heating of the land and sea surfaces via insolation, and the continuous low-level introduction of cooler marine air over from the Gulf of Maine to the land by the synoptic-scale wind. Forecasters can expect SC6 SB and MAR events to occur

when u_G is negative (toward the land), and NSB events to occur when u_G is positive (toward the sea). Sea breezes do not occur at Pease with SC3 or SC5 because cold-air advection on the west side of the cyclone prevents the development of a strong landward mesoscale PGF. In addition, the cross-shore wind component may be greater than 12 ms^{-1} , shown in Chapter 3 to prevent the sea breeze from reaching Pease, regardless of the strength of $\delta\theta/\delta x$. In SC4 and SC6 cases, the time that TENVs crosses from the Weak Exclusion Zone into the Transition Zone cannot be used to predict whether a sea breeze will reach the Pease airport.

The research described in Chapters 5 and 6 compared meso- β variations in the sea-breeze circulation, gravity current, and front, to routinely available meso- α forcing variables: The cross-shore potential temperature gradient ($\delta\theta/\delta x$), and the cross-shore wind component at 925 hPa (u_{925}). The latter was substituted for the surface geostrophic cross-shore wind component (u_G ; used in Chapters 3 and 4) because it also accounts for the synoptic-scale temperature gradient between the surface and 925 hPa via the thermal wind relation.

In Chapter 5, meso- β near-surface potential temperature and wind fields were examined for twelve case-studies from the year

2001. The potential temperature fields were used to explore the response of the sea-breeze gravity current, and the wind fields were used to explore the response of the sea-breeze circulation. The potential temperature (isentropic) fields evolved between 15 "patterns," some of which were associated with sea-breeze events. Most of them exhibited considerable along-shore variation. The most developed (mature) patterns associated with the sea breezes were the Lowlands, Split S, and Inland Shore-Parallel patterns (Figure 5.5). In the first, the sea-breeze gravity current moved inland and filled the low-lying areas (below 150 m ASL) in the northern and southern lowlands areas (NLA and SLA; Figure 5.4). In the second, the gravity current moved up onto the higher ground west of the NLA, and along the Mount Agamenticus-Lake Winnepesaukee line (MALW; Figure 5.4). In the third, the gravity current moved onto the high ground west of the SLA as well, resulting in the formation of a well-defined, roughly linear, shore-parallel thermodynamic sea-breeze front about 40 to 50 kilometers inland. The most developed isentropic pattern the sea-breeze gravity current achieved was a function of the meso- α [$\delta\theta/\delta x, u_{925}$] forcing.

The wind (kinematic) fields evolved between 24 patterns, all but two of which occurred on sea breeze days. In some of them, the kinematic sea breeze occurred along some parts of the coast, but

did not occur along other parts of the coast. The strongest sea breezes were associated with the COL1 through COL5 kinematic patterns (Figure 5.13). In COL1, a well-developed kinematic sea-breeze front was on the coast, with southeasterly flow seaward of the front, and westerly or northwesterly flow west of the front. In COL2, the front became deformed and began to move inland. In COL3, the front traced out the inland limits of the NLA and SLA (Figure 5.4). COL4 occurred when the front moved onto the higher ground along the MALW line, between the NLA and SLA, and COL5 occurred when the front moved further inland, often past the northwestern boundary of the study area, approximately 65 kilometers inland. The time of the sea-breeze circulation's first contact with the coast (in the study area), and its most advanced inland distance, were both functions of the meso- α [$\delta\theta/\delta x, u_{925}$] forcing.

Two scales of meso- β kinematic (SBC) response to mesoscale forcing were evident: One that corresponded to the larger meso- α forcing estimated by the Nowcast Diagram (Figure 5.3), and another that corresponded to the smaller thermal forcing produced by the meso- β potential temperature fields associated with the sea-breeze gravity current. When the meso- α forcing was weak, details of the

wind field mirrored details of the potential temperature field, and the sea breeze behaved as a true gravity current. When the meso- α was strong, the correspondence of the wind field (defining the sea-breeze circulation) and the potential temperature field (defining the sea-breeze gravity current) weakened considerably.

In Chapter 6 it was shown that the New England sea-breeze front is a complex structure with at least two distinguishable components: The convergence zone associated with the landward edge of the sea-breeze circulation, called the kinematic sea-breeze front (SBFkn), and the zone of maximum isentropic gradient separating the marine and continental airmasses, called the thermodynamic sea-breeze front (SBFth). Both the SBFkn and SBFth were subject to bifurcation, resulting from diabatic airmass modification over the land surface, and surface roughness differences between the sea surface, the coastal lowlands and the inland highlands. When bifurcation occurred, there was an inland component (which may or may not have been shore-parallel, depending on meso- α forcing and topography) and a coastal component. The magnitudes of the two components usually peaked twice during the life-cycle of the sea breeze -- once in mid-afternoon, and once in early evening. The reduction in magnitude between the two peaks resulted from a combination of diabatic

heating, changes in surface roughness (as one or both fronts moved further inland), and changes in the wind direction seaward of the sea-breeze front.

The results presented in Chapter 6 are useful to weather forecasters concerned with predicting several aspects of sea-breeze frontal behavior. When the meso- α forcing is strong, as determined by the Nowcast Diagram developed in Chapters 3 and 4, decoupling of the sea-breeze circulation and the sea-breeze gravity current results in spatial and temporal separation of the SBFkn and SBFth. Forecasters can expect multiple sea-breeze frontal passages at a given location, associated with temporally-separate changes in wind velocity and air temperature. When meso- α forcing is weaker, the two components are more closely associated, and forecasters can expect a single sea-breeze front causing simultaneous changes in wind velocity and air temperature at a given location.

The strongest SBFkn and SBFth occur when the cross-shore wind component near the top of the planetary boundary layer is about 5 ms^{-1} , and the meso- α cross-shore potential temperature gradient is between -10 and $-15 \text{ }^\circ\text{C} (100\text{km})^{-1}$. This is the same range of meso- α forcing in which the two components of the SBF occur in the same *place* at the same *time*, resulting in the strongest

measurable meso- β sea-breeze frontogenesis.

A zone of convergence commonly extends along a line from Lawrence, Massachusetts through Portsmouth, New Hampshire, and further northeast into the Gulf of Maine, but more research is needed to determine its cause. The SBFkn sometimes develops when this line rotates in a counter-clockwise direction, its southern half moving toward the coast from the land, and its northern half moving toward the coast from the sea. Weak, secondary convergence zones sometimes develop within the SBC during the afternoon, eventually replacing the primary SBFkn.

Directions for Future Research

The SBS system is a highly complex system composed of many smaller phenomena. In Chapters 5 and 6, my results show that at least three of its constituent components (the SBC, SBG, and SBF) are themselves highly complex systems. This picture is at odds with the description of the sea breeze offered in many meteorology texts, and there are many questions yet unanswered.

There are a few obvious directions for future research. One route for improving the research described in this dissertation is the utilization of better 925 hPa wind data. A radar wind profiler,

installed at the Pease airport in late 2001 by the NOAA Aeronomy Laboratory, and brought to full operational capability in mid-2002, is capable of providing these data. A mesoscale *network* of these profilers would be an even better source of information.

The relationship between the sea breeze and ozone events pollution on the central New England coastline should be more closely quantified. Some work has already been done in this area [e.g. *Pagnotti, 1987*], but has not utilized areal coverage on the fine scale UNH is capable of producing with its mesoscale weather network. There is already evidence that the SBG plays a significant role in differentiating between moderate and severe ozone pollution events, as shown in Figure 7.1.

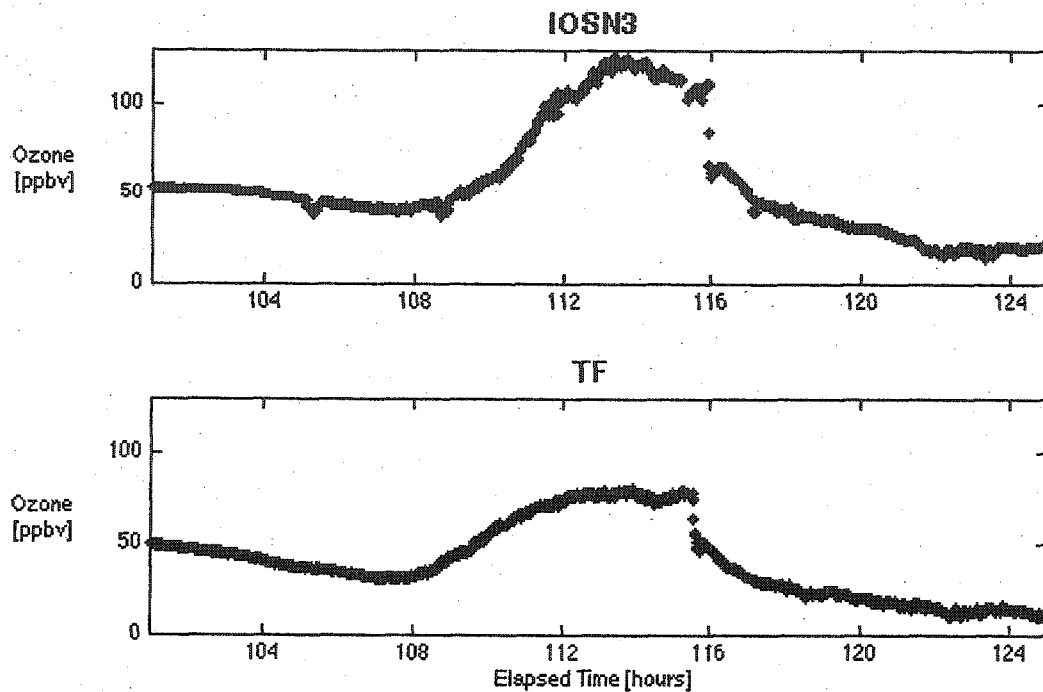


Figure 7.1: Ozone recorded at Isles of Shoals (IOSN3) and Thomson Farm (UNH) site on 23 July 2002. IOSN3 is approximately 10 kilometers offshore of Portsmouth, New Hampshire; Thomson Farm is approximately 10 kilometers inland. Horizontal axes are labeled in hours since the beginning of the time-series, and run from 23 July 2002, 0000 local time through 24 July 2002, 0000 local time.

Figure 7.1 shows ground-level ozone recorded at two locations near the coast on 23 July 2002, as part of the New England Air Quality Study pilot project. The synoptic-scale surface wind was southwesterly, with a cold front approaching from the west. Prior to the passage of the cold front (visible as a sharp drop in the ozone

level in both time-series), the offshore site (Isles of Shoals, or IOSN3; approximately 10 kms east-southeast of Portsmouth, New Hampshire) recorded peak ozone levels nearly twice that of the inland site (Thomson Farm, or TF, in Durham, New Hampshire; approximately 10 kms inland). The sea breeze system was active on the day these observations were recorded, suggesting that the difference in the two peak ozone levels was the result of recording ozone in two different airmasses: the marine airmass -- with a shallow mixing depth -- at IOSN3, and the pre-frontal continental airmass -- with a greater mixing depth -- at TF. This hypothesis is supported by the temperature plots shown in Figure 7.2.

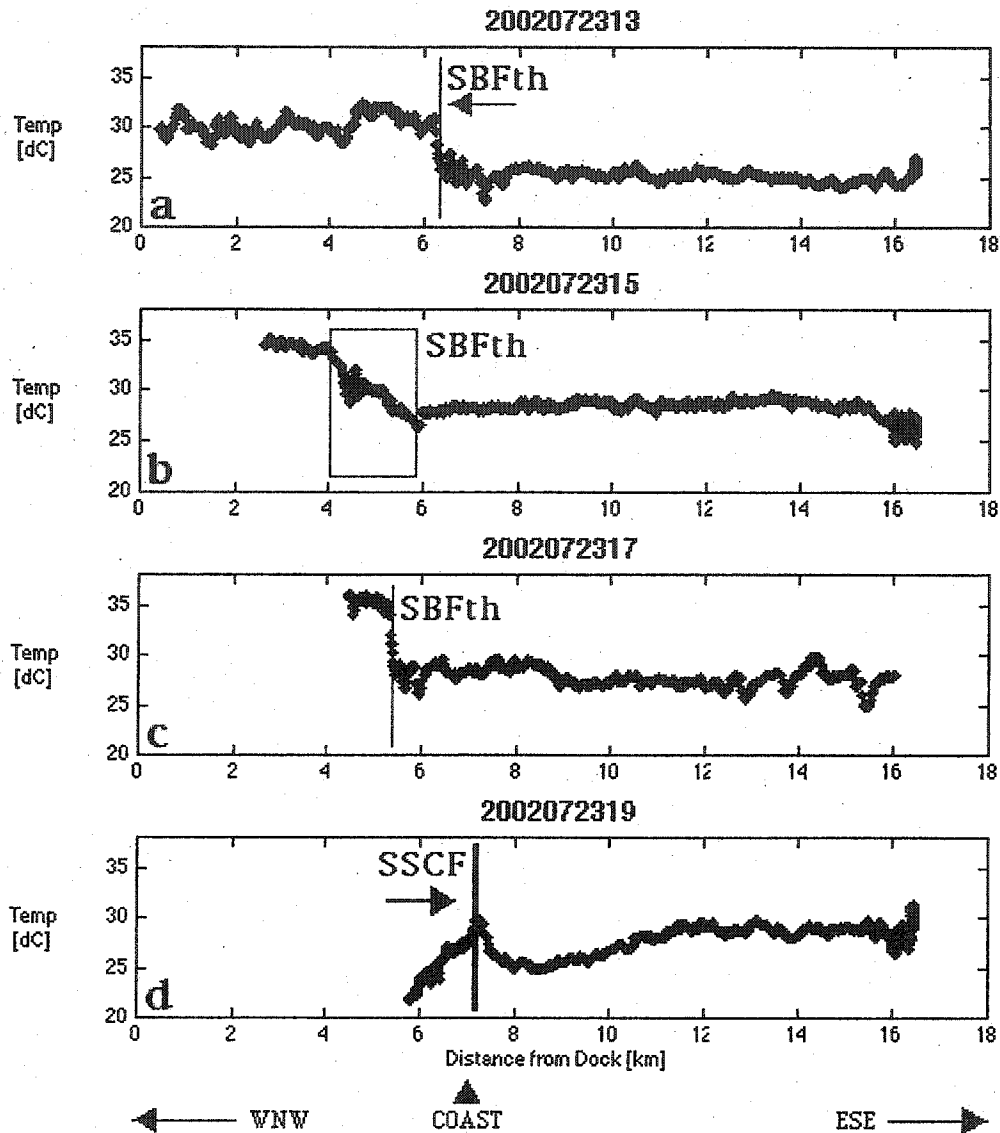


Figure 7.2: Air temperature recorded during ferry trips between Portsmouth and the Isles of Shoals on 23 July 2002. Horizontal scale is distance (kms) from the dock in Portsmouth. A one-way trip takes ~ 1 hr. a) Series beginning 1300 UTC (0800 LST) - Outbound (Portsmouth to IOSN3). Thin blue line indicates position of SBFth. Blue arrow indicates direction of movement. b) Beginning 1500 UTC (1000 LST) -- Inbound. SBFth difficult to localize. Diffuse airmass transition zone indicated with box. c) Beginning 1700 UTC (1200 LST) - Outbound. SBFth visible at coast. d) Beginning 1900 UTC (1400 LST) - Inbound. Synoptic-scale cold front (SSCF) indicated with thicker blue line.

Figure 7.2 shows the air temperature recorded by a GPS-equipped instrument mounted on the Isles of Shoals Ferry during four trips on 23 July 2003 [Rawlins, 2003]. The dock, in Portsmouth, New Hampshire, is on the left-hand side of each series, and the Isles of Shoals are on the right-hand side of each series. (The ferry travels from Portsmouth to the Isles of Shoals several times a day during spring, summer, and autumn. A one-way trip takes approximately one hour.) In panel a, the thermodynamic sea-breeze front (SBFth) can be seen approximately 6.5 kilometers from the dock, which is within 1/2 kilometer of the coast. In panel b (approximately two hours later), mid-day diabatic heating has washed out the SBFth, making it difficult to localize precisely. In panel c), a new SBFth has formed at the coast, reflecting the pattern of SBFth redevelopment seen in case-study field files. In panel d, the synoptic-scale cold front (SSCF) that caused a dramatic drop in ozone levels at both stations can be seen crossing the coast. (The depression in temperatures east of the front may have been caused by a thunderstorm downdraft). Panels a, b, and c suggest that stations IOSN3 and TF were in different airmasses. The ozone concentration was much higher in the marine airmass than it was in the continental airmass ahead of the SSCF. Gridded (meso- β) wind and temperature data created with observations from UNH's

mesoscale weather network should be compared with these series to a) refine the findings in this dissertation about the behavior and characteristics of the sea-breeze front, and b) establish the characteristics of the SBC during high-ozone episodes.

Another obvious direction for additional work is pushing the scale of investigation down further, into the meso- γ (2 - 20 km) and microscale (< 2 km) ranges [Fujita, 1986]. Because of UNH's collaboration with the C-10 Research and Education Foundation (C-10/REF), access to a coastal-zone meso- γ -scale data set is available. The study area used in this dissertation was deliberately extended southward to include the C-10/REF network, so that future work could be performed relating my findings with results from the C-10/REF network. The C-10/REF network (Figure 7.3) is composed of approximately 20 closely-spaced, research-grade anemometers, which record surface (10-meter) wind direction and speed at one-minute intervals. In the vicinity of Newburyport, Massachusetts, the sensor spacing is on the order of one kilometer.

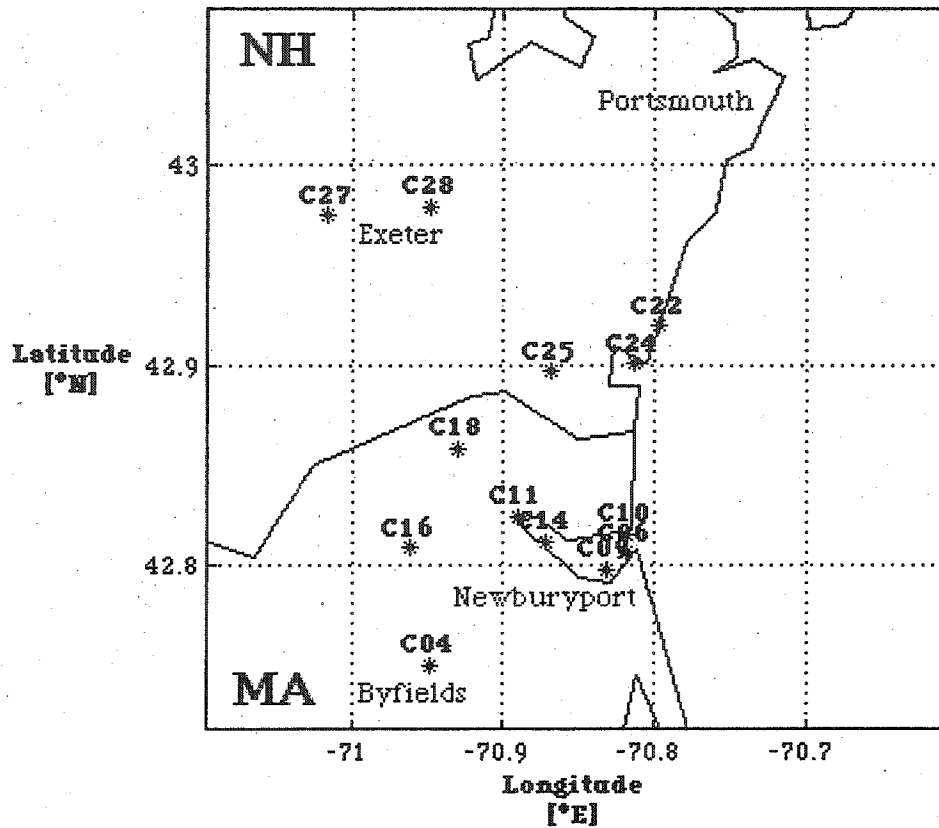


Figure 7.3: C-10 Research and Education Foundation meso- γ environmental monitoring network. Each station (indicated with an asterisk and three-character identifier) is equipped with a research-grade anemometer. Stations record wind at one-minute intervals.

The network covers the region from Byfields, Massachusetts through Exeter, New Hampshire, and extends eastward from this line to the coast. The C-10/REF data offer the ability to look into sea-breeze events at very high spatial and temporal resolution. These data should be used to examine the behavior of the SBF, for

variations in its width, intensity (magnitude of horizontal convergence), relative complexity (qualitatively, and via curl calculations), and speed of propagation under varying synoptic- and mesoscale scenarios.

Concluding Remarks

At the time of this writing, I have been a working meteorologist for more than 22 years. I have worked as weather forecaster and observer at locations throughout North America and in the Middle East. Drawing on my background, I chose the sea breeze as the subject for my dissertation because I assumed that it would present a relatively straightforward research problem. Along with the members of my doctoral committee (and most other meteorologists), I believed that the sea breeze was a simple phenomenon. I was quickly relieved of this illusion.

“Completely” describing the central New England sea breeze proved to a virtually bottomless task. The main difficulty faced when writing up my work was deciding what to leave out. (Enough has been excluded from this dissertation to account for at least another chapter.) And as may be obvious from the suggested courses of future research noted above, I did not accomplish

everything I originally imagined when the project was first conceived. Hopefully, someone will carry the work forward, examine the sea breeze down to the meso- γ scale, and make a comprehensive study of its relationship to ground-level ozone.

The sea breeze is a rich source of discovery, and Isaac Newton once said something that describes my relationship to it pretty well:

I was like a boy playing on the sea-shore, and diverting myself now and then finding a smoother pebble or a prettier shell than ordinary, whilst the great ocean of truth lay all undiscovered before me.

REFERENCES

REFERENCES

_____, *International Cloud Atlas*, Geneva, Switzerland, World Meteorological Organization, 156 pgs., 1956.

_____, *Guide to Meteorological Instruments and Methods of Observation (WMO-No. 8)*, Sixth edition, Geneva, Switzerland, World Meteorological Organization, 1996.

_____, *Air Force Manual 15-111: Surface Weather Observations*, 1998, available on the World-Wide Web at <http://afpubs.hq.af.mil/>

Abbs, D.J., and W.L. Physick, Sea-breeze observations and modelling: a review, *Aust. Meteor. Mag.*, 41, 7 - 19, 1992.

Adams, Ed, Four ways to win the sea breeze game, *Sailing World*, March 1997, 44 - 49, 1997.

AIRMAP, The New England Air Quality Study, Draft Science Plan, October, 2001. <http://www.al.noaa.gov/neaqs/>

Anderson, D.A., J.C. Tannehill, and R.H. Pletcher, *Computational Fluid Mechanics and Heat Transfer*, Hemisphere Publishing Corporation, 599 pgs., 1984.

Angell, J.K., and D.H. Pack, A study of the sea breeze at Atlantic City, New Jersey using tetroons as lagrangian tracers, *Mon. Wea. Rev.*, 93 (8), 475 - 493, 1965.

Anthes, R.A., The height of the planetary boundary layer and the production of circulation in a sea breeze model, *J. Atmos. Sci.*, 35, 1231 - 1239, 1978.

Apel, J.R., *Principles of Ocean Physics*, London, Academic Press, 634 pgs., 1987.

Arritt, R.W., Effects of the large-scale flow on characteristic features of the sea breeze, *J. Appl. Meteor.*, 32, 116 - 125, 1992.

Asai, T., and S. Mitsumoto, Effects of an inclined land surface on the land and sea breeze circulation: A numerical experiment, *J. Meteor. Soc. Japan*, 56 (6), 559 - 570, 1978.

Asimakopoulos, D.N., C.G. Helmis, K.H. Papadopoulos, J.A. Kalogiros, P. Kassomenos, and M. Petrakis, Inland propagation of sea breeze under opposing offshore wind, *Meteorol. Atmos. Phys.*, 70, 97 - 110, 1999.

Atkins, N.T., R.M. Wakimoto, and T.M. Weckwerth, Observations of the sea-breeze front during CaPE, Part II: Dual-doppler and aircraft analysis, *Mon. Wea. Rev.* 123, 944 - 969, 1995.

Banta, R.M., L.D. Olivier, and D.H. Levinson, Evolution of the Monterey Bay sea-breeze layer as observed by pulsed doppler radar, *J. Atmos. Sci.*, 50 (24), 3959 - 3982, 1993.

Barbato, J.P., *The sea breeze of the Boston area and its effect on the urban atmosphere*, Ph.D. dissertation, Boston University Graduate School, 1975.

Barkan, J., and Y. Feliks, Observations of the diurnal oscillation of the inversion over the Israeli coast, *Bound-Lay. Meteorol.*, 62, 393 - 409, 1993.

Barnes, S.L., A technique for maximizing details in numerical weather map analysis, *J. Appl. Meteor.*, 3, 396 - 409, 1964.

Biggs, W.G., and M.E. Graves, A lake breeze index, *J. Appl. Meteor.*, 1, 474 - 480, 1962.

Brümmer, B., B. Hennemuth, A. Rhodin, and S. Thiemann, Interaction of a cold front with a sea-breeze front: Observations, *Tellus*, 47A, 383 - 402, 1995.

Brown, W.S., Boundary flux measurements in the coastal ocean, *The Sea*, 10, 399 - 418, 1998.

Brown, W.S., and J.D. Irish, The annual variation of water mass structure in the Gulf of Maine: 1986 - 1987, *J. Mar. Res.*, 51, 53 - 107, 1993.

Buckley, R.L., and R.J. Kurzeja, An observational and numerical study of the nocturnal sea breeze, Part I: Structure and circulation. *J. Appl. Meteor.*, 36, 1577 - 1598, 1997.

Camberlin, P., and O. Planchon, Coastal precipitation regimes in Kenya. *Geogr. Ann.*, 79 A (1-2), 109 - 119, 1997.

Carbone, R.E., J.W. Wilson, T.D. Keenan, and J.M. Hacker, Tropical island convection is the absence of significant topography. Part I: Life cycle of diurnally forced convection, *Mon. Wea. Rev.*, 128, 3459 - 3480, 2000.

Carnahan, B., H.A. Luther, and J.O. Wilkes, *Applied Numerical Methods*, Malabar, Florida, Krieger Publishing Company, 604 pgs., 1990.

Cenedese, A., M. Miozzi, and P. Monti, A laboratory investigation of land and sea breeze regimes, *Exp. Fluids* [suppl.], S291 - S299, 2000.

Chiba, O., The turbulent characteristics in the lowest part of the sea breeze front in the atmospheric surface layer, *Bound-Lay. Meteorol.*, 65, 181 - 195, 1993.

Chiba, O., F. Kobayashi, G. Naito, and K. Sassa, Helicopter observations of the sea breeze over a coastal area, *J. Appl. Meteor.*, 38, 481 - 492, 1999.

Clappier, A., A. Martilli, P. Grossi, P. Thunis, F. Pasi, B.C. Krueger, B. Calpini, G. Graziani, and H. van den Bergh, Effect of sea breeze on air pollution in greater Athens area, Part I: Numerical simulations and field observations, *J. Appl. Meteor.*, 39, 546 - 562, 2000.

Clark, W.A.V., and P.L. Hosking, *Statistical Methods for Geographers*, New York, John Wiley & Sons, 518 pgs., 1986.

Clarke, R.H., Some observations and comments on the sea breeze, *Aust. Meteor. Mag.*, 11, 47 - 68, 1955.

Clarke, R.H., Colliding sea-breezes and the creation of internal atmospheric bore waves: two-dimensional numerical studies, *Aust. Meteor. Mag.*, 32, 207 - 226, 1984.

Coutant, V., and V.L. Eichenlaub, *Theophrastus De Ventis*, Notre Dame, Indiana, University of Notre Dame Press, 105 pgs., 1975.

Craig, R.A., I. Katz, and P.J. Harney, Sea breeze cross sections from psychrometric measurements, *Bull. Amer. Meteor. Soc.*, 26 (10), 405 - 410, 1945.

Dalu, G.A., and R.A. Pielke, An analytical study of the sea breeze, *J. Atmos. Sci.*, 46 (12), 1815 - 1825, 1989.

Druilhet, A., A. Herrada, J.P. Pages, J. Saïssac, C. Allet, and M. Ravaut, Étude expérimentale de la couche limite interne associée à la brise de mer. *Bound-Lay. Meteorol.*, 22, 511 - 524, 1982.

Elliott, D.L., and J.J. O'Brien, Observational studies of the marine boundary layer over an upwelling region, *Mon. Wea. Rev.*, 105, 86 - 98, 1977.

Estoque, M.A., The sea breeze as a function of the prevailing synoptic situation, *J. Atmos. Sci.*, 19, 244 - 250, 1962.

Federovich, E., F.T.M. Nieuwstadt, and R. Kaiser, Numerical and laboratory studies of horizontally evolving convective boundary layer, Part II: Effects of elevated wind shear and surface roughness, *J. Atmos. Sci.*, 58, 546 - 560, 2001.

Feliks, Y., A numerical model for estimation of the diurnal fluctuation of the inversion height due to a sea breeze, *Bound-Lay. Meteorol.*, 62, 151 - 161, 1993.

Feng, H., *Wind-induced responses of the western coastal Gulf of Maine during Spring and Summer, 1994*, Master's Thesis, University of New Hampshire, 104 pgs, 1996.

Finkele, K., J.M. Hacker, H.Kraus, and R.A.D. Byron-Scott, A complete sea- breeze circulation cell derived from aircraft observations, *Bound- Lay. Meteorol.*, 73, 299 - 317, 1995.

Finkele, K., Inland and offshore propagation speeds of a sea breeze from simulations and measurements, *Bound-Lay. Meteorol.*, 87, 307 - 329, 1998.

Fisher, E.L., An observational study of the sea breeze, *J. Meteorol.*, 17, 645 - 660, 1960.

Fofonoff, N.P., and R.C. Millard, Jr., *Algorithms for computation of fundamental properties of seawater*, Unesco/SCOR/ICES/IAPSO Joint Panel on Oceanographic Tables and Standards and SCOR Working Group 51, 53 pgs., 1983.

Fosberg, M.A., and M.J. Schroeder, Marine air penetration in central California, *J. Appl. Meteor.*, 5, 573 - 589, 1966.

Franchito, S.H., V.B. Rao, J.L. Stech, and J.A. Lorenzetti, The effect of coastal upwelling on the sea-breeze circulation of Cabo Frio, Brazil: a numerical experiment, *Ann. Geophysicae*, 16, 866 - 881, 1998.

Frizzola, J.A., and E.L. Fisher, A series of sea breeze observations in the New York City area, *J. Appl. Meteor.*, 2, 722 - 739, 1963.

Gangoiti, G., L. Alonso, M. Navazo, A. Albizuri, G. Perez-Landa, M. Matabuena, V. Valdenebro, M. Maruri, J.A. Garcia, and M.A. Millán, Regional transport of pollutants over the Bay of Biscay: analysis of an ozone episode under a blocking anticyclone in west-central Europe, *Atmos. Environ.*, 36, 1349 - 1361, 2002.

Garratt, J.R., and W.L. Physick, The inland boundary layer at low latitudes: II, Sea-breeze influences, *Bound-Lay. Meteorol.*, 33, 209 - 231, 1985.

Gaza, R.S., Mesoscale meteorology and high ozone in the northeast United States, *J. Appl. Meteor.*, 37, 961 - 977, 1998.

Geisler, J.E., and F.P. Bretherton, The sea-breeze forerunner, *J. Atmos. Sci.* 26, 82 - 95, 1969.

Gibbs, M.T., Detecting a response to weak sea breezes in the New South Wales coastal ocean, *New Zeal. J. Mar. Fresh.*, 34, 669 - 680, 2000.

Godske, C.L., T. Bergeron, J. Bjerknes, and R.C. Bundgaard, *Dynamic Meteorology and Weather Forecasting*, Boston, Massachusetts, American Meteorological Society, 800 pgs., 1957.

Gryning, S.E., and E. Batchvarova, Analytical model for the growth of the coastal internal boundary layer during onshore flow, *Quart. J. R. Met. Soc.*, 116, 187 - 203, 1990.

Hadi, T.W., T. Horinouchi, T. Tsuda, H. Hashiguchi, and S. Fuhao, Sea- breeze circulation over Jakarta, Indonesia: A climatology based on boundary layer radar observations, *Mon. Wea. Rev.*, 130, 2153 - 2166, 2002.

Halliday, D., R. Resnick, and J. Walker, *Fundamentals of Physics*, New York, John Wiley & Sons, Inc., 1306 pgs., 1993.

Helmis, C.G., D.N. Asimakopoulos, D.G. Deligiorgi, and D.P. Lalas, Observations of sea-breeze fronts near the shoreline, *Bound-Lay. Meteorol.*, 38, 395 - 410, 1987.

Helmis, C.G., K.H. Papadopoulos, J.A. Kalogiros, A.T. Soilemes, and D.N. Asimakopoulos, Influence of background flow on evolution of Saronic Gulf sea breeze, *Atmos. Environ.*, 29 (24), 3689 - 3701, 1995.

Hess, S.L., *Introduction to Theoretical Meteorology*, Malabar, Florida, Krieger Publishing Company, 362 pgs., 1959.

Holmer, B., and M. Haeger-Eugensson, Winter land breeze in a high latitude complex coastal area, *Phys. Geogr.*, 20 (2), 152 - 172, 1999.

Holton, J.R., *An Introduction to Dynamic Meteorology*, San Diego, California, Academic Press, Inc., 511 pgs., 1992.

Hsu, S.A., *Coastal Meteorology*, San Diego, California, Academic Press, Inc., 260 pgs., 1988.

Intrieri, J.M., C.G. Little, W.J. Shaw, R.M. Banta, P.A. Durkee, and R.M. Hardesty, The Land/Sea Breeze Experiment (LASBEX), *Bull. Amer. Meteor. Soc.*, 71 (5), 656 - 664, 1990.

Jehn, K.H., *A Sea Breeze Bibliography, 1664 - 1972*, Report No. 37, National Science Foundation Grant GA-16167, Atmospheric Science Group, College of Engineering, The University of Texas, Austin Texas, 51 pgs., 1973.

Johnson, R., *Elementary Statistics*, Boston, Massachusetts, PWS-Kent Publishing Company, 730 pgs, 1992.

Kalthoff, N., I. Bischoff-Gauß, M. Fiebig-Wittmaack, F. Fiedler, J. Thurauf, E. Novoa, C. Pizarro, R. Castillo, L. Gallardo, R. Rondanelli, and M. Kohler, Mesoscale wind regimes in Chile at 30°S, *J. Appl. Meteor.*, 41, 953 - 970, 2002.

Kanda, M., Y. Inoue, and I. Uno, Numerical study on cloud lines over an urban street in Tokyo, *Bound-Lay. Meteorol.*, 98, 251 - 273, 2001.

Kitada, T., Turbulence structure of sea breeze front and its implication in air pollution transport -- application of k-e turbulence model, *Bound-Lay. Meteorol.*, 41, 217 - 239, 1987.

Kraus, H., J.M. Hacker, and J. Hartmann, An observational aircraft-based study of sea-breeze frontogenesis, *Bound-Lay. Meteorol.*, 53, 223 - 265, 1990.

Kraus, H., Turbulence frontogenesis, *Meteorol. Atmos. Phys.*, 48, 309 - 215, 1992.

- Kottmeier, C., P. Palacio-Sese, N. Kalthoff, U. Corsmeier, and F. Fiedler, Sea breezes and coastal jets in southeastern Spain, *Int. J. Climatol.*, 20, 1791 - 1808, 2000.
- Kozo, T.L., An observational study of sea breezes along the Alaskan Beaufort sea coast: Part I, *J. Appl. Meteor.*, 21 (7), 891 - 905, 1982.
- Kuelegan, G.H., An experimental study of the motion of saline water from locks into fresh water channels, *13th Progress Report on Model Laws for Density Currents*, U.S. National Bureau of Standards, No. 5168, 1957.
- Laird, N.F., and D.A.R. Kristovich, Lake Michigan lake breezes: Climatology, local forcing, and synoptic environment, *J. Appl. Meteor.*, 40, 409 - 424, 2001.
- Lapworth, A., Observations of atmospheric density currents using a tethered balloon-borne turbulence probe system, *Quart. J. Roy. Meteor. Soc.*, 126, 2811 - 2850, 2000.
- List, R.J., *Smithsonian Meteorological Tables*, Washington, D.C., Smithsonian Institution Press, 527 pgs., 1968.
- Lee, H.D.P., *Aristotle VII Meteorologica*, Cambridge, Massachusetts, Harvard University Press, 432 pgs., 1952.
- Lericos, T.P., H.E. Fuelberg, A.I. Watson, and R.L. Holle, Warm season lightning distributions over the Florida peninsula as related to synoptic patterns, *Weather. Forecast.*, 17, 83 - 98, 2002.
- Liu, H.P., and J.C.L. Chan, Boundary layer dynamics associated with a severe air-pollution episode in Hong Kong, *Atmos. Environ.*, 36, 2013 - 2025, 2002.

Luhar, A.K., B.L. Sawford, J.M. Hacker, and K.N. Rayner, The Kwinana coastal fumigation study: II - Growth of the thermal internal boundary layer, *Bound-Lay. Meteorol.*, 89, 385 - 405, 1998.

Lutgens, F.K., and E.J. Tarbuck, *The Atmosphere An Introduction to Meteorology*, Upper Saddle River, New Jersey, Prentice Hall, 484 pgs., 2001.

Lyons, W.A., The climatology and prediction of the Chicago lake breeze, *J. Appl. Meteor.*, 11, 1259 - 1270, 1972.

Lyons, W.A., E.R. Sawdey, J.A. Schuh, R.H. Calby, and C.S. Keen, An updated and expanded coastal fumigation model, *Air Pollution Control Association 74th Annual Meeting, Philadelphia, Pennsylvania, June 21 - 26, 1981*.

Masselink, G., and C.B. Pattiaratchi, The effect of sea breeze on beach morphology, surf zone hydrodynamics and sediment resuspension, *Mar. Geol.*, 146, 115 - 135, 1998.

Mathews, J.H., The sea-breeze -- Forecasting aspects, *Aust. Met. Mag.*, 30, 205 - 209, 1982.

McKendry, I., and N. Roulet, Sea breezes and advective effects in southwest James Bay, *J. Geophys. Res.*, 99 (D1), 1623 - 1634, 1994.

McPherson, R.D., A numerical study of the effect of a coastal irregularity on the sea breeze, *J. Appl. Meteor.*, 9, 767 - 777, 1970.

Melas, D., and H.D. Kambezidis, The depth of the internal boundary layer over an urban area under sea-breeze conditions, *Bound-Lay. Meteorol.*, 61, 247 - 264, 1992.

Melas, D., I. Ziomas, O. Klemm, and C.S. Zerefos, Anatomy of the sea-breeze circulation in Athens area under weak large-scale ambient winds, *Atmos. Environ.*, 32 (12), 2223 - 2237, 1998.

Melas, D., A. Lavagnini, and A. Sempreviva, An investigation of the boundary layer dynamics of Sardinia island under sea-breeze conditions, *J. Appl. Meteor.*, 39, 516 - 524, 2000.

Militellow, A., and N.C. Kraus, Generation of harmonics by sea breeze in nontidal water bodies, *J. Phys. Oceanogr.*, 31, 1639 - 1647, 2001.

Miller, J.E., On the concept of frontogenesis, *J. Meteorol.*, 5, 169 - 171, 1948.

Miller, S.T., *Air-Sea Heat Flux in the Gulf of Maine: Meteorological Forcing and Oceanic Response*, Master's Thesis, University of New Hampshire, 232 pgs., 1999.

Mitsumoto, S., H. Ueda, and H. Ozoe, A laboratory experiment on the dynamics of the land and sea breezes, *J. Atmos. Sci.*, 40, 1228 - 1240, 1983.

Mizuma, M., General aspects of land and sea breezes in Osaka Bay and surrounding area, *J. Meteor. Soc. Japan*, 73 (6), 1029 - 1040, 1995.

Mizuma, M., General aspects of land and sea breezes in Western Seto Inland Sea and surrounding areas, *J. Meteor. Soc. Japan*, 76 (3), 403 - 418, 1998.

Neumann, J., On the rotation rate of the direction of sea and land breezes, *J. Atmos. Sci.*, 34 (8), 1913 - 1917, 1977.

Neumann, J., and Y. Mahrer, A theoretical study of the land and sea breeze circulation, *J. Atmos. Sci.*, 28, 532 - 542, 1971.

Nielsen, J.W., In situ observations of Kelvin-Helmholtz waves along a frontal inversion, *J. Atmos. Sci.*, 49 (5), 369 - 386, 1992.

Oliphant, A.J., A.P. Sturman, and N.J. Tapper, The evolution and structure of a tropical island sea/land-breeze system, northern Australia, *Meteorol. Atmos. Phys.*, 78, 45 - 59, 2001.

Ohashi, Y., and H. Kida, Observational results of the sea breeze with a weak wind region over the northern Osaka urban area, *J. Meteor. Soc. Japan*, 79 (4), 949 - 955, 2002.

Pagnotti, V., A meso-meteorological feature associated with high ozone concentrations in the northeastern United States, *JAPCA*, 37 (6), 720 - 722, 1987.

Panel on Coastal Meteorology, *Coastal Meteorology -- A Review of the State of the Science*, Washington, D.C., National Academy Press, 99 pgs., 1992.

Pearce, R.P., The calculation of a sea-breeze circulation in terms of differential heating across the coastline, *Quart. J. Roy. Meteor. Soc.*, 81, 351 - 381, 1955.

Pearson, R.A., G. Carboni, and G. Brusasca, The sea breeze with mean flow, *Quart. J. Roy. Meteor. Soc.*, 109, 809 - 830, 1983.

Physick, W.L., Numerical experiments on the inland penetration of the sea breeze, *Quart. J. Roy. Meteor. Soc.*, 106, 735 - 746, 1980.

Physick, W.L., and D.J. Abbs, Flow and plume dispersion in a coastal valley, *J. Appl. Meteor.*, 31, 64 - 73, 1992.

Pielke, R.A., *Sea breeze-induced mesoscale systems and severe weather*. NASA Project Progress Report, 1985.

Pielke, R.A., A. Song, P.J. Michaels, W.A. Lyons, and R.W. Arritt, The predictability of sea-breeze generated thunderstorms, *Atmosfera*, 4, 65 - 78, 1991.

Planchon, O., and S. Cautenet, Rainfall and sea-breeze circulation over south-western France, *Int. J. Climatol.*, 17, 535 - 549, 1997.

Prahba, T.V., R. Venkatesan, E. Mursch-Radlgruber, G. Rengarajan, and N. Jayanthi, Thermal internal boundary layer characteristics at a tropical coastal site as observed by a mini-SODAR under varying synoptic conditions, *Proc. Indian Acad. Sci. (Earth Planet Sci.)*, 111 (1), 63 - 77, 2002.

Rao, P. ., and H.E. Fuelberg, An investigation of convection behind the Cape Canaveral sea-breeze front, *Mon. Wea. Rev.*, 128, 3437 - 3458, 2000.

Rawlins, W.T, Personal Communication, 2003. Dr. Rawlins (rawlins@psicorp.com) is a research scientist with Physical Sciences, Inc., and was responsible for installing ozone instrumentation on the Isle of Shoals Ferry for the New England Air Quality Study summer-2002 pilot study.

Raynor, G.S., S. Sethuraman, and R.M. Brown, Formation and characteristics of coastal internal boundary layers during onshore flows, *Bound-Lay. Meteorol.*, 16, 487 - 514, 1979.

Reible, D.D., J.E. Simpson, and P.F. Linden, The sea breeze and gravity-current frontogenesis, *Quart. J. Roy. Meteor. Soc.*, 119, 1 - 16, 1993.

Rotunno, R., On the linear theory of the land and sea breeze, *J. Atmos. Sci.*, 40, 1999 - 2009, 1983.

Rogers, R.R., and M.K. Yau, *A Short Course in Cloud Physics*, Woburn, Massachusetts, Butterworth-Heinemann, 290 pgs., 1989.

Rubes, M.T., H.J. Cooper, and E.A. Smith, A study of the Merritt Island, Florida sea breeze flow regimes and their effect on surface heat and moisture fluxes, NASA Contractor Report 4537, 141 pgs., 1993.

Sawford, B.L., A.K. Luhar, J.H. Hacker, S.A. Young, I.-H. Yoon, J.A. Noonan, J.N. Carras, D.J. Williams, and K.N. Rayner, The Kwinana coastal fumigation study: I - Program overview, experimental design, and selected results, *Bound-Lay. Meteorol.*, 89, 359 - 384, 1998.

Schoellhamer, D.H., Factors affecting suspended-solids concentrations in South San Francisco Bay, California, *J. Geophys. Res.*, 101 (C5), 12,087 - 12,095, 1996.

Schoenberger, L.M., Doppler radar observation of a land-breeze cold front, *Mon. Wea. Rev.*, 112, 2455 - 2464, 1984.

Schumann, E.H., W.K. Illenberger, and W.S. Goschen, Surface winds over Algoa Bay, South Africa, *S. Afr. J. Sci.*, 87, 202 - 207, 1991.

Seaman, N.L., and S.A. Michelson, Mesoscale meteorological structure of a high-ozone episode during the 1995 NARSTO-Northeast Study, *J. Appl. Meteor.*, 39, 384 - 398, 2000.

Sha, W., T. Kawamura, and H. Ueda, A numerical study on sea-land breezes as a gravity current: Kelvin-Helmholtz billows and inland penetration of the sea-breeze front, *J. Atmos. Sci.*, 48 (14), 1649 - 1665, 1991.

Sha, W., T. Kawamura, and H. Ueda, A numerical study of nocturnal sea breezes: Prefrontal gravity waves in the compensating flow and inland penetration of the sea-breeze cutoff vortex, *J. Atmos. Sci.*, 50 (8), 1076 - 1087, 1993.

Shair, F.H., E.J. Sasaki, D.E. Carlan, G.R. Cass, W.R. Goodin, J.G. Edinger, and G.E. Schacher, Transport and dispersion of airborne pollutants associated with the land breeze-sea breeze system, *Atmos. Environ.*, 16 (9), 2043 - 2053, 1982.

Shearer, D.L. and R.J. Kaleel, Critical review of studies on atmospheric dispersion in coastal regions (NUREG/CR-2754), Pacific National Laboratory (PNL-4292), 41 pgs., 1982.

Silva Dias, M.A.F., and A.J. Machado, The role of local circulations in summertime convective development and nocturnal fog in São Paulo, Brazil, *Bound-Lay. Meteorol.*, 82, 135 - 157, 1997.

Simpson, J.E., A comparison between laboratory currents and atmospheric density currents, *Quart. J. Roy. Meteor. Soc.*, 95, 758 - 765, 1969.

Simpson, J.E., *Sea Breeze and Local Wind*, Cambridge, England, Cambridge University Press, 234 pgs., 1994.

Simpson, J.E., Diurnal changes in sea-breeze direction, *J. Appl. Meteor.*, 35, 1166 - 1169, 1996.

Simpson, J.E., *Gravity Currents in the Environment and the Laboratory*, Cambridge, England, Cambridge University Press, 244 pgs., 1997.

Simpson, J.E., D.A. Mansfield, and J.R. Milford, Inland penetration of sea-breeze fronts, *Quart. J. Roy. Meteor. Soc.*, 103, 47 - 76, 1977.

Simpson, J.E., and R.E. Britter, A laboratory model of an atmospheric mesofront, *Quart. J. Roy. Meteor. Soc.*, 106, 485 - 500, 1980.

Simpson, J.E., and P.F. Linden, Frontogenesis in a fluid with horizontal density gradients, *J. Fluid Mech.*, 202, 1 - 16, 1989.

Smith, R.K., N. Crook, and G. Roff, The Morning Glory; An extraordinary atmospheric undular bore, *Quart. J. Roy. Meteor. Soc.*, 108, 937 - 956, 1982.

Stephan, K., H. Kraus, C.M. Ewenz, and J.M. Hacker, Sea-breeze front variations in space and time, *Meteorol. Atmos. Phys.*, 70, 81 - 95, 1999.

Stull, R.B., *An Introduction to Boundary Layer Meteorology*, Dordrecht, The Netherlands, Kluwer Academic Publishers, 670 pgs., 1988.

Tijm, A.B.C., and A.J. van Delden, The role of sound waves in sea-breeze circulation, *Quart. J. Roy. Meteor. Soc.*, 125, 1997 - 2018, 1999.

Tijm, A.B.C., A.A.M. Holtstag, and A.J. van Delden, Observations and modeling of the sea breeze with the return current, *Mon. Wea. Rev.*, 127, 625 - 640, 1999.

Venkatram, A., A model of internal boundary-layer development, *Bound- Lay. Meteorol.*, 11, 419 - 437, 1977.

Walsh, J.E., Sea breeze theory and applications, *J. Atmos. Sci.*, 31, 2012 - 2026, 1974.

Weckwerth, T.M., J.W. Wilson, and R.M. Wakimoto, Thermodynamic variability within the convective boundary layer due to horizontal convective rolls, *Mon. Wea. Rev.*, 124, 769 - 784, 1996.

Weckwerth, T.M., J.W. Wilson, R.M. Wakimoto, and N.A. Crook, Horizontal convective rolls: Determining the environmental conditions supporting their existence and characteristics; *Mon. Wea. Rev.*, 125, 505 - 526, 1997.

Wood, R., I.M. Stromberg, and P.R. Jonas, Aircraft observations of sea- breeze frontal structure, *Quart. J. Roy. Meteor. Soc.*, 125, 1959 - 1995, 1999.

Xian, Z., and R.A. Pielke, The effects of width of landmasses on the development of sea breezes, *J. Appl. Meteor.*, 30, 1280 - 1304, 1991.

Xu, Q., Density currents in shear flows -- A two-fluid model, *J. Atmos. Sci.*, 49, 511 - 524, 1992.

Yoshikado, H., Numerical study of the daytime urban effect and its interaction with the sea breeze, *J. Appl. Meteor.*, 31, 1146 - 1164, 1992.

Yu, T.W., and N.K. Wagner, Diurnal variations of onshore wind speed near a coastline, *J. Appl. Meteor.*, 9, 760 - 766, 1970.

Zhong, S., and E.S. Takle, An observational study of sea- and land-breeze circulation in an area of complex coastal heating, *J. Appl. Meteor.*, 31, 1426 - 1438, 1992.

APPENDICES

APPENDIX I

TERMINOLOGY

Adiabatic. An adiabatic process is one in which a system (or parcel of air) does not exchange energy with its surroundings.

AGL. Above Ground Level.

Anticyclonic. Horizontal circulation associated with areas of high atmospheric pressure, and clockwise (counter-clockwise) rotation in the Northern (Southern) Hemisphere.

Appalachian Lee Trough (APLT). A trough of low pressure that forms east of the Appalachian mountains on days when the 700 - 500 hPa flow has a significant westerly component.

Backing. Counter-clockwise rotation of the wind direction.

Buys Ballot's Law. A law describing the geostrophic wind. *If you stand with your back to the wind in the Northern Hemisphere, lower pressure is on your left and higher pressure is on your right. The relation is reversed in the Southern Hemisphere.*

Circulation. A scalar quantity that represents a macroscopic measure of rotation over a finite area of fluid in two dimensions.

Coastal Upwelling. See upwelling.

Convection. Vertical heat transfer by fluid flow. This occurs when the atmosphere is thermodynamically unstable, *i.e.*, when warmer (lighter) air underlies colder (denser) air.

Convective Internal Boundary Layer (CIBL). Well-mixed region within the marine airmass over land, adjacent to Earth's surface.

Coriolis Force. An apparent force causing objects moving over the surface of Earth to be deflected to the right in the Northern Hemisphere, and to the left in the Southern Hemisphere.

Cu. Fair-weather cumulus.

Cutoff Vortex. See Undular Bore.

Cyclonic. Horizontal circulation associated with areas of low atmospheric pressure, and counter-clockwise (clockwise) rotation in the Northern (Southern) Hemisphere.

Diabatic. A diabatic process is one in which a system (or parcel of air) exchanges energy with its surroundings.

Diffusion. The transport of matter solely by random motions of individual molecules (a.k.a. molecular diffusion), or due to the effects of turbulent motion (a.k.a. dispersion).

Ekman Pumping. Upward or downward vertical motion in the surface ocean resulting from the balance of the Coriolis force and wind stress on the sea surface.

Frontogenesis. The formation or amplification of a front, due to an increase in the magnitude of the associated gradients. Results from the convergence of two dissimilar airmasses.

Frontolysis. The dissipation or weakening of a front, due to a decrease in the magnitude of the associated gradients.

Fumigation. Rapid downward mixing of an elevated plume of air pollution as it crosses from a stable layer into a turbulent mixed layer, such as a Convective Internal Boundary Layer.

Geostrophic Wind. Theoretical wind resulting from balance between the horizontal pressure gradient and Coriolis forces.

Gravity Current. A flow driven by horizontal density contrasts.

Hectopascal (hPa). Unit of pressure equivalent to 100 Pascals, or one millibar. The mean atmospheric sea-level pressure on Earth's surface is about 1013 hectopascals.

Horizontal Convective Roll (HCR). Overturning cylindrically-shaped wind structures whose axis of rotation is parallel to Earth's surface.

Hydrostatic. Theoretical condition wherein the vertical pressure gradient force is balanced by gravity. There is no net vertical acceleration.

Inviscid. An inviscid (or *ideal*) fluid is one in which all surface forces exerted on the boundaries of each small element of the fluid act normal (perpendicular) to these boundaries.

Isobar. A line of equal atmospheric pressure.

Isotropic. Having the same properties in all direction.

Kelvin-Helmholtz Billow (KHB). Wave structures seaward of the sea-breeze head, along the top of the sea-breeze gravity current.

Kinematic. Pertaining to pure motion without regard to force, momentum, or energy.

Kinematic (Sea-Breeze) Front. The location of maximum near-surface (100 meters AGL) wind convergence.

L-B Index. Lake-Breeze Index.

LHS. Left-Hand Side.

Mesoscale. Size scale of meteorological phenomena between 2 and 2000 kilometers across. The meso- α scale consists of phenomena between 200 and 2000 kilometers across, the meso- β scale consists of phenomena between 20 and 200 kilometers across, and the meso- γ scale consists of phenomena between 2 and 20 kilometers across.

Mesoscale Pressure Gradient Force (Mesoscale PGF).

Pressure gradient force created by the local density difference between the marine and continental airmasses. It points from the sea to the land.

Microscale. Size scale of meteorological phenomena less than 2 kilometers across.

Morning Glory. Pronounced undular bore that occurs in northern Australia.

NEAQS. New England Air Quality Study. Joint project of the U.S. National Oceanic and Atmospheric Administration, the University of New Hampshire, and others, to understand the inter-relationships in New England's air quality, meteorology, and climate phenomena.

Nocturnal Stable Layer. Shallow, thermodynamically-stable region of the atmosphere in contact with Earth's surface that is created by the emission of infra-red radiation during hours of darkness.

Planetary Boundary Layer (PBL). Region of the troposphere directly influenced by Earth's surface.

Potential Temperature (θ). The temperature a parcel of air would have if it were transported adiabatically to 1000 hPa.

Pressure Gradient Force (PGF). Horizontal force pointing from higher pressure to lower pressure, perpendicular to the isobars.

Prevailing Wind (PW). Wind flow resulting from synoptic-scale systems.

Pyroclastic Flow. Downslope flow of hot volcanic ash and cinders.

Radiational (or Radiative) Cooling. The nocturnal emission of infra-red radiation from Earth's surface. Typically occurs on calm, clear nights, and results in a nocturnal stable layer.

Richardson Number (Ri). The ratio of static (thermodynamic) stability to kinetic energy of shear.

RHS. Right-Hand Side.

Roll Vortex. See Undular Bore.

Sea-Breeze Circulation (SBC). Vertically-rotating, closed circuit of wind flow caused by a mesoscale cross-shore temperature gradient.

Sea-Breeze Front (SBF). The landward edge of the sea-breeze system. The SBF consists of two main components: The thermodynamic SBF (SBF_{th}), and the kinematic SBF (SBF_{kn}). The former is characterized a strong cross-shore temperature gradient, and marks the landward edge of the sea-breeze gravity current. The latter is characterized by a change in wind direction and speed, and marks the landward edge of the sea-breeze circulation.

Sea-Breeze Gravity current (SBG). Landward movement of cool marine air near Earth's surface.

Sea-Breeze Head (SBH). The raised wave-like structure at the leading edge of the sea-breeze gravity current.

Sea-Breeze System (SBS). Includes all aspects of the group of phenomena collectively called the sea breeze.

SSCF. Synoptic-Scale Cold Front -- The boundary between two synoptic-scale airmasses, with the colder (denser) airmass advancing onto an area of Earth's surface previously dominated by the warmer (lighter) airmass.

Synoptic Scale. Size scale of meteorological phenomena more than 2000 kilometers across.

Thermal Pressure Gradient Force (Thermal PGF). See mesoscale pressure gradient force.

Thermodynamic (Sea-Breeze) Front. The location within the PBL where the mean thermodynamic properties of the air begin to differ from those of the ambient (continental) air.

Thermodynamic Stability. The ability of a fluid to become turbulent or laminar due to the effects of buoyancy; a measure of the potential for convective overturning in a region of the atmosphere.

Turbidity Current. Gravity current in which a limited volume of turbid (muddy) water moves relative to the surrounding water because of the current's greater density.

Turbulence. Irregular, unpredictable fluctuations in fluid media, generally occurring in all three spatial dimensions.

Undular Bore. A solitary wave that forms when the leading edge of the SBG (beneath the SBH) separates from the remainder of the marine airmass and propagates inland independently.

Upwelling. The vertical transport of subsurface water to points nearer the sea surface.

Urban Heat Island (UHI). Region of atmosphere above and near urban areas, that, because of the presence of urban structures, is warmer than the air above the surrounding countryside.

Veering. Clockwise rotation of the wind direction.

APPENDIX II

SUMMARY OF SYMBOLS

Table A2.1: Summary of Symbols.

Symbol	Description
C_a	Circulation
c_p	Specific heat coefficient of air (constant pressure)
C_D	Drag coefficient
C_T	Heat flux coefficient
d	Vertical depth of sea breeze
\bar{d}	Mean vertical depth of sea breeze
D/Dt	Material derivative
f	Coriolis parameter
F	Entrainment coefficient
g	Gravitational acceleration
h	Height of CIBL
H	Horizontal scale
k	Constant; von Karman constant
L	Vertical scale
P, P_0, P_1	Atmospheric pressure
Q	Heat
R	Specific gas constant for air
t	Time
T, T_1, T_2	Temperature
$\bar{T}, \bar{T}_1, \bar{T}_2$	Mean temperature
u	Eastward component of net wind vector
\bar{U}	Mean wind speed
$ U $	Scalar wind speed
u_{FRONT}	Rate of advance of sea-breeze front
u_g	Eastward component of geostrophic wind; cross-shore wind speed in continental airmass
u_h	Cross-shore wind component at upper part of CIBL

Table A2.1 (Continued): Summary of Symbols.

u_{SB}	Wind velocity behind sea-breeze front
v	Northward component of net wind vector
v_g	Northward component of geostrophic wind
w	Vertical component of net wind vector
x	Cross-shore dimension
y	Along-shore dimension
z	Vertical dimension
α	Angle
β	Expansion coefficient of air
ϵ	Lake breeze index
ϕ	Latitude
γ	Vertical temperature lapse rate
K, K_H, K_V	Coefficient of heat diffusion
θ	Potential temperature
ρ, ρ_a	Air density
ω	Diurnal cycle of heating and cooling

APPENDIX III

SCALING AND LIMITATIONS OF THE KINEMATIC FRONTOGENESIS FUNCTION

Scaling

The theoretical development of the three-dimensional kinematic frontogenesis function (KFF) is discussed in *Miller et al.* [2003a]. The version of the function involving potential temperature (equation 2.13), and the physical interpretation of its terms, are discussed in Chapter 2 of this dissertation. The base variables (and their assumed values) used for scaling the right-hand side of the KFF are listed in Table A3.1.

Table A3.1: Base variables for scaling the KFF.

Variable	Description	Assumed Scale Value
L	Horizontal domain dimension	10^5 m
H	Vertical domain dimension	100 m
U	Horizontal wind component	10 ms^{-1}
W	Vertical wind component	10^{-1} ms^{-1}
ΔT	Horizontal temperature range	10°C
$-\gamma \approx -\Gamma d$	Vertical temperature gradient	$10^\circ \text{C km}^{-1}$ ($10^{-2}^\circ \text{C m}^{-1}$)
$K_H \approx K$	Heat diffusion coefficient scale, Horizontal heat diffusion scale	$1 \text{ m}^2 \text{ s}^{-1}$
$K_V \approx 10^3 \times K$	Vertical heat diffusion scale	$10^3 \text{ m}^2 \text{ s}^{-1}$

where the scale values of K_H and K_V were found via experimentation.

Using these values, the terms on right-hand side of the KFF scale as follows:

- Term 1: 10^{-8}
- Term 2: 10^{-8}
- Term 3: 10^{-8}
- Term 4: 10^{-14}
- Term 5: 10^{-14}
- Term 6: 10^{-6}

From the scale analysis, it is evident that terms 4 and 5 (the horizontal diffusion terms) are relatively unimportant, and need not be calculated in a first-order analysis. Terms 1, 2, and 3 (convergence, horizontal rotation, and vertical rotation) are six orders of magnitude larger, but are also still two orders of magnitude smaller than term 6 (related to vertical heat diffusion).

From this, one might conclude that the last term is all that is necessary for a first-order calculation. This assumes that equally useful knowledge of the appropriate scalars in all three spatial dimensions is available, which is usually not the case. This paper utilizes gridded values of potential temperature and horizontal wind

components near Earth's surface, which are sufficient for calculating the gradients required in the first two terms of the frontogenesis function. Knowledge of vertical gradients is not available in the required detail, so the KFF was reduced from a 3-D model to a 2-D model, describing the horizontal plane at 10 meters AGL..

Finite-Difference Modeling

The KFF was converted to a finite-difference equation as described in *Anderson et al.* [1984]. Once the required differences were calculated for all points in the gridded domain, the first two terms on the right-hand side of (1) were calculated by:

$$\left[- \frac{\partial u}{\partial x} \theta_x \right]_{i,j,k} \sim - \left(\frac{u_{i,j+1,k} - u_{i,j-1,k}}{2\Delta x} \right) [\theta_x]_{i,j,k} \quad (A1)$$

$$\left[- \frac{\partial v}{\partial x} \theta_y \right]_{i,j,k} \sim - \left(\frac{v_{i,j+1,k} - v_{i,j-1,k}}{2\Delta x} \right) [\theta_y]_{i,j,k} \quad (A2)$$

Model Limitations

There are a number of limitations that should be understood before attempting to use the KFF. Some of these are discussed in Table A3.2.

Table A3.2. Summary of KFF model limitations when using in the horizontal plain.

Observation	Conclusion
Model kinematics diagnose <i>changes</i> in cross-shore airmass transition zone, not the location of transition zone.	Model can not be used for localizing the position of the seabreeze front.
Model kinematics assume that the transition zone grows stronger if it is acted upon in such a way as to increase the cross-shore temperature gradient, and grows weaker if it is acted upon in such a way as to decrease the cross-shore temperature gradient.	Sea-breeze frontogenesis occurring because of convergence in the along-shore direction will not be diagnosed.
Model kinematics do not include a term for rotation resulting from along-shore variation in the cross-shore wind component.	Sea-breeze frontogenesis occurring because of rotation due to along-shore variation in the wind's u-component will not be diagnosed.
The model uses a rectangular grid rotated so that the x-direction is pointed toward 120 degrees, and the y-direction is pointed toward 30 degrees. Model kinematics assume that the coastline is a straight line parallel to the y-direction. Any significant departures from this assumption (those departures "visible" to the model) will result in a false diagnosis, especially by term 2 -- the along-shore rotation term.	The model may only be safely used to diagnose changes in the cross-shore airmass transition zone at some distance inland of the coast, i.e., at a point far enough removed from the coast so that "small" variations in the shape of the coastline are not "visible" to the model.

APPENDIX IV

COMPLETE LIST OF YEAR-2001 SEA-BREEZE, MARGINAL, AND NON-SEA-BREEZE EVENTS AND THEIR ASSOCIATED SYNOPTIC CLASSES

Table A4.1: List of Year-2001 Events and Associated Synoptic Classes.

Date [MM/DD/YYYY]	Hour of Onset [GMT]	Type of Event (at KPSM)	Synoptic Class
01/01/2001	NA	Non-Sea Breeze	2
01/02/2001	NA	Non-Sea Breeze	1
01/07/2001	NA	Non-Sea Breeze	3
01/10/2001	NA	Non-Sea Breeze	2
01/12/2001	NA	Non-Sea Breeze	2
01/17/2001	NA	Non-Sea Breeze	2
01/22/2001	NA	Non-Sea Breeze	1
01/23/2001	23	Sea Breeze	4
01/25/2001	NA	Non-Sea Breeze	2
01/26/2001	21	Marginal	6
01/28/2001	NA	Non-Sea Breeze	2
02/03/2001	NA	Non-Sea Breeze	3
02/07/2001	NA	Non-Sea Breeze	2
02/10/2001	NA	Non-Sea Breeze	3
02/11/2001	NA	Non-Sea Breeze	2
02/12/2001	23	Sea Breeze	1
02/15/2001	NA	Non-Sea Breeze	3
02/18/2001	NA	Non-Sea Breeze	1
02/19/2001	NA	Non-Sea Breeze	4
02/20/2001	24	Marginal	4
02/21/2001	NA	Non-Sea Breeze	3
02/22/2001	22	Sea Breeze	1
02/24/2001	NA	Non-Sea Breeze	2
02/26/2001	NA	Non-Sea Breeze	3
02/27/2001	NA	Non-Sea Breeze	7
02/28/2001	NA	Non-Sea Breeze	1
03/01/2001	NA	Non-Sea Breeze	2
03/04/2001	17	Sea Breeze	6

Table A4.1 (Continued): List of Year-2001 Events and Associated Synoptic Classes.

03/08/2001	18	Sea Breeze	1
03/15/2001	NA	Non-Sea Breeze	3
03/16/2001	NA	Non-Sea Breeze	2
03/17/2001	17	Sea Breeze	6
03/20/2001	17	Sea Breeze	6
03/24/2001	NA	Non-Sea Breeze	5
03/26/2001	18	Sea Breeze	6
03/27/2001	NA	Non-Sea Breeze	2
03/28/2001	NA	Non-Sea Breeze	2
04/03/2001	18	Sea Breeze	2
04/04/2001	18	Sea Breeze	1
04/05/2001	NA	Non-Sea Breeze	2
04/07/2001	19	Sea Breeze	6
04/14/2001	NA	Non-Sea Breeze	3
04/15/2001	19	Sea Breeze	2
04/16/2001	16	Sea Breeze	6
04/19/2001	NA	Non-Sea Breeze	2
04/20/2001	19	Sea Breeze	4
04/25/2001	23	Sea Breeze	1
04/26/2001	16	Sea Breeze	1
04/28/2001	NA	Non-Sea Breeze	6
04/29/2001	NA	Non-Sea Breeze	1
05/01/2001	18	Sea Breeze	4
05/02/2001	NA	Non-Sea Breeze	2
05/03/2001	NA	Non-Sea Breeze	5
05/06/2001	16	Sea Breeze	6
05/07/2001	19	Sea Breeze	1
05/08/2001	17	Sea Breeze	4
05/09/2001	15	Sea Breeze	4
05/10/2001	18	Sea Breeze	1
05/11/2001	16	Sea Breeze	2
05/13/2001	NA	Non-Sea Breeze	6
05/14/2001	NA	Non-Sea Breeze	3
06/05/2001	NA	Non-Sea Breeze	2
06/06/2001	NA	Non-Sea Breeze	2
06/07/2001	NA	Non-Sea Breeze	2
06/08/2001	19	Sea Breeze	2
06/09/2001	25	Marginal	2
06/14/2001	18	Sea Breeze	7
06/16/2001	21	Sea Breeze	4
06/18/2001	26	Sea Breeze	2
06/19/2001	NA	Non-Sea Breeze	5
06/25/2001	19	Sea Breeze	6
06/26/2001	21	Marginal	2
06/27/2001	NA	Non-Sea Breeze	2
06/28/2001	NA	Non-Sea Breeze	2
07/02/2001	NA	Non-Sea Breeze	2
07/06/2001	NA	Non-Sea Breeze	2
07/07/2001	20	Marginal	1
07/13/2001	NA	Non-Sea Breeze	3
07/15/2001	17	Sea Breeze	2

Table A4.1 (Continued): List of Year-2001 Events and Associated Synoptic Classes.

07/16/2001	16	Sea Breeze	2
07/20/2001	17	Sea Breeze	2
07/23/2001	NA	Non-Sea Breeze	4
07/21/2001	18	Sea Breeze	1
07/24/2001	NA	Non-Sea Breeze	4
07/25/2001	NA	Non-Sea Breeze	3
07/27/2001	23	Marginal	1
07/28/2001	18	Sea Breeze	1
07/31/2001	19	Marginal	6
08/01/2001	15	Sea Breeze	6
08/02/2001	NA	Non-Sea Breeze	4
08/06/2001	NA	Non-Sea Breeze	2
08/07/2001	NA	Non-Sea Breeze	2
08/09/2001	NA	Non-Sea Breeze	2
08/11/2001	16	Sea Breeze	6
08/13/2001	NA	Non-Sea Breeze	7
08/14/2001	18	Sea Breeze	6
08/15/2001	15	Sea Breeze	6
08/16/2001	NA	Non-Sea Breeze	2
08/18/2001	NA	Non-Sea Breeze	2
08/22/2001	16	Sea Breeze	2
08/23/2001	NA	Non-Sea Breeze	2
08/24/2001	16	Sea Breeze	6
08/25/2001	15	Sea Breeze	6
08/26/2001	18	Sea Breeze	4
08/29/2001	NA	Non-Sea Breeze	2
09/02/2001	20	Sea Breeze	1
09/04/2001	NA	Non-Sea Breeze	4
09/05/2001	NA	Non-Sea Breeze	6
09/07/2001	NA	Non-Sea Breeze	4
09/08/2001	NA	Non-Sea Breeze	4
09/09/2001	NA	Non-Sea Breeze	4
09/10/2001	20	Sea Breeze	4
09/11/2001	NA	Non-Sea Breeze	2
09/12/2001	18	Sea Breeze	6
09/13/2001	NA	Non-Sea Breeze	5
09/15/2001	18	Sea Breeze	6
09/16/2001	21	Sea Breeze	1
09/17/2001	17	Sea Breeze	6
09/18/2001	17	Sea Breeze	6
09/26/2001	NA	Non-Sea Breeze	5
09/27/2001	NA	Non-Sea Breeze	3
09/29/2001	17	Sea Breeze	6
09/30/2001	15	Sea Breeze	6
10/01/2001	23	Marginal	6
10/03/2001	NA	Non-Sea Breeze	4
10/04/2001	NA	Non-Sea Breeze	4
10/05/2001	NA	Non-Sea Breeze	4
10/07/2001	NA	Non-Sea Breeze	2
10/08/2001	NA	Non-Sea Breeze	2
10/09/2001	NA	Non-Sea Breeze	1

Table A4.1 (Continued): List of Year-2001 Events and Associated Synoptic Classes.

10/10/2001	21	Sea Breeze	4
10/11/2001	22	Sea Breeze	4
10/15/2001	NA	Non-Sea Breeze	7
10/18/2001	NA	Non-Sea Breeze	2
10/19/2001	20	Sea Breeze	4
10/20/2001	NA	Non-Sea Breeze	5
10/21/2001	NA	Non-Sea Breeze	4
10/22/2001	NA	Non-Sea Breeze	2
10/28/2001	21	Sea Breeze	1
10/29/2001	NA	Non-Sea Breeze	4
10/30/2001	NA	Non-Sea Breeze	6
11/02/2001	NA	Non-Sea Breeze	4
11/06/2001	NA	Non-Sea Breeze	3
11/07/2001	NA	Non-Sea Breeze	3
11/09/2001	NA	Non-Sea Breeze	3
11/11/2001	NA	Non-Sea Breeze	6
11/12/2001	NA	Non-Sea Breeze	1
11/13/2001	22	Sea Breeze	1
11/15/2001	NA	Non-Sea Breeze	4
11/17/2001	21	Sea Breeze	6
11/18/2001	NA	Non-Sea Breeze	4
11/19/2001	NA	Non-Sea Breeze	4
11/21/2001	22	Sea Breeze	4
11/23/2001	19	Sea Breeze	1
12/01/2001	NA	Non-Sea Breeze	5
12/07/2001	NA	Non-Sea Breeze	3
12/09/2001	NA	Non-Sea Breeze	6
12/10/2001	23	Marginal	4
12/11/2001	21	Sea Breeze	7
12/16/2001	NA	Non-Sea Breeze	6
12/19/2001	NA	Non-Sea Breeze	5
12/22/2001	NA	Non-Sea Breeze	1
12/25/2001	NA	Non-Sea Breeze	2
12/28/2001	24	Marginal	2
12/29/2001	NA	Non-Sea Breeze	2
12/30/2001	NA	Non-Sea Breeze	2
12/31/2001	NA	Non-Sea Breeze	2

APPENDIX V

MISCELLANEOUS TABLES

Table A5.1: Description of Isentropic Patterns.

Pattern	Description	Fig(s)
Elongate S (ES)	Warm air extended northeastward from the southwest boundary, over the Great Bay, and further offshore. Cold air extended southwestward from the northeast boundary, south of KIWI (Figure 3), and inland over the central portion of the study area.	5.5a
Coastal S (CS)	Isentropes were approximately shore-parallel in the study area, except for a small seaward "kink" indicating an extension of warm air into the area offshore of KSFM.	5.5b
Coastal Shore-Parallel; Warm Air Over Land (CSP-Wland)	Isentropes were shore-parallel, with warmer air over land, and cooler air over the sea. A sharp gradient, indicative of a SBFth, may or may not be present near the coastline.	5.5c and 5.6d
Split S (SS)	Isentropes were generally parallel to the straight section of coastline, with cold air offshore, and warm air over land. The isentropes indicated a sharp, cross-shore potential temperature gradient in two locations: One approximately 40 kilometers inland in the northern half of the study area, and one along the coast throughout the study area. The former was the "inland component," and the latter was the "coastal component." The inland and coastal components merged diagonally across the MALW line (Figure 7b), forming a single, very wide SBFth in the southern half of the study area.	5.5d
Inland Shore-Parallel (ISP)	Closely-spaced shore-parallel isentropes, coinciding approximately with 2ML. Represented a unified, well-defined SBFth, with relatively unmodified marine air to the east, and continental air to the west.	5.5e

Table A5.1 (Continued): Description of Isentropic Patterns.

Lowlands (LL)	Closely-spaced isentropes, aligned in a pattern that approximately coincided with inland edges of the NLA and SLA (150-meter ASL topographic contour; Figure 7b). Indicative of relatively unmodified marine air flooding into the NLA, the SLA, or both (Figure 7b), in the form of a sea-breeze gravity current. The isentropic gradients tended to be weaker than those associated with SS, indicating gradual modification of the marine airmass from the shore inland.	5.5f
Cold Northwest and Warm Southwest (KNWWSW)	Cold air (K) was located in the northwest corner, and warm air (W) was located along the southwestern boundary of the study area.	5.6a
Cold Northwest and Warm Southeast (KNWWSE)	Cold air (K) was located in the northwest corner, and warm air (W) was located in the offshore area of the southeast corner of the study area.	5.6b
Coastal Shore-Parallel; Cold Air Over Land (CSP-Kland)	Isentropes generally parallel to the straight section of coastline, with warm air offshore, and cold air over land.	5.6c
Cold Air East (KE)	Cold air was located in the northern half of the offshore area, and warmer air was located in the southwest. The isentropes crossed the coast at an oblique angle throughout most of the study area.	5.6e
Cold Air North (KN)	Cold air was located in the northeast corner of the offshore area, associated with the cold, along-shore current in the GOM (Figure 9). Warmer air was over the land surface to the southwest. Isentropes crossed the coast at an oblique angle in the northern half of the study area, and at right angle in the southern half.	5.6f
Central Inland Cold Pocket (CICP)	A pocket of cold air was centered in the hilly region east of the circular Ossipee formation in New Hampshire, and west of Sanford, in southern Maine (KSFM; Figure 3). This area is surrounded by narrow strips of lowlands, most of them containing rivers or lakes.	5.7a
Lake Winnepesaukee Warm Pocket (LWWP)	A pocket of warm air was centered above Lake Winnepesaukee, along the central portion of northwest boundary. Lake Winnepesaukee is a relatively large lake, with a surface area of approximately 185 km ² , and is surrounded by hilly terrain.	5.7b

Table A5.1 (Continued): Description of Isentropic Patterns.

Mount Washington Drainage Event (MWN Drainage)	A narrow finger of cold air extended southeast from the New Hampshire Presidential Range (White Mountains) toward KSFM, and offshore. Occurred at all times of the year, generally after 2200 LST, and was often visible in early-morning isentropic fields.	5.7c
Cold South - Warm Central - Cold North (KWK)	Cold air was offshore of the southeast corner of the study area (vicinity of CA) and offshore of KPWM in the northeast corner of the study area; warm air was centered over the Great Bay (Portsmouth, New Hampshire), and sometimes extended northwest toward the White Mountains. KWK appeared on NSB days..	5.7d

Table A5.2: Description of Kinematic Patterns.

Pattern	Description	Fig(s)
Trough (T)	The flow in the study area was cyclonically curved and generally towards the sea. The trough axis could be oriented in from northwest to southeast, northeast to southwest, or east to west.	5.8
Southwesterly flow, primarily perpendicular to the coast (SWX1, SWX2, SWX3).	SWX1: Generally smooth flow; weak convergence and/or divergence. Weak troughs and ridges were sometimes embedded in the flow.	5.9a
	SWX2: A strong axis of convergence dominated the study area. Flow north of this line was either westerly or northwesterly.	5.9b
	SWX3: There was divergence in the flow field, with or without minor regions of convergence.	5.9c
Southwesterly flow, primarily parallel to the coast (SWP1, SWP2, and SWP3).	SWP1: Generally smooth flow. Wind speeds over water may have been greater than over land; wind inland may have been very light or calm. In some cases the wind flow inland showed some evidence of following the topographic contours.	5.9d
	SWP2: Oblique landward crossing of the wind at the coast, with weak convergence along an inland line parallel to the coast, indicating the development of a weak SBC. A weak divergence region sometimes appeared along an offshore line parallel to the coast.	5.9e
	SWP3: Oblique seaward crossing of the wind at the coast, with weak divergence along an inland line parallel to the coast, and weak convergence along an offshore line parallel to the coast.	5.9f
Southwesterly flow, both parallel and perpendicular to the coast (SWM1, SWM2, and SWM3).	SWM1: Flow offshore and in the near-coastal inland region was parallel to the coast, or crossing seaward at an oblique angle. Flow in the southwestern corner was southerly or southeasterly, and a divergence line extended northward from KASH.	5.10a
	SWM2: Similar to SWX1, but with more pronounced waves. Flow over the northern offshore area was cyclonic, and sometimes became shore-parallel, or even crossed back toward the land at an oblique angle.	5.10b
	SWM3: Well developed onshore flow was in the northern half of the study area, and convergent shore-parallel flow was in the southern half. A mesoscale cyclonic circulation was sometimes present on the coast, near KPWM, or at some point further inland along a shore-perpendicular line extending northwestward from KPWM.	5.10c

Table A5.2 (Continued): Description of Kinematic Patterns.

Northeasterly flow (NE1 through NE6).	NE1: Flow was generally shore-parallel. In some cases the wind flow inland followed the topographic contours.	5.11a
	NE2: Obliquely seaward-crossing wind was at the coast, with weak divergence along an inland line parallel to the coast, and weak convergence was along an offshore line parallel to the coast.	5.11b
	NE3: Flow was generally in a broad cyclonic arc from the northeast Gulf of Maine, inland toward the White Mountains (near KIZG and KLCI; see Figure 3), and back offshore across Cape Ann (see Figure 7). Wind offshore followed the contour of the coastline. A convergence line was created along the coast in the southern portion of the study area, where the shore-crossing wind inland met the shore-parallel flow offshore. A calm or very light wind region sometimes developed seaward of this convergence line. There was some evidence of terrain-following inland.	5.11c
	NE4: Obliquely landward-crossing wind at the coast, with weak convergence along an inland line parallel to the coast. A weak region of divergence sometimes appeared along an offshore line parallel to the coast.	5.11d
	NE5: Convergence line in NE4 rotated and crossed the coast at an angle. Flow south of this line was landward, and flow north of the line was either shore-parallel or crossing seaward at an oblique angle.	5.11e
	NE6: The convergence line in NE5 traced out the shape of the NLA and SLA. Flow east of the line was landward, crossing the shore at an oblique angle. Flow west of the line was generally shore-parallel, and sometimes followed the topographic contours.	5.11f
Northwesterly flow, generally perpendicular to the Coast (NW1, NW2, and NW3).	NW1: Generally smooth flow; weak convergence and/or divergence. Weak troughs and ridges were sometimes embedded in the flow, and the wind sometimes followed the topographic contours over land. A region of calm or very light winds sometimes developed in the southern offshore region north of Cape Ann.	5.12a
	NW2: A strong axis of convergence cut across the study area, crossing the coast at a right angle.	5.12b
	NW3: Northwesterly flow field exhibited regions of both divergence and convergence.	5.12c

Table A5.2 (Continued): Description of Kinematic Patterns.

Convergence line approximately parallel to the coast, with generally northwesterly flow west the line, and southerly to southeasterly flow east of the line (COL1, COL2, COL3, COL4, and COL5).	COL1: Shore-parallel convergence line, generally in the immediate vicinity of the coast, with northwesterly flow inland and southwesterly flow over water.	5.13a
	COL2: Convergence line in COL1 rotated so that some portion of it was no longer parallel to the coast. Flow over water backed toward the east. Flow was northeasterly in the southern offshore area, southeasterly in the central offshore area, and southerly in the northern offshore area.	5.13b
	COL3: The convergence line traced out the approximate inland limits of the SLA and NLA, marking out the 150-meter topographic contour. Wind within the SLA and NLA rotated cyclonically. Wind along the MALW line was northwesterly almost all the way down to the coast.	5.13c
	COL4: Convergence line pushed inland. The onshore flow to the east of the line showed no evidence of being trapped in the low-lying regions near the coast. Calm, very light, or cyclonically-rotating wind regions sometimes developed along the line.	5.13d
	COL5: Convergence line pushed further inland, reaching or exceeding the western extreme of the study area. Flow throughout the study area was southeasterly and diffluent.	5.13e

Table A5.3: Sequence of Isentropic and Kinematic Patterns with Sea-Breeze and Marginal Events.

Date MMDDYYYY	Type	Isentropic Pattern Sequence	Kinematic Pattern Sequence	Notes
01/23/2001	SB	MWN Drainage By 15: CSP-KLand By 17: ES By 22: CSP-KLand By 02: MWN Drainage By 04: KNWWSE	T By 13: SWM1 By 14: SWP1 By 18: SWP2 By 23: SWP1 By 00: SWP3 By 01: SWP1 By 03: SWP3	T axis oriented NNW - SSE.
04/03/2001	SB	CICP + LWWP + ES By 14: CSP-Wland + KE By 16: KN By 19: LL (SLA) + CSP-Wland (N) By 22: CSP-Wland (N + S) By 23: KN By 02: MWN Drainage	T By 13: NW1 By 14: NW2 By 16: NW1 By 19: COL3 (SLA) + NW1 (N) By 21: COL3 (SLA) + NE1 (N) By 23: COL3 (SLA) + COL1 (N) By 00: COL3 (SLA) + NE1 (N) By 02: NW3	NE half of study area beneath synoptic-scale shield of middle and high clouds. A.M. T axis oriented NNE - SSW.
05/09/2001	SB	Elongate S + LWWP By 13: Coastal S + LWWP By 14: Coastal S By 17: Lowlands (SLA + NLA) By 22: ISP By 00: KN By 03: CICP	SWP1 By 13: SWM3 By 15: COL5	
05/10/2001	SB	ES + LWWP By 13: KE By 16: CS By 20: SS By 22: LL (NLA + SLA) By 02: KN By 04: KNWWSE	COL3 (SLA) + COL1 (N) By 13: NW3 By 14: T By 16: COL3 (NLA + SLA) By 19: COL2 By 22: COL1 By 01: T By 03: NW2	A.M. T axis parallel to coast. P.M. T axis NW - SE.

Table A5.3 (Continued): Sequence of Isentropic and Kinematic Patterns with Sea-Breeze and Marginal Events.

05/11/2001	SB	<p>KWK</p> <p>By 16: SS</p> <p>By 21: ISP + CS</p> <p>By 00: LL (NLA + SLA)</p> <p>By 03: KN</p>	<p>NW2</p> <p>By 13: NE3</p> <p>By 15: COL2</p> <p>By 16: COL3</p> <p>By 19: COL4</p> <p>By 20: SWP2</p> <p>By 01: SWP1</p> <p>By 02: SWP3</p> <p>By 03: SWM1</p>	<p>ISP peaks at 23.</p> <p>Portion of kinematic sequence beginning at 20 caused by Coriolis-induced veering.</p>
06/14/2001	SB	<p>CS + LWWP</p> <p>By 16: CS</p> <p>By 19: SS</p> <p>By 22: ISP</p> <p>By 00: KE</p> <p>By 04: KWK</p>	<p>SWX2</p> <p>By 14: SWM3</p> <p>By 16: SWP2</p> <p>By 03: SWP1</p>	<p>SWP2 cnvrgnce line near NW edge of study area by 16; retreats toward coast after 16.</p>
07/07/2001	MAR	<p>KWK</p> <p>By 19: ES</p> <p>By 20: KWK</p> <p>By 00: ES</p> <p>By 02: ES + LWWP</p>	<p>SWM2</p> <p>By 17: SWP2</p> <p>By 20: SWM2</p> <p>By 21: SWP1</p> <p>By 02: SWP2</p> <p>By 03: SWP1</p>	<p>SWP2 develops in NLA by 17 and along entire coast by 19.</p>

Table A5.3 (Continued): Sequence of Isentropic and Kinematic Patterns with Sea-Breeze and Marginal Events.

07/28/2001	SB	<p>(Weak pattern)</p> <p>By 13: CSP-Wland By 16: CS By 19: SS By 23: LL (NLA + SLA) + LWWP By 03: KNWWSE + LWWP</p>	<p>NW2</p> <p>By 15: T (N) + NW3 (S) By 16: COL1 By 18: COL3 (NLA + SLA) By 20: COL5 By 22: SWP2 By 01: SWM1</p>	<p>Split S peaks at 21.</p> <p>T axis oriented parallel to coast.</p> <p>Coriolis-induced veering causes portion of kinematic sequence beginning after 20.</p>
09/29/2001	SB	<p>KNWWSW</p> <p>By 14: KE By 15: CS By 16: CSP-Wland By 18: CS By 19: LL (NLA) + CSP-Wland (S) By 20: CSP-Wland By 23: CICP + LWWP By 00: MWN Drainage By 02: CICP By 03: KNWWSE</p>	<p>NE1</p> <p>By 13: NE2 By 15: NE1 By 17: NE5 By 23: NE6 (NLA + SLA) By 00: NE4 and NE5 (oscillating)</p>	

Table A5.4: Summary of $|\nabla\theta|$ and $\nabla \cdot \mathbf{v}$ field evolution during Sea-Breeze and Marginal events.

Date MMDDYYYY	$ \nabla\theta $ Fields	$\nabla \cdot \mathbf{v}$ Fields
01/23/2001	<p>By 16: Cross-shore gradients with values of about $0.10 \text{ }^\circ\text{C km}^{-1}$ replaced earlier along-shore gradients.</p> <p>By 17 - 20: Cross-shore gradients weakening.</p> <p>By 23: No detectable gradients.</p> <p>Aft 00: Along-shore gradients redeveloped.</p>	<p>By 15: Axis of convergence marking the position of the SBFkn from vicinity of KLWM through KPSM, and further offshore towards the northeast. Peak negative $\nabla \cdot \mathbf{v}$ approx. $0.050 \text{ m s}^{-1} \text{ km}^{-1}$.</p> <p>By 18: SBFkn shore-parallel along coast. Peak negative values $0.125 \text{ m s}^{-1} \text{ km}^{-1}$.</p> <p>By 20: Peak negative values $0.250 \text{ m s}^{-1} \text{ km}^{-1}$.</p> <p>By 22: SBFkn weakened and rotated back toward 15 position.</p> <p>By 00: Peak convergence diminished to $0.050 \text{ m s}^{-1} \text{ km}^{-1}$.</p>
04/03/2001	<p>By 15: Earlier shore-oblique gradient destroyed by insolation.</p> <p>By 18: Cross-shore gradient established (peak negative values of $0.10 \text{ }^\circ\text{C km}^{-1}$) in the southern half of the study area, from Cape Ann, through Newburyport and Portsmouth.</p> <p>By 20: SBFth position indicated by meso-β gradient along inland boundary of SLA.</p> <p>By 21: Gradient weakened; fell below $0.10 \text{ }^\circ\text{C km}^{-1}$ by 22.</p> <p>Aft 00: Along-shore gradients only.</p>	<p>By 16: Organized axis of convergence appeared (marking the SBFkn) in the same place it appeared in the January 23, 2001 SB event. Peak values approx. $0.050 \text{ m s}^{-1} \text{ km}^{-1}$.</p> <p>By 17: Convergence increased to $\geq 0.100 \text{ m s}^{-1} \text{ km}^{-1}$, with weaker values in the north.</p> <p>By 19: Strong SBFkn (peak negative values $\geq 0.175 \text{ m s}^{-1} \text{ km}^{-1}$ inland; higher offshore) traced out inland limits of the SLA. Highest inland convergence values along the northern edge of the SLA, where sea breeze converged with ambient northwesterly flow.</p> <p>By 23: Convergence weakened; became undetectable by 00.</p>

Table A5.4 (Continued): Summary of $|\nabla\theta|$ and $\nabla \cdot \mathbf{v}$ field evolution during Sea-Breeze and Marginal events.

05/09/2001	<p>By 14: Weak cross-shore isentropic gradient developed at the coastline indicating development of SBFth.</p> <p>By 17: Well-defined SBFth traced out the inland limits of the SLA and NLA.</p> <p>By 18: SBFth marked by peak (negative) gradient values of more than $0.30 \text{ }^\circ\text{C km}^{-1}$ at the inland extreme of the NLA. Peak negative values at the inland extreme of the SLA were more than $0.25 \text{ }^\circ\text{C km}^{-1}$.</p> <p>By 21: SBFth advanced beyond the NLA and SLA and onto higher terrain (above 150 m ASL), resulting in the development of shore-parallel front well inland. Peak gradients fell from 0.30 to about $0.20 \text{ }^\circ\text{C km}^{-1}$.</p> <p>By 23: Gradient reintensified to $0.30 \text{ }^\circ\text{C km}^{-1}$.</p> <p>By 00: Cross-shore gradients undetectable.</p>	<p>By 13: Shore-parallel axis of convergence developed with peak negative values of approx. $0.025 \text{ m s}^{-1} \text{ km}^{-1}$.</p> <p>By 14: Strong center of convergence developed along the SBFkn immediately east of York, Maine, with peak negative values $\geq 0.175 \text{ m s}^{-1} \text{ km}^{-1}$.</p> <p>By 15: As leading edge of SBC rapidly moved inland, the intense center of convergence migrated to western end of the NLA. Remainder of SBFkn trailed along a shore-parallel line toward the southwest.</p> <p>By 16: SBFkn moved out of the study area (toward the northwest), and a new line of convergence (secondary SBFkn) developed in SLA.</p> <p>By 17: Secondary SBFkn migrated northward, bisecting the SLA from southwest through northeast. Moved further north and weakens considerably by 18.</p> <p>19 - 20: Entire $\nabla \cdot \mathbf{v}$ field weakened further, with peak negative values dropping below $0.025 \text{ m s}^{-1} \text{ km}^{-1}$.</p> <p>Aft 00: New SBFkn developed at the coast; peak negative values of $0.175 \text{ m s}^{-1} \text{ km}^{-1}$ vicinity of KPSM.</p>
------------	---	---

Table A5.4 (Continued): Summary of $|\nabla\theta|$ and $\nabla \cdot V$ field evolution during Sea-Breeze and Marginal events.

<p>05/10/2001</p>	<p>By 16: Cross-shore gradient appeared on the coast, marking the formation of the SBFth. Peak negative values were on the order of $0.30 \text{ }^\circ\text{C km}^{-1}$.</p> <p>By 19: Secondary SBFth developed inland in the northern half of the study area.</p> <p>By 21: Inland SBFth continued to intensify through 21, while the coastal front remains in place without weakening.</p> <p>By 22: Inland SBFth moved back toward the sea. Peak inland negative isentropic gradient fell from more than $0.25 \text{ }^\circ\text{C km}^{-1}$ to less than $0.20 \text{ }^\circ\text{C km}^{-1}$.</p> <p>By 23: Peak negative gradient reintensified back to more than $0.25 \text{ }^\circ\text{C km}^{-1}$ by 00, peaking above $0.30 \text{ }^\circ\text{C km}^{-1}$.</p>	<p>By 14: SBFkn appeared, stretching (as in the January 23, 2001 sea-breeze event) from KLWM through KPWM, then further northeast into the Gulf of Maine.</p> <p>By 15: SBFkn traced out inland contours of the SLA and NLA.</p> <p>By 16: Peak inland convergence began to increase, reaching maximum of about $0.175 \text{ m s}^{-1} \text{ km}^{-1}$ in NLA, and about $0.200 \text{ m s}^{-1} \text{ km}^{-1}$ in SLA.</p> <p>By 19: Peak convergence increased to $\geq 0.450 \text{ m s}^{-1} \text{ km}^{-1}$ in NLA. Peak convergence values remained greater than $0.350 \text{ m s}^{-1} \text{ km}^{-1}$ until 23.</p> <p>By 23: SBFkn moved back toward coast.</p> <p>Aft 00: Entire convergence field weakened considerably.</p>
-------------------	--	--

Table A5.4 (Continued): Summary of $|\nabla\theta|$ and $\nabla \cdot V$ field evolution during Sea-Breeze and Marginal events.

<p>05/11/2001</p>	<p>By 14: Early-morning along-shore gradients destroyed by insolation.</p> <p>By 15: Cross-shore gradients developed on coast, indicating position of the SBFth.</p> <p>By 19: Inland SBFth developed and reached same magnitude as the coastal SBFth. Peak negative isentropic gradients exceeded $0.25 \text{ }^\circ\text{C km}^{-1}$ along the entire coastal SBFth, as well as along the inland SBFth in the northern half of the study area.</p> <p>20 - 22: Inland SBFth weakens, with peak negative isentropic gradient values falling to about $0.20 \text{ }^\circ\text{C km}^{-1}$.</p> <p>By 23: Inland SBFth reintensified (peak negative values of more than $0.25 \text{ }^\circ\text{C km}^{-1}$).</p> <p>By 00: Entire $\nabla\theta$ field collapsed, leaving no discernible gradients in the study area.</p>	<p>By 14: Offshore light wind region appears as a region of weak divergence north of Cape Ann.</p> <p>By 15: SBFkn visible as a weak convergence zone from KLWM, across KPSM, and out over the Gulf.</p> <p>By 16: SBFkn moved to the western ends of the SLA and NLA. Peak convergence values in the south exceeded $0.200 \text{ m s}^{-1} \text{ km}^{-1}$, while in the north, peak values only reached about $0.050 \text{ m s}^{-1} \text{ km}^{-1}$.</p> <p>By 17: Convergence increased to more than $0.275 \text{ m s}^{-1} \text{ km}^{-1}$ in the north.</p> <p>By 18: SBFkn moved out of the lowlands and onto the MALW line separating the SLA and NLA. The regions of peak convergence in the NLA and SLA began to merge along 2ML.</p> <p>By 19: Convergence regions weakened slightly, and SBFkn shifted about 10 kilometers back toward the sea.</p> <p>By 20: SBFkn on the coast at the northern end of the NLA, but still more than 50 kms inland (along 2ML) in the south.</p> <p>21 - 23: Convergence field was very weak.</p> <p>By 00: Convergence redeveloped at the coast.</p>
-------------------	---	--

Table A5.4 (Continued): Summary of $|\nabla\theta|$ and $\nabla \cdot V$ field evolution during Sea-Breeze and Marginal events.

<p>06/14/2001</p>	<p>By 16: Coastal SBFth exhibited its peak values (of about $0.35 \text{ }^\circ\text{C km}^{-1}$). Northern half of the coastal SBFth weakened for the remainder of the day. Southern coastal SBFth maintains a relatively constant magnitude.</p> <p>By 19: The inland SBFth developed in the north at 1900, with peak negative values of about $0.25 \text{ }^\circ\text{C km}^{-1}$, then weakened slightly for the following two hours.</p> <p>22 - 23: Inland SBFth intensified slightly, but never regained its original peak values.</p>	<p>At 12: KLWM-KPSM-GOM convergence line in place.</p> <p>By 15: Northern end of the line rotated toward the northwest, moved closer to the shore, and became more shore-parallel.</p> <p>By 17: Well-developed SBFkn was visible, parallel to the coast along the SLA, and moving inland in the NLA. Peak convergence values increased to $0.175 \text{ m s}^{-1} \text{ km}^{-1}$ in the north, and $0.125 \text{ m s}^{-1} \text{ km}^{-1}$ in the south.</p> <p>By 20: Secondary SBFkn developed offshore.</p> <p>By 21: Original SBFkn was near northwestern boundary of the study area, while the secondary SBFkn moved into place along the KLWM-KPSM-GOM line</p> <p>By 22: Inland SBFkn weakened and moved seaward; coastal SBFkn intensified.</p> <p>By 22: Inland SBFkn vanished; coastal SBFkn reached its peak intensity of $\geq 0.125 \text{ m s}^{-1} \text{ km}^{-1}$.</p> <p>By 23: Over-water flow veered from southeasterly to southwesterly, and coastal SBFkn slowly weakened.</p>
-------------------	--	---

Table A5.4 (Continued): Summary of $|\nabla\theta|$ and $\nabla \cdot \mathbf{v}$ field evolution during Sea-Breeze and Marginal events.

07/28/2001	<p>By 16: Coastal SBFth initially appeared, with peak gradients of about $0.15 \text{ }^\circ\text{C km}^{-1}$.</p> <p>By 20: Inland SBFth appeared in the northern half of the study area.</p> <p>By 21: Northern coastal SBFth weakened as the inland SBFth continued to intensify. The southern SBFth maintained a steady peak of about $0.15 \text{ }^\circ\text{C km}^{-1}$.</p> <p>By 22: Inland SBFth reached peak negative values of about $0.13 \text{ }^\circ\text{C km}^{-1}$, while northern coastal front weakened to about $0.05 \text{ }^\circ\text{C km}^{-1}$ and the southern SBFth weakened to about $0.10 \text{ }^\circ\text{C km}^{-1}$.</p>	<p>By 15: Convergence line developed along the KLWM-KPWM-GOM line, with peak values southeast of KDAW.</p> <p>By 16: SBFkn rotated into a shore-parallel position along the coast and increased in strength. Intensification of the SBFkn continued through 18, and it moved into the NLA and SLA.</p> <p>By 20: SBFkn moved beyond northwestern boundary of the study area, and minor axes of convergence and divergence were aligned in the shore-perpendicular dimension.</p> <p>By 21: Entire $\nabla \cdot \mathbf{v}$ field weakened throughout the study area.</p> <p>By 22: KLWM-KPSM-GOM convergence line developed.</p>
------------	---	--

Table A5.4 (Continued): Summary of $|\nabla\theta|$ and $\nabla \cdot V$ field evolution during Sea-Breeze and Marginal events.

09/29/2001	<p>This sea-breeze event was marked by a very weak $\nabla\theta$ field over its entire duration. The highest negative value associated with the sea breeze was about $0.10 \text{ }^\circ\text{C km}^{-1}$, indicating the absence of a well-defined SBFth.</p>	<p>By 17: SBFkn developed approximately 15 kilometers inland. Divergence was in a roughly shore-parallel region approximately 40 kilometers offshore.</p> <p>By 18: SBFkn temporarily weakened.</p> <p>By 19: SBFkn reintensified.</p> <p>By 21: SBFkn about halfway into the NLA, and near the coast in the SLA. Peak convergence values exceeded $0.100 \text{ m s}^{-1} \text{ km}^{-1}$ in the north, and $0.075 \text{ m s}^{-1} \text{ km}^{-1}$ in the south.</p> <p>By 23: Magnitude of the SBFkn increased further. Peak values in the NLA increased to more than $0.125 \text{ m s}^{-1} \text{ km}^{-1}$. Convergence increased in the south as well, but the centroid of the convergence zone began drifting back toward the northwest corner of Cape Ann, so it is difficult to attribute peak convergence values there (exceed $0.325 \text{ m s}^{-1} \text{ km}^{-1}$) entirely to the SBFkn.</p> <p>Aft 00: Entire $\nabla \cdot V$ field weakened.</p>
------------	--	---